An Exploratory Study On The Functional Significance Of Eosinophil Residency In The Small Intestine Under Homeostatic Conditions

THÈSE N^{O} 7333 (2018)

PRÉSENTÉE LE 14 DÉCEMBRE 2018

À LA FACULTÉ DES SCIENCES DE LA VIE

UNITÉ DE LA PROF. HARRIS

PROGRAMME DOCTORAL EN APPROCHES MOLÉCULAIRES DU VIVANT

ÉCOLE POLYTECHNIQUE FÉDÉRALE DE LAUSANNE

POUR L'OBTENTION DU GRADE DE DOCTEUR ÈS SCIENCES

PAR

Kathleen SHAH

acceptée sur proposition du jury:

Prof. E. Oricchio, présidente du jury
Prof. N. Harris, directrice de thèse
Prof. A. Oxenius, rapporteuse
Prof. D. Velin, rapporteur
Prof. M. De Palma, rapporteur

ÉCOLE POLYTECHNIQUE
FÉDÉRALE DE LAUSANNE

Suisse
2018

An Exploratory Study On The Functional Significance Of Eosinophil Residency In The Small Intestine Under Homeostatic Conditions

ABSTRACT

The small intestine is a highly dynamic and complex cellular ecosystem, which serves as the primary interface between the host and its environment. A critical component of this ecosystem is the microbiota, which plays a pivotal role in shaping both immune and physiological homeostasis of the host from the moment of birth. However, interaction with the microbiota is a double-edged sword – and the inappropriate establishment of host-microbiota crosstalk could lead to detrimental consequences.

Eosinophils are multi-functional granulocytes, recruited into the intestine in early life – but the relevance of this phenomenon has remained enigmatic, given the dogmatic view of these cells as drivers of pathophysiology in type-II immune mediated disorders. Understanding the functional significance of their residency in this tissue under homeostatic conditions warrants further investigation and may provide invaluable insight into their dysregulation in disease.

In this thesis, I report our investigation of the contributions of eosinophils to small intestinal homeostasis through a broad characterization of changes in various intestinal functions consequent of eosinophil-deficiency. We approached this expansive question through a combination of histological, cellular and transcriptional analyses, which have afforded us unprecedented insight to eosinophil function in this tissue. Using Δdbl.GATA1 mice, a model of constitutive eosinophil deficiency, we provide evidence for a central role for eosinophils in tissue integrity maintenance in response to the microbiota. We report herein that eosinophil-mediated tissue protection is largely driven by epithelial-derived alarmins, released in response to barrier stress – which equips eosinophils with the capacity to maintain small intestinal integrity and homeostasis through the regulation of extracellular matrix remodelling.

In summary, our work provides a functional rationale for the early life recruitment of eosinophils in the small intestine, implicating these cells as key facilitators in the establishment of appropriate host-microbiota crosstalk.

RÉSUMÉ

L’intestin grêle est un écosystème cellulaire complexe et dynamique, servant d’interface entre l'hôte et son environnement. Le microbiome intestinal en est un composant essentiel du fait de son rôle d'éducation du système immunitaire local et de mise en place de la physiologie intestinale, et ce dès la naissance. Dès alors, toute altération dans l'élaboration et la composition du microbiome intestinal peut donner lieu à des développements pathologiques.

Les éosinophiles sont des granulocytes aux multiples fonctions. Dans l’intestin, ils sont recrutés très tôt en terme de développement. Bien que cette observation soit connue depuis longtemps, son importance fonctionnelle n’a malheureusement pas été suffisamment adressée. En effet, la plupart des études sur les éosinophiles ont focalisé sur leur rôle en conditions pathophysiologiques, se limitant à l'établissement d’un dogme soutenant que les éosinophiles sont à l’origine des pathophysiologies causées par les réponses immunitaires de type 2. L'étude du rôle des éosinophiles en conditions physiologiques pourrait donc ouvrir des portes vers une meilleure compréhension de leurs rôles et permettre le développement de nouvelles approches pour remédier à leurs dysfonctionnements pathologiques.

Dans cette thèse, je rapporte notre étude du rôle des éosinophiles dans la physiologie intestinale. Notre approche a été d'étudier les conséquences fonctionnelles - tant physiologiques que nutritionnelles ou immunitaires - de l’absence d'éosinophiles. Pour ce faire, nous avons focalisé sur le modèle murin Δdbl.GATA1 qui en présente une déficience constitutive. Nous avons pu montrer que les éosinophiles jouent un rôle crucial pour la maintenance de l'intégrité tissulaire en réponse au microbiome intestinal. Suivant un stress, les cellules épithéliales de la barrière intestinale produisent des alarmines qui activent les éosinophiles pour un remodèlement optimal de la matrice extracellulaire.

Pour conclure, notre travail montre que les éosinophiles sont des acteurs clefs de la communication entre le microbiome intestinal et l'hôte, permettant de preserver l’integrite de la barrière intestinale.

ABBREVIATIONS

15-HETE 15-hydroxyeicosatetraenoic acid
Acadl acyl-acoa dehydrogenase
Actn2 actinin alpha 2
Adamdec adam like decysin
Adra1 adrenergic receptor 1
Angptl4 angiopoetin-like 4
APRIL a proliferation-inducing ligand
ATP adenosine tri-phosphate
BAFF b-cell activating factor
BEC blood endothelial cells
Bgn biglycan
BMP bone morphogenic 2
BrdU 5-bromo-2'-deoxyuridine
C1q- complement component 1 q
Cacna calcium voltage-gated channel
Car3 carbonic anhydrase 3
CCL- c-c motif chemokine
Ccr3 chemokine receptor type 3
Col collagen
CXCL chemokine (c-x-c motif) ligrand
DAMP danger-associated molecular pattern
DC dendritic cell
Drd2 dopamine receptor d2
DUO duodenum
ECM extracellular matrix
ECP eosinophil cationic protein
EDN eosinophil-derived neurotoxin
EoE eosinophilic esophagitis
EPO/EPX eosinophil peroxidase
FAP fibro/adipogenic progenitor cells
Fgf- fibroblast growth factor
FOXP3 Forkhead box P3
Gag glycosaminoglycans
GATA-1 gata binding protein-1
GATA-3 gata binding protein-3
GC goblet cells
GF germ-free
GFAP glial-fibrillary acidic protein
GM-CSF granulocyte-macrophage colony stimulating factor
GMP Granulocyte-monocyte progenitor
Gria glutamate ionotrophic receptor
HFD high fat diet
Hmcn2 hemicentin 2
Hmgcs2 3-hydroxy-3-methylglutaryl-coa synthase 2
IBD inflammatory bowel disease
IEC intestinal epithelial cells
IEL intra-epithelial lymphocytes
Ifi interferon induced
IFN interferon
Ig- immunoglobulin
IL- interleukin
ILC innate lymphoid cell
ILE ileum
ILF isolated lymphoid follicles
Itga7 integrin alpha 7
JEJ jejunum
Kcnq potassium voltage-gated channel subfamily kqt
Lama1 laminin 1
LEC lymphatic endothelial cells
LP lamina propria
LTb Lymphotoxin beta
LTB4 leukotriene b4
LTC4 leukotriene c4
LTi lymphoid tissue inducer
M2 alternatively activated macrophages
MBP1 major basic protein 1
MFI mean fluorescence intensity
MHCII major histocompatibility complex II
Mmp- metalloprotease
MRI magnetic resonance imaging
MYD88 myeloid differentiation primary response 88
Myh myosin heavy chain
Myom1 myomesin 1
Mytl1 myelin transcription factor 1 like
Ncan neurocan
Nell- neural egfl like 1
Ngf nerve growth factor
Nrtn neurturin
Oprd1 opioid receptor delta 1
Oxtr oxytocin receptor
P2X purinoreceptor
P4ha3 prolyl 4-hydroxylase-subunit alpha 3
Pdk4 pyruvate dehydrogenase kinase 4
Pex11a peroxisomal biogenesis factor 11 a
PGP9.5 protein gene product 9.5
PMD piece-meal degranulation
PPAR-α peroxisome-proliferator activated receptor alpha
PRR pattern-recognition receptor
Roryt rar-related orphan receptor gamma
SCFA Short chain fatty acids
SI small intestine
Slc25a20 solute carrier family 25 member 20
SPF specific-pathogen free
ST2/il1rl1 il-1 receptor like 1
TCR- t-cell receptor
TEM transmission electron microscopy
TGF- transforming growth factor
Tnbx tenascin-x
Tnf- tumor-necrosis factor
Vcan versican
VEGFR2 vascular endothelial growth factor 2
VIP vasoactive peptide
α-SMA alpha smooth muscle actin

TABLE OF CONTENTS

LIST OF FIGURES

CHAPTER 1 - INTRODUCTION

CHAPTER 2 -RESULTS

CHAPTER 3 - RESULTS

CHAPTER 4 - RESULTS

CHAPTER 5 - RESULTS

CHAPTER 6 - RESULTS

CHAPTER 7 – MATERIALS AND METHODS / SUPPLEMENTARY FIGURES

CHAPTER 7 – MATERIALS AND METHODS / SUPPLEMENTARY TABLES

ACKNOWLEDGMENT OF CONTRIBUTORS TO THESIS CONTENT

Fig. 2,3: complete figures obtained from Nature Immunology Reviews – *with permission*
Fig. 5B: EM image obtained from J. Bernier-Latmani (Petrova lab)
Fig. 6: Wholemount sample acquired from (Petrova lab; UNIL)
Fig. 9: Complete data (Experimental planning/procedure/analysis) acquired from KD McCoy lab (U Calgary)
Fig. 10: Staining was conducted by the Histology facility at the EPFL
Fig. 11A: Staining was conducted by the Histology facility at the EPFL
Fig. 11B, C: Staining and quantifications completed by J. Bernier-Latmani (Petrova lab; UNIL)
Fig. 12A, B: Staining was conducted by the Histology facility at the EPFL
Fig. 13: Complete data (Experimental planning/procedure/analysis) acquired from KD McCoy lab (U Calgary)
Fig. 14: Quantifications completed by J. Bernier-Latmani (Petrova lab; UNIL)
Fig. 23: Complete data (Experimental planning/procedure/analysis) acquired from J. Bernier-Latmani (Petrova lab; UNIL)
Fig. 24: J. Bernier-Latmani (Petrova lab; UNIL) helped in the analysis using Angiotool
Fig. 30: Complete data (Experimental planning/procedure/analysis) acquired from J. Bernier-Latmani (Petrova lab; UNIL)
Fig. 31: Representative images taken by J. Bernier-Latmani (Petrova lab; UNIL)
Fig. 34: Complete data (Experimental planning/procedure/analysis) acquired from J. Bernier-Latmani – (Petrova lab; UNIL)
Fig. 47, 49: B. Wenger – Gachon Lab (NRI) sourced the mice and setup the restricted feeding regime

Dr. J. Bernier-Latmani -Petrova lab(UNIL) made the initial observation of villous defects in dbl.GATA1 mice, established the wholemount protocol in our lab, and provided technical support. He also conducted all the cardiac perfusions and dissection for most wholemount experiments. In addition, he established the triglyceride analysis experiment in the lab, and led the pilot experiment.

Dr. M. Moyat (Harris lab; EPFL) provided ample assistance for large harvests involving flowcytometry, and technical support for various experiments in chapter 6.

Dr. T. Bouchery (Harris lab; EPFL), N. Katanyeva (Oricchio lab; EPFL) provided technical assistance for the chimera experiments by performing all I.V injections. They also provided technical support on the maintenance of the chimeric mice.

Prof. KD McCoy established all the germ-free strains during her tenure at U Bern

All electron microscopy experiments were conducted in collaboration with the EM facility at EPFL – headed by Dr. G. Knott

All RNA-seq experiments were conducted in collaboration with the GCEF facility at the EPFL – headed by Dr. B. Mangeat

All RNA-seq analysis (i.e. processing of raw sequencing files, statistical analysis) – Dr. N. Wong (Monash U)

The author (K. Shah) is otherwise responsible for the quality of content (i.e. planning, experimental, data interpretation) presented herein

Chapter 1: Introduction

1.1 THE SMALL INTESTINE

The small intestine is the largest organ (per area) in the body – and is a focal point for host interactions with the external environment. Its immense complexity and dynamic nature is reflective of the diverse functions it serves for the maintenance of total organismal homeostasis[1,2].

In principle, the main function of the small intestine is nutrient absorption, with outcomes in this tissue influencing both local and systemic processes. The small intestine is also home to the largest number of immune cells in the body - anatomically and functionally compartmentalized to prevent pathogen infiltration, while simultaneously facilitating controlled, mutualistic interaction between the host and commensal microbiota residing in the intestinal lumen. Each intestinal region and compartment are distinct in terms of cellular composition and function.

Furthermore, it is also a highly mechanical organ – with coordinated, contractile movements necessary to support intestinal functions such as nutrient absorption, immune defense and regeneration[3,4].

1.1.1 Regional specialization of the small intestine

The small intestine is densely covered with villi, increasing surface area for optimal nutrient absorption. They vary in size from the proximal (largest) to the distal (shorted) end of the intestine **(Figure 1A)**. This seems to be, for the most part, a developmentally regulated process, as discrepancies in villous size between regions are already dictated pre-natally[5] – independent of environmental signals (*i.e.* microbiota, diet). In general, villous and small intestine development follows a wave-like temporal pattern, with the proximal structures forming first[6]. The entire small intestinal tissue can be subdivided into 3 morphologically distinct regions - Duodenum, Jejunum and Ileum **(Figure 1A, B)**.

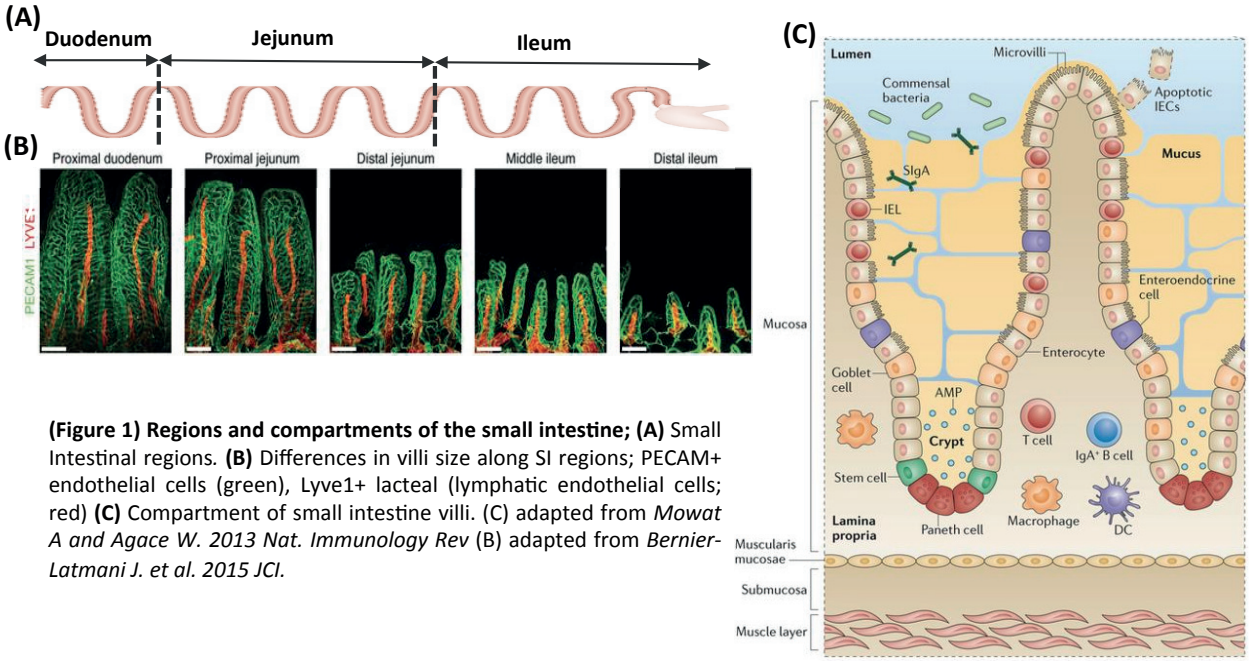

(Figure 1) Regions and compartments of the small intestine; (A) Small Intestinal regions. **(B)** Differences in villi size along SI regions; PECAM+ endothelial cells (green), Lyve1+ lacteal (lymphatic endothelial cells; red) **(C)** Compartment of small intestine villi. (C) adapted from *Mowat A and Agace W. 2013 Nat. Immunology Rev* (B) adapted from *Bernier-Latmani J. et al. 2015 JCI.*

The Duodenum, the most proximal, is a region corresponding directly after the pyloric sphincter and terminates at the duodenal-jejunal junction (demarcated by the ligament of trietz). It is the shortest (in length) of all 3 regions, but harbours the largest villi - the most vascular in the small intestine[7,8]. Its primary function is to process partially digested food (*i.e.* chyme) coming in from the stomach - mediating its complete, chemical digestion through provision of various enzymes and molecules (*e.g.* lipases, bile salts) supplied by the pancreas, liver and gallbladder. Peristaltic activity from the muscularis layer, facilitate mixing of these secretions with the chyme – ensuring optimal liberation/digestion of dietary products for absorption as it passes down the gastrointestinal tract. In addition to this function, the duodenum (along with the proximal jejunum) is the primary site for the absorption of dietary lipids.

Following the duodenum is the jejunum, accounting for 40% of the small intestine following the duodenal-jejunal junction. It has a primary role in the absorption of all nutrients. This is reflected by its large to moderately sized villi, along with a thick muscularis layer - in comparison to the ileum - required for managing great mechanical strain and facilitating strong peristaltic movement in response to the incoming bolus/chyme[9,10]. Similarly to the duodenum, jejunal villi are also extensively vascularized.

The ileum, accounts for the distal 60% following the duodenal-jejunal flexture. While there are no morphological markers to adequate distinguish this region, the villi here are significantly shorter in comparison to the other regions. The primary function of the ileum is to resorb bile salts/acids from the lumen for recirculation into the liver, along with other nutrients that were not absorbed in the proximal regions[8].

1.1.2 Structural compartmentalization of small intestinal mucosa

Each small intestinal (SI) compartment can be further divided into 4 distinct layers, with the majority of intestinal processes taking place in the mucosa (*i.e.* epithelium, lamina propria), submucosa and muscularis. While each compartment has distinct contributions, they collectively address the diverse functional requirements of the intestine **(Figure 1C)**.

Epithelial barrier

The small intestinal epithelial barrier is a physicochemical barrier that facilitates absorption of nutrients while serving as a primary interface for host-microbiota interactions. In total there are 5 functionally distinct epithelial cell subsets[1]. Enterocytes are the predominant subtype and is important for nutrient absorption and sensing. Goblet cells are responsible for generating the mucus layer – critical for the physical separation, and reinforcement of the epithelial layer against microorganisms and other luminal contents. Mucus density follows a gradient of increasing density from the proximal to the distal SI, correlating with increasing microbiota density. Paneth cells secrete antimicrobial peptides, which are released into the mucus layer. Enteroendocrine cells produce gastrointestinal peptides and hormones that are important for various metabolic processes. Lastly, Tuft cells – recently discovered, as a district population of intestinal epithelial cells (IEC), are critical in the initiation of anti-helminth responses through its provision of epithelial-derived alarmin IL-25[11,12].

Intertwined within the epithelial barrier resides a small, but significant population of intraepithelial lymphocytes (IELs). CD8αα+ (TCRαβ, TCRγδ) t-cells comprise the majority of this pool. They are termed 'natural' – in that their differentiation and recruitment are developmentally determined[13]. In contrast, CD4+ TCRαβ and CD8αβ+ TCRαβ t-cells are induced in response to luminal signals, particular the microbiota – and gradually increase in frequency with age[13,14]. Despite these differences, most IELs rely on similar survival signals (e.g. IL-15, IL-7, CCL25) acquired

from epithelial cells, and mononuclear phagocytes[1,13,15,16]. In turn, IELs support the epithelial barrier – not only through their immune-surveillance activities, but also by aiding in reparative responses.

The epithelial barrier is replenished every 4-5 days with cells sourced and differentiated from the intestinal crypts in the submucosa, where the epithelial stem cell niche is located[1]. Under homeostatic conditions, luminal signals from the microbiota influence this process, as exhibited by decreased epithelial turnover rate in germ-free/axenic animals[17]. Accelerated epithelial turnover of the epithelium, is thought to be an adaptive mechanism by the host to maintain optimal epithelial fitness in response to microbial-induced damage. The turnover rate is further accelerated in response to tissue-injury/infection[18–21]. The maintenance of epithelial barrier integrity and function is pivotal not only to local tissue homeostasis, but also overall metabolic health. Disruption of this layer results in the maladaptive activation of underlying immune cells within the lamina propria – leading to significant pathophysiology.

Sitting between the epithelium and the lamina propria is a thin network of sub-epithelial fibroblasts, which provides a critical source of factors regulating epithelial cell activation and survival. Together with IECs, they are a major source of extracellular matrix in this layer, collectively forming the basal lamina - providing both structural support, and function as a scaffold for mucosal derived factors influencing epithelial barrier function and maintenance[2].

Lamina propria and Submucosa

The lamina propria has the highest cellular heterogeneity out of all intestinal layers and is a focal area for various intestinal processes. It consists of loosely packed connective tissue, interspersed with various stromal and immune cells – collectively forming the villous scaffold.

Immune cells

Various innate and adaptive immune cells reside in the lamina propria (LP) under homeostatic conditions. However, their relative proportions vary within a given intestinal region, and are highly influenced by the presence of exogenous signals (*e.g.* microbiota composition, diet). These cells are involved in the maintenance of epithelial barrier integrity, tolerance to commensal microbiota and innocuous antigens, and protection against pathogens[2]. During homeostasis, the innate

immune compartment of the LP consists of various antigen-presenting cells (*e.g.* dendritic cells (DCs), macrophages), innate lymphoid cells (*e.g.* ILC3, ILC2) and granulocytes (*e.g.* eosinophils, mast cells). The adaptive immune compartment of the LP consists primarily of CD4+ T helper (Th) cell subsets (*i.e.* Th2, Th17, T-regulatory cells), CD8 t-cells and IgA-secreting plasma cells. In addition to being an effector site, the LP serves as an activation site for dendritic cells (DC) that migrate to the gut-associated lymphoid structures (*e.g.* Peyer's patches, mesenteric lymph node) to prime adaptive immune responses[1].

Stromal cells

An extensive network of stromal cells, which extend into the submucosa, support the Immune cells within the lamina propria, and serve as a rich source of molecules that regulate immune cell activation and survival. These stromal-derived factors also impact on other stromal cells, and on the overlying epithelium, regulating its architecture/organization, development and maintenance[24–26]. The major stromal cell subsets in the LP include: 1) blood endothelial cells (BECs; GP38- CD31+) which form the tissue vasculature, 2) lymphatic endothelial cells (LECs; GP38+ CD31+), which form the lymphatic vasculature and lacteals, 3) fibroblasts (GP38+ CD31-) which represent a heterogeneous population comprising of cells such as, myofibroblasts and fibroblastic reticular cells, 4) double-negative cells (GP38- CD31-) which are also a heterogeneous population comprised of neurons, glial cells and rare stromal cells. Small intestinal stromal cells (particularly myofibroblasts) also participate in wound reparative responses, and in the maintenance of the intestinal stem cell niche[24,26].

Furthermore, stromal cells also participate in nutritional absorptive processes. For example, lacteals are formed from conduits of LECs important for lipid transport into the central lymphatics/circulation, in a process aided by the contractile activity of myofibroblasts[27].

Extracellular matrix

The extracellular matrix (ECM; otherwise called 'interstitium') is a mesh-like network of molecules, fundamental to both the form and function of the intestine. There is a multitude of molecules that comprise the ECM, and its composition is highly dependent on the ongoing processes within a given tissue[28–30].

The ECM primarily consists of elastic fibers (generating tissue elasticity/compliance), collagen fibrils (generating tissue stiffness/strength), plus glycosaminoglycans (GAGs) and other related proteoglycans (generating compressive stiffness/strength). The proportions of the various ECM constituents within a given tissue collectively define the tissues mechanical properties. The ECM also functions as a reservoir for molecules (*e.g.* cytokines, growth factors, chemokines) secreted by cells located within the tissue. ECM binding to such factors can regulate their bioavailability[31–34]. In addition, the ECM can also directly influence the activation of cells via integrins expressed on the cell's surface[30,35,36].

Cells within the intestine establish the extracellular matrix (ECM) during development. However, throughout life, bi-directional crosstalk between immune and stromal cells (a primary source of ECM substrates) facilitates its maintenance in addition to remodelling events that allow the tissue to adapt to environmental changes and/or undergo repair in response to disease and injury[24,37]. In healthy tissues, changes in the mechanical properties of the ECM during reparative responses can alter cellular activation, which then leads to a feedback response from the cell to deposit matrix substrates/remodelling enzymes to revert the physical properties of the matrix back to its 'pre-stress state'[30]. However, dysregulation of these complementary homeostatic processes could lead to fibrosis, mechanical/structural failure or other pathologies.

Muscularis externa

The muscularis externa (muscle layer) is primarily comprised of 2 layers of densely bundled smooth muscle layers (*i.e.* circular, longditudinal). Intercalated in the muscles of both layers is the muscularis propria – a highly innervated connective tissue, containing the myenteric plexus (complex network of neurons and glial cells) responsible for the coordination of contractile activity in the circular/longdituinal muscle, that are critical for peristaltic activity. The myenteric plexus connects both submucosal plexus and neurons/glia from the LP – suggesting that the enteric nervous system collectively integrate signals from the lumen to the muscularis to influence a wide variety of intestinal processes[38].

In comparison to the other layers, immune cells in the muscularis are sparse, and mostly consist of muscularis macrophages and mast cells – which can interact with neurons in a bi-directional manner. Under homeostatic conditions, these interactions fine-tune peristaltic processes.

However, they may also participate in tissue-protective processes (*i.e.* immune defense, tissue repair) under pathophysiological conditions[39,40].

1.1.3 Role of the microbiota in shaping the intestinal microenvironment

The intestinal mucosa is colonized by the largest and most distinct repertoire of microbial communities in the body[41]. Microbiota colonization results in significant changes in intestinal function and homeostasis from birth, and throughout the course of life. They are important for directing the maturation of the intestine, not only through their stimulation and regulation of immune cell populations – but also by initiating the development of lymphoid structures that facilitate and sustain local immune responses. The microbiota also has critical implications for physiological outcomes of key intestinal functions such as nutrient absorption and barrier integrity[2,42–44].

The composition and activation of immune cells within a given tissue are highly dependent on the microbiota. These microorganisms function as a unit, critical for setting the immunological tone of the tissue microenvironment[45]. Indeed, this is best illustrated through studies using axenic/germ-free mice – which are devoid of all microorganisms[46]. These mice present with reduced numbers of immune cell populations in the intestine, and have compromised immune function. The microbiota regulates immune cell homeostasis through direct, and indirect mechanisms. For example, it can trigger immune responses directly via release of bacterial-derived molecules (priming DCs to trigger T-helper cell differentiation), or indirectly through regulating the production of metabolites such as short-chain fatty acids (SCFA, a by-product of microbiota fermentation of dietary fibres) that influence the activation and maintenance of immune, epithelial and stromal cell populations[42,47].

As mentioned above the microbiota also plays a critical role in the development of lymphoid structures – particularly isolated lymphoid follicles (ILFs), which develop from cryptopatches in the small intestine in response to microbial colonization[48]. This process requires association with LTbr+ stromal cells and RORyt+ LTi ILC3s in the presence of microbial-derived signals – and mediates the recruitment of DCs and naive B-cells. Under conditions of epithelial barrier breach, stromal cells themselves can be activated by the microbiota – contributing to both effector responses through provision of inflammatory molecules, and tissue repair[26,49,50].

There is growing evidence that differences in microbiota composition and diet can shape the immunological microenvironment of the intestinal tissue and thus impact on the outcome of immune cell-microbial interactions within the host. Therefore, in disorders such as IBD that are associated with microbial dysbiosis, this crosstalk can become detrimental, resulting in chronic inflammation and extensive tissue remodelling[51,52].

In addition to the ability of the microbiota to shape host immunity and tissue architecture – it also has a key impact on the mechanical homeostasis of the intestine. Germ-free mice are known to exhibit significant intestinal dysmotility causing slowed intestinal transit, and recent work has shed light on this phenomenon[39,53]. Studies have shown that the microbiota is critical for the activation of muscularis macrophages, which in colonized mice – express BMP2 which signals to enteric neurons, thereby regulating the peristaltic activity of the muscularis. Furthermore, the microbiota has also been shown to be important for the maturation of enteric glia[54]. This also has implications for peristalsis, as the pattern and frequency of contractions is mediated by glial-neuron circuitry.

1.2 THE EOSINOPHIL

The small intestine is home to the largest pool of eosinophils in the body under homeostatic conditions[55,56]. Nonetheless, the significance of their residency remains enigmatic.

Eosinophils are granulocytic cells, capable of producing a wide array of molecules **(Figure 2)** stored pre-formed in various granules and lipid bodies throughout their cytoplasm[57,58,59]. While this renders eosinophils with vast potential to influence a wide variety of processes, most studies of eosinophils have traditionally focused on its purported role in anti-helminthic responses – where eosinophilia is a hallmark phenotype[60]. Furthermore, eosinophils have also been implicated in driving pathophysiological processes in various type II immune disorders (*e.g.* asthma, allergy), thought to be an adverse consequence of a dysregulated and misdirected anti-helminth response[57,58,61–63]. However, this fatalistic view of eosinophil effector function has been challenged, based on the fact that these cells have been shown to participate in processes that transcend type-II immunity, along with their accumulation in sites of injury/repair, and presence in healthy tissues under homeostatic conditions[57,64–67].

In addition to its commonly cited role in tissue damage in various disorders, eosinophils also participate in ongoing processes through immune regulation and tissue remodelling, which has important implications on shaping the tissue microenvironment[68,69]. What is intriguing about these cells, is that mechanisms that drive eosinophil function as a 'tissue destructive cell' has also been implicated in being important for its tissue protective function. Therefore, it is of particular interest to decipher and understand the factors that regulate eosinophil function in both health and disease.

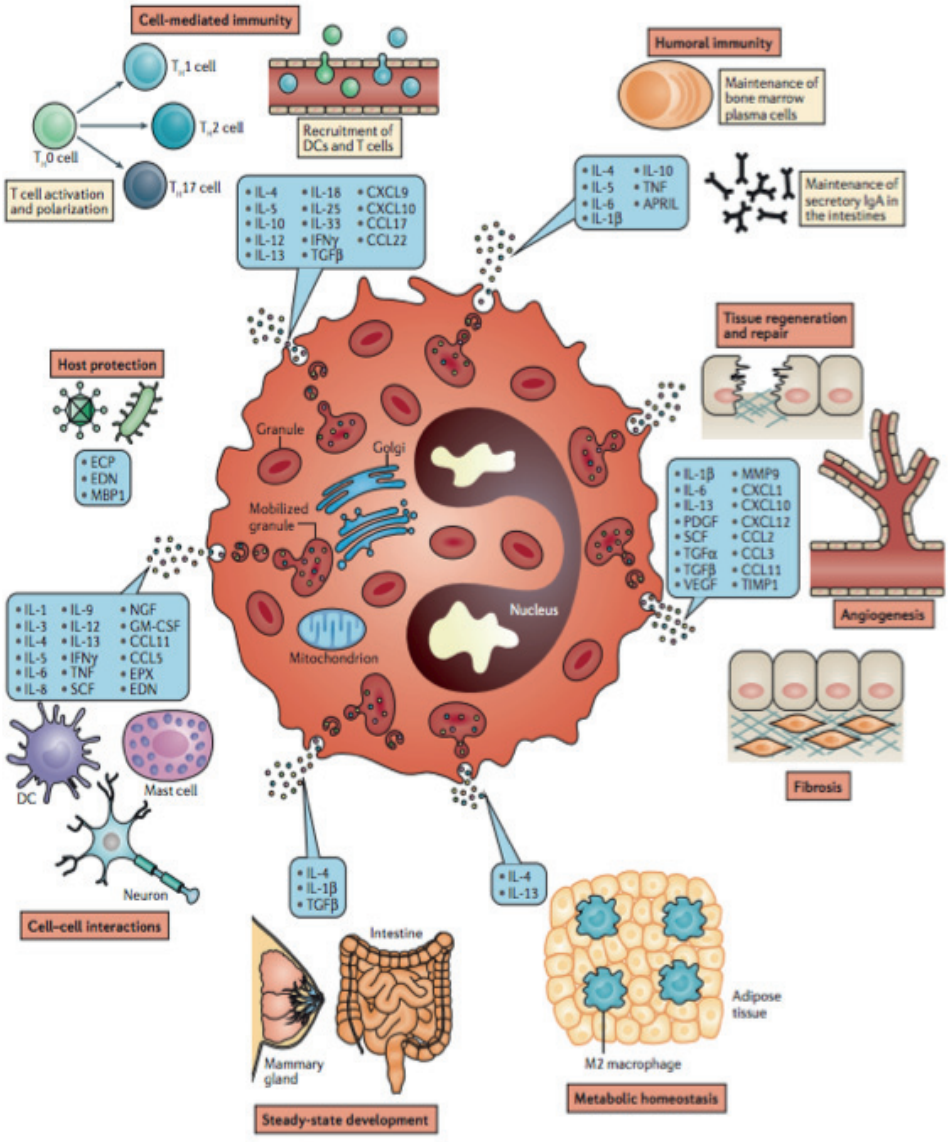

(Figure 2) Eosinophil-derived molecules and their functions: CC-chemokine ligand (CCL); CXC- chemokine ligand (CXCL); dendritic cell (DC); eosinophil cationic protein (ECP); eosinophil derived neurotoxin (EDN); eosinophil derived peroxidase (EPX); granulocyte-macrophage colony stimulating factor (GM-CSF); interferon-γ (IFN-γ); Major Basic Protein 1 (MBP1); matrix metalloprotease 9 (MMP); nerve growth factor (NGF); platelet-derived growth factor (PDGF); stem cell factor (SCF); transforming growth factor (TGF); tissue inhibitor of metalloproteases 1 (TIMP1); tumor necrosis factor (TNF); vascular endothelial cell growth factor (VEGF). Figure adapted from Weller and Spencer, 2017 Nature Immunology reviews *(with permission).*

1.2.1 Identification and ultra-structural characterization of eosinophils

Eosinophils are highly granular cells that can be easily observed using conventional light microscopy[70]. Mature eosinophils posses a multi-lobbed nucleus, whereas immature eosinophils present with a 'doughnut shaped' nucleus. Due to the acidic properties of their cytoplasmic granules, acidophilic histological dyes such as Eosin give eosinophils a 'pink-like' appearance. However, unlike other granulocytes such as Mast cells, light microscopy is not sufficient to distinguish fully intact (*i.e.* non-degranulated) from spent/degranulated eosinophils.

By flowcytometry, eosinophils can be identified as SSC^{hi} cells that express surface markers Siglec-f, F4/80 and CCR3. Siglec-f is the most dependable marker for distinguishing eosinophils – as eosinophil expression of other markers such as F4/80, CCR3, tend to vary in a tissue-specific manner[71–73]. Furthermore, Siglec-f is primarily expressed by eosinophils, whereas cells such as macrophages and Th2 cells ubiquitously express F4/80 and CCR3, respectively. Other cell types constitutively expressing Siglec-f are rare, with expression limited to alveolar macrophages (low expression), and Tuft cells (in the intestine), in addition to eosinophils[12,74]. A limitation of flowcytometric analysis of eosinophils is the lack of reliable markers that can distinguish differences in eosinophil activation states – particularly with regards to degranulation. For example, surface expression of lysosome protein CD63/LAMP-3 (also expressed in the granule membrane) is often used as a marker of eosinophil degranulation but can only be sufficiently detected in highly degranulated cells[75]. In order words, it may not be able to detect subtle changes in eosinophil degranulation/activation.

Currently, Electron microscopy (particularly transmission election microscopy; TEM) is the golden standard used in the field to distinguish morphological changes in eosinophil activity[70,76,77]. Mature eosinophils are a rich source of various molecules, which they store, pre-formed, in various granules and lipid bodies scattered throughout their cytoplasm **(Figure 3)**. Eosinophil granules are unique compared to other granulocytic cells, due to their distinct morphology. These granules can be observed to have a spheroid-circle like shape, with a central crystalline core. The space surrounding this core is called the 'outer matrix' where chemokines, cytokines and granule-derived proteins (*e.g.* EDN, EPX, ECP) are stored. Numerous pre-formed cytokines, chemokines and growth factors are also stored within these granules[57,70]. The crystalline core is primarily made up of MBP-1 aggregates, which collectively form a dense, cylinder-like structure **(Figure 3A)**.

In addition to granules, lipid bodies are also stored throughout the cytoplasm of eosinophils. These dense, circular structures contain pre-formed stores of various lipid mediators such as various eicosanoids, leukotrienes and other arachidonyl phospholipids[70,78,79]. Lipid bodies also serve as a storage site for substrates and enzymes required for the *de novo* synthesis/modification of these factors. Additionally, some factors such as TNF-α and Fibroblast growth factors are also known to be stored in lipid bodies.

Modes of Eosinophils degranulation

Eosinophil release of factors can occur in three distinct ways: Piece-meal degranulation (PMD), cytolysis or classical-exocytosis **(Figure 3C)**.

PMD, the most commonly occurring mode, is described as any condition in which eosinophils progressively secrete granule contents while the cell stays relatively intact. Given the large repertoire of factors eosinophils are able to secrete, PMD allows for differential release of molecules, depending on the type of stimuli – and requires a complex process of protein sorting and export (*via* vesiculotubular structures in the cytoplasm) to the extracellular space[76,77]. On this note, the extent of PMD is dependent on the intensity and concentration of the stimulant(s). It is estimated that in resting cells (under steady state), 70% of eosinophils had fewer than 10% of their granules undergoing PMD – whereas, upon stimulation with CCL11, granules become considerably emptied with a significant number of eosinophils exhibiting more than 90% of their granules undergoing PMD[70]. Hallmarks of ongoing PMD are granules that have disorder in their core and/or surrounding matrix. This is accompanied by formation of vesiculotubular structures, which morphologically, are hollow vesicles, scattered throughout the cytoplasm (either in 'sombrero-shape' or tubular)**(Figure 3C)**.

Sorting and vesicular transport of eosinophil granule-derived factors is best described for cytokine, IL-4 **(Figure 3C)**[80]. Using a combination of immune-blotting and Immuno-gold EM studies, pre-formed IL4r-α was found in the granules of eosinophils, and that upon stimulation with CCL11, it was mobilized into the intragranular compartment as a means to sequester pre-formed IL-4 stored in the granule matrix. This coincides with an upregulation of IL4r-α as well, perhaps as an effort of the cell to replenish pre-formed stores. IL4r-α from the granules (bound to IL-4; tracked by immune-gold labelling for IL4r-α) is then budded off the granules – enclosed by vesiculotubular

structures, which form on the granule periphery **(Figure 3C)**. The cytoplasm also reveals a significant number of cytoplasmic vesiculotubular structures positive for IL4r-α, suggesting that this phenomenon is a mechanism with which eosinophils are able to differentially sort and release specific molecules based on the stimuli.

Compound exocytosis, is a more drastic form of degranulation and is a form of degranulation utilized by other granulocytes – basophils, mast cells - upon crosslinking of their Fc Epsilon receptors[59,81]. This mode of degranulation is described as the release of entire granule contents, into the extracellular space upon fusion with the plasma membrane **(Figure 3B)**. Eosinophils have also been shown to utilize this mode of degranulation, but only in upon contact with helminthic parasites *in vitro*. It has yet to be observed *in vivo*. Finally, cytolysis – another degranulation mode – is associated with the loss of membrane integrity and subsequent release and deposition of intact, cell-free membrane bound granules **(Figure 3D)**. Cell-free granules have been observed in tissues biopsies from patients with severe allergic disorder (*e.g.* atopic dermatitis, nasal polyps), and eosinophil-mediated disorders such Eosinophilic esophagitis (EoE)[82].

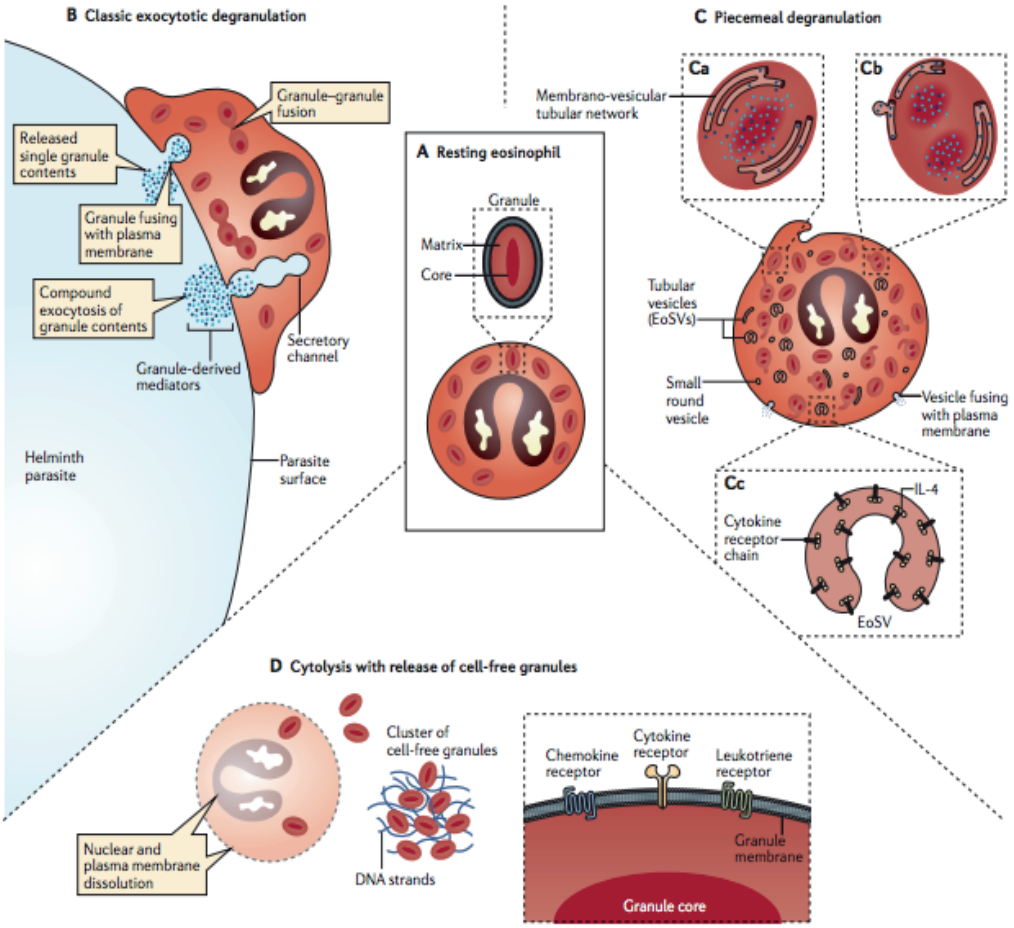

(Figure 3) Modes of eosinophil degranulation: A) Resting eosinophils have a well-defined crystalline core, surrounded by a relatively translucent matrix **B)** *Classical exocytotic degranulation* - intracellular granules fuse with the plasma membrane, creating a secretory pore through which the entire granule contents are released. **C)** Piecemeal degranulation (PMD) – differential release of granule-derived proteins via transport by vesiculotubular structures which traverse the cytoplasm and fuse with the plasma membrane to release their granule-derived cargo. PMD exhibit varying degrees of ultrastructural alteration, including an apparent reorganization of electron-dense contents and the appearance of a membranous network of tubules within granules. **D)** *Cytolytic degranulation* – requires cytolytic death of eosinophil, characterized by dissolution of the nuclear and plasma membranes, extrusion of DNA nets and expulsion of intact granules as clusters of cell-free extracellular granules within tissues. A portion of cell-free, extracellularly deposited eosinophil granules retain an intact outer membrane, express functional receptors and remain competent to undergo stimulus-dependent secretion within tissues. Figure adapted from Weller and Spencer, 2017 Nature Immunology reviews *(with permission).*

1.2.2 Factors that regulate eosinophil development and survival

Eosinophils represent less than 5% of total circulating leukocytes under homeostatic conditions. In the bone marrow, they are generated from GATA1+ common granulocyte-monocyte precursor (GMP), which also give rise to basophils and mast cells[70]. Their differentiation program is distinguished from other granulocytes, due to the high expression of the transcription factor GATA1+ required for their development. They are released from the bone marrow and into the peripheral circulation as mature, terminally differentiated cells with a half-life of around ~18h. Eosinophil survival is often prolonged upon their migration to peripheral tissues – suggesting that this process is highly dependent on tissue-trophic cues. Their migration and extravasation into tissues is dependent on the receptor CCR3, which has a high affinity for chemotactic factor CCL11/eotaxin-1. However, CCR3 can also recognize other eotaxins (*e.g.* CCL24/eotaxin-2). The primary sources of eotaxins are stromal in origin (*e.g.* fibroblasts/smooth muscle cells, endothelial cells), but can also be produced by epithelial cells[55,83–85].

IL-5 is a canonical, eosinophil-specific factor, which plays a central role in various aspects of eosinophil activation and survival in different tissues[70,86,87]. Furthermore, IL-5 can promote the expansion of eosinophil-progenitors in the bone marrow. IL-5 is known to prime eosinophils, lowering their threshold for degranulation in response to CCL11. Genetic deletion and antibody blockade of either CCL11, and IL-5 results in significant decrease of eosinophils in all peripheral sites[59,70]. However, it does not result in total ablation – suggesting that other factors may be influencing this process.

Similarly to IL-5, other type-II immune cytokines such as IL-4 and IL-13 can also promote eosinophil activation. Although these factors are signature products of Th2 cells, innate immune cells are also potential sources. For example, granulocytes such as Mast cells and basophils are noted to release IL-4/13 and IL-5 – promoting eosinophilia in various allergy models[59,88–90]. However, the contributions of Innate lymphoid cell (ILC2s) in sourcing these factors – particularly IL-5 – is arguably the most significant, as they not only produce these factors under type II inflammatory conditions, but are also a steady source in various tissues where eosinophils are noted to reside under homeostatic conditions[91–93].

Apart from cytokines, various receptors expressed by eosinophils on their surface can also regulate their activation and survival[94–96]. Siglec-f is expressed on the surface of eosinophils, which mediates eosinophil apoptosis upon cross-linkage or ligand binding to other sialylated/sulphated glycans. Surface expression of Siglec-f correlates with eosinophil activity, and is noted to be an important negative feedback mechanism limiting eosinophilia under inflammatory conditions. SIRP1α/CD172a also plays a critical role in limiting eosinophil-mediated effector responses[97]. Crosslinking of eosinophil surface-bound CD172a inhibits their degranulation and promotes survival.

Eosinophils can also regulate their own survival and activation through release of autocrine-signals. For example, upon contact with extracellular matrix protein fibronectin via VLA-4 mediated adhesion, eosinophil survival is prolonged through autocrine release of GM-CSF and IL-3[98,99]. Autocrine production of IL-5 can also be induced in response to stimulation of eosinophils by antibody immune complexes (*i.e.* IgA, IgG)[100,101]. IL-5, GM-CSF and IL-3 are known eosinopoetins and can function synergistically to sustain eosinophil activation and survival in peripheral tissues, and support eosinophil development in the bone marrow[58,102].

Eosinophil regulation by epithelial derived alarmins

The epithelial-derived alarmin IL-33, is also an important regulator of eosinophil homeostasis[88,103,104,105]. The IL-33 receptor ST2 is expressed on the surface of eosinophils both at steady state, and under inflammatory conditions. Eosinophilia is a major hallmark phenotype of in *vivo* IL-33 administration - which regulates eosinophil activation and expansion both directly (*via* ST2-signalling on eosinophils) and indirectly (*via* ILC2s)[106,107,92,108]. For example, transfer of ST2ko eosinophils into recipient mice, subjected to allergen challenge resulted in decreased eosinophil numbers in the lung – despite normal migratory capacity[109]. This suggests that *in vivo*, tissue derived IL-33 can act directly on eosinophils to sustain their survival. In addition, IL-33 also functions as a potent activator of eosinophil function. While IL-33 does not induce eosinophil degranulation, a study by Bouffi et *al.* (2013) has shown that IL-33 stimulation of eosinophils resulted in the alteration of over 500 genes – resulting in the upregulation of various factors such as IL-6, IL-13, CCL17 and TGF-β[88]. In addition, IL-33 stimulation of eosinophils results in autocrine production of IL-4, which synergizes with ongoing IL-33 signalling to regulate the eosinophil transcriptome through an NFkB-dependent mechanism. However while the IL-4 autocrine-loop

seemed to amplify IL-33 mediated activation of eosinophils, it did not account for all noted alterations, as upregulation of genes such as IL-6, IL-13 seemed to be independent of this process. Eosinophil-mediated disorders such as asthma, EoE and IBD – are known to have significant input from IL-33 signalling[110–112]. However, it is unclear whether dysregulation of IL-33 (and consequently – responsive cells such as eosinophils) is involved in the initiation of the inflammatory response, or, is rather involved in its propagation.

IL-33 can also impact on eosinophil function through indirect mechanisms. IL-33 is known to be a potent activator of ILC2s – promoting their expansion and cytokine production in tissues. ILC2s are lineage-negative, GATA3+ cells that are a major source of IL-13, IL-5 and amphiregulin in the early phase of type II inflammatory responses (*e.g.* helminth infection, asthma, allergy)[93]. ILC2 effector function in inflammation is achieved primarily through its regulation of eosinophils (*via* IL-5) and goblet cell hyperplasia/mucus secretion (*via* IL-13). However, they are also a source of these Type-II cytokines in certain tissues (*e.g.* adipose, intestine) under homeostatic conditions[92,113]. IL-33 can also influence eosinophils indirectly, by inducing CCL11 production in fibroblasts resulting in eosinophil recruitment[114,115].

Another epithelial-derived cytokine capable of regulating eosinophil function is IL-25, which signals through IL17RB[93,116,117]. Similar to IL-33, IL-25 can also induce expansion of ILC2s and stimulate their production of IL-5/13 – highlighting a degree of redundancy in terms of their function. However, unlike IL-33 receptor ST2, it is still unclear whether or not eosinophils truly express the IL17RB receptor under homeostatic conditions. Eosinophil upregulation of surface IL17RB has been observed in a few studies, but always in the context of inflammatory responses (*e.g.* allergic asthma)[118]. Interestingly, eosinophils themselves can also be a source of IL-25 – thus amplifying ongoing type II immune response through further activation of ILC2s – sustaining eosinophil survival and activation in inflamed tissue.

1.2.3 Effector functions of eosinophils under homeostatic conditions

Helminth infection

The dogmatic view of eosinophil function is that they evolved exclusively as part of an early innate immune response against parasitic helminths[60,119,120]. This is largely due to eosinophilia, being a dominant hallmark of helminth infections – in addition to early studies showing helminth-killing activities of eosinophils through compound exocytosis – upon contact with helminths *in-vitro*[121,122,123]. Intriguingly, the generation of eosinophil-deficient mouse strains over the past couple of decades have put this dogma into question – showing that eosinophil-effector function against parasites *in vivo* is largely nominal, or at least redundant, and that it may be limited to a subset of helminth species (*e.g.* filarial nematodes)[60]. It is important to note however, that helminth interact with their host in species-specific manner, shaped by millennia of co-evolution. In this regard, while there are more similarities than are differences between human and mouse eosinophils, an anti-parasitic role for eosinophils in humans has yet to be ruled out, which could be attributable to species-specific functions of this cell[60,124].

In contrast to the dogmatic view of evolutionary selection for the eosinophil lineage solely for participation in anti-helminthic responses, a few studies have even shown a peculiarity in which eosinophils may actually prove beneficial for helminths – aiding in their survival in the host[125,126]. Eosinophils confer benefit to the parasite through altering the metabolic environment surrounding the larvae – to one conducive to larval growth.

Asthma

Eosinophilia is a hallmark of asthma; in addition to airway hyperactivity, and mucus production and tissue remodelling (*e.g.* smooth muscle expansion, ECM deposition)[127,128]. In this regard, tissue remodelling is defined as an imbalance between tissue regeneration and repair mechanisms – which under chronic inflammatory conditions leads to fibrosis.

Eosinophils have capacity to produce various pro-fibrotic mediators (*e.g.* TGF-β, MBP, EPO, IL-6) suggested to drive pathophysiology in asthma[62,127]. As a result, limiting eosinophilia has been the target of many anti-asthma therapies, but conflicting data in this field suggests that its role in driving disease pathology is unclear. For example, in various human clinical trials and mouse studies wherein eosinophils were depleted – loss/reduction of eosinophils did not necessarily

confer any protective effect in asthma exacerbations suggesting that eosinophilia is not a sole driver of pathophysiology in this disease[129]. The only thing that can be agreed upon is that eosinophils are driving changes in tissue remodelling in the lung in response to challenge[130,131].

Inflammatory bowel disease (IBD)

IBD is characterized by a maladaptive immune response directed towards luminal microbiota resulting in chronic tissue-destruction of the mucosa. In addition, excessive tissue remodelling is also a hallmark of IBD progression and severity[132,133]. Neutrophils are the predominant cell type driving IBD. Nonetheless, eosinophil numbers in the gut increase during disease progression and there is much evidence for their activation in this context[59,115,134]. This is exhibited by the marked increase in the concentration of eosinophil-derived granules (*e.g.* EPO) in the intestinal lumen of patients suffering from IBD[135].

The detrimental role of eosinophils in this disorder are thought to be dependent on the presence of inflammatory cytokines such as GM-CSF in the microenvironment[75]. The ensuing inflammatory response is further exacerbated through eosinophil release of TNF-α and IL-13. This could perhaps suggest that the activation phenotype of eosinophils under this context are more inflammatory, in comparison to eosinophils residing in the intestine under homeostatic conditions, although this has not been addressed.

Furthermore, eosinophils may influence the fibrogenesis observed in this disorder through their ability to regulate intestinal fibroblast function – thereby contributing to stricture formation (*i.e.* scar tissue/matrix stiffening) associated with Crohn's disease (a subtype of IBD)[115]. Yet a simple tissue-destructive role for eosinophils is not entirely clear, as there is also evidence of a critical role for these cells in epithelial repair after inflammatory injury – attributed to the ability of eosinophils to release anti-inflammatory cytokines such as TGF-β[136,137].

Food Allergy

The aetiology of food allergies is multi-factorial and the precise mechanisms that initiate adverse immunological responses to food antigens remain an enigma even today. Nonetheless, food allergy is thought to be a predominantly type-II immune disorder – unlike IBD, and asthma, which have significant inputs from Th1/Th17 immune responses.

Food allergies are a maladaptive type II immune response against common dietary allergens[138]. Similarly to asthma, they are driven in response to antigen-challenge, thereby requiring a priming event. The most common type of food allergy is a type-I immediate hypersensitivity, which is highly dependent on IgE-mediated activation of basophils/mast cells resulting in their degranulation – and in severe cases, triggering anaphylaxis. Hallmarks of food allergy include intestinal eosinophilia, elevated IgE-levels and the presence of allergen-reactive, CD4+ T-cells (*i.e.* Th2) [139]. Th2 cells are critical for the propagation of this response, and are the primary source of IL-4, IL-5 and IL-13 once the disease is established.

Eosinophils were thought to be an end-stage effector cell in this disorder, becoming highly activated and releasing their granules once in the intestine due to the presence of a highly inflammatory, Th2-driven microenvironment. Recent studies have expanded our understanding of the role of eosinophils in food allergy – showing that resident eosinophils are also critical for the initiation of the allergic responses in the intestinal lamina propria[71]. Eosinophils, through their release of EPO, were able to control CD103+ DC activation and CCR7-dependent migration to the mesenteric lymph node – allowing the priming/differentiation of Th2 cells. However, it has yet to be determined as to what factors lie upstream of eosinophil activation that could have led eosinophils to trigger such a response.

Eosinophilic esophagitis (EoE)

EoE is characterized by eosinophilia within the esophagus, which occurs concurrently with excessive tissue remodelling and tissue dysfunction, resulting in food impaction/dysphagia, abdominal pain and disordered gastrointestinal motility[61,68]. It is similar to standard food allergies in that it is largely driven in response to food antigens – as exhibited by disease amelioration in the context of an exclusively elemental (amino-acid based) diet[140]. EoE is also driven by type-II cytokines – however, unlike food allergies, IgE is not necessary for this disorder[141,142].

Similar to asthma, where airway hyper reactivity is associated with increased neuronal branching, patients with EoE often have higher levels of neurotrophins (*i.e.* factors inducing survival, development, function of neurons)[143–145]. This is thought to contribute to the dysphagia, and altered gastrointestinal motility observed in afflicted patients – and suggests that eosinophils can

impact on peripheral neurons. Whether this is a consequence, or driver, of eosinophil-mediated responses under these conditions is unclear.

Anti-tumoral responses in cancer

Eosinophils are frequently found to reside in solid tumors[146]. Nonetheless, their role in this context is still not entirely defined – with some studies showing that eosinophils in tumors are a sign of severity (*e.g.* oral squamous neck carcinomas, Hodgkin's lymphoma)[146,147], whereas in others, their presence correlates with a good prognosis (*e.g.* gastrointestinal, head and neck tumors)[148,149]. These discrepancies may be attributable to differences in the tumor microenvironment, which is likely to play a role in shaping the phenotype/transcriptome of the eosinophil – thereby dictating whether these cells play a pro or anti-tumorgenic role. However such questions have not yet been addressed. It is widely known in the field that eosinophils are drawn to tissues by 'danger-signals' (DAMPs) emanating from necrotic cells[150]. They also thrive in hypoxic environments – which might explain their presence in tumors[151].

In vitro co-cultures of eosinophils and tumor cells have laid the foundation for the hypothesis that eosinophils have a tumorcidal function[152]. This was attributed to their release of the pro-inflammatory mediators TNF-α, ECP and granzyme A – resulting in tumor cell killing. Although *in vivo* research addressing this phenomenon is still lacking, a recent study by Carretero et *al.* 2015 - has demonstrated a role for eosinophils in tumor rejection using a mouse model of melanoma[153]. Eosinophils were shown to contribute to this process indirectly by modulating the tumor microenvironment – with the absence of eosinophils resulting in impaired tumor rejection and decreased survival following T-regulatory cell depletion. The presence of eosinophils in the tumor coincided with the upregulation of pro-inflammatory cytokines (*e.g*. TNF-α, IFN-γ, IL-6), chemokines (*e.g.* CCL5, CXCL10) and nitric oxide, which are chemo attractants for CD8+ T-cells, and drivers of M1 (classically activated macrophage)-polarization. Furthermore, after T-regulatory cell depletion, the presence of eosinophils was required for the normalization of tumor vasculature – and consequently improved intra-tumoral infiltration of cytotoxic, CD8+ T-cells.

1.2.4 Homeostatic functions of eosinophils

Tissue Regeneration

In the context of inflammatory disease (such as IBD) eosinophils are often recruited to sites of injury – and partake in perpetuating the ongoing inflammatory response through provision of inflammatory mediators, and promoting tissue remodelling. However, under certain circumstances, eosinophils may also be recruited to sites of injury and in contrast – partake in tissue regenerative processes[154,155]. This dichotomous nature of the eosinophil is intriguing, highlighting the importance of the given microenvironment in dictating the outcome of their function.

For example, in a model of cardio-toxin muscle injury, eosinophils have been shown to drive regenerative responses. Eosinophils play a critical role in the regulation of IL-4rα+ fibrocyte-adipocyte progenitors (FAPs), preventing their differentiation to adipocytes through provision of IL-4/IL-13[65]. FAPs then provide signals that promote a stromal environment favourable for myocyte differentiation, in addition to phagocytic removal of necrotic muscle fibers – which is pivotal for appropriate muscle repair. Similarly, in a model of tetrachloride-induced liver injury, eosinophils are the predominant IL-4 expressing cells, with eosinophil release of IL-4 directly stimulating liver regeneration *via* IL-4ra signalling. This is concurrent with an increase in tissue IL-6 levels, known to amplify hepatocyte proliferation. Eosinophil recruitment in this context is mediated by injured hepatocytes enhancing local production of CCL11, likely through release of alarmins, thereby facilitating eosinophil recruitment.

Mammary gland development and uterine maintenance

Puberty hormones and growth factors trigger mammary gland development, which is characterized by the elongation and branching of the prenatal rudimentary ductal tree. Studies have reported that eosinophils, in combination with alternatively activated macrophages (M2), are critical for driving this process through provision of soluble mediators (*e.g.* TGF-β, MMPs) that shape the activity of the surrounding stroma[156]. Whilst the exact mechanism(s) by which this occurs are still unclear, it is apparent that eosinophils contribute to ductal branching – whilst M2 macrophages regulate the elongation of the ductal tree.

Eosinophils are also recruited to the healthy uterus in the degradation cycle (*i.e.* oestrus to metoestrus). Similarly to the mammary gland, eosinophil recruitment to the uterus is dependent on CCL11, where eosinophil recruitment and degranulation coincides with tissue-degradation and subsequent uterine repair and remodelling processes[157,158]. However, despite this observation – eosinophil-deficient mice exhibit normal pregnancy/parturition – suggesting that the role of eosinophils in this process is redundant, or that adaptation takes place to compensate for its absence. Nonetheless, a recent study by Miguel et *al.* (2017) suggests that eosinophils at least play a critical role in endometrial maintenance during infection with *C. trachomatis*, by promoting endometrial proliferation and tissue repair[159].

Metabolic homeostasis in the adipose tissue

Unlike the muscle, uterus and mammary gland, eosinophils are found to constitutively reside in adipose tissue under homeostatic conditions. Recent studies have shown a critical role for eosinophils in the maintenance of M2 macrophages in this tissue by releasing IL-4[113]. This in turn allows the immune milieu of the adipose tissue to be maintained in an anti-inflammatory state – which is favourable for the maintenance of metabolic homeostasis. ILC2-derived IL-5 contributes to this outcome by sustaining eosinophils in this tissue[160]. The loss of eosinophils is thought to result in low-grade, type-I inflammation in the adipose due to the loss of M2 macrophages. This coincided with increased susceptibility to high-fat diet induced obesity, and insulin tolerance.

Immune regulation in the small intestine

Research on intestinal eosinophils has been done, mainly in the context of infection or pathophysiology (discussed previously). Nonetheless, a few studies over the past five years have started to shed light on the functional significance of eosinophil residency in this tissue under homeostatic conditions.

Four independent studies have shown that eosinophils are important in regulating immune homeostasis in this tissue[64,161–163]. The first two, have shown that eosinophils are required for the maintenance of IgA+ plasma cells in the small intestine – however, they attribute this outcome to different mechanisms. Chu et *al.* (2014), suggested that eosinophil-derived BAFF, TGF-β and IL-6 production mediate the survival of IgA+ plasma cells[163]. By contrast Jung et *al.* (2015), showed that eosinophils did not contribute to IgA production *via* release of these factors, but rather *via* their

production of IL-1β and lymphotoxins[162]. The third study, conducted by Sugawara et *al.* (2016) – didn't examine IgA+ plasma cells, but instead showed that eosinophils repressed Th17 cells *via* IL-1Rα – which has antagonistic activities against IL-1β mediated Th17 differentiation[161]. The final study, by Buonomo et al. 2016, did not look at the immune regulatory function of eosinophils – but instead showed that eosinophils are required for the maintenance of barrier integrity during infection with *Clostridium Difficile* – thereby decreasing intestinal inflammation caused by this bacterial pathogen[64]. However, the mechanism for this remains unclear.

Overall, the consensus is that in one way or another – eosinophils are mediating tissue protective processes in the intestine, either through regulating barrier integrity, immune cell homeostasis or both. However, the precise mechanisms eosinophils utilize to achieve this remains unclear. Moreover the discrepancies apparent between these studies likely highlight the influence the microenvironment and/or the microbiota may have in promoting differential eosinophil function within the intestine. Further studies - in which environmental factors (including the diet and microbiota) are carefully controlled – will be necessary to elucidate the exact function of eosinophils within the healthy intestine.

1.3 RATIONALE FOR THESIS

The small intestine has important functions as a physicochemical barrier and a nutrient absorptive site. In addition, it also functions as a reservoir for the largest number of mature immune cells within the body. It is also extensively colonized with microbial organisms in the post-natal state, and serves as the primary interface for host-microbiota interactions. Therefore, this tissue is tasked with maintaining a delicate balance by facilitating nutrient uptake – whilst maintaining adequate vigilance (immunological-armistice) towards the luminal microbiota. This balance is essential to maintain tissue homeostasis and its disturbance can result in disease.

The microbiota provides much value to the host - but in order to do so, host-microbial interactions must be established and maintained correctly. However, the precise mechanisms that facilitate this establishment remain unclear. Eosinophils are recruited to this small intestine in early-life, and are sustained in this tissue in substantial numbers throughout life - in both mice and humans. However, the functional significance of their residency is still enigmatic. Given the extensive variation of processes in which eosinophils have been noted to take part (in both health and disease), and the multi-functionality of these cells, understanding the full extent of their function within complex tissues like the small intestine warrant further investigation.

In addition, understanding how eosinophils are recruited to, or activated within, the small intestine under homeostatic conditions may provide invaluable insight into the mechanisms responsible for their dysregulation during disease.

This thesis was designed to explore the role of eosinophils resident in small intestine, taking a holistic view of small intestinal function as a physicochemical barrier, immunological niche and a nutrient absorptive site.

1.4 THESIS OBJECTIVES

To study the impact of eosinophils in small intestinal homeostasis, we utilized a mouse model of eosinophil-deficiency, the Δdbl.GATA1 mice, which is commonly utilized in the field of eosinophil biology. Δdbl.GATA1 mice were generated through the targeted deletion of a high-affinity palindromic ('double') GATA1 binding site upstream of the gata1 promoter[164]. GATA1 is noted to autoregulate its own transcription through this site. The removal of this site does not result in ablation of Gata1 expression, and Gata1 is still expressed in Δdbl.GATA1 mice at a basal level. However, deletion of this site results in cells not being able to acquire a high expression of GATA1 rendering eosinophil-progenitors incapable of eosinophil differentiation. As a result, eosinophils are completely absent throughout the body of Δdbl.GATA1 mice.

Using this mouse model as a means to study the impact of eosinophil-deficiency – we designed a series of objectives to *broadly assess the functional significance of eosinophil residency in the small intestine.* These objectives are listed below:

1) To conduct a spatiotemporal characterization of eosinophils within the small intestine - and to assess the impact of the microbiota on their activation
2) To investigate the impact of eosinophils on barrier function and immune homeostasis in the intestine
3) To assess the impact of eosinophils on the tissue architecture of the small intestine
4) To identify pathways influencing eosinophil-mediated functions within the small intestine
5) To determine whether eosinophils impact on intestinal function as an absorptive organ

Chapter 2: Spatio-temporal characterization of small intestinal eosinophils and regulation by the microbiota

The Small Intestine (SI) has the highest frequency of eosinophils in the body under homeostatic conditions. While this phenomenon has been reported in the literature, fundamental information about their distribution and localization in this tissue remain unclear, largely due to limitations in the methods commonly used to analyse eosinophils (*e.g.* histological, flowcytometric). Furthermore, whether key regulators of the intestinal microenvironment (*e.g.* microbiota) have an impact on overall eosinophil homeostasis is relatively unknown. We initiated our studies with a broad characterization of eosinophil localization and recruitment in the SI, and assessed the impact of the microbiota on their activation. Addressing these fundamental questions were a crucial foundation for the generation of hypotheses that conferred invaluable insight into eosinophil function within the SI.

2.1. IDENTIFICATION, DISTRIBUTION AND LOCALIZATION OF SI EOSINOPHILS UNDER HOMEOSTATIC CONDITIONS

2.1.1 Distribution and Characterization of Resident Eosinophils in the SI

In order to understand the contributions of resident eosinophils to small intestinal homeostasis, we first wanted to characterize the relative distribution of these cells in different SI compartments. We observed eosinophils (identified as SSC^{hi}, Siglec-f+ cells) to be enriched in the proximal intestine (*i.e.* Duodenum, Jejunum) in comparison to the ileum, which is concurrent with previous reports **(Figure 4B)**[71]. Given the functional specialization of different intestinal region, and the enrichment of eosinophils in the proximal gut – we focused much of our analysis on the jejunum.

Eosinophils residing in the Jejunum represent 5-30% of total CD45+ cells, and are noted to express a distinct set of surface markers in comparison to more terminal (*e.g.* ileum, colon) regions of the intestine[72,165]. These differences may perhaps be a reflection of differential activity of these cells under the influence of their given microenvironment [71]. We found jejunal eosinophils to express $F4/80^{int}$ $CD11b^{hi}$ $CD11c^{hi}$ $CD44^{hi}$ $CCR3^{hi}$ $Ly6c^{lo}$ and $CD103^{int}$, which are in-line with previous studies **(Figure 4C)**[71,72]. However, contrary to previous reports[166], we saw low expression of MHCII

suggesting that jejunal eosinophils in the lamina propria have little to no antigen-presentation activity under homeostatic conditions **(Figure 4C)**.

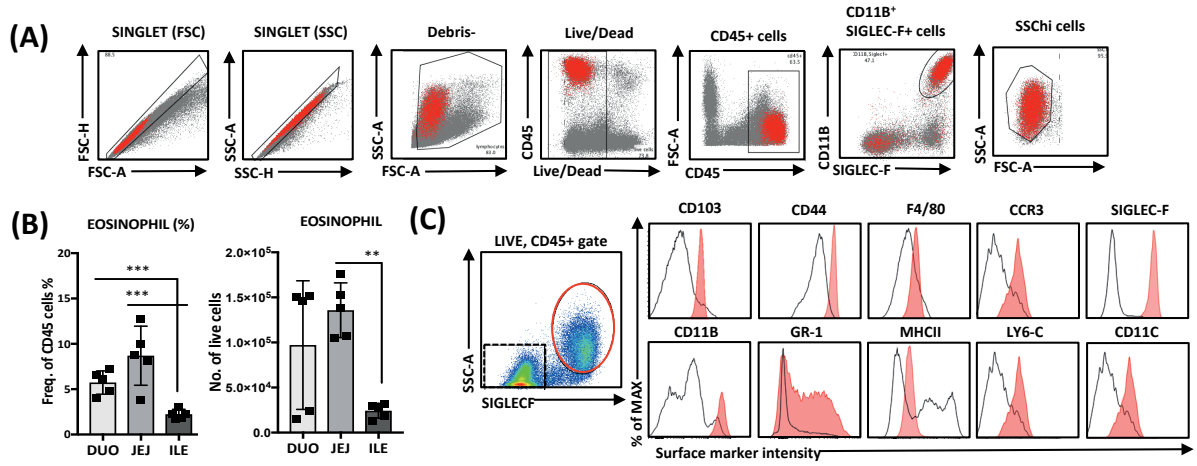

(Figure 4) Identification and distribution of Eosinophils in the SI under homeostatic conditions.
(A) Gating strategy for identification of small intestinal (SI) eosinophil (live, CD45+ SSChi Siglec-f+ cells) **(B)** Duodenum (DUO) represents the first 5 cm of the SI; Jejunum (JEJ) corresponds to a region 10cm distal to the DUO; Ileum (ILE) denotes the last 10cm of the SI proximal to the cecum - shows frequency of Eosinophils within total CD45 cells; absolute cell counts of eosinophil. **(C)** Surface marker analysis of Eosinophils isolated from the Jejunum (red – SSC^{hi}, $Siglecf^{+}CD45^{+}$ cells) shown as Mean fluorescence intensity (MFI); compared to all other $CD45^{+}$ (dotted line – $Siglecf^{-}$ $CD45^{+}$ cells) in the lamina propria. Statistical analysis (One-way ANOVA; $p<0.001$***, $p<0.01$**); Error bars represent SD within group.

2.1.2 Localization of Eosinophils in the SI

To gain insight on novel functions of resident eosinophils, we utilized a wholemount staining protocol, which enabled us to identify eosinophil localization within the SI with high resolution[7]. Furthermore, it allowed us to analyze the villus in its entirety – providing us with the advantage of visualizing eosinophils in their native microenvironment. In the intestine, we found that resident Eosinophils (identified as Siglecf+ cells[i] in the lamina propria) preferentially reside in the villous lamina propria – adjacent to functionally significant structural cells such as blood endothelial cells (BECS; identified by expression of VEGFR2) and myofibroblasts (distinguished by expression of α-SMA) **(Figure 5A)**. They can

[i] **Note:** Tuft cells (specialized- IEC) also express Siglecf in addition to Eosinophils. However, they can be easily distinguished from eosinophils based on their morphology (i.e. bottle-like/oblong) and their epithelial layer localization *(vs. lamina propria localization by; segmented nuclei of - eosinophils)*

also be found to reside near PGP9.5+ enteric neurons **(Figure 5D)** and GFAP+ glial cells **(Figure 5E)**

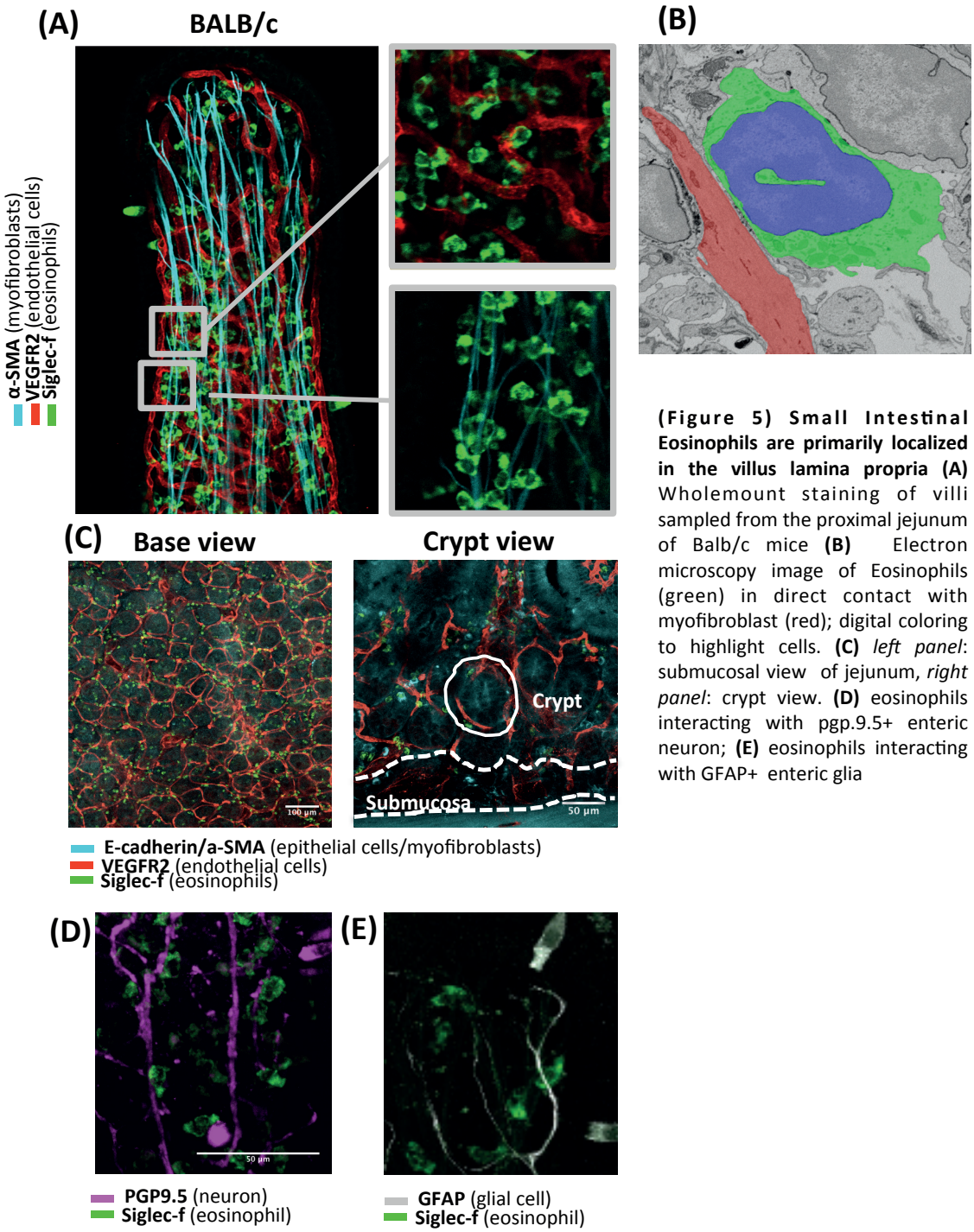

(Figure 5) Small Intestinal Eosinophils are primarily localized in the villus lamina propria (A) Wholemount staining of villi sampled from the proximal jejunum of Balb/c mice **(B)** Electron microscopy image of Eosinophils (green) in direct contact with myofibroblast (red); digital coloring to highlight cells. **(C)** *left panel*: submucosal view of jejunum, *right panel*: crypt view. **(D)** eosinophils interacting with pgp.9.5+ enteric neuron; **(E)** eosinophils interacting with GFAP+ enteric glia

We also observed by electron microscopy (EM) that some eosinophils are also in direct contact with these cells **(Figure 5B)**. To a lesser extent, eosinophils can also be found near vessels in the peri-cryptal region of the villous **(Figure 5C** – left panel**)**. However, they are virtually absent in the muscularis mucosa in adult mice **(Figure 5C** – right panel**)**.

2.2 MICROBIOTA REGULATION OF EOSINOPHIL SURVIVAL, RECRUITMENT AND ACTIVATION IN THE SI

2.2.1 Eosinophil recruitment into the SI is microbiota-independent

One of the peculiarities of eosinophils that make a case for these cells as functionally important for intestinal homeostasis, is the early life recruitment of these cells into the SI[167]. Eosinophils are recruited into this tissue as early as E17.5 in a wave that starts from the proximal to distal region **(Figure 6)**. This coincides with the formation of villus, which also follows the same spatio-temporal pattern albeit starting at E15[5]. At this developmental stage, we observed eosinophils to be residing at the base of the villi, and only migrate up the villus starting at post-natal P2 (sparsely), only reaching adult levels at ~P14 (personal observations; data not shown). While the precise factors mediating this recruitment from the base to the tip of the villus is unknown, this correlates with a period within which pups mature to have enhanced capacity to utilize Vitamin A for conversion to retinoic acid – a factor which is important for the migration and survival of eosinophils [168,169].

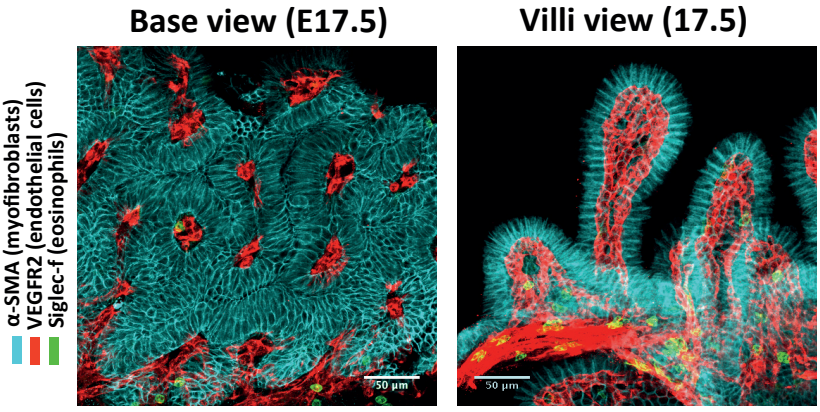

(Figure 6) Early life recruitment of eosinophil in the small intestine: Wholemount imaging of basement membrane (left) and villi (right) of Balb/c mice at E17.5.

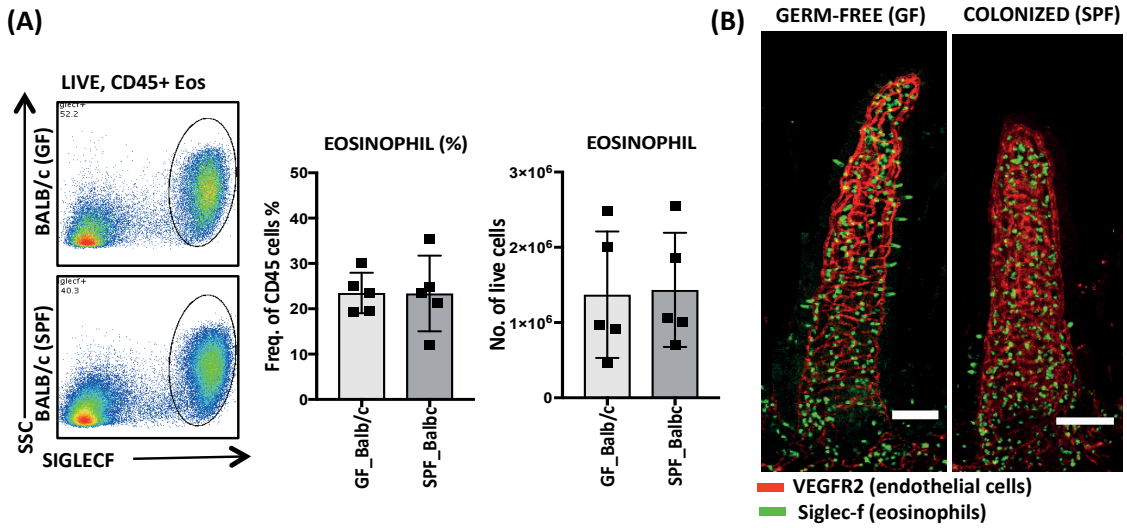

(Figure 7) Microbiota colonization-status does not influence Eosinophil localization and residency in the SI under homeostatic conditions: (A) Representative plots from FACS analysis of from jejunum of Balb/c mice (GF vs. SPF); FACS data quantification (Frequency and cell number) of SI eosinophils **(B)** Wholemount imaging of villi from GF (left) and SPF (right) Balb/c mice, sampled from jejunum. Statistical analysis (student-t test; not significant with $p>0.05$) Error bars represent SD between samples.

Given the immense potential of the microbiota to regulate both physiological, and immune homeostasis in the intestine – we wanted to see whether colonization status influences resident eosinophils by comparing eosinophil numbers in the jejunum of Germ-free (GF) and Specific-pathogen free (SPF) colonized Balb/c mice. We observed similar quantities of resident eosinophils in both conditions **(Figure 7A)** suggesting that the extent of eosinophil recruitment in the intestine under homeostasis is independent of the microbiota, inline with previous reports. Similarly, we also did not observe changes in the localization and migration of eosinophils into the villus lamina propria in Germ-free vs. SPF mice **(Figure 7B)** – all of which suggest that eosinophil recruitment/localization in the intestine is a developmentally regulated process at steady-state.

2.2.2 Microbiota regulation of survival, recruitment and activation in the SI

As discussed previously, an accurate depiction of eosinophil activation status is difficult to obtain using conventional methods (*i.e.* flowcytometric, histological). This is due to the lack of surface markers delineating eosinophil degranulation or activation. Eosinophils can be readily analyzed by methods such as electron microscopy due to their unique, granule and lipid-body dense cytoplasm, in addition to an intricate network of vesicles scattered throughout this compartment. In order to assess the impact of the microbiota on eosinophils activation in the small intestine, we

used TEM imaging to characterize ultrastructural changes resulting from microbial exposure in SI eosinophils.

Using this method, we compared parameters such as granule number and degranulation status in Germ-free (GF) and Colonized Balb/c mice (SPF). We did not observe any differences in degranulation status and granule number between GF and SPF eosinophils imaged from the proximal jejunum under homeostatic conditions **(Figure 8A, B)**. Interestingly, most of the changes we observed between the two groups were occurring not in the granules/lipid bodies but rather - in the cytoplasm itself - where, eosinophils from SPF mice exhibited more pronounced formation of vesiculo-tubular structures compared to microbiota-deficient GF mice **(Figure 8C)**. These pleomorphic networks are responsible for the movement of eosinophil-derived proteins from cytoplasmic stores and to the plasma membrane for cellular release[76]. We also observed a dramatic increase in free ribosomes throughout the cytoplasm in SPF vs. GF eosinophils **(Figure 8C)**.

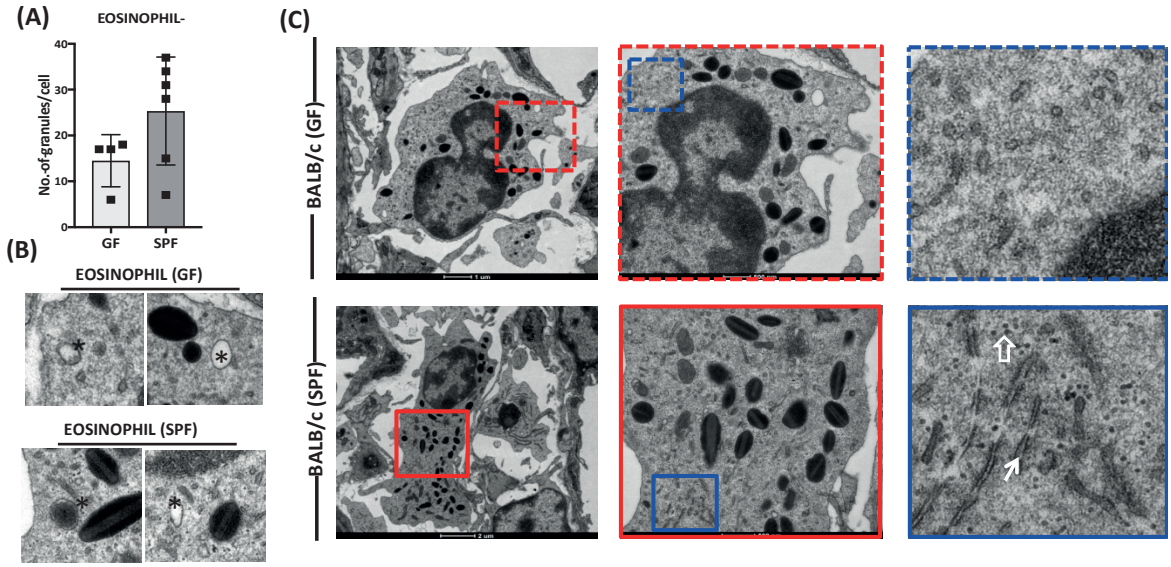

(Figure 8) SI eosinophils from SPF-colonized mice exhibit increased cytoplasmic activity: (A) Quantification of granules in the cytoplasm of eosinophils resident in the proximal jejunum by Transmission electron microscopy (TEM) from GF and SPF Balb/c. **(B)** Examples of emptied (full, partial) granules *indicated by astetrix* (*), secondary to piecemeal degranulation **(C)** TEM images at various magnifications; colored boxes correspond with location of magnified image. Note that SPF mice have increased cytoplasmic free ribosomes (*dot-like structures* - Open arrow) and vesiculotubular structures (*tubular structures* – closed arrow) compared to GF mice. Images representative of >6 TEM images per mouse (n=2 per condition).

Free ribosomes function to synthesize protein for internal consumption, and not for extracellular transport[17]. An increase of these structures in SPF mice may suggest a higher activation status compared to GF mice. Increased free ribosome number in SPF mice, may be indicative of the cell replenishing released pre-formed factors stored in cytoplasmic granules/lipid bodies.

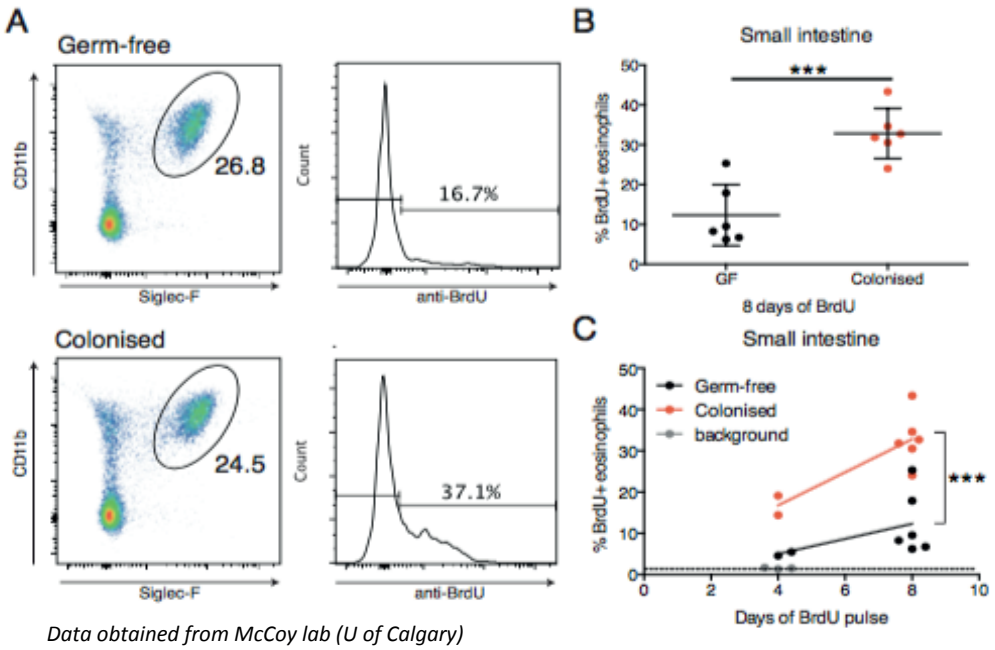

Data obtained from McCoy lab (U of Calgary)

(Figure 9) Microbiota regulates homeostatic turnover of SI eosinophils: (A-C) Small intestinal eosinophils were analyzed in GF or SPF colonized conditions, and received BrdU in drinking water for 10 days, **(A)** Representative FACS plot of data from **(B)** which shows % of BrdU+ SI eosinophils at day 8 of continuous BrdU+ intake between Gf and colonized (SPF) mice. % of BrdU proliferation of eosinophils were analyzed at day 4 and 8, quantification includes a linear regression curve fit between day 4 and 8 **(C)**. Statistical analysis – student t-test (unpaired) *** $p<0.001$

In addition to the small intestine harbouring the largest population of eosinophils in the body, eosinophils in this tissue are also longer-lived in comparison to other tissues in the body where other eosinophils reside under homeostatic conditions[72]. It is widely suggested that micro-environmental cues, specific to the intestine, may be involved in the regulation of eosinophil survival. Given our preliminary observations for a role of the microbiota in regulating eosinophil activity, we hypothesized that these observations may indicate changes in this eosinophil survival. To address this, our collaborators (K McCoy lab; University of Calgary) conducted an experiment comparing turnover rates of small intestinal eosinophils under GF and colonized (SPF) conditions. Through a BrdU-pulse chase experiment over the course of 10 days, they report that eosinophil turnover is delayed in GF compared to SPF mice **(Figure 9)**. Under SPF conditions, almost 40% of SI eosinophils were positive for BrdU incorporation compared to only 10% of eosinophils from GF

mice at day 8 post-BrdU feeding **(Figure 9C)**. Since the SI eosinophil numbers are comparable between GF and SPF mice **(Figure 7A)**, it can be concluded that this decrease in BrdU+ eosinophils in SPF mice is due to eosinophils turning over at a faster rate and not due an increase in proliferation. Overall, these findings suggest that commensal microbiota (through direct or indirect mechanisms) may be accelerating eosinophil turnover in the SI.

2.3 DISCUSSION

Eosinophil distribution correlates with changes in villous size, noted to decrease in area from the proximal (largest) to the distal (smallest) small intestine **(Figure 4B, 1A)**. This variation in villus size across the SI is developmentally determined. Under homeostatic conditions, stromal cells within the villous are the primary eotaxin-1 producers (which is required for SI recruitment of eosinophils)[55,167,170]. Given that the cellular density – particularly that of the stromal compartment – is concurrent with villous size, it may be that the increased enrichment of eosinophils in the proximal intestine is a mere reflection of the quantity of eotaxin-1 producing cells within the villous [5,171].

Wholemount imaging of eosinophils in the small intestine, has provided us the advantage of accurately visualizing eosinophil localization and distribution within its native microenvironment at a level not previously attained by conventional histological imaging. This technique has enabled us to capture the villus at its entirety, instead of being restricted to a cross section (*e.g.* immunohistogical staining of paraffin/OCT sections). From this work, we were able to appreciate the large quantity of eosinophils within the villus, in agreement with high eosinophil frequencies we observe by FACS analysis **(Figure 5)**. We also report that eosinophil recruitment in the intestine is independent of microbiota-colonization status **(Figure 7)**.

The villous lamina propria housed most of eosinophils found in the intestine (followed by pericryptal regions) **(Figure 5)**. Furthermore, we observed eosinophils to be in close contact with blood vessels, myofibroblasts and components of the enteric nervous system (*i.e.* glia, neurons) **(Figure 5)**. Their close proximity under homeostasis may be suggestive of ongoing crosstalk between these cells and eosinophils under homeostatic conditions; a concept explored in later chapters.

Ultrastructural analysis of SI eosinophil morphology under GF vs. SPF conditions by TEM imaging revealed microbiota-induced changes in cytoplasmic structures, particularly the increased prominence of vesiculo-tubular networks and free ribosomes **(Figure 8C)**. These structures have been observed in other studies of eosinophil activation, and represent hallmark characteristics associated with increased eosinophil activity[76,78]. At current, ultrastructural evaluation of eosinophil activity within the intestinal microenvironment has primarily been studied in the context of eosinophil-mediated disorders[172–174]. Therefore, it is quite difficult to gauge what these differences may reflect with regards to eosinophil homeostasis, and overall host physiology at steady-state. One hypothesis that has been presented is that increased formation of free ribosomal structures may be an effort by the eosinophils to restock cytoplasmic stores due to increased extra-cellular release of proteins from the cell[70]. Concurrent with this, increased prominence of cytoplasmic, vesiculotubular networks may be reflective of increased sorting and trafficking of molecules tagged for export[76,175].

Based on the ultrastructural features we observed, SI eosinophils are likely releasing molecules through Piecemeal Degranulation (PMD), which allows for the regulated (partial/differential) release of molecules from cytoplasmic secretory granules – without necessitating the collapse and exocytosis of entire granular compartments[172,175]. Hallmarks of PMD were observed in all eosinophils examined in our analysis, irrespective of condition **(Figure 8B)** – and does not seem to depend on microbial colonization status. Nonetheless, in light of other observations (*i.e.* increase in vesiculotubular structures, free ribosomes) it is likely that this process may be enhanced in response to the microbiota.

It remains unclear whether the microbiota may be regulating eosinophil activation through a direct or indirect mechanism. Eosinophil degranulation status in the intestine has been noted to correlate with injury/trauma[56]. Therefore, it is possible that the microbiota may be indirectly regulating eosinophil activation through induction of tissue stress and damage. Alternatively, eosinophils are noted to express various PRRs – and it is also possible that eosinophil activation may be a direct consequence of bacterial recognition[176]. Regardless, an increased activation status of eosinophils in response to the microbiota correlates with its faster turnover, as the extent of eosinophil degranulation/activation is negatively correlated with its survival[97].

In consideration of all the observations reported here, we conclude that signals either directly from, or in consequence to, microbiota colonization results in an increased state of eosinophil activation, and alterations in survival – providing further evidence for a important role of the small intestinal microenvironment in shaping and regulating tissue-specific functions of resident eosinophils.

Chapter 3: Eosinophil regulation of Barrier and Immune Homeostasis in the Small Intestine

In addition to its fundamental role in nutrient absorption processes, the intestinal epithelial barrier is a critical facilitator of microbiota host crosstalk, with implications on various physiological and immunological processes.

The intestinal epithelial barrier is largely comprised of various classes of differentiated epithelial cells, adhered together by a network of tight-junctions and adhesion molecules[177]. Intraepithelial lymphocytes are also present throughout this layer – reinforcing the immune-surveillance capacity of the barrier, by keeping the microbiota (both commensal and pathogenic) in check[13,178]. Underlying the epithelial monolayer are sub-epithelial fibroblasts and various ECM components (*i.e.* ECM proteins, modifiers, associated proteins) that support the overlying IEC serving as a bio-active scaffold that facilitates processes involved in wound healing, cell migration and overall epithelial homeostasis/maintenance[179].

3.1 EOSINOPHIL REGULATION OF IEC HOMEOSTASIS

Epithelial turnover is a critical factor for overall intestinal homeostasis. It can be summarized in to 3 parts: proliferation, apoptosis and migration – factors that need to be in balance for maintenance of barrier integrity. We explore the impact of eosinophils in this process.

3.1.1 Eosinophils are dispensable for crypt homeostasis and IEC differentiation

In addition to the villous lamina propria, Eosinophils are also found to reside in the peri-cryptal region of the SI, where they are in close interaction with blood vessels and SMA+ myofibroblasts surrounding the crypt - key cellular populations that function as part of a regulatory niche maintaining intestinal stem cell homeostasis [180].

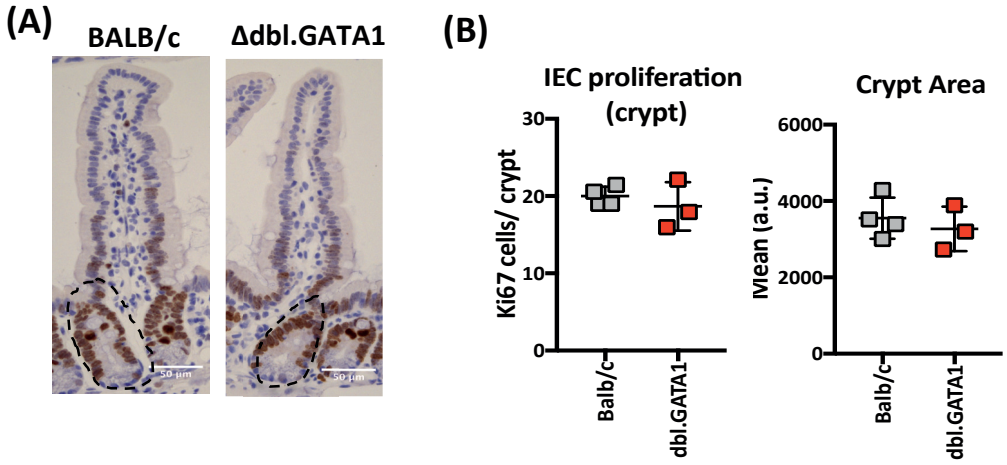

(Figure 10) Δdbl.GATA1 mice have normal crypt proliferation under homeostatic conditions: (A) Representative images of immunohistochemical (IHC) staining for Ki67 of jejunal villi from Balb/c mice – dotted line denotes crypt region used for analysis (example) **(B,** left**)** Quantifications of ki67+ cells per crypt; crypt area **(B,** right**).** Each data point is an average of >20 randomly sampled crypts per mouse (n=3-4 mice). Error bars represent SD within group.

To assess the impact of eosinophil-deficiency on crypt homeostasis, we assessed the proliferative activity of crypts from the jejunum of Δdbl.GATA1 mice using Ki67-positivity as a marker of cell proliferation. We did not observe any differences in number of Ki67+ nuclei within the crypt, suggesting that eosinophils are not important for regulating epithelial proliferation **(Figure 10B;** left**)**. In addition, we also did not observe any differences in crypt area compared to control mice **(Figure 10B**; right**)**. Differentiated IEC subsets such as Paneth cells, Goblet cells and Tuft cells were also quantified - with no differences observed between Δdbl.GATA1 and control mice **(Figure 11)**. This suggests that SI eosinophils have no influence on the differentiation of IECs under homeostatic conditions.

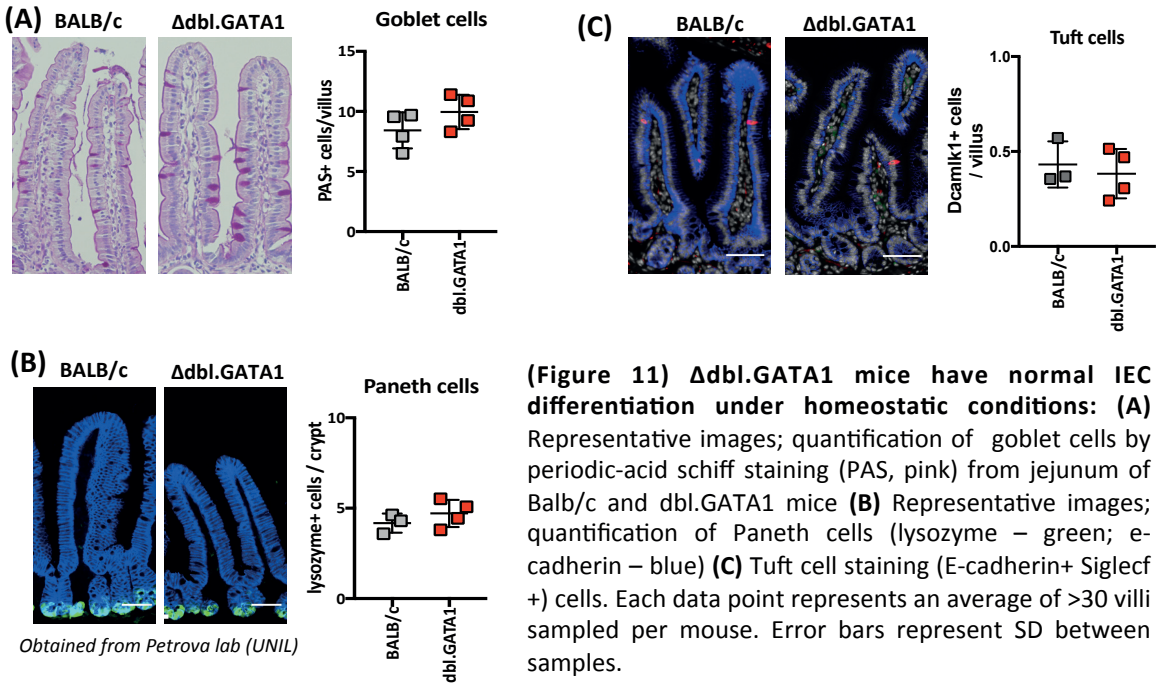

Obtained from Petrova lab (UNIL)

(Figure 11) Δdbl.GATA1 mice have normal IEC differentiation under homeostatic conditions: (A) Representative images; quantification of goblet cells by periodic-acid schiff staining (PAS, pink) from jejunum of Balb/c and dbl.GATA1 mice **(B)** Representative images; quantification of Paneth cells (lysozyme – green; e-cadherin – blue) **(C)** Tuft cell staining (E-cadherin+ Siglecf +) cells. Each data point represents an average of >30 villi sampled per mouse. Error bars represent SD between samples.

3.1.2 IEC turnover dynamics is altered in Δdbl.GATA1 mice

SI epithelial cells undergo continuous apoptosis/shedding, and robust restitution of displaced cells is required for optimal barrier integrity[20,181]. This delicate balance between IEC apoptosis and replacement must be maintained to ensure epithelial barrier homeostasis. Using Caspase-3 to identify apoptotic cells, and EdU-incorporation for tracking migrating cells along the villous – we sought to determine whether homeostatic IEC turnover was affected by eosinophil-deficiency.

Caspase-3 staining was sparely found in the villus, which is expected at steady-state conditions. With focus on the epithelial barrier, we found caspase-3+ epithelial cells **(Figure 12A)**, in addition to staining in IEC-associated cells – which by morphology are likely to be IELs and sub-epithelial fibroblasts **(Figure 12B)**. Upon quantification, we observed no significant differences in the apoptosis rate of IEC and IEC-associated cells in the epithelial barrier of Δdbl.GATA1 mice in comparison to Balb/c controls.

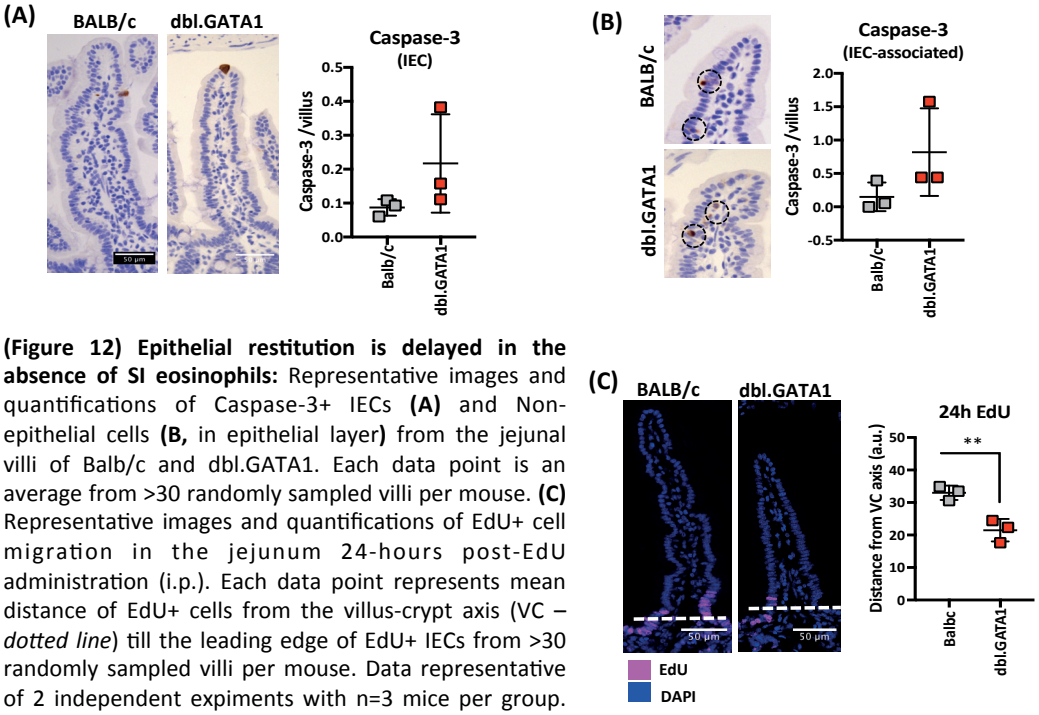

(Figure 12) Epithelial restitution is delayed in the absence of SI eosinophils: Representative images and quantifications of Caspase-3+ IECs **(A)** and Non-epithelial cells **(B,** in epithelial layer**)** from the jejunal villi of Balb/c and dbl.GATA1. Each data point is an average from >30 randomly sampled villi per mouse. **(C)** Representative images and quantifications of EdU+ cell migration in the jejunum 24-hours post-EdU administration (i.p.). Each data point represents mean distance of EdU+ cells from the villus-crypt axis (VC – *dotted line*) till the leading edge of EdU+ IECs from >30 randomly sampled villi per mouse. Data representative of 2 independent expiments with n=3 mice per group. Statistical analysis unpaired student t.test ($p<0.001$**). Error bars represent SD between samples

Next, we looked at whether there were any discrepancies in epithelial restitution; a process achieved by IEC migration, and replacement of displaced/apoptotic epithelial cells. This was accomplished by tracking the migration of EdU+ cells, with the rate of migration measured as a distance from the villus-crypt axis 24h post-EdU injection. Here, we saw a modest but robust (~30%) delay in the migration of IECs of Δdbl.GATA1 mice from the villus-crypt axis. This suggests that eosinophils are able to influence epithelial cell migration, despite being located in the villus core.

3.1.3 Δdbl.GATA1 have increased barrier permeability

A delay in epithelial restitution is indicative of perturbations in intestinal barrier function, potentiating risk for intestinal leakage and consequent microbiota-induced pathophysiology. To further examine the impact of eosinophil-deficiency on barrier homeostasis, our collaborators (K McCoy lab – University of Calgary) conducted a barrier permeability assay on Δdbl.GATA1 mice under SPF vs. GF conditions.

In brief, the assay used an Ussing Chamber to measure the influx of FITC-dextran from the mucosal side of the small intestine, to the serosal, serving as a functional read-out of paracellular

permeability within the epithelial layer. FITC-dextran influx was measured at the chamber facing the serosal side of the intestinal tissue at various timepoints (0, 20, 40, 60mins).

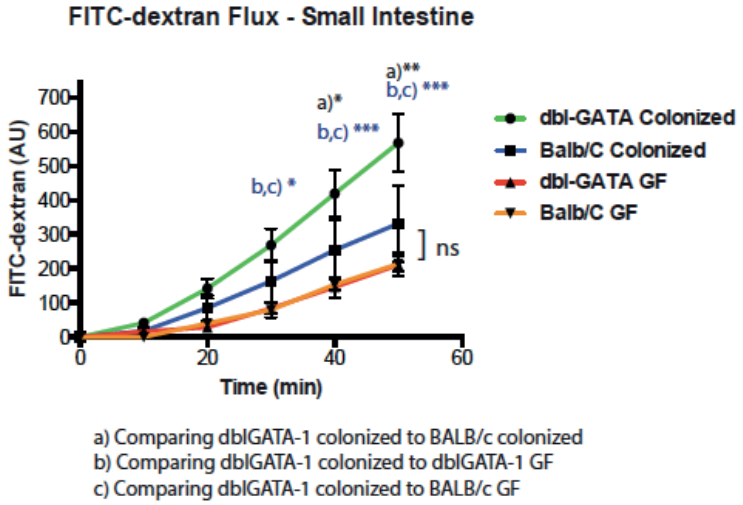

(Figure 13) Δdbl.GATA1 mice have increased barrier permeability in response to microbiota colonization: Signal/intesity/ concentration of FITC-dextran (serosal side, SI) Statistical analysis **(A)** comparing Δdbl.GATA1 SPF-colonized to Balb/c (B) dbl.GATA1 SPF-colonized **(B)** Δdbl.GATA1 germ-free (GF) **(C)** Δdbl.GATA1 SPF-colonized to Balb/c GF.

Data acquired from K McCoy lab (Ucalgary)

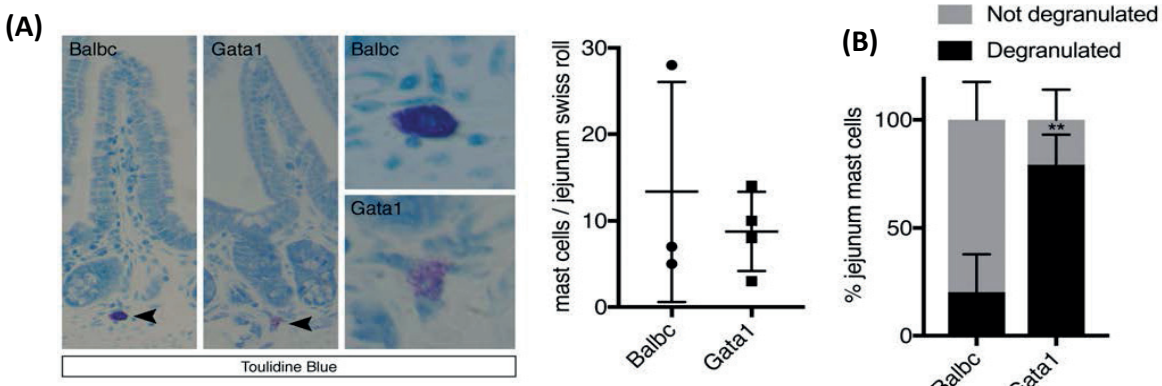

Quantifications by Petrova lab (from JBL)

(Figure 14) SI mast cell degranulation is increased in the absence of Eosinophils: (A) Representative images and quantification of Mast cells in Balb/c and dbl.GATA1 mouse SI, Mast cells were chemically-stained with toluidine blue – with degranulation corresponding to decreased cytoplasmic staining **(B)** Ratio of degranulated/total mast cells in the SI.

Concurrent with previous findings, we found that intestinal barrier permeability in microbiota-colonized mice is increased compared to germ-free mice – indicated by an increase in FITC-dextran influx at later time points of the experiment **(Figure 13)**[182]. Under germ-free conditions, no differences were found between the paracellular permeability of Δdbl.GATA1 and Balbc control mice. Interestingly however, this microbiota-induced increase in barrier permeability was exaggerated in the absence of eosinophils – a finding that, along with delayed IEC migration, highlight the importance of eosinophils in the homeostatic maintenance of barrier integrity at steady state conditions.

To further corroborate our findings, we looked at Mast-cell degranulation, known to correlate with increased barrier permeability[183,184]. Mast cells are primarily present in the submucosal layer of the intestine under homeostatic conditions, and are easily identifiable using basic histological dyes such as toluidine blue. Toluidine blue stains mast cell granules (i.e. heparin, histamine) dark blue/purple, with degranulation identified by decreased cytoplasmic staining (i.e. pink). While Δdbl.GATA1 had comparable mast cell numbers to Balb/c mice **(Figure 14A)**, we observed a significant increase in the proportion of degranulated mast cells **(Figure 14B)** in the absence of eosinophils compared to Balb/c controls. This is concurrent with the increased intestinal permeability we observed in Δdbl.GATA1 mice.

3.1.4. RNA-seq from epithelial barrier of Δdbl.GATA1 at under homeostatic conditions

To gain better insight on the mechanisms that may be driving the epithelial barrier defects observed in Δdbl.GATA1 mice, we proceeded to do a comparative, RNA-seq analysis on the epithelial fraction from the jejunum of Balb/c and Δdbl.GATA1 mice.

In total, 67 genes were differentially regulated between Δdbl.GATA1 and Balb/c controls. From this gene set only 19 genes were significantly downregulated, for which we performed a Gene Set Enrichment Analysis (GSEA; Molecular signature database – Broad Institute). Out of the 15 genes recognized by the database, 7 belonged to the PPAR-a pathway, a critical driver of fatty acid metabolism – particularly in the oxidization of fatty acids in mitochondria mediating ketone and triacylglycerol metabolism **(Figure 15B; supplementary table 5)**. This suggests that eosinophils are involved in induction of PPAR-a signalling in intestinal epithelial cells.

Next, we looked at genes that were significantly increased in expression from our Δdbl.GATA1 mice relative to Balb/c. When we ran our targets through the GSEA database (FDR 0.05; FClog2 >1.5), we saw enrichment for pathways involved in extracellular matrix remodelling (*e.g.* MMP13, MMP2, Col6a4) and complement system (*e.g.* C1Qa, C1Qb, C1Qc) **(Figure 16B; Supplementary table 6)**. These findings are indicative of active remodelling, and increased barrier dysfunction in the absence of eosinophils.

(A)

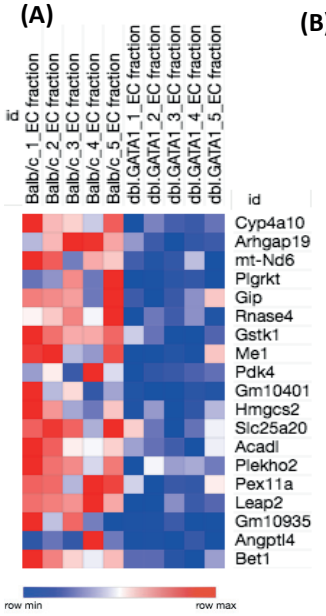

(B)

Gene Set Name [# Genes (K)]	Description	# Genes in Overlap (k)	k/K	p-value	FDR q-value
REACTOME_FATTY_ACID_TRIACYLGLYCEROL_AN_AND_KETONE_BODY_METABOLISM [168]	Genes involved in Fatty acid, triacylglycerol, and ketone body metabolism	6		$6.39\ e^{-12}$	$8.5\ e^{-9}$
REACTOME_METABOLISM_OF_LIPIDS_AND_LIPOPROTEINS [478]	Genes involved in Metabolism of lipids and lipoproteins	6		$3.43\ e^{-9}$	$2.04\ e^{-6}$
KEGG_PPAR_SIGNALING_PATHWAY [69]	PPAR signaling pathway	4		$4.6\ e^{-9}$	$2.04\ e^{-6}$
REACTOME_PPARA_ACTIVATES_GENE_EXPRESSION [104]	Genes involved in PPARA Activates Gene Expression	4		$2.43\ e^{-8}$	$8.09\ e^{-6}$

(Figure 15) RNA-seq of Epithelial fraction of Δdbl.GATA1 mice (downregulated genes) at steady-state conditions: (A) Heatmap shows top genes downregulated in dbl.GATA1 mice (epithelial fraction) relative to Balb/c (epithelial fraction) FC >0.3, FDR 0.05 (p<0.001). Genes are ranked from lowest (most significant) to highest (least significant) p-value. Downregulated genes, were analyzed through Gene set enrichment analysis (Highest overlap, GSEA; Molecular signatures – H Hallmark gene set) FDR 0.05. **(B)** Out of 19 downregulated genes, 15 were identified by the database. Table extracted from MSigDB. Each sample is a biological replicate (n=5 / group) Details about sample collection and analysis is found in the methods section.

(A)

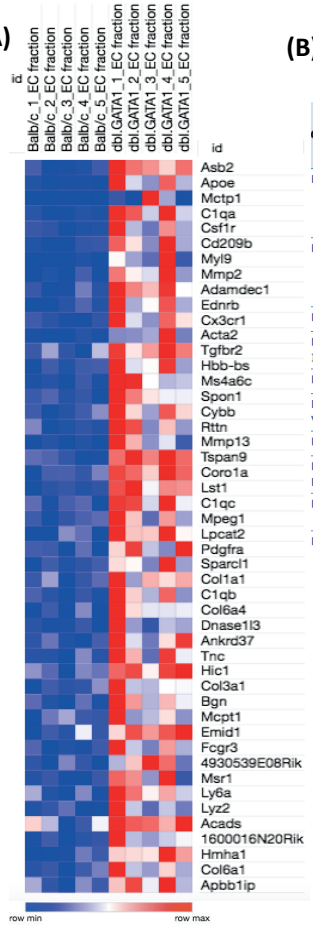

(B)

Gene Set Name [# Genes (K)]	Description	# Genes in Overlap (k)	k/K	p-value	FDR q-value
NABA_MATRISOME [1028]	Ensemble of genes encoding extracellular matrix and extracellular matrix-associated proteins	14		$9.73\ e^{-14}$	$1.29\ e^{-10}$
NABA_CORE_MATRISOME [275]	Ensemble of genes encoding core extracellular matrix including ECM glycoproteins, collagens and proteoglycans	8		$9.67\ e^{-11}$	$6.43\ e^{-8}$
PID_AVB3_INTEGRIN_PATHWAY [75]	Integrins in angiogenesis	5		$6.36\ e^{-9}$	$2.82\ e^{-6}$
REACTOME_EXTRACELLULAR_MATRIX_ORGANIZATION [87]	Genes involved in Extracellular matrix organization	5		$1.35\ e^{-8}$	$4.49\ e^{-6}$
KEGG_FOCAL_ADHESION [201]	Focal adhesion	6		$2.2\ e^{-8}$	$5.85\ e^{-6}$
REACTOME_CREATION_OF_C4_AND_C2_ACTIVATORS [10]	Genes involved in Creation of C4 and C2 activators	3		$7.3\ e^{-8}$	$1.62\ e^{-5}$
BIOCARTA_CLASSIC_PATHWAY [14]	Classical Complement Pathway	3		$2.21\ e^{-7}$	$4.19\ e^{-5}$
REACTOME_INITIAL_TRIGGERING_OF_COMPLEMENT [16]	Genes involved in Initial triggering of complement	3		$3.39\ e^{-7}$	$5.03\ e^{-5}$
PID_INTEGRIN1_PATHWAY [66]	Beta1 integrin cell surface interactions	4		$3.41\ e^{-7}$	$5.03\ e^{-5}$
BIOCARTA_COMP_PATHWAY [19]	Complement Pathway	3		$5.86\ e^{-7}$	$7.79\ e^{-5}$

(Figure 16) RNA-seq of Epithelial fraction of Δdbl.GATA1 mice (upregulated genes) under homeostatic conditions: (A) Heatmap shows total upregulated in dbl.GATA1 mice (epithelial fraction) relative to Balb/c (epithelial fraction), FDR 0.05 (p<0.001). Genes are ranked from lowest (most significant) to highest (least significant) p-value. **(B)** Upregulated genes, were analyzed through Gene set enrichment analysis (Top 10 overlap, GSEA; Molecular signatures – C2 Canonical pathways (CP: Curated gene sets)) FDR 0.05, log2>1.5. Each sample is a biological replicate (n=5 / group). Out of 39 downregulated genes, 33 were identified by the database. Table extracted from MSigDB. Details about sample collection and analysis is found in the methods section.

3.2 EOSINOPHIL REGULATION OF IMMUNE HOMEOSTASIS IN THE LAMINA PROPRIA (LP)

3.2.1 IEL homeostasis is altered in Δdbl.GATA1 mice

In addition to the function of the intestinal epithelial barrier as a physiochemical barrier, it also functions as reservoir for various intraepithelial lymphocytes (IELs). Primarily composed of CD8α+ lymphocytes, these immune sentinels play a key role for protective immunity against pathogenic entities at the barrier, while simultaneously maintaining epithelial homeostasis through the provision of important survival/activation signals[13]. In Balb/c mice, IELs are dominated by CD8αα TCRγδ+ (CD8γδ) t-cells and CD8αα TCRαβ+ (CD8αα) t-cells. Microbiota-induced CD8αβ TCRαβ (CD8αβ) t-cells, which have a 'memory-phenotype', are the least represented out of the 3 major IEL type. However, the precise proportion of the total IEL pool is likely to change depending on the strain of the mouse, diet and microbial communities present in a given cohort of mice.

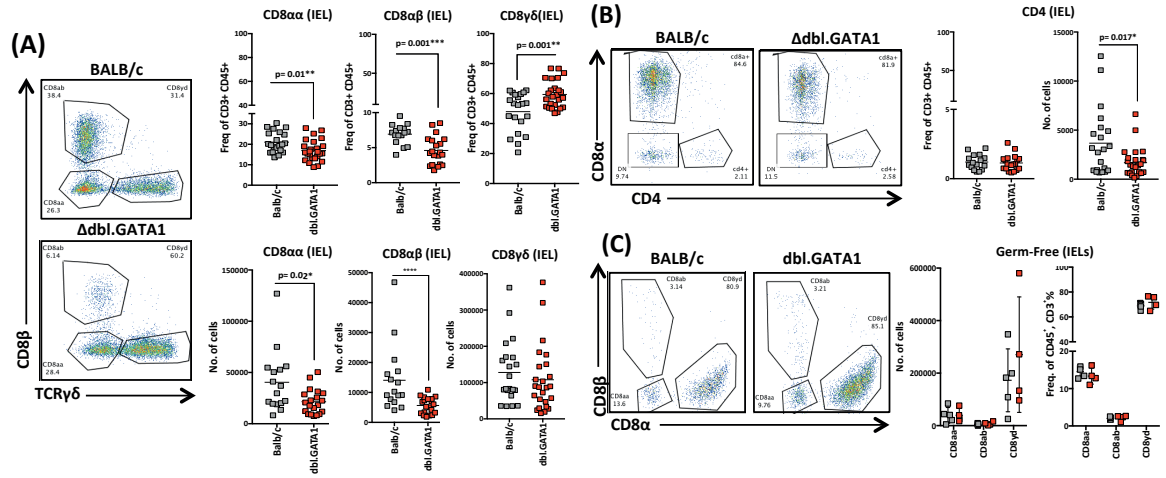

(Figure 17) CD8αα, CD8αβ IELs are reduced in the absence of Eosinophils: (A) Representative FACS plot identifying CD8 t-cells in the epithelial fraction (IELs); cells were pre-gated as live, CD45+ CD3+Cd8α+. Quantification of Cd8αα, Cd8αβ, Cd8γδ IEL within total CD45+ cells from jejunal epithelial fraction of SPF mice. **(B)** Representative FACS plot and Quantification of CD4+ IEL (pre-gated live CD45+ CD3+). **(C)** Representative FACS plot and Quantification of CD8+ IEL (pre-gated live CD45+ CD3+CD8α+), from germ-free mice. Data pooled from 3-4 independent experiments (n=3-5 per group). Statistical test unpaired student test ($p<0.0001$****, or p-value as reported in figure) – non-significant ($p>0.05$) p-values are not reported; Mann-Whitney test correction was conducted if SD values >0.05. Error bars represent SD between samples.

Given our previous findings of perturbed epithelial barrier homeostasis in Δdbl.GATA1 mice, we wanted to examine the impact of eosinophil-deficiency on IEL populations in this compartment. The frequency and number of CD8αα, CD8αβ, CD8γδ and CD4+ t-cell populations were assessed from total epithelial cell fraction, which in addition to IELs is comprised primarily of IECs and rare quantities of sub-epithelial fibroblasts that may have been shed off during the EDTA treatment

needed for IEC detachment from the lamina propria. Gating on live, CD45+ CD3+ cells, we observe a significant decrease in CD8αα+, CD8αβ+ t-cells in both frequency and number in Δdbl.GATA1 compared to control mice **(Figure 17A)**. Conversely, CD8γδ t-cells were increased in frequency, but are consequential to the loss of CD8αα+ and CD8αβ+ t-cells, as no increase was reported in cell number. This reduction in CD8αα+ and CD8αβ+ t-cells in Δdbl.GATA1 mice compared to Balb/c control mice is abolished in GF conditions – suggesting that their maintenance is dependent on microbiota-activation of eosinophils **(Figure 17B)**. We also examined CD4+ t-cells in the epithelial fraction, which are rare under homeostatic conditions – and no differences were found between Δdbl.GATA1 and Balb/c controls **(Figure 17C)**.

3.2.2 CD8 t-cell populations are unchanged in the SILP of Δdbl.GATA1 mice

Recent studies have highlighted a role for eosinophils in the regulation of immune cells in the lamina propria, but varying result across independent reports[161–163,165]. We therefore wanted to characterize and compare changes in various immune cell populations in the lamina propria that have been noted to be altered in Δdbl.GATA1 mice, to mice bred and raised in our SPF facility (both control and Δdbl.GATA1 groups).

First, we looked at CD8αα+, CD8αβ+ t-cells within the small intestinal lamina propria (SILP) compartment. We did not observe any changes in these populations in both number and frequency in Δdbl.GATA1 relative to the control **(Figure 18B)**. Therefore, it is likely that our previous observation of a decrease in CD8αα, CD8αβ IELs is particular to the intestinal epithelial compartment.

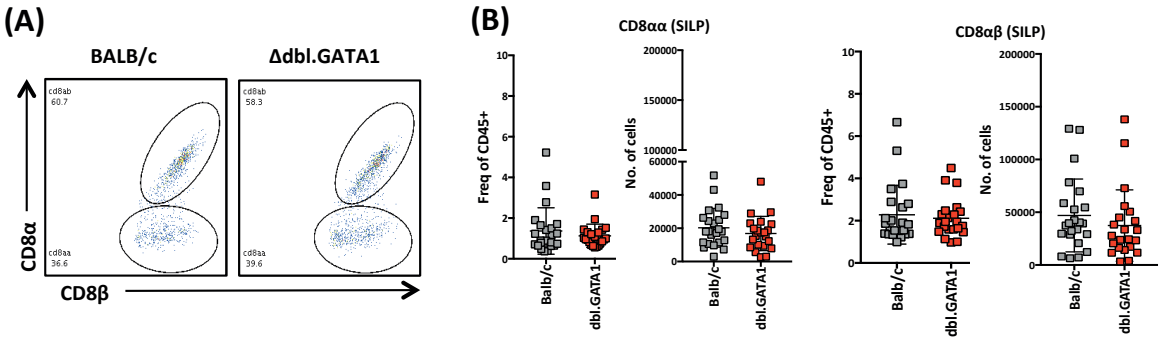

(Figure 18) Eosinophil-deficiency does not impact CD8+ T-cells in the lamina propria (LP) of the SI: (A) Representative FACS plot for CD8aa, CD8ab (pre-gated on live Siglecf- CD45+ CD3+ Cd8a+) **(B)** Quantification of CD8aa, CD8ab frequencies and absolute number from lamina propria of SI (jejunum). Data pooled from 3 independent experiments (n=3-5 per group). Error bars represent SD between samples. Statistical analysis (student-t test; not significant with p>0.05)

3.2.3 T-helper cell populations are unchanged in the SILP of Δdbl.GATA1

Next, we compared changes across the major T-helper cell populations (*i.e.* T-regulatory, Th17, Th2) in the lamina propria. We focused our analysis on these subsets as they have been reported to either increase or decrease in previous studies on SI eosinophil function[163]. T-regulatory cells are largely identified by their expression of transcription factor FOXP3+. However, they are noted to have various subtypes, with a significant proportion co-expressing transcription factors GATA3+ or RORγt+, required for differentiation of naïve-t helper cells into Th2, and Th17 cells respectively. As we did not notice a change in the frequency and number of FOXP3+GATA3+ and RORγt+FOXP3+ T-regulatory cells (data not shown), we collectively identified T-regulatory cells as total live CD4+ CD3+ FOXP3+ cells in our analysis. We observed no differences were observed in total T-regulatory cells between Balb/c and Δdbl.GATA1 **(Figure 19A)**. This finding is concurrent with observations from Sugawara et *al.* 2016 and Jung et *al.* 2015 [161,162]. Similarly, we did not observe any difference in Th17 and Th2 populations **(Figure 19B)** in Δdbl.GATA1 mice. Th17 and Th2 cells were identified as CD4+CD3+ Rorγt+ and CD4+ CD3+ GATA3+ cells, respectively. The absence of changes in Th2 populations in Δdbl.GATA1 mice was in agreement with all studies that have characterized T-helper cell populations in this strain. However, Sugawara et al. reported that eosinophils to be important for restraining Th17 populations (which are increased in Δdbl.GATA1 mice in their study) which does not agree with our findings[161].

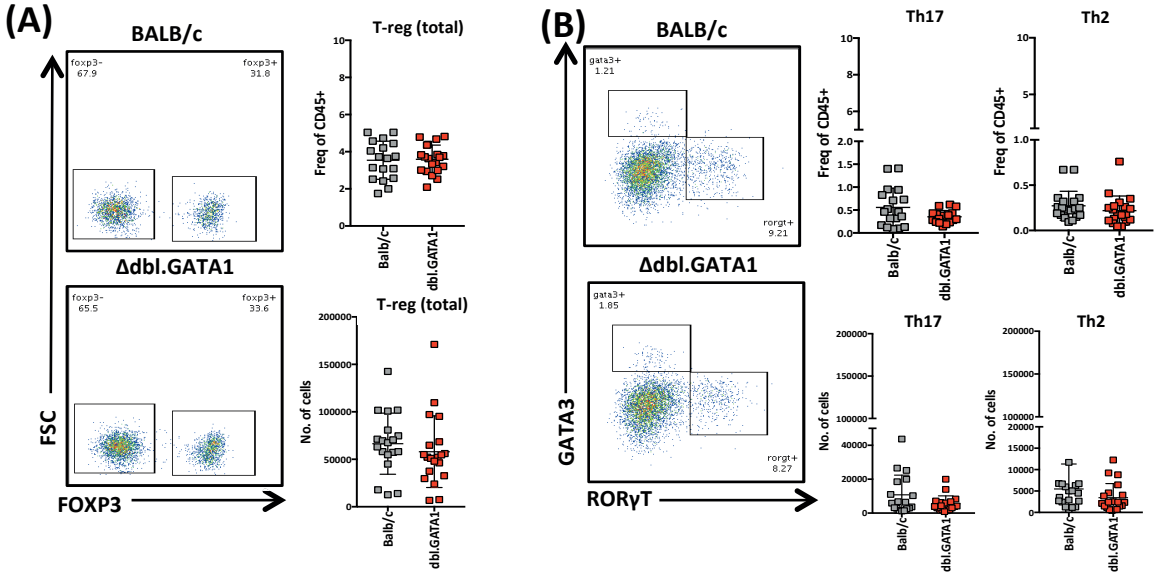

(Figure 19) Eosinophil-deficiency does not impact T-helper populations in the SI: (A) Representative FACS plot for T-regulatory cells (FOXP3+; pre-gated on live, CD45+ CD3+ CD4+), quantifications. **(B)** Representative FACS plot for Th17 (Roryt+) and Th2 (GATA3+) populations (pre-gated as live, CD45, CD3 CD4+), quantifications. Data pooled from 3-4 independent experiments (n=3-5 mice per group). Statistical analysis (student-t test; not significant with p>0.05). Error bars represent SD between samples.

3.2.4 Innate lymphoid cell populations are unchanged in Δdbl.GATA1 mice

Innate lymphoid cell (ILC) populations, particularly ILC3s are reportedly reduced in Δdbl.GATA1 mice[162]. Therefore, we sought to determine whether this population is also changed in our mice, in addition to extending our analysis to ILC2s populations in the lamina propria. We identified ILC3s as RORγt+ CD3- cells, and delineated various subsets of ILC3s with the natural killer-cell marker Nkp46 expressed by a fraction of ILC3s. In contrary to the findings by Jung et al. 2015, we did not see any changes in both frequency and number of either Nkp46+ or Nkp46- ILC3s **(Figure 20A)**. ILC2s were identified as CD3- GATA3+ cells, that were SSC^{lo} – in order to rule our possible contamination by basophils which are SSC^{int} due to the presence of cytoplasmic granules on their surface. While we identified a significant decrease in this population in terms of frequency in Δdbl.GATA1 mice, only a trend was observed in cell number – making it difficult to make a conclusion on whether or not a decrease is truly present **(Figure 20B)**.

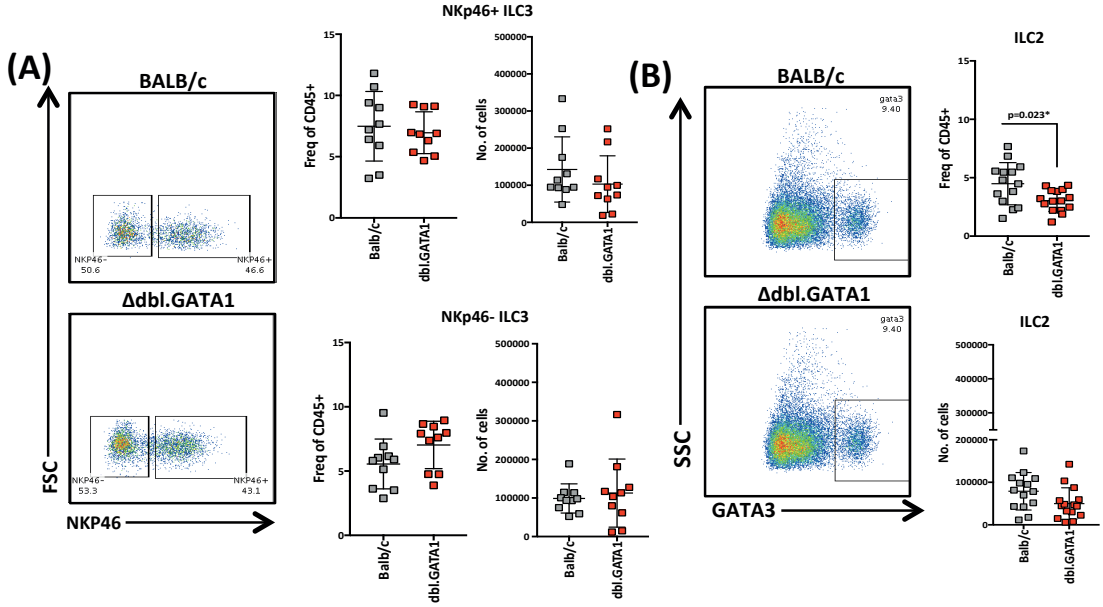

(Figure 20) Eosinophil-deficiency does not impact ILC2, ILC3 populations in the SI: (A) Representative FACS plot for ILC3s (Nkp46 +/-); pre-gated as live, CD45+ CD3- Roryt+, quantifications. **(B)** Representative FACS plot for ILC2 (GATA3+); pre-gated as live, CD45+ CD3- SSClo, quantifications. Data pooled from 2-3 independent experiments (n=3-5 mice per group). Statistical analysis (student-t test; $p<0.05$* or not significant with $p>0.05$). Error bars represent SD between samples.

3.2.5 CD103+ DCs and IgA+ Plasma cells are unchanged in Δdbl.GATA1 mice

Work by Chu et *al.* 2014, showed that eosinophil-deficiency led to decreased survival and numbers of IgA-producing plasma cells (IgA+ PCs) in the intestinal lamina propria – a primary focus of their study[163]. This finding was supported by similar observations from Jung et *al.* 2015[162]. In the former study, it was reported that CD103+ DCs, in addition to IgA+ PCs were decreased in Δdbl.GATA1 mice – and we proceeded to determine whether changes in these 2 populations were also present in our cohort of Δdbl.GATA1 mice. Since there are many subsets of CD103+ DCs that persist in the intestine under homeostatic conditions – we aligned our analysis to that of Chu et *al.*, 2014 - focusing our assessment of DCs to total MHCII+ CD103+ CD11c+ DCs without any further stratification. IgA+ PCs were identified as cells positive for surface IgA+, Ly6-c and MHCII^{int}, as this is the predominant subclass of microbiota-induced IgA PCs in the intestine[185]. Using these parameters, we failed to see any differences in both CD103+ DCs and IgA+ plasma cells in the SI of Δdbl.GATA1 mice **(Figure 21)**.

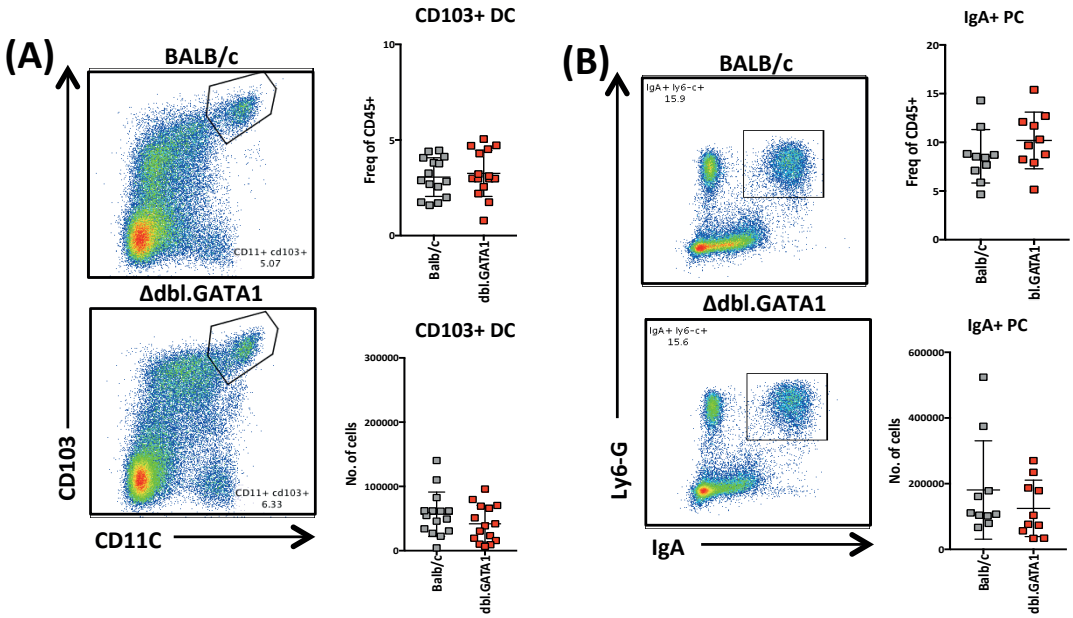

(Figure 21) Eosinophil-deficiency does CD103+ DCs nor IgA+ plasma cell populations in the SI: (A) Representative FACS plots; quantifications for CD103+ DC (pre-gated as live, CD45+ MHCII+) population **(B)** Representative FACS plot; quantification for IgA+ plasma cells (pre-gated as live, CD45+). Data pooled from 2-3 independent experiments (n=3-5 mice per group). Statistical analysis (student-t test; not significant with p>0.05). Error bars represent SD between samples.

3.3 DISCUSSION

Some intestinal eosinophils reside in close proximity to the vasculature surrounding the epithelial stem-cell niche, and we first hypothesized that there may be a functional impact of this spatial-interaction in the maintenance of IEC progenitors. However, this was not the case, as eosinophil-deficiency did not result in gross epithelial defects, with regards to the proliferation and differentiation of these cells into specialized subsets **(Figure 10, 11)**. Instead, we identified a role for eosinophils in regulating epithelial turnover – not at the level of survival, but rather in the restitution/migration of epithelial cells along the villi, which is delayed in the absence of eosinophils **(Figure 12)**. Concurrent with this delay in epithelial turnover, is increased intestinal leakage in response to microbiota colonization – a finding supported by increased mast cell degranulation in Δdbl.GATA1 **(Figure 13, 14)**. Collectively, these defects are indicative of ongoing barrier instability – which could have detrimental consequences to intestinal homeostasis, due to an insufficient barrier response against luminal commensal microbiota.

Impact of eosinophil-deficiency on epithelial barrier homeostasis

Intestinal barrier integrity is dependent on many factors, such as the epithelial-epithelial cell junctions, anti-microbial peptide and mucus secretion. We observed that expression of genes encoding for molecules involved in these processes are not changed in our RNA-seq analysis **(supplementary table 5,6)**, which is concurrent with our findings for normal numbers of specialized epithelial cells such as paneth and goblet cells.

Δdbl.GATA1 mice presented with increased intestinal permeability and delayed epithelial restitution. In an attempt to identify altered pathways that could account for these differences, we conducted GSEA on differentially regulated (upregulated) genes in the Δdbl.GATA1 mice relative to Balb/c controls **(Figure 16; supplementary table 6)**. Interestingly, we found this data set to be enriched for genes that encode for factors within the ECM/matrisome and remodelling enzymes (45% of dataset; *e.g.* MMP2, Adamdec1, MMP13, ADAM33). It is known that MMPs could increase intestinal barrier permeability through the modifications of tight junction/adhesion molecules at a protein level[186,187]. Therefore, although we do not see changes in barrier related genes at a transcriptional level, upregulation of modifiers and other ECM components could have consequences on barrier function that may be occurring at the level of protein modification. Furthermore, it is also well established that alterations in ECM composition and organization

change the mechanical properties of a given cellular layer, thereby impacting the migratory capacity of cells[18,30]. It is tempting to suggest that perhaps, in addition to providing a possible explanation for the increased leakage we see in Δdbl.GATA1 mice – these alterations in ECM could also account for the delayed IEC migration/turnover we observed.

It is important to note however, that despite the defects we observed in Δdbl.GATA1 mice – we did not observe any overt signs of increased morbidity in these mice under homeostatic conditions. We speculate that under conditions of significant dysbiosis or infection with pathogens – there may be enough damage/stimulatory signals that could tip this threshold and where we could observe the consequences of the defects we observed under homeostatic conditions. Indeed, in this regard, Buonomo et *al.* (2016) has shown resident SI eosinophils to be protective against *Clostridium difficile* infection, with eosinophil-deficiency resulting increased morbidity in infected mice[64]. They show eosinophils confer increased survival, not through protective immunity (bacterial burdens remained the same), but rather through the maintenance of epithelial barrier integrity – as depletion of eosinophils resulted in significant intestinal leakage in response to infection. However, the mechanism downstream of eosinophil-mediated maintenance of barrier integrity is currently unknown.

RNA-seq analysis reveals significant downregulation of molecular targets within the PPAR-a signalling pathway

In addition to potential changes in the ECM, our RNA-seq analysis has also revealed unexpected changes in the PPAR-α pathway in the absence of eosinophils. GSEA analysis of downregulated genes revealed enrichment (~50%) for known targets of PPAR-a signalling **(Figure 15; supplementary table 5)**. PPAR-α signalling has primarily been studied in the context of metabolism (particularly fatty acid oxidization) in the liver[188], but studies have slowly accumulated over the past decade, showing functions for this pathway beyond lipid metabolism. Indeed, this pathway has been shown to be important for the regulation of innate-immune responses, anti-microbial defense, and epithelial barrier homeostasis[189,190].

A study by Bünger et *al.* (2007) characterized the transcriptional changes resulting from PPAR-α deficiency in the small intestine – which yielded very similar transcriptional signatures to what we have observed in Δdbl.GATA1 deficiency[189]. It's important to note that some of the targets

reported to be downregulated in this study were not recognized components of the curated genes from the PPAR-α signalling pathway in the GSEA database we used – showing the limitation of publically available databases. Nonetheless, ~50% of the genes downregulated in PPAR- α ko mice matched with our own RNA-seq analysis (*e.g.* Cyp4a10, Pdk4, Slc25a20). In addition, genes that they have shown to be increased by PPAR-α stimulation (*e.g.* Angptl4, Hmgcs2, Acadl and Pex11a) are also seen downregulated in our RNA-seq **(Figure 15, supplementary table 5)**.

As mentioned previously, genes belonging to the complement pathway (*i.e.* C1qb, C1qc, C1qa) and ECM-related proteins (*i.e.* Mmp13, Mmp2, Adamdec1) to be significantly upregulated in Δdbl.GATA1 mice **(Figure 16, supplementary table 6)**. This observation is concurrent with genes known to be upregulated in response to PPAR-a deficiency based on the study by Bünger et al, 2007 – which further supports the possibility PPAR-α signalling is reduced in the absence of eosinophils. These findings are surprising, given that our RNA-seq analysis was confined to cells isolated from the intestinal epithelial layer, whereas the data set from Bünger et *al.* 2007 was conducted on full PPAR-α ko mice. Indeed, RNA-seq analysis of the lamina propria fraction of Δdbl.GATA1 mice (discussed in chapter 4) did not reveal any changes in PPAR-α targets. These genes were also expressed at low levels even in both Δdbl.GATA1 mice and Balb/c controls. Furthermore, expression of PPAR-α-associated genes, were very low in the lamina propria fraction (for both Δdbl.GATA1 and Balb/c mice) relative to the epithelial fraction (data not shown). Overall these findings suggest that epithelial cells are the primary cell type expressing PPAR-α in the intestine.

However, it remains unclear whether downregulation of PPAR-α signalling is due to the loss of an eosinophil-derived agonist(s) that drives tonic PPAR-α signalling in the intestine, or whether it is secondary to ongoing barrier dysfunction[190,191]. Eosinophils are known to produce various lipid mediators (*e.g.* LTC4, LTB4, 15-HETE), and to our knowledge – only LTB4 is a known canonical PPAR- α agonist[59,79,192,193]. As characterization of lipid mediators has not been done on intestinal resident eosinophils, it is possible that eosinophils could be generating even more PPAR-α agonists in a manner specific to the small intestine. Indeed, given their capacity for arachidonic acid metabolism – they are equipped with the machinery to generate PPAR- α agonists[79,192,193].

Eosinophil regulation of immune homeostasis

Our characterization of immune population differences between Balb/c and Δdbl.GATA1 mice revealed few differences when comparing T-cell (i.e. CD8αα, CDαβ, Th2, Treg, Th17), IgA-producing PC, Innate lymphoid (i.e. ILC2, ILC3) and CD103+ DC populations in the intestinal lamina propria – suggesting that, at least under homeostatic conditions SI eosinophils do not appear to regulate these cell subsets. Interestingly however, we do note a consistent reduction in CD8αα and CDαβ IEL populations in Δdbl.GATA1 mice compared to Balb/c mice **(Figure 17)**.

Microbiota colonization seems to enhance the survival/differentiation of CD8αα and CDαβ IELs, as these populations are reduced in GF mice. However, this induction in response to the microbiota only occurs in the presence of eosinophils – as Δdbl.GATA1 mice had comparable numbers of these two populations to GF mice. This seems to be a phenomenon restricted to the epithelial layer, as these populations did not differ in the lamina propria of Balb/c and Δdbl.GATA1 mice.

It's important to note that no differences were observed when comparing CCR9 nor CD103 expression in these IEL populations - suggesting that deficiency in homing to the intraepithelial layer is not to blame for their decreased numbers in Δdbl.GATA1 mice (data not shown). We also do not think that this defect is accounted for by decreased survival signals for the following reasons (1) Cd8γδ t-cells share similar requirement for survival as CD8αα and CD8αβ T-cells (*e.g.* IL-7, IL-15, CCL25) and given that CD8γδ t-cells are present in normal frequencies, it seems unlikely that the defect observed in Δdbl.GATA1 mice is due to a reduction in canonical survival factors commonly utilized by IELs (2) RNA-seq analysis did not reveal any changes in the expression of these factors – at least at a transcriptional level (data not shown).

Taking into account the fact these populations are decreased under GF conditions, it is quite possible that the issue is at the level of induction by DCs at secondary lymphoid sites (e.g. Peyer's patches, mesenteric lymph node). CD103+ DCs are ubiquitous in the small intestine, and have a strong capacity to sample luminal antigens and promote the differentiation of IELs[2,14]. While we did not see a difference in this population between Δdbl.GATA1 and Balb/c, there is a large diversity of CD103+ DC subtypes and it could be possible that a special subset that preferentially induces microbiota-induced IEL responses is defective in the absence of eosinophils. More in depth analysis of subtypes of CD103+ DCs would be needed to address this question.

Addressing inconsistencies between our findings and the literature

It is important to note that our observation of relatively normal immune cell homeostasis in Δdbl.GATA1 mice is contrary to previous literature focused on eosinophil function in the small intestine. Below, we address some key caveats that may account for these inconsistencies.

Findings from 4 independent studies have shown significant alterations in immune homeostasis in the absence of eosinophils under homeostatic conditions. Chu et *al.* 2014, reported a decrease in IgA+ producing B-cells, CD103+ DCs and CD4 T-cells populations – which they largely attributed to the capacity of eosinophils to induce active TGF-β signalling (secretion or activation of latent TGF-β via MMP9 release) and, production of B-cell survival factors BAFF and APRIL[163]. Jung et *al.* 2015, reported a similar decrease in IgA-producing B-cells and ILC3s but reported no other changes in other immune cell types in the SI lamina propria[162]. Furthermore, they reported that this was through a mechanism dependent on IL-1β – reporting no differences in TGF- β, APRIL and BAFF production. Chu et al. 2014, did not observe any changed in IgA-producing B-cells under homeostatic conditions[71]. Finally, a more recent study from Sugawara et al. 2016, showed that eosinophils were required for restraining Th17 responses in a mechanism dependent on eosinophil production of IL-1Rα[161]. Whilst they did not look at any of the other immune populations discussed in the two prior studies, Th17 populations were reported to be increased due to unregulated IL-1β signalling; a finding that in disagreement with previous studies.

Given that microbiota composition is known to change between facilities, we suggest that this may account for the discrepancy between our findings and those reported in the literature. For example, the pathobiont Segmentous Filamenous Bacteria (SFB) are potent stimulators of IgA-producing B-cells, ILC3s and (especially) TH17 populations[194]. This strain is absent in the microbiome of mice bred in our facility, and as a consequence, the immune microenvironment in our study may not be conducive to the manifestation of defects observed in the other studies. Regardless, its an intriguing possibility that the detrimental consequences of the epithelial barrier defects we observed in this study may become more apparent in facilities with SFB, as SFB-colonized mice have a heightened-immune environment presenting with more opportunity to observe dysregulated immune responses that would occur. Furthermore, they are also adherent to the epithelium – and may cause overt inflammatory responses in mice with a compromised intestinal epithelial barrier[195].

Taken together, we believe it is increasingly important that future studies on the homeostatic function of eosinophils elaborate on certain aspects of colony maintenance such as, whether littermate controls were used, dietary composition/food and information about the general composition of microbes present in maintained mouse colonies (particularly if these facilities harbour strongly immunogenic pathobionts such as SFB). Discussing these peculiarities and inconsistencies within the literature, particularly in the study of tissue resident eosinophil populations will be necessary in order to advance our collective understanding of their homeostatic contributions. Furthermore, identifying the factors that contribute to these inconsistencies will be beneficial as it may itself, provide invaluable clues to and insight on the true function of eosinophils in the intestine.

Chapter 4: Eosinophil-mediated villous maintenance in response to the microbiota

In the previous chapter, we provide evidence for a critical role of eosinophils in the maintenance of barrier integrity in response to microbiota colonization. However, it is unclear whether eosinophils influence other aspects of intestinal homeostasis beyond immunity.

In the Chapter 2, we identified eosinophils to preferentially reside in the villous lamina propria in close proximity to functionally relevant structural cells (e.g. endothelial cells, myofibroblasts). Eosinophils are known to crosstalk with stromal cells in diseased conditions such as asthma and IBD – where eosinophils have been identified to have pathological role by driving excessive tissue remodelling. However, whether small intestinal eosinophils impact on tissue architecture and remodelling under homeostatic conditions has never been explored to date.

In this chapter, we characterize the architectural changes in the small intestinal villous resulting from eosinophil deficiency under homeostatic conditions.

4.1 EOSINOPHILS ARE REQUIRED FOR THE MAINTENANCE OF SI VILLI

4.1.1 Δdbl.GATA1 mice exhibit decreased villous surface area

To investigate the contributions of resident eosinophils to villous homeostasis, we utilized wholemount imaging as a tool to characterize and identify changes in tissue-architecture that may occur in the absence of eosinophils. To do this, we did a comparative analysis of intestinal tissue from Balb/c vs. Δdbl.GATA1 mice, sampled from 5 different regions of the SI **(Methods - Figure 50)**. For visualization purposes, we often used VEGFR2+ staining to identify blood endothelial cells (BECs) – in order to visualize the overall area of the villus - using the blood vessel cage area as a proxy.

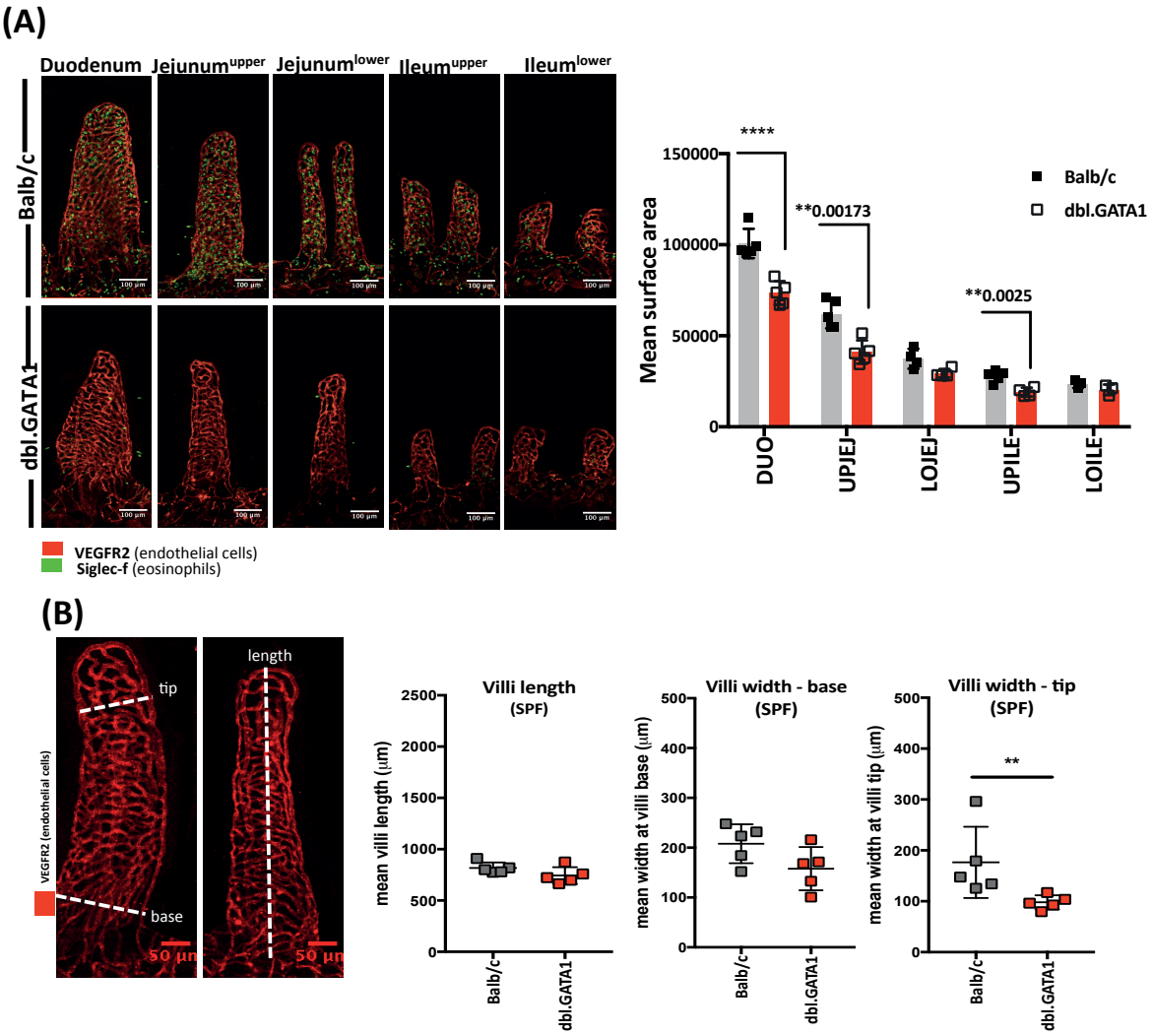

(Figure 22) Villous surface area is decreased in the small intestine of dbl.GATA1 mice: (A) Representative images of villi sample from different intestinal compartments (by wholemount imaging) and corresponding quantifications of villus area. Blood vessel cage area (VEGFR2 staining) was used a proxy for villus area**. (B)** Schematic for quantification of villus width/length from the samples measured in (A); Width/length measurements of villi from upper jejunum region of Balb/c (grey bar) and dbl.GATA1 (red bar) under homeostatic conditions**.** *Each data point represents the mean surface area of more than >30 villi per mouse*. VEGF2 staining (red) was used for determination of villous boundary. More details about sampling can be found in methods. Statistical analysis two-way ANOVA ($p<0.01$**, $p<0.0001$****). Error bars represent SD within group.

The visualization of the blood vasculature also allowed us to delineate between the lamina propria and the epithelial barrier. Furthermore, it allows is to better estimate eosinophil localization within this tissue. Overall, we saw a significant decrease of the global villous surface area of the small intestine – particularly the Duodenum (~27%), Upper Jejunum (~35%) and Upper ileum (~30%) in the absence of eosinophils **(Figure 22A)**. On average, this decrease was mostly attributed to decreased width of the villus, rather than differences in villous length **(Figure 22B)**.

We also checked whether there were any structural abnormalities in blood vessel and lymphatic branching, as eosinophils are known to secrete factors that promote angiogenesis in previous studies[196–198]. We did not see any differences in either lymphatic **(Figure 23)** or vasculature networks **(Figure 24)** between Balb/c and Δdbl.GATA1 mice. Although, parameters such as lacteal length and vessel length were generally decreased in Δdbl.GATA1 mice compared to controls, these differences were lost when normalized to villus size, suggesting they are simply proportional to – rather than causative of – decreased villus size.

Lastly, we looked at the relative frequencies of various stromal cell subsets in the lamina propria. CD45- Stromal cells in the LP of Balb/c and Δdbl.GATA1 mice were categorized into 4 major subsets; $GP38^{+}$ $CD31^{-}$ (GP38+ fibroblasts), $GP38^{+}$ $CD31^{+}$ (LECS), $GP38^{-}$ $CD31^{+}$ (BECS) and $GP38^{-}$ $CD31^{-}$ cells (DN) – a gating strategy followed from a resource paper by Stzepourginski et *al.* (2015)[199]. Frequencies of these 4 stromal cells subsets were comparable between Δdbl.GATA1 and Balb/c mice suggesting that the villous phenotype observed in the absence of eosinophils is not due to decreased stromal cells **(Figure 25B)**. Nonetheless, this does not rule out changes in the activation status of these cells, which could contribute/account for the villous defect observed in Δdbl.GATA1 mice – a possibility discussed in later sections of this thesis.

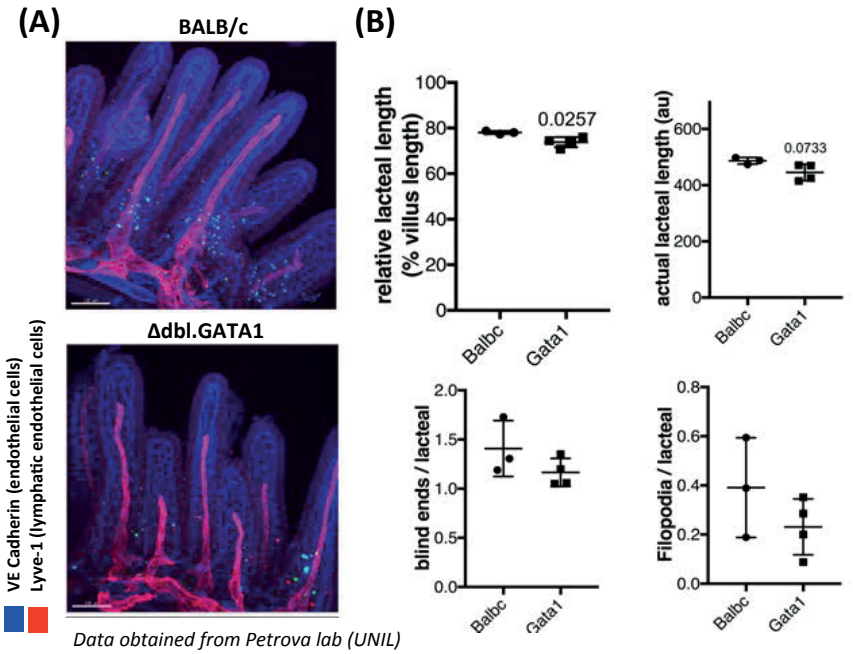

Data obtained from Petrova lab (UNIL)

(Figure 23) No gross defects in villous lymphatics of dbl.GATA1 mice :
(A) Representative images of villi sampled from jejunum with lacteals/ lymphatics (red: VEGFR2) length, filopodia number and 'blind ends' quantified in **(B)** (with the latter 2 being hallmarks of active lymphangiogenesis) by our collaborators (JBL-petrova lab).

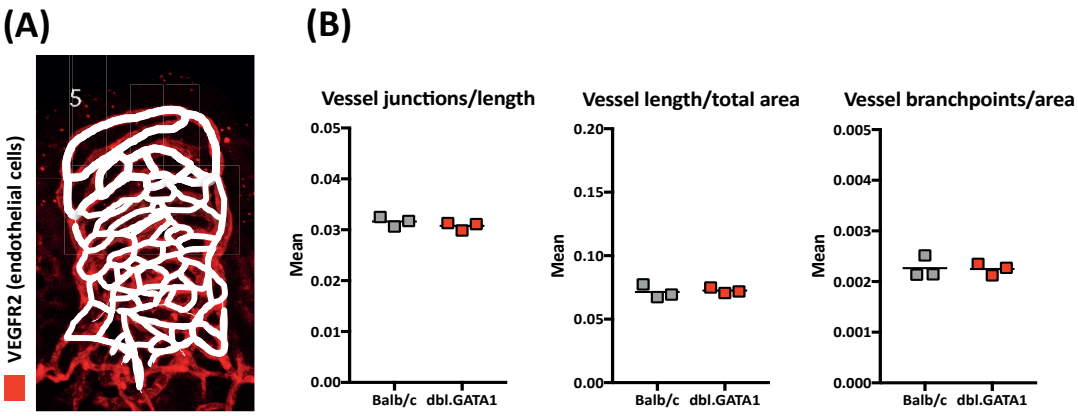

(Figure 24) No gross defects of villous blood vasculature network in dbl.GATA1 mice : (A) Representative image of traced vessel networks – transposed to original image; vessels were traced from villi images manually and ran on Angiotool software – readouts were average number of junctions and branchpoints in the vessel network, in addition to vessel length **(B)**. All readouts were normalized to surface area. Villi with VEGFR2 staining blood endothelial cells. Each data point represents a mean of >15 villi per mouse.

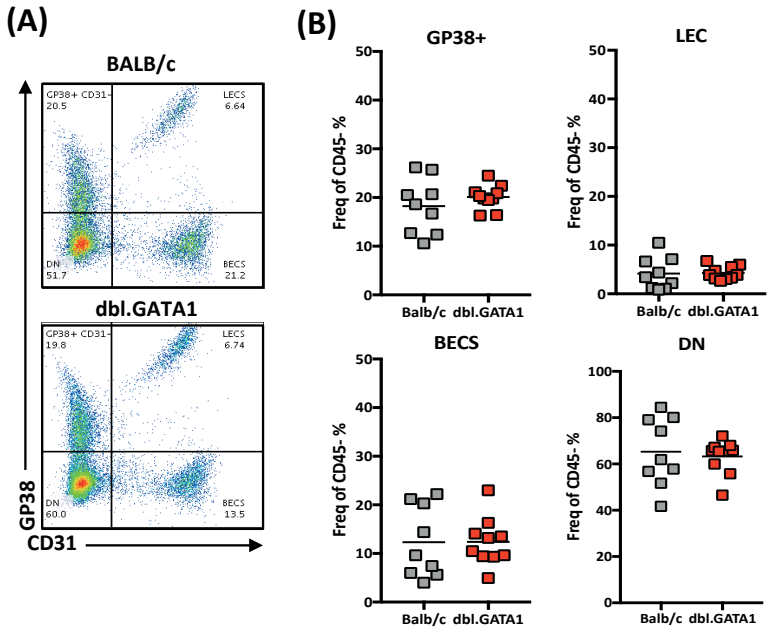

(Figure 25) SI stromal cell populations are present at normal frequencies in Δdbl.GATA1 mice: (A) Representative FACS plot of gating for intestinal stromal subsets; GP38+ (podoplanin), lymphatic endothelial cells (LECS; CD31+ gp38+), blood endothelial cells (BECS, CD31+ gp38-) and double negative cells (DN, gp38-CD31-) were quantified **(B)** in frequency of live CD45- cells in the intestine (jejunum). Data pooled from 2 independent experiments with (n=4-5 mice per group). Error bars represent SD within group

4.1.2. Carriage of Δdbl.GATA1 mutation in CD45- cells does not contribute to villous defect

In an effort to validate our observations, we generated bone-marrow chimeras and determined whether we see an induction of, or recovery from, the villous shrinkage-phenotype associated with eosinophil-deficiency. For this purpose we performed lethal irradiation of Balb/c mice, which were reconstituted with marrow from Δdbl.GATA1 donors (eosinophil-deficient), and compared these to irradiated Δdbl.GATA1 mice reconstituted with Balb/c marrow (eosinophil competent). We saw that reconstitution of eosinophils in ΔdblGATA1 mice by transfer of Balb/c bone marrow was sufficient to induce villous recovery in recipient, Δdbl.GATA1 mice **(Figure 26A)**. Conversely, irradiated Balb/c mice reconstituted with of Δdbl.GATA1 marrow resulted in reduced villous area **(Figure 26B)**. These data indicate that eosinophil-competency is the primary factor responsible for the villous defect observed in Δdbl.GATA1 mice, rather than being driven by off-target effects of Δdbl.GATA1 mutation in non-hematopoietic cells.

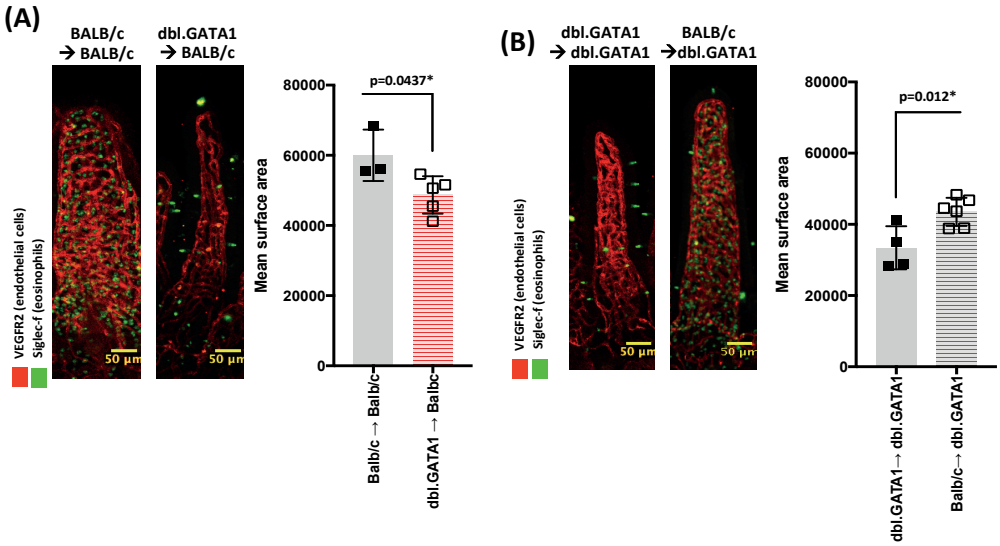

(Figure 26) Villous phenotype in dbl.GATA1 mice is not due to expression of GATA1 mutation in non-hematopoietic compartment: (A) Representative image and quantification of mean villous surface area of irradiated Balbc mice reconstituted with either bone marrow from Balb/c (grey bar) or dbl.GATA1 (red-striped bar) donor mice **(B)** irradiated dbl.GATA1 mice reconstituted with either bone marrow from age, gender-matched dbl.GATA1 (grey bar) or Balb/c (red-striped bar) donor mice. All analysis conducted >9 weeks post-reconstitution. VEGF2 staining (red) was used for determination of villous boundary. Each data point represents a mean average surface area >30 villi sampled per mice. Statistical analysis by student t-test (p-values as indicated in graph). Error bars represent SD within group

4.1.3. Mice deficient in γc-/- signalling present with similar villous defect to Δdbl.GATA1 mice

Common-γ chain signalling has been shown to be critical for eosinophil survival in the small intestine[72]. This is a tissue-specific trait that is not required for eosinophil survival in other tissues such as the thymus, lung and uterus where eosinophils also reside under homeostatic conditions rendering these mice a useful model to further validate a role for SI eosinophils in regulating villous size **(Figure 27A)**. To further validate that the loss eosinophils accounts for reduced villous area observed in Δdbl.GATA1 mice – we proceeded to compare the villi of NOD.SCID vs. NOD.SCID x $\gamma c^{-/-}$. [ii]Concurrent with our findings in Δdbl.GATA1 mice, we found that mice deficient for the common-γ chain exhibit a reduction in villous surface area **(Figure 27B)**.

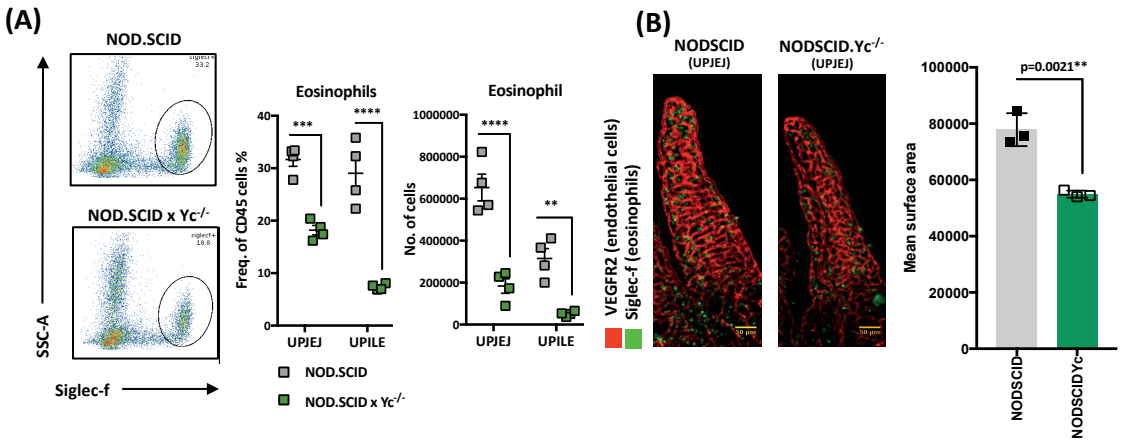

(Figure 27) Common γ chain deficient mice have decreased SI eosinophils and present similar villous area defect as dbl.GATA1 mice: (A) Representative FACS plot for Eosinophils (Siglecf+, SSChi) pre-gate as live CD45+ cells from upper jejunum of either NOD.SCID or NOD.SCIDYc-/- mice; along with quantifications presented as freq of eosinophils within CD45+ cells, and absolute number – n=3-4 mice per group. Statistical analysis two-way ANOVA p<0.01**, p<0.001***, p<0.00001****) **(B)** Representative wholemount images of Villi from UPJEJ of NODSCID (grey bar), NODSCID.Yc-/- mice (green bar) alongside quantifications of villous size – VEGF2 staining (red) was used for determination of villous boundary. Each data point represents mean surface area of >30 villi sampled per mouse. Error bars represent SD within goup

[ii] **Note:** NOD.SCID vs NOD.SCID Yc-/- mice were used as single common-γ chain mice were not readily available at our facility for these pilot experiments

4.1.4 Cellularity does not contribute to the maintenance of villous surface area

Previous studies show that Δdbl.GATA1 mice exhibit reduced cellularity in the SI, marked by a decrease in cells such as IgA-producing B-cells, CD4 T-cells and ILC3s – which make up a considerable percentage of total cells in the intestine[162,163]. Although we did not see these differences in our own experiments, we decided to test whether cellularity had an impact on villous size using Rag2$^{-/-}$ mice – which are deficient in both T and B-cells. Compared to control C57.B6 mice, we did not observe any changes in mean villous area suggesting that reduced cellularity does not have an impact on villous size **(Figure 28)**. Furthermore, it also suggests that T/B cells do not contribute to eosinophil-regulation of villous homeostasis.

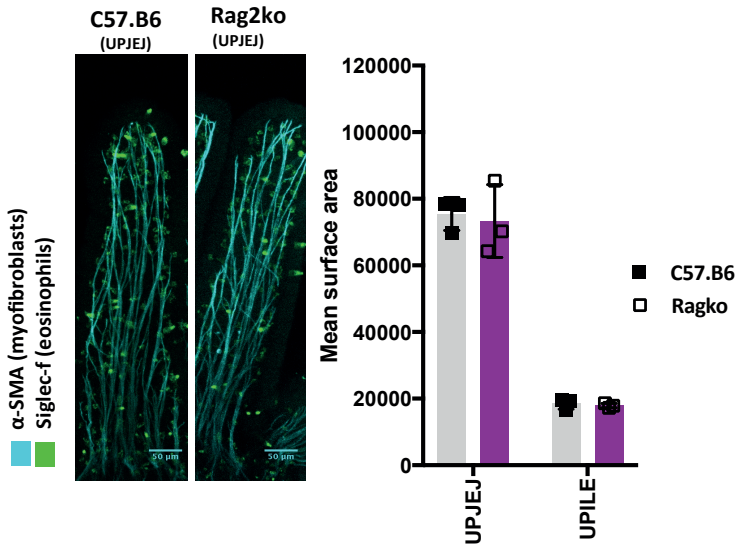

(Figure 28) Cellularity does not impact villous size: Representative wholemount image of villi from the upper jejunum (UPJEJ) and upper ileum of C57.B6 and Rag2ko mice – myofibroblasts (a-SMA, cyan) was used to determine villi boundary **.** Quantifications of mean surface area, each data point is average of >30 sampled villi (n=3 mice per group). Error bars represent SD within group.

4.1.5 IL-4r signalling is dispensable for eosinophil-mediated villous maintenance

Eosinophils are noted to be the primary IL-4 expressing cells in the small intestine under homeostatic conditions. Given that several studies have attributed Eosinophil-dependent IL-4 signalling as a key mechanism linking these cells to the maintenance of tissue homeostasis, we wanted to test whether the loss of IL-4 signalling has an impact on villous size[65,113,159]. Using IL4r-α ko mice, we observed no changes in villous area compared to control C57.B6 mice – which makes the contributions of homeostatic IL-4 signalling on the maintenance of villous area unlikely **(Figure 29).**

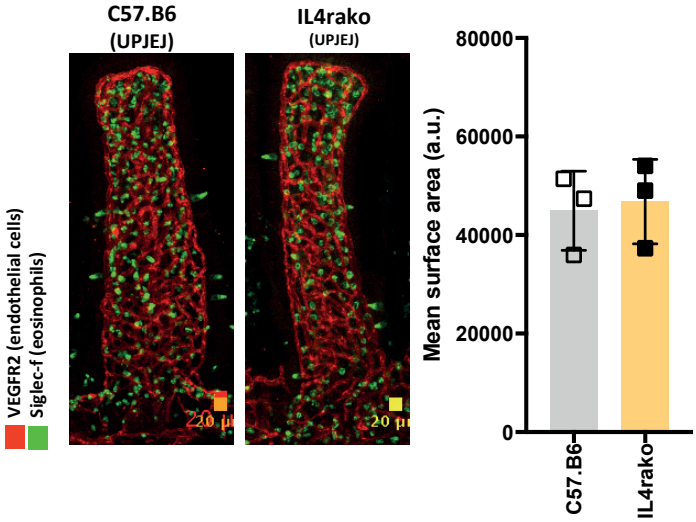

(Figure 29) IL-4r signaling is dispensable for eosinophil-mediated villous maintenance: Representative wholemount image of villi from the upper jejunum (UPJEJ) of C57.B6 and IL4rako mice. Vessel cage area (VEGFR2, ref) was used to determine villus boundary. Quantifications of mean surface area, each data point is average of >30 sampled villi (n=3 mice per group). Error bars represent SD within group.

4.2. VILLOUS DEFECT IN EOSINOPHIL-DEFICIENT MICE IS INDUCED IN RESPONSE TO MICROBIAL COLONIZATION

4.2.1 Villous defect in Δdbl.GATA1 mice presents shortly before the suckling-weaning transition period

In order to gain insight on the mechanism responsible for driving the villous defect observed in Δdbl.GATA1 mice, we sought to identify the approximate developmental period within which this phenotype arises. As mentioned in Chapter 2.2, eosinophils are present in the SI in fetal life, but only fully migrate into the villous lamina propria shortly before the suckling-weaning period. Given the rapid nature of developmental processes (*i.e.* villus formation, tissue growth) during this period, it was imperative for us to do our analysis on littermate controls - as even discrepancies in birth time of a few hours can give drastic, artifactual differences in villus morphology this early in life, making it difficult for us to conduct an accurate assessment. Therefore, we compared the villous surface area of littermate-controlled mice Balb/c and Δdbl.GATA1 mice, generated from heterozygous breedings (Δdbl.GATA1$^{+/MUT}$ x Δdbl.GATA1$^{+/MUT}$) at P7 and P10 post-natal life. Both VEGFR2 and α-SMA were used as markers for endothelial and myofibroblasts/smooth muscle cells, respectively – serving as structural cues that make it easier to visualize the overall villous architecture within which eosinophils lie.

We observed that at P7, all villi are positive for eosinophils – with these cells mostly localized at the lower ½ of the villous. At this stage, we did not see any differences in villous surface area between Balb/c and Δdbl.GATA1 mice **(Figure 30A)**. However, when we looked at a slightly later stage of development at P10, we see a dramatic decrease in villous surface area (~50%) in the absence of eosinophils **(Figure 30B)**. This finding is very interesting, as this phenotype arises just before the time when many environmental changes are noted to occur such as dietary transition to solid food and when the neonatal microbiota undergoes a period a rapid change, growing in increasing complexity both in diversity and abundance[200]. Also of note, the ~50% decrease in villous area is more notable than what we observed in adults, suggesting that some sort of compensation/adaptation may be occurring in later life.

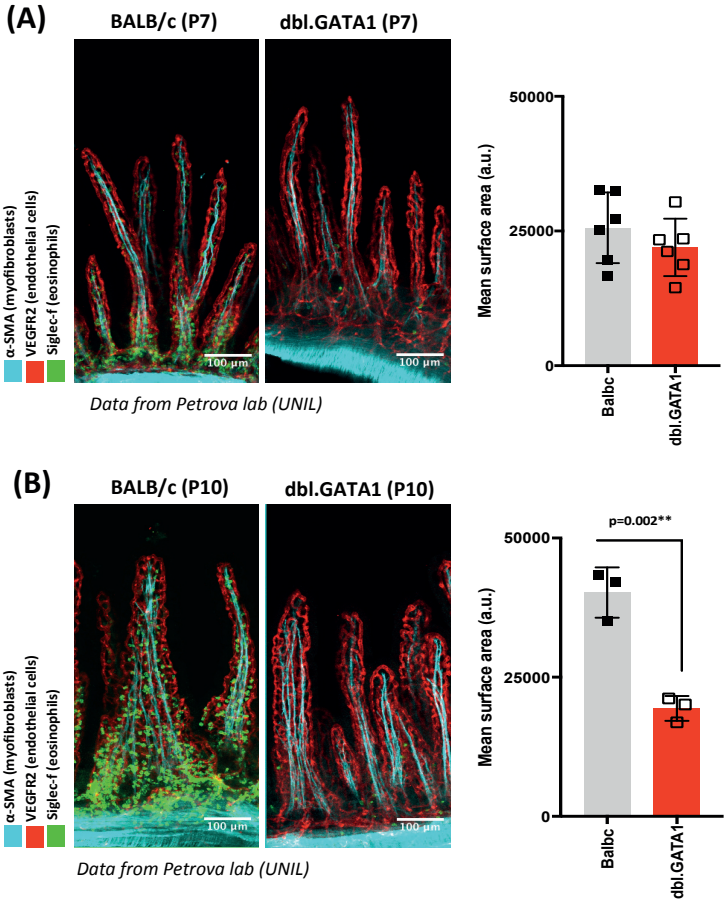

(Figure 30) Villous defect observed in eosinophil-deficient mice occurs shortly before sucking-weaning transition period:
(A) Representative wholemount images and corresponding villous area quantifications from Balb/c and dbl.GATA1 (littermate) mice at day 7 post-natal **(A)** and day 10 post-natal **(B)** For quantification of villous area VEGFR2 staining was used to determine villous boundary. Each data point corresponds to mean surface area >20 villi sampled from the proximal intestine per mouse. Data pooled from 2-3 breedings. Statistical analysis (unpaired) Student-test p<0.01** Error bars represent SD within group.

4.2.2 Eosinophils mediate villous protective effect in response to the microbiota

The microbiota is known to influence a wide variety of cellular and physiological processes in the intestine. Eosinophils are equipped with a multitude of immune sensors, enabling ample opportunity for these cells to respond to microbial-derived cues[59,176]. As previously discussed, our preliminary TEM data suggests that microbial colonization status influences cellular activity of SI eosinophils **(Figure 8)**. This observation, coupled with the identification of villous defects occurring at P10 – has lead us to speculate that the villous phenotype we observe may occur in response to the microbiota. To test this hypothesis, we compared the villous surface area of Balb/c and Δdbl.GATA1 mice under germ-free conditions.

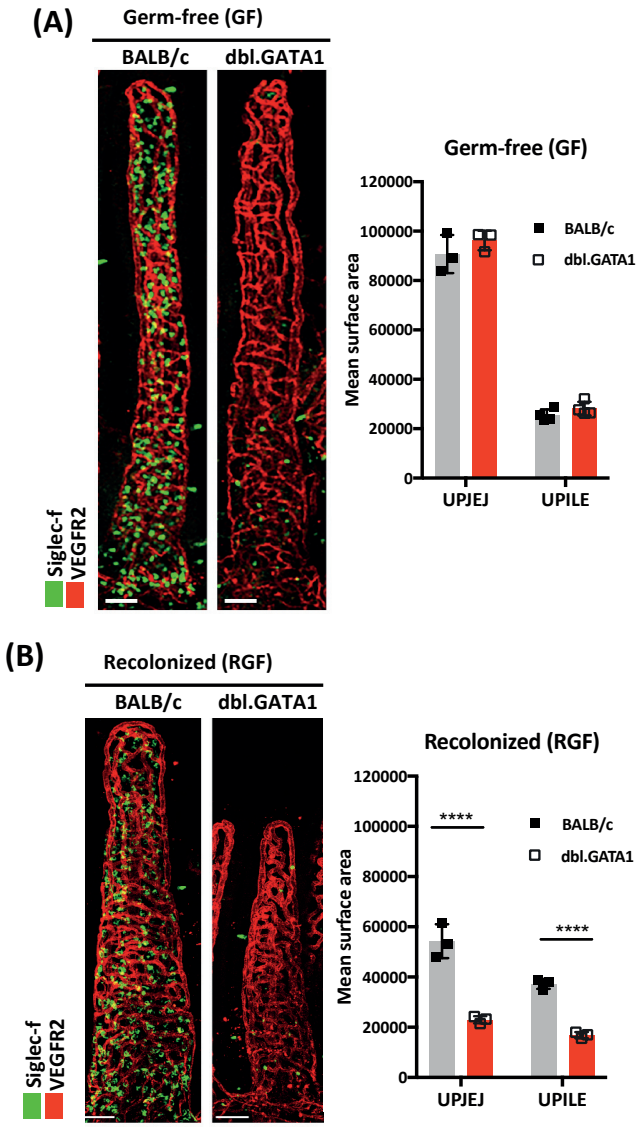

(Figure 31) Villous defect observed in dbl.GATA1 mice is dependent on microbial-colonization status: (A) Representative wholemount images and corresponding villous area quantifications from the upper jejunum and ileum of Germ-free (GF) Balb/c and dbl.GATA1 mice **(A)** and recolonized (previously GF) Balb/c and dbl.GATA1 mice (>4-weeks post recolonization) **(B).** For quantification of villous area, VEGFR2 staining was used to determine villous boundary. Each data point corresponds to mean surface area >30 villi sampled per mouse. Data is representative of at least 2 independent experiments. Statistical analysis two-way ANOVA $p<0.01$**, $p<0.05$* Error bars represent SD

Upon analysis of the upper jejunum (UPJEJ) and upper ileum (UPILE) of these mice, we observed that the villus area of both GF strains revealed no differences in both the upper jejunum and ileum – which makes it clear that the villous defect observed in the absence of eosinophils is in response to microbial colonization **(Figure 31A)**. To explore further, we recolonized previously GF Balb/c and Δdbl.GATA1 mice with a fecal transfer (by oral gavage) from SFP Balb/c donors - ensuring that the colonizing species do not have discrepancies in community composition. We analyzed the villi of these mice >4 weeks post-colonization, and sampled tissue from the upper jejunum and ileum **(Figure 31B)**. Based on the villus area, it is apparent that microbial colonization itself naturally decreased the villous surface area of Balb/c mice – as GF mice have significantly larger villi that

SPF mice; a phenomenon reported in the literature [201,202]**(Figure 31)**. However, this decrease in villous area is exaggerated in the absence of eosinophils, which is noted by a clear decrease in villous area of (~50%) in the upper jejunum and (~50%) ileum in comparison to RGF Balb/c mice. Taken together, these findings provide support for a critical role of eosinophils in the homeostatic maintenance of villus size in response to microbial colonization.

4.2.3 Analysis of villous protective pathways altered in Δdbl.GATA1 mice using RNA-seq

We explored factors that might help explain this villous shrinkage observed in Δdbl.GATA1 mice. From this analysis, we were able to rule out the contribution of cellularity/T-B cell and IL4ra-signalling to this phenotype. We know it is not due to decreased number of structural cells, or due to different numbers of immune cell populations. However, since as our analysis was restricted to just characterizing immune cell numbers and wholemount analysis, this does not rule out that there are changes at the level of cell activation. To gain a broader perspective on what processes might be dysregulated in the lamina propria of Δdbl.GATA1 mice we conducted RNA-seq analysis on this compartment.

We found a total of 587 genes to be differentially expressed in Δdbl.GATA1 mice relative to Balb/c controls. First, we conducted a GSEA analysis on the 323 genes downregulated in the absence of eosinophil. Amongst the downregulated dataset, eosinophil-associated genes (e.g. EPX, CCR3, ALOX15) were significantly decreased as expected **(supplementary table 8)**. Other than this we found that out of the downregulated genes recognized by the database, the highest overlap was with pathways involved in the extracellular matrix (8%; matrisome) **(Figure 32B; supplementary table 7)**. Interestingly, this was followed by overlap to pathways involved in nervous system processes (7%, receptor interaction, synapses, maintenance). Furthermore, we also observe enrichment for genes involved in muscle maintenance/contraction (3%, cardiomyopathy targets).

(A)

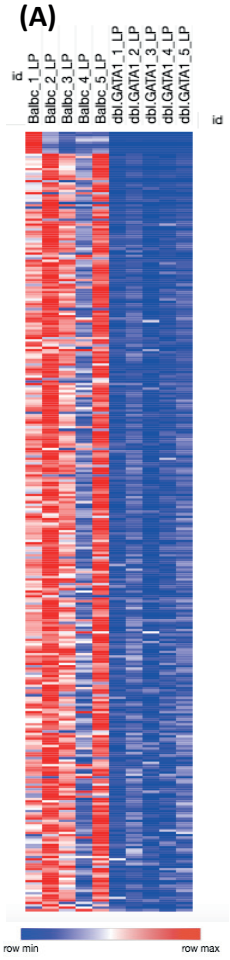

(B)

Gene Set Name [# Genes (K)]	Description	# Genes in Overlap (k)	k/K	p-value	FDR q-value
REACTOME_NEURONAL_SYSTEM [279]	Genes involved in Neuronal System	21		$1.93\ e^{-16}$	$2.57\ e^{-13}$
KEGG_NEUROACTIVE_LIGAND_RECEPTOR_INTERACTION [272]	Neuroactive ligand-receptor interaction	16		$3.3\ e^{-11}$	$2.19\ e^{-8}$
REACTOME_VOLTAGE_GATED_POTASSIUM_CHANNELS [43]	Genes involved in Voltage gated Potassium channels	8		$3.05\ e^{-10}$	$1.35\ e^{-7}$
REACTOME_POTASSIUM_CHANNELS [98]	Genes involved in Potassium Channels	10		$8.4\ e^{-10}$	$2.79\ e^{-7}$
KEGG_CALCIUM_SIGNALING_PATHWAY [178]	Calcium signaling pathway	12		$2.11\ e^{-9}$	$5.62\ e^{-7}$
KEGG_ARRHYTHMOGENIC_RIGHT_VENTRICULAR_AR_CARDIOMYOPATHY_ARVC [76]	Arrhythmogenic right ventricular cardiomyopathy (ARVC)	8		$3.3\ e^{-8}$	$7.31\ e^{-6}$
REACTOME_TRANSMISSION_ACROSS_CHEMICAL_AL_SYNAPSES [186]	Genes involved in Transmission across Chemical Synapses	11		$3.87\ e^{-8}$	$7.34\ e^{-6}$
NABA_MATRISOME [1028]	Ensemble of genes encoding extracellular matrix and extracellular matrix-associated proteins	24		$6.68\ e^{-8}$	$1.11\ e^{-5}$
KEGG_DILATED_CARDIOMYOPATHY [92]	Dilated cardiomyopathy	8		$1.49\ e^{-7}$	$2.2\ e^{-5}$
REACTOME_GPCR_LIGAND_BINDING [408]	Genes involved in GPCR ligand binding	14		$4.84\ e^{-7}$	$6.43\ e^{-5}$

(Figure 32) RNA-seq of lamina propria fraction of Δdbl.GATA1 mice (downregulated genes) under homeostatic cnditions: (A) Heatmap shows differentially *downregulated genes* in dbl.GATA1 mice (lamina propria fraction) relative to Balb/c (lamina propria fraction) FC >1, FDR 0.05 ($p<0.001$). (B)Genes are ranked from lowest (most significant) to highest (least significant) p-value. Down regulated genes, were analyzed through Gene set enrichment analysis (Top 10 overlap, GSEA; Molecular signatures – C2 Canonical pathways (Top 10 overlap, CP: Curated gene sets)) FDR 0.05 (A, table top). Each sample is a biological replicate (n=5 / group). Out of 322 gene, 294 were identified by the database. Each Tables extracted from MSigDB. Details about sample collection and analysis is found in the methods section.

Next, we proceeded to do a GSEA analysis on genes that were upregulated (264 genes) in the absence of eosinophils. Out of genes recognized by the database **(Figure 33B; supplementary table 8)**, the highest overlap was for pathways involved in extracellular matrix processes (30% - matrisome, matrisome associated, secreted factors), followed by enrichment for genes involved in inflammatory processes (15% - rhodopsin-like receptors, complement pathway, GPCR ligand binding).

(A)

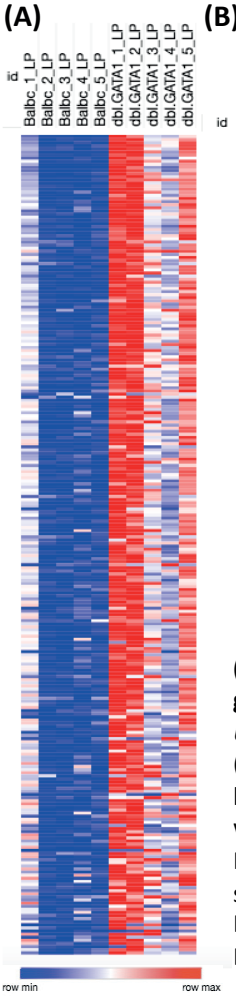

(B)

Gene Set Name [# Genes (K)]	Description	# Genes in Overlap (k)	k/K	p-value	FDR q-value
NABA_MATRISOME [1028]	Ensemble of genes encoding extracellular matrix and extracellular matrix-associated proteins	55		$6.74\ e^{-46}$	$8.96\ e^{-43}$
NABA_MATRISOME_ASSOCIATED [753]	Ensemble of genes encoding ECM-associated proteins including ECM-affilaited proteins, ECM regulators and secreted factors	39		$1.02\ e^{-31}$	$6.78\ e^{-29}$
REACTOME_GPCR_LIGAND_BINDING [408]	Genes involved in GPCR ligand binding	21		$2.55\ e^{-17}$	$8.92\ e^{-15}$
REACTOME_CLASS_A1_RHODOPSIN_LIKE_RECEPTORS [305]	Genes involved in Class A/1 (Rhodopsin-like receptors)	19		$2.68\ e^{-17}$	$8.92\ e^{-15}$
NABA_SECRETED_FACTORS [344]	Genes encoding secreted soluble factors	19		$2.47\ e^{-16}$	$6.56\ e^{-14}$
KEGG_CYTOKINE_CYTOKINE_RECEPTOR_INTERACTION [267]	Cytokine-cytokine receptor interaction	17		$9.38\ e^{-16}$	$1.96\ e^{-13}$
REACTOME_IMMUNE_SYSTEM [933]	Genes involved in Immune System	27		$1.03\ e^{-15}$	$1.96\ e^{-13}$
NABA_CORE_MATRISOME [275]	Ensemble of genes encoding core extracellular matrix including ECM glycoproteins, collagens and proteoglycans	16		$2.75\ e^{-14}$	$4.57\ e^{-12}$
REACTOME_PEPTIDE_LIGAND_BINDING_RECEPTORS [188]	Genes involved in Peptide ligand-binding receptors	14		$4.01\ e^{-14}$	$5.92\ e^{-12}$
KEGG_COMPLEMENT_AND_COAGULATION_CASCADES [69]	Complement and coagulation cascades	9		$9.53\ e^{-12}$	$1.27\ e^{-9}$

(Figure 33) RNA-seq of lamina propria fraction of Δdbl.GATA1 mice (upregulated genes) under homeostatic conditions: (A) Heatmap shows differentially *Upregulated genes* in dbl.GATA1 mice (lamina propria fraction) relative to Balb/c (lamina propria fraction) FC log2 >1, FDR 0.05 ($p<0.001$). **(B)** Genes are ranked from lowest (most significant) to highest (least significant) p-value. Up regulated genes, were analyzed through Gene set enrichment analysis (Top 10 overlap, GSEA; Molecular signatures – C2 Canonical pathways (Top 10 overlap, CP: Curated gene sets)) FDR 0.05 (A, table top). Out of 264 gene, 183 were identified by the database. Each sample is a biological replicate (n=5 / group). Tables extracted from MSigDB. Details about sample collection and analysis is found in the methods section.

4.3 Discussion

Based on our observations that eosinophils reside near structural cells such as myofibroblasts, blood vessels and enteric neurons within the villus, we sought to determine whether these interactions had any implications on the maintenance of intestinal homeostasis – particularly in the context of tissue architecture.

We report that mice deficient for eosinophils have defective villous architecture, characterized by a reduction in villous size (shrinkage) – coinciding with the epithelial barrier defects we reported in Chapter 3. This phenotype is absent in germ-free conditions and early life, suggesting that eosinophil-mediated villous protection is triggered in response to microbiota colonization.

Of particular note, our RNA-seq analysis revealed many changes relating to ECM remodelling and deposition in Δdbl.GATA1 mice (**Figure 32, 33; supplementary table 7, 8)**. It is likely that the target cells of eosinophil-mediated changes in RNA expression are stromal in origin, as the downregulated genes involved in muscular contraction and maintenance (*e.g.* Myom1, Myh6, Actn2, Myh10, Itga7, Car3) are primarily expressed by contractile cells such as smooth muscle cells, myofibroblasts and fibroblastic reticular cells. This is also true for the ECM related genes (*e.g.* Tnbx, Hmgcn2, Nell1/2, P4ha3, Elastin), which were downregulated in the Δdbl.GATA1 mice. Of note, these genes encode for molecules that give tissues structural rigidity/integrity. For example, Tenascin X (TNBX) facilitates proper interactions between collagens and elastin, with the abrogation of TNBX function leading to severe weakening/fragility of connective tissues[31,203–206]. Similar findings have been noted for NELL1/2 ko mice, which are noted to have increased fragility and decreased ECM stiffness in bone connective tissue[207,208]. Hemicentin-2 (HMCN2) plays an important role in mesenchymal cell migration and tissue organization (*e.g.* epidermal-dermal junction formation)[209,210]. Prolyl 4-hydroxylase-subunit alpha 3 (P4HA3) is required for proper 3D folding/bundling of newly synthesized pro-collagen chains[211,212]. Furthermore, expression of fibroblast derived growth factors such as Fgf14, Fgf16 are also downregulated, along with some collagens (e.g. Col1a1, Col8a2) – suggesting that reparative responses and fibroblast homeostasis is altered in the absence of eosinophils.

In addition to these findings, we also observed a decrease in pathways involved in neuron-related processes. This includes a wide array of receptors (*e.g.* Gria1/2, Oxtr, Oprd1, Drd2, Adra1a), genes

involved in firing/excitability (*e.g.* various KCNQ-family, and CACNA-family members) – in addition to regulators of neuron cell fate (*e.g.* Mytl1) and attachment/growth (*e.g.* Ncan, Nrtn). Nonetheless, it is unclear whether eosinophils impact neuron-related processes directly through release of neuroactive molecules (such as NGF – which it has been shown to express, and is downregulated in Δdbl.GATA1 mice), or whether it is secondary to alterations in the ECM mechanics itself. Indeed, multiple studies have shown that alterations in stiffness /matrix properties could influence neuronal differentiation and firing[35,213,214].

Interestingly, when we looked at genes upregulated in the absence of eosinophils – we also saw enrichment in ECM-related pathways. Notably, genes encoding for various ECM components (*e.g.* Lama1, Col18a1, Col14a1, Vcan, Bgn) and ECM degradation (e.g. Adamts3, Adamdec1, Mmp9, Mmp10) were upregulated, alongside various inflammatory genes involved in the complement pathway (*e.g.* C1qa-c, C3ra1, C5ar1), type-I interferons (*e.g.* Ifi16, Ifi44) and chemokine receptors (*e.g.* Ccr2/5/1, Cx3cr1).

Eosinophil regulation of ECM homeostasis through positive and negative feedback

Our RNA-seq data indicates that eosinophils may be important for both the induction and suppression of ECM production and organization. This finding indicates a probable role for eosinophils in regulating homeostatic, tissue remodelling processes in the small intestine.

In terms of induction of genes involved in ECM remodelling we saw that genes such as Tnbx/Nell-1/2, and Hmcn2 were decreased in **Δ**dbl.GATA1 mice. Reduced gene expression of these ECM-associated could in part explain defects associated with eosinophil-deficiency such as villous shrinkage (due to weakening/reduced ECM stiffness) and delayed epithelial turnover (due to erroneous epithelial anchorage to the basal lamina) respectively. These findings are complementary to the downregulation of genes involved in myofibroblast differentiation/contraction in Δdbl.GATA1 mice, which could be a direct consequence of decreased matrix stiffness. It is unclear however whether ECM dysregulation came first (with myofibroblast, neuronal abnormalities as a consequence) or whether eosinophil-deficiency resulted in decrease deposition by structural cells, which then led to ECM dysregulation. Alternatively, downregulation of these ECM components could have an impact beyond tissue mechanics. For example, Tenascin-X can also regulate the bioavailability of factors such as TGF-β –

through sequestration (either TGF-β and/or TGF-β complex), and may therefore aid in the unmasking of the mature form upon conformational change[31]. Such alterations in the bioavailability of could also have ramifications on global ECM homeostasis and composition.

In terms genes involved in ECM remodelling that are suppressed by eosinophils, we observed the upregulation of various metalloproteases (*e.g.* Mmp-9/12/13, Adam-ts3/28/dec1), alongside deposition of ECM components such as proteoglycans (*e.g.* Vcn, Bgn), laminins (*e.g*. Lama1), collagens (*e.g.* Col18a1, Col14a1), and fibroblast growth factors (*e.g.* Fgf10/9/7) in the Δdbl.GATA1 mice. This is interesting when considering the decreased myofibroblast-associated gene signature observed in Δdbl.GATA1 mice, as factors such as biglycan (Bgn) are known to be negatively correlated with myofibroblast differentiation[215].

Concurrent with these changes are the rise of various inflammatory signatures such as increased expression of complement related genes (*e.g.* C1qa-c, C3ar1, C5ar1), chemokine receptors and interferon-inducible genes. These findings are suggestive that eosinophils additionally reinforce villous integrity by limiting ECM turnover induced by the microbiota[216].

Based on these findings we suggest that the loss of eosinophils results in reduced structural rigidity – which could lead to an attempt of cells within the microenvironment to compensate for the loss of structural integrity through the upregulation of ECM substrates, and promotion of reparative responses (*e.g.* upregulation of Fgfs, collagen). However, this process may not be sufficient or correct leading to ensuing inflammation – which then furthers the abhorrent remodelling process.

Potential contributions of the microbiota to ECM homeostasis

Given that the villous defect observed in Δdbl.GATA1 mice is driven in response to the microbiota, it's important to understand where colonization status might fit in ECM homeostasis. Microbial colonization induces many physiological changes in the host, with factors such as increased intestinal motility, permeability - having a potential impact on ECM turnover kinetics/composition[42,43,216,201].

Based on our data, we observed that villous shrinkage and increased epithelial barrier permeability occurs in response to microbial colonization. While we did not test it in our own model, the microbiota is also known to be important for facilitating intestinal motility – with peristalsis severely decreased in germ-free animals[39,202]. Moreover, microbiota-induced peristalsis – could lead to increased mechanical loading in the intestine. Increases in mechanical loading has been noted to positively correlate with both ECM synthesis and degradation – with the latter, serving as part of a negative feedback loop in order to maintain mechanical homeostasis in motile connective tissue[30]. Taken together, these changes are indicative of altered ECM dynamics (e.g. turnover, composition/deposition) and changes in the mechanical properties of the ECM in response to the microbiota.

In summary our data indicate that eosinophils play a critical role for maintaining villous architecture, likely by promoting a balanced ECM remodelling in response to microbial colonization.

Chapter 5: Contributions of epithelial-derived alarmins in eosinophil-mediated villous maintenance

In the previous chapters, we present evidence for small intestinal eosinophils are important mediators of appropriate microbiota-host interactions, with eosinophil-deficiency resulting in significant barrier defects and structural abnormalities following microbial colonization. However, the means by which the microbiota regulates eosinophil responses are unclear.

In chapter 5, we attempt to identify the mechanism responsible for eosinophil-mediated villous protective effects in response to microbiota.

5.1 MYD88-SIGNALLING IS REQUIRED FOR EOSINOPHIL-MEDIATED VILLOUS MAINTENANCE

Our previous findings show that the microbiota regulate SI eosinophils through a direct/indirect mechanism, leading to alterations in eosinophil cytoplasmic ultrastructure – particularly, inducing the formation of complex vesiculo-tubular structures and free ribosomes. We also observed that these microbiota-induced changes in eosinophil activity must be important for intestinal maintenance as eosinophil-deficiency results in villous and barrier defects in response to microbiota colonization.

In an attempt to determine the precise signalling pathway mitigating eosinophil-microbiota crosstalk, we investigated MYD88-deficient mice. MYD88 is a critical adapter protein downstream of many PRR (*e.g.* TLRs) signalling pathways that could be triggered in response to eosinophil sensing of microbial-derived cues[217]. Using VEGFR2 to visualize blood vessels and, α-SMA+ (myofibroblast) coverage to define villus surface area, we observed a decrease in villus size (~20%) in MyD88-deficient mice compared to C57.B6 controls **(Figure 34)**. This is in accordance with decreased surface area we observe in SPF Δdbl.GATA1 mice **(Figure 22A)**, suggesting that this pathway may indeed be necessary for eosinophil-mediated villous maintenance.

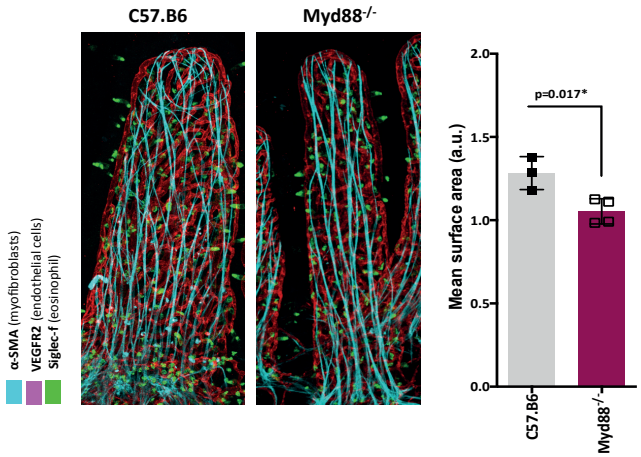

(Figure 34) MyD88-signalling is required for eosinophil-mediated villous maintenance: Representative wholemount images and corresponding villous area quantifications from the upper jejunum of C57.B6 and MyD88ko mice. For quantification of villous area VEGFR2 staining (red) and a-SMA staining (cyan) was used to determine villous boundary. Each data point corresponds to mean surface area >30 villi sampled per mouse. Statistical analysis (p-values as indicated in graph) Student-test $p<0.05$* Error bars represent SD within group.

Data obtained from Petrova lab (UNIL)

5.2 EOSINOPHIL-INTRINSIC IL33/25 SIGNALLING IS REQUIRED FOR VILLOUS MAINTENANCE

Myd88 signalling is not restricted to innate immune sensing, and also functions as an adaptor used by cytokines from the IL-1r family[218]. Called 'Alarmins', most of these cytokines share a common receptor chain IL1RAcp, which possesses a Toll-1R (TIR) domain that initiates a similar signalling cascade to Toll-like receptors (TLRs) with regards to the requirement of MYD88[219,220]. Most notable of the alarmins in this family – in the context of eosinophil regulation in the intestine - is IL-33. IL33 signals through the IL-33 receptor complex, comprised of IL-1RAcp and ST2[110,219]. As previously discussed in chapter 1, IL-33 regulation of eosinophils has been noted in driving inflammation and tissue remodelling in models of asthma and IBD – but whether this relationship holds homeostatic significance under steady state conditions is unclear.

5.2.1 Characterization of IL-33 expression in the SI

In order to test whether the villous defect observed in Myd88-deficient mice is due to lack of IL-33 signalling, we utilized a mouse model – ST2.IL17rbko[iii] – deficient in IL-33 receptor ST2 (in addition to IL-25 receptor IL17rb) which we used for our preliminary analysis. In contrast to IL17rb expression, ST2 is highly expressed by small intestinal eosinophils at steady state conditions **(Figure 35A)**[104,219]. Interestingly, we observed that despite the literature showing that bone-marrow derived eosinophils require IL-33 for their survival[102], ST2.IL17rbko mice exhibited normal eosinophil numbers in the small intestine by FACS analysis **(Figure 35B)** suggesting that –

[iii] **Note:** Ideally, ST2-single ko mice would have been a better system to use for this analysis but due to practical reasons – ST2xIL17rbko mice were used as they were readily available from our collaborators (Marsland lab – CHUV/UNIL). We are aware that these experiments will need to be repeated with single ST2ko – which is planned by our collaborators in University of Calgary (McCoy lab – Ucalgary).

at least under homeostatic conditions – IL-33 (nor IL-25) are required for eosinophil recruitment and maintenance in this tissue.

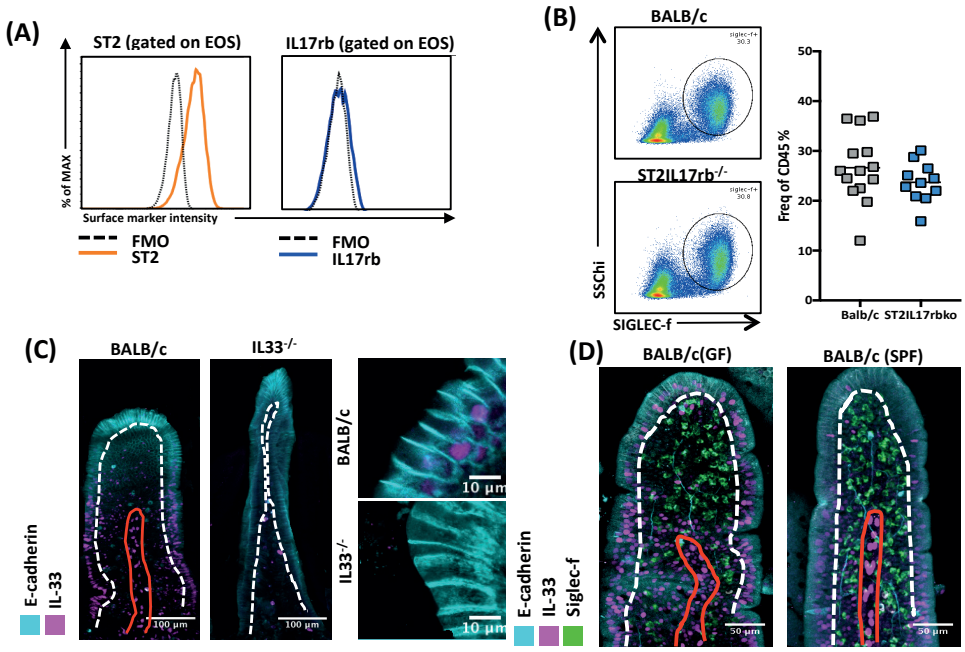

(Figure 35) ST2, a Myd88-dependent receptor for alarmin IL-33 is highly expressed in SI eosinophils: (A) Representative MFI curves from Balb/c, SI-eosinophils (jejunum; live SSChi, CD45+ Siglecf+) – fluorescence minus one (FMO) control (dotted-line), transposed with MFI of either ST2 (orange) or IL17rb (blue). **(B)** Representative FACS plot and quantifications of eosinophil frequency (within CD45% cells) in the jejunum of Balb/c an ST2IL17rbko mice (data pooled from 2-3 independent experiments) . **(C)** Wholemount staining of villi from upper jejunum of either Balb/c or IL-33ko mice. **(D)** wholemount images of villi (jejunum) from GF and SPF ('colonized') Balbc mice. For **(C,D)** - dotted line (white) denotes boundary between epithelial layer and lamina propria, (red) indicates location of lacteal**.**

In terms of distribution, much has been done on the characterization of IL-25, which has been reported to be restricted to Tuft-cells (cytoplasmic-localization)[11,91]. Tuft cells are sparse under homeostatic conditions, and are only noted to arise after the weaning-transition period (~3-4 weeks) in a manner independent of microbial colonization[91]. Furthermore, they are only noted to expand and release IL-25 in response to infection with intestinal helminths/protozoa[11]. In contrast, using wholemount staining, we report that IL-33 is ubiquitously present in the small intestine – localized in the nucleus of enterocytes at steady state **(Figure 35C)**. They are also expressed in pericryptal fibroblasts and lymphatic endothelial cells (LECS), an observation concurrent with published studies[49]. IL-33, which functions as a 'danger signal', is released in response to cellular damage and mechanical stress[110,219,221].

It is important to note that our lab is the first to report the presence of nuclear IL-33 in enterocytes under homeostatic conditions. Therefore, in an effort to corroborate our findings – we utilized IL33ko mice as a staining control for our wholemount analysis. The absence of IL-33 staining in the wholemount preparation of IL-33ko mice, compared to Balb/c controls – confirms our observation that nuclear IL-33 is constitutively present in SI enterocytes under homeostatic conditions **(Figure 35C)**. Interestingly, we observed a discrepancy in nuclear IL-33 distribution between GF and SPF mice **(Figure 35D)**. Under GF settings, nuclear IL-33 is often present within enterocytes throughout the villi - whereas under SPF conditions, IL-33 staining is rarely found in the villus tip, this absence of nuclear IL-33 staining at the villous tip is suggestive of IL-33 release from cells located here into the microenvironment in response to microbiota colonization[219].

5.2.2 Mice deficient in ST2/IL17rb signalling present with similar villous abnormalities to Δdbl.GATA1 mice

Given that SI eosinophils express ST2, and that IL-33 may be released from enterocytes in response to microbiota colonization – we wanted to determine whether ablation of this signalling pathway (using ST2IL17rbko mice) would result in similar villous defect (reduced area) that we observed in Δdbl.GATA1 and MYD88ko mice by wholemount analysis. Using α-SMA+ myofibroblast coverage as a proxy for villous area, we observed decreased villous area in ST2IL17rbko mice (similar to that present in the Δdbl.GATA1 cohort) in comparison to Balb/c samples **(Figure 36A)**. This suggests that ST2/IL17rb-signalling somehow participates in eosinophil-mediated villous protection.

To see whether this villus defect is induced in response to the microbiota, we wanted to test whether this decrease in villus area was already present in ST2-deficient mice under germ free conditions. For this purpose, we acquired GF ST2-ko[iv] mice and compared it to GF Balb/c controls. We observed that ST2ko mice do not exhibit reduced villous surface area under GF conditions compared to GF Balb/c mice, and present comparable villus size to other GF Balb/c and GF Δdbl.GATA1 mice analyzed in this thesis. Similar to findings from SPF Δdbl.GATA1 mice reported previously, villous defects were only observed in ST2-deficient mice (ST2IL17rbko)

[iv] **Note:** GF ST2ko mice were used instead of GF *ST2IL17rbko* mice, as the latter strain was not available/re-derived in axenic conditions from our collaborators (McCoy/MacPherson lab – Ubern).

under SPF conditions **(Figure 36B)**– suggesting that ST2/IL17rb signalling is critical for villous maintenance in response to microbial colonization.

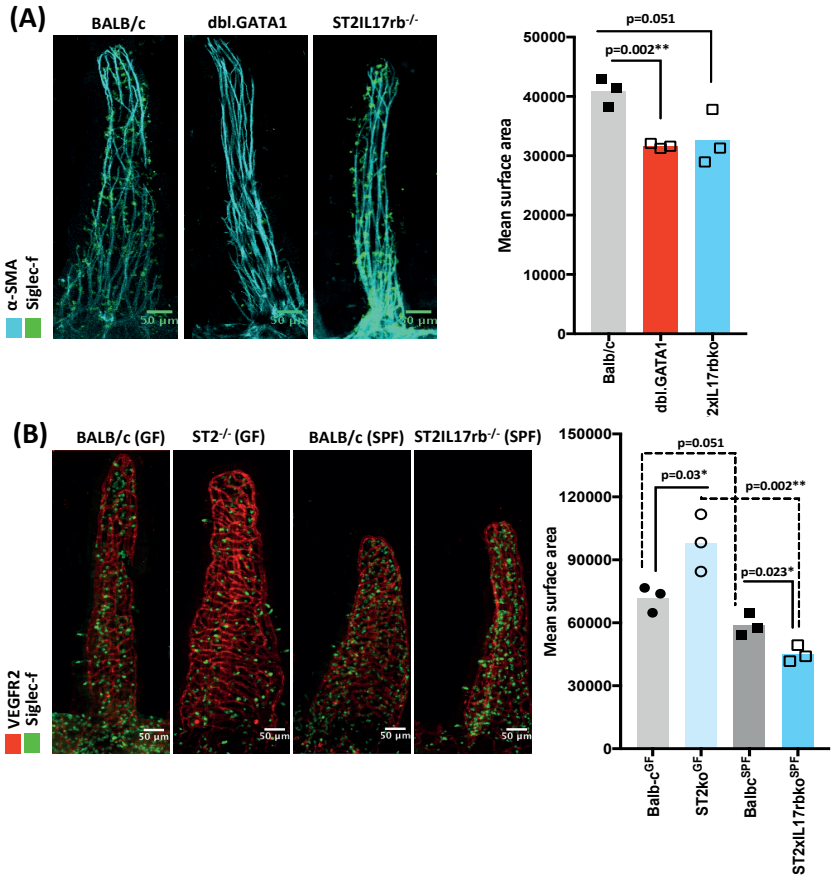

(Figure 36) Mice deficient in IL33/25 mediated signaling exhibit similar villous defects observed in dbl.GATA1 mice: (A) Representative wholemount images of villi from upper jejunum from Balb/c, dbl.GATA1 and ST2IL17rbko mice – alongside quantification of villous surface area – myofibroblast coverage (a-SMA staining, cyan) was used as an indicator of the villous boundary. **(B)** Representative images of villi from upper jejunum of germ-free (Balb/c, ST2ko mice) and colonized (SPF) Balb/c and ST2IL17rbko mice – alongside quantifications of villous surface area – VEGFR2 staining (red) enables identification of blood vessel cage network which was used to visualize the villous boundary, used for quantification of area. Each data point represents the mean villous area >30 villi sampled per mouse. Data representative of 2 independent experiments (n=3-4 mice per group). Statistical analysis student t-test (p=values are indicated in the graph).

5.2.3 Eosinophil-intrinsic sensing of epithelial-derived alarmins is required for villous maintenance

To provide direct evidence for the importance of IL-33/25 signalling in mediating villous protective function of eosinophils, we needed to generate a model wherein eosinophils express deficiency for ST2/IL17rb while other hematopoietic populations retain competency for these receptors.

For this purpose, we generated mixed bone marrow chimeras. In brief, Balb/c mice (recipients) were lethally irradiated and were reconstituted with bone marrow from Balb/c, Δdbl.GATA1 or ST2.IL17rbko donors – with these 3 groups serving as "*controls*" (all lines congenic to the Balb/c strain). These groups were compared to 2 "*test*" groups, which were reconstituted with bone marrow mixed at a 1:4 ratio – with 75% acquired from Δdbl.GATA1 donors, and the remaining

25% acquired from either Balb/c or ST2.IL17rbko donors. The first test group enabled us to do a comparison wherein eosinophil-specific, villous protective effects could be studied without potential off-target contribution from other hematopoietic cells. The second test group enabled us to evaluate whether eosinophil-specific, villous protective effects could be achieved in the absence of ST2.IL17rb signalling competency under the same conditions.

Using wholemount analysis to compare the villus area of mice from the 5 different treatments/conditions – we observed a significant resemblance of our ST2.IL17rbko *test* group to our ST2.IL17rbko *control*, with regards to decreased villous area – in comparison to both our Balb/c *test* and Balb/c *control* group **(Figure 37A)**. Furthermore, this decreased surface area is concurrent with the decrease we observed in the Δdbl.GATA1 *control* group. We also report that this decrease in area was mostly attributed to a reduction in width rather than the length of the villus – similar to that observed in Δdbl.GATA1 mice **(Figure 37B)**.

Next, we wanted to compare the rate of epithelial restitution between these 5 groups. This was achieved through an EdU+ pulse-chase experiment – where we looked at the rate of migration of EdU+ cells, through the measurement of distance travelled from the villus-crypt axis 24h post-EdU injection. We observed delayed migration of EdU+ cells in the ST2IL17rbko *test* group similar to Δdbl.GATA1 and ST2.IL17rbko *controls* – in comparison to the Balb/c *test*, and Balb/c *control* group **(Figure 37C)**.

Taken together, these data indicate an important role for eosinophils in the maintenance of villous homeostasis through cell intrinsic-IL33/25 signalling via ST2/IL17rb receptor(s).

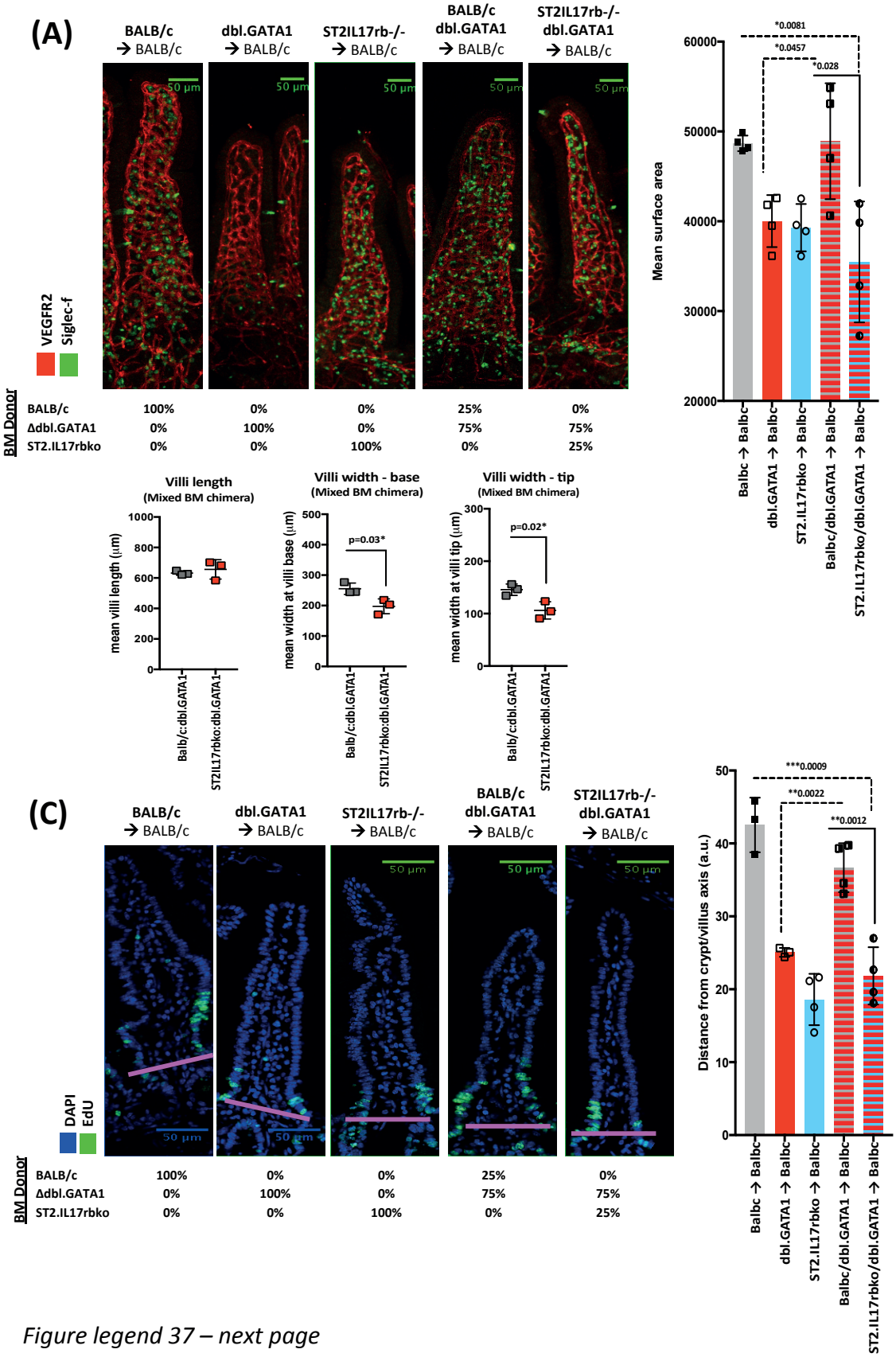

Figure legend 37 – next page

(Figure 37) Eosinophils require cell-intrinsic IL33/25 signalling to mediate villous protective effects: (A) Representative images from mixed-BM chimera experiment. Quantification of mean vlllus surface area (upper jejunum) from irradiated Balb/c mice reconstituted with either (marrow from Balb/c, dbl.GATA1 or ST2IL17rbko donors – 'control' group) and (chimeric marrow from either Balb/c: dbl.GATA1 or ST2IL17rbko:dbl.GATA1 – mixed at a 1:3 ratio 'test' group). Each data point is an average surface area from >30villi randomly sampled per mouse**. (B)** Width, length analysis of villi from same data set as (A)**. (C)** same mice used in (A) were injected with EdU (i.p.) 24hours before harvest – to normalize, harvest time was timed to match EdU injection time. Each data point is an average measurement of distance travelled by EdU+ cells from the villus crypt axis, to the leading edge of EdU+ cells randomly sampled from >30 villi per mouse. Statistical test unpaired student test (p-values are as indicated); Mann-Whitney test correction was conducted if SD values >0.05 Error bars represent SD within group.

5.2.4 IL33/25-signalling is not required for microbiota-induced ultrastructural changes in SI eosinophils

Our data suggest that ST2/IL17rb-mediated signalling in eosinophils play a crucial role in mitigating microbiota crosstalk with SI eosinophils. However, it is unclear whether this crosstalk is responsible for the microbiota-induced ultrastructural changes observed in eosinophils from colonized mice. To test whether or not epithelial derived alarmins - IL33/25 - play a role in these changes, we compared the ultrastructure of SI eosinophils from SPF-colonized ST2.IL17rbko mice to that of GF and SPF-colonized Balb/c mice using TEM imaging.

We observed that in comparison to eosinophils from GF Balb/c mice, both SPF Balb/c and SPF ST2.IL17rbko eosinophils had increased free ribosome numbers throughout its cytoplasm – indicating increased activity **(Figure 38)**. However, eosinophils from ST2IL17rbko mice exhibit a peculiarity, in that they seem to have more circular vesicular networks on average – unlike in SPF eosinophils where you get a combination of both tubular and circular vesicular networks. At current, not much is known about whether circular or tubular networks have different functions.

Taken together, our preliminary observations suggests that IL33/25 signalling (*via* ST2/IL17rb) is not responsible for the increased secretory activity/protein translation machinery observed in eosinophils from SPF-colonized Balb/c mice relative to GF Balb/c mice. Nonetheless, this does not rule out an impact of IL33/25-signalling in shaping the mRNA profile of the eosinophil transcriptome in the small intestine[88].

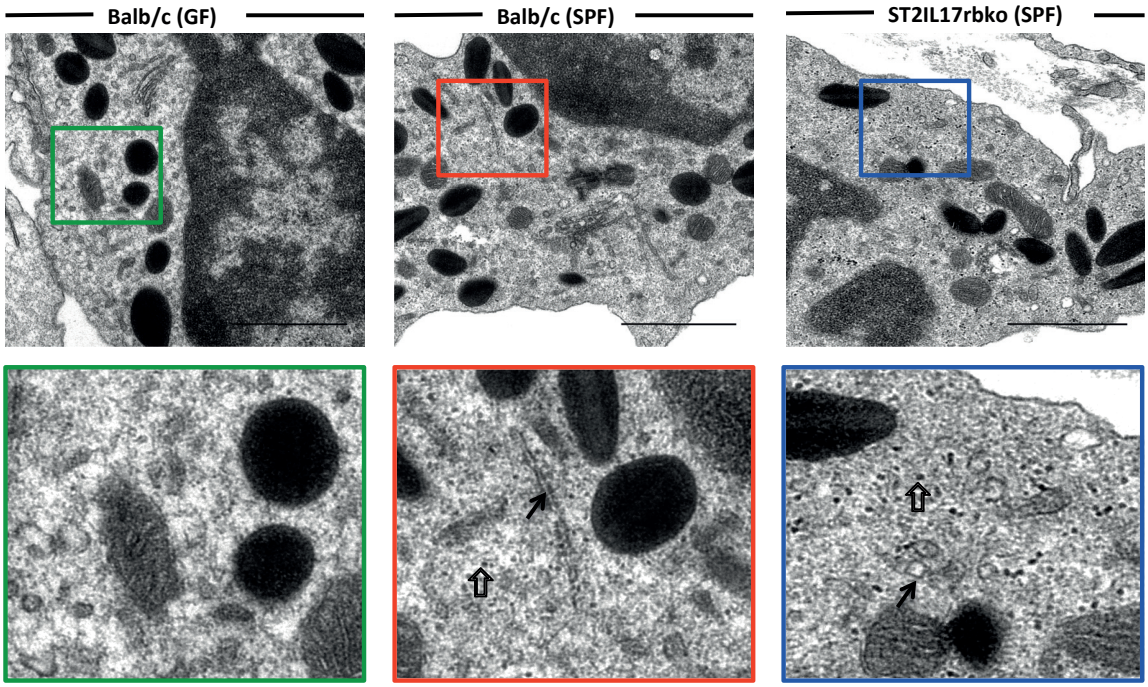

(Figure 38) IL33/25 signalling is not required for microbiota colonization induced ultrastructural changes in eosinophil cytoplasm: Representative TEM images of SI eosinophils in the upper jejunum of germ-free (GF) Balb/c (magnified in green box), colonized (SPF) Balb/c (magnified in red box) and ST2IL17rbko mice (magnified in blue box). Examples of cytoplasmic free ribosomes (*dot-like structures* - Open arrow) and vesiculotubular structures (*tubular structures* – closed arrow). Images representative of >10 TEM images per mouse (n=2 per condition).

5.2.5 Comparative analysis of RNA-seq from LP fraction of Δdbl.GATA1 and ST2IL17rbko mice

To investigate the impact of IL33/25 signalling on SI eosinophils under homeostatic conditions, we conducted RNA-seq of the lamina propria fraction (jejunum) of SPF-colonized ST2.IL17rbko and Balb/c mice. Out of 640 differentially expressed genes (relative to Balb/c mice), 610 genes were downregulated **(Figure 39B; supplementary table 9)**. We conducted a GSEA analysis on downregulated genes and observed that from the 565 genes recognized by the database, the highest enrichment was in pathways involved in ECM-related processes (~10% - matrisome). This is followed by changes in nervous system processes (7% - receptor interaction, synapses, maintenance). Amongst these downregulated genes were il1rl1 (ST2) and IL17rb, which is expected **(supplementary table 9)**. In contrast, only 30 genes were upregulated in ST2.IL17rbko mice relative to Balb/c controls. GSEA analysis on this gene set did not reveal enrichment for any pathway **(supplementary table 10).**

(A)

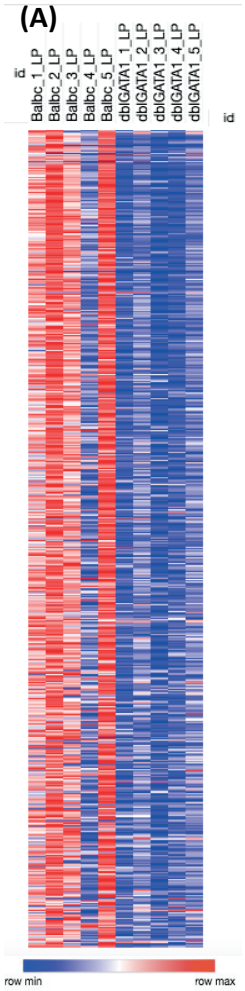

(B)

Gene Set Name [# Genes (K)]	Description	# Genes in Overlap (k)	k/K	p-value	FDR q-value
REACTOME_NEURONAL_SYSTEM [279]	Genes involved in Neuronal System	38		$5.64\ e^{-28}$	$7.5\ e^{-25}$
NABA_MATRISOME [1028]	Ensemble of genes encoding extracellular matrix and extracellular matrix-associated proteins	55		$1.02\ e^{-19}$	$6.78\ e^{-17}$
REACTOME_POTASSIUM_CHANNELS [98]	Genes involved in Potassium Channels	19		$1.32\ e^{-17}$	$5.27\ e^{-15}$
NABA_CORE_MATRISOME [275]	Ensemble of genes encoding core extracellular matrix including ECM glycoproteins, collagens and proteoglycans	28		$1.59\ e^{-17}$	$5.27\ e^{-15}$
KEGG_CALCIUM_SIGNALING_PATHWAY [178]	Calcium signaling pathway	22		$7.87\ e^{-16}$	$2.09\ e^{-13}$
REACTOME_VOLTAGE_GATED_POTASSIUM_CHANNELS [43]	Genes involved in Voltage gated Potassium channels	13		$3.34\ e^{-15}$	$7.4\ e^{-13}$
REACTOME_TRANSMISSION_ACROSS_CHEMICAL_SYNAPSES [186]	Genes involved in Transmission across Chemical Synapses	21		$2.24\ e^{-14}$	$4.25\ e^{-12}$
KEGG_NEUROACTIVE_LIGAND_RECEPTOR_INTERACTION [272]	Neuroactive ligand-receptor interaction	24		$7.91\ e^{-14}$	$1.31\ e^{-11}$
NABA_ECM_GLYCOPROTEINS [196]	Genes encoding structural ECM glycoproteins	20		$6.36\ e^{-13}$	$9.39\ e^{-11}$
REACTOME_AXON_GUIDANCE [251]	Genes involved in Axon guidance	19		$4.32\ e^{-10}$	$5.74\ e^{-8}$

(Figure 39) RNA-seq of lamina propria fraction of ST2IL17rbko mice (downregulated genes) under homeostatic conditions: (A) Heatmap shows differentially *downregulated genes* in ST2IL17rbko mice (lamina propria fraction) relative to Balb/c (lamina propria fraction) log 2 FC >1, FDR 0.05 ($p<0.001$). Genes are ranked from lowest (most significant) to highest (least significant) p-value. **(B)** Down regulated genes, were analyzed through Gene set enrichment analysis (Top 10 overlap, GSEA; Molecular signatures – C2 Canonical pathways (Top 10 overlap, CP: Curated gene sets)) FDR 0.05 (A, table top). Each sample is a biological replicate (n=5 / group). Out of 605 gene, 565 were identified by the database. Each Tables extracted from MSigDB. Details about sample collection and analysis is found in the methods section.

A great degree of overlap was found when comparing downregulated genes (239 genes) between the Δdbl.GATA1 and ST2IL17rbko, supportive for a role of IL33/25 in driving eosinophil-mediated villous maintenance **(Figure 40A)**. These commonly downregulated genes account for ~74% of genes downregulated in Δdbl.GATA1 and ~43% in ST2.IL17rbko mice **(Figure 40A)**. We ran this commonly downregulated gene set through the GSEA database, and it was enriched for the same pathways seen in the Δdbl.GATA1 mice dataset (*i.e.* matrisome, neuron-related pathways, muscle maintenance/contraction) **(Figure 40B; supplementary table 11).**

Lastly, we wanted to see which pathways were enriched in the ~60% of downregulated genes observed in ST2IL17rbko, but not Δdbl.GATA1 mice. We found that 11% of this gene set was involved in ECM-related processes, followed by neuron-related pathways (6%; receptor interactions, synapses) **(Figure 41; supplementary table 12)**. This indicates that alarmins may regulate ECM remodelling through both eosinophil-dependent and independent pathways.

(A)

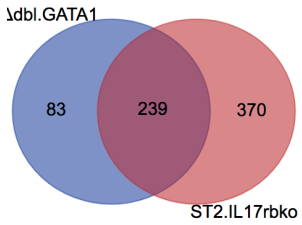

(B)

Gene Set Name [# Genes (K)]	Description	# Genes in Overlap (k)	k/K	p-value	FDR q-value
REACTOME_NEURONAL_SYSTEM [279]	Genes involved in Neuronal System	17		$7.48\ e^{-14}$	$9.94\ e^{-11}$
KEGG_NEUROACTIVE_LIGAND_RECEPTOR_INTERACTION [272]	Neuroactive ligand-receptor interaction	13		$1.35\ e^{-9}$	$6.2\ e^{-7}$
KEGG_CALCIUM_SIGNALING_PATHWAY [178]	Calcium signaling pathway	11		$1.77\ e^{-9}$	$6.2\ e^{-7}$
REACTOME_VOLTAGE_GATED_POTASSIUM_CHANNELS [43]	Genes involved in Voltage gated Potassium channels	7		$1.87\ e^{-9}$	$6.2\ e^{-7}$
REACTOME_POTASSIUM_CHANNELS [98]	Genes involved in Potassium Channels	8		$3.48\ e^{-8}$	$9.25\ e^{-6}$
REACTOME_TRANSMISSION_ACROSS_CHEMICAL_AL_SYNAPSES [186]	Genes involved in Transmission across Chemical Synapses	9		$4.39\ e^{-7}$	$9.71\ e^{-5}$
NABA_CORE_MATRISOME [275]	Ensemble of genes encoding core extracellular matrix including ECM glycoproteins, collagens and proteoglycans	10		$1.36\ e^{-6}$	$2.59\ e^{-4}$
NABA_MATRISOME [1028]	Ensemble of genes encoding extracellular matrix and extracellular matrix-associated proteins	17		$1.75\ e^{-5}$	$2.9\ e^{-3}$
REACTOME_DEVELOPMENTAL_BIOLOGY [396]	Genes involved in Developmental Biology	10		$3.27\ e^{-5}$	$4.83\ e^{-3}$
KEGG_ARRHYTHMOGENIC_RIGHT_VENTRICULAR_AR_CARDIOMYOPATHY_ARVC [76]	Arrhythmogenic right ventricular cardiomyopathy (ARVC)	5		$3.99\ e^{-5}$	$4.88\ e^{-3}$

(Figure 40) Comparative analysis of RNA-seq from lamina propria fraction (downregulated genes) of Δdbl.GATA1 and ST2IL17rbko mice under homeostatic conditions: (A) Venn diagram showing degree of overlap between downregulated genes identified in Δdbl.GATA1 and ST2L17rbko mice; FDR 0.05 (p<0.001), log2 FC>1) **(B)** Genes are ranked from lowest (most significant) to highest (least significant) p-value. Down regulated genes, were analyzed through Gene set enrichment analysis (Top 10 overlap, GSEA; Molecular signatures – C2 Canonical pathways (Top 10 overlap, CP: Curated gene sets)) FDR 0.05 (A, table top). Each sample is a biological replicate (n=5 / group). Out of 322 gene, 294 were identified by the database. Each Tables extracted from MSigDB. Details about sample collection and analysis is found in the methods section.

Gene Set Name [# Genes (K)]	Description	# Genes in Overlap (k)	k/K	p-value	FDR q-value
NABA_MATRISOME [1028]	Ensemble of genes encoding extracellular matrix and extracellular matrix-associated proteins	38		$4.2\ e^{-16}$	$5.58\ e^{-13}$
REACTOME_NEURONAL_SYSTEM [279]	Genes involved in Neuronal System	21		$2.97\ e^{-15}$	$1.97\ e^{-12}$
NABA_CORE_MATRISOME [275]	Ensemble of genes encoding core extracellular matrix including ECM glycoproteins, collagens and proteoglycans	18		$3.12\ e^{-12}$	$1.38\ e^{-9}$
REACTOME_POTASSIUM_CHANNELS [98]	Genes involved in Potassium Channels	11		$1.78\ e^{-10}$	$5.91\ e^{-8}$
NABA_ECM_GLYCOPROTEINS [196]	Genes encoding structural ECM glycoproteins	14		$2.64\ e^{-10}$	$7.01\ e^{-8}$
REACTOME_TRANSMISSION_ACROSS_CHEMICAL_AL_SYNAPSES [186]	Genes involved in Transmission across Chemical Synapses	12		$1.59\ e^{-8}$	$3.51\ e^{-6}$
KEGG_CALCIUM_SIGNALING_PATHWAY [178]	Calcium signaling pathway	11		$9.81\ e^{-8}$	$1.86\ e^{-5}$
REACTOME_TRANSMEMBRANE_TRANSPORT_OF_SM_SMALL_MOLECULES [413]	Genes involved in Transmembrane transport of small molecules	15		$5.2\ e^{-7}$	$8.65\ e^{-5}$
REACTOME_VOLTAGE_GATED_POTASSIUM_CHANNELS [43]	Genes involved in Voltage gated Potassium channels	6		$7.21\ e^{-7}$	$1.07\ e^{-4}$
REACTOME_NEUROTRANSMITTER_RECEPTOR_BINDING_AND_DOWNSTREAM_TRANSMISSION_IN_IN_THE_POSTSYNAPTIC_CELL [137]	Genes involved in Neurotransmitter Receptor Binding And Downstream Transmission In The Postsynaptic Cell	9		$8.67\ e^{-7}$	$1.15\ e^{-4}$

(Figure 41) Analysis of genes only downregulated in ST2IL17rbko mice (lamina propria) under homeostatic conditions: Analysis of genes of downregulated in ST2IL17rbko mice not shared with dbl.GATA1 mice (lamina propria fraction) relative to Balb/c (lamina propria fraction) FC log2 >1, FDR 0.05 (p<0.001). Gene set enrichment analysis (Top 10 overlap, GSEA; Molecular signatures – C2 Canonical pathways (Top 10 overlap, CP: Curated gene sets)) FDR 0.05 (A, table top). Each sample is a biological replicate (n=5 / group). Out of 605 gene, 565 were identified by the database (370 genes were differentially downregulated). Each Tables extracted from MSigDB.Each Tables extracted from MSigDB. Details about sample collection and analysis is found in the methods section.

5.3 Discussion

In this chapter, we identified a critical role for epithelial-derived alarmins in the initiation of eosinophil-mediated villous protective responses towards luminal microbiota.

This was achieved by first exploring pathways we hypothesized may be altered in response to the microbiota. We observed that both MYD88 and IL33/25 signalling are important for eosinophil maintenance of villus volume, with eosinophil-intrinsic ST2/IL17rb-signalling sufficient to mediate villous protection in response to microbial colonization. Furthermore, we also did a comparative analysis of our RNA-seq data from the Δdbl.GATA1 and ST2.IL17rbko datasets – and found a great degree of overlap between downregulated genes from the two strains further supporting that IL33/25-signalling is a key facilitator of eosinophil-mediated changes to ECM-related processes (*e.g.* turnover/composition) and in maintenance of contractile cells in the intestinal lamina propria.

Microbiota-induced release of epithelial-derived alarmin IL-33

Through this work, we show that epithelial-derived alarmin IL-33 is stored constitutively in intestinal epithelial cells under homeostatic conditions **(Figure 35)**. To our knowledge, we are the first to demonstrate this – as previous studies were only able to detect nuclear IL-33 in intestinal epithelial cells under inflammatory conditions. Epithelial IL-33 can be readily detected at a transcriptional level, but various groups were not able to detect IL-33 at a protein level using conventional, immunofluorescence microscopy under homeostatic conditions[49,219,222].

We used the wholemount technique to stain for IL-33, which requires the use of a fixation buffer containing Picric acid – a gentler fixative, known for its good preservation of antigenicity and precipitation of proteins[223,224]. However, conventional histology methods often require fixation with 4% paraformaldehyde over long incubation periods – which alters protein conformation, masking protein antigenicity over time. We propose that this discrepancy between our findings and others is solely due to technical differences. Indeed, we were able to confirm the validity of our staining using wholemount staining of IL-33ko mice – which were negative for nuclear IL-33.

With regards to the release of IL-33 following microbial-colonization, there are two possible reasons, that we did not have the ability to address in our studies. The first possibility is that SPF-colonized mice have increased mechanical load compared to GF mice, due to increased peristaltic activity in response to microbial colonization. It is known that IL-33 is released in response to mechanical stress – and activities that stimulate peristaltic activity such as feeding (discussed in Chapter 6) could account for this[221,225]. The second possibility is that epithelial IL-33 is released in response to the microbiota due to cellular stress[226,227]. Extracellular accumulation of ATP, which signals through P2X receptors, is a known 'danger signal' and previous studies have shown that this could trigger IL-33 release from epithelial cells. Given that the microbiota themselves could be a source of extracellular ATPs shown to influence a wide variety of processes in the intestine; it is possible that microbial-induced enterocyte release of IL-33 follows this mechanism[228,229].

In the small intestine, eosinophils are the most abundantly ST2-expressing cells, which are in close proximity to various stromal cells in the lamina propria. Therefore, microbiota-induced release of IL-33 could lead to eosinophil activation and release of factors directly to stromal cells – which could lead to changes in their activation status, thereby facilitate the maintenance of villous homeostasis in response to the microbiota.

Comparative analysis of RNA-seq from the lamina propria of Δdbl.GATA1 and ST2.IL17rbko mice

As mentioned previously, Tnbx, Nell1/2, p4ha3 and Hmcn2 are key genes in the maintenance of ECM rigidity and architecture – both through the provision of ECM substrates, and the appropriate bundling/interaction of these molecules. We observed that these genes are commonly downregulated in both Δdbl.GATA1 and ST2IL17rbko mice **(Figure 40, supplementary table 11)**. Furthermore, this was accompanied by downregulation of genes involved in myocyte striation/contraction. As these two strains exhibit significant villous defects, the potential contributions of these genes (and potentially other commonly downregulated genes) on protection against microbiota-induced villus shrinkage is likely, given their established roles in development and maintenance of tissue architecture and homeostasis.

Interestingly, although eosinophil-deficiency led to both downregulation and upregulation of genes that encode for matrix remodelling and inflammatory molecules, the upregulation of such

genes is absent in ST2IL17rbko mice **(supplementary table 10)**. While there are many possible interpretations for this, we propose a possible scenario whereby IL33/25-driven expression of genes encoding for ECM substrates could be dysregulated/imbalanced in the absence of eosinophils. As a consequence of this imbalanced deposition and disorganization of ECM-components, cells embedded throughout the matrix could potentially sense detrimental alterations in the mechanical properties of the ECM (*e.g.* via integrins, other mechanosensors) and could attempt to compensate for this through up regulation of other ECM-substrates, and remodel the existing matrix through release of metalloproteases[30,36]. However, despite this attempt to repair/remodel the ECM – the matrix instability resulting from the loss of key structural ECM components in Δdbl.GATA1 and ST2IL17rbko mice may not be sufficient to rescue the villus defect.

In addition to upregulation of ECM-associated genes, an increased inflammatory gene signature was also observed in Δdbl.GATA1 mice, which was not found in ST2.IL17rbko mice. This finding was particularly surprising, as there were no changes in lamina propria immune cell populations between Δdbl.GATA1 and control mice that could reflect this increased inflammatory gene signature **(chapter 3.2)**. Out of the upregulated genes in Δdbl.GATA1 that were inflammation related, a striking number belonged to the type-I IFN pathway (*e.g.* Cxcl10, Ifi44, Ifi16, Ifit3, Ifitm1, Oas3 – **supplementary table 8**)[230]. Type I-IFN upregulation can be induced in response to stimulation of cytoplasmic pattern recognition receptors such as TLR3/7/9, by nucleic acids such as dsRNA, ssRNA and DNA itself – in both immune and non-hematopoetic cells. This type of inflammatory signature is a critical component of immune response against pathogens[230–232], but has also been noted in tissue-damage[233], fibrotic-autoimmune disorders (*e.g.* systemic sclerosis)[234,235,236] and cellular senescence[237–239].

Eosinophils and IL-33 have been noted in driving the progression of fibrosis in a vast number of chronic inflammatory disorders such as asthma and IBD. However, within fibrotic tissue, senescent cells are also present[237,238]. Studies comparing the transcriptional signature of senescent vs. fibrotic cells have revealed Type-I interferon and MMP-related gene upregulation, being a primarily senescence-dependent signature[237,240]. In addition, senescent cells are accompanied by a decline in ECM production[238,241]. This is in contrast to other cells within fibrotic/injured tissue, which are largely enriched for genes involved in wound-healing and ECM-

production[237,238]. Therefore, it would be interesting to see how IL-33 driven fibrosis, in the presence or absence of eosinophils, could influence the maintenance/induction of cellular senescence in fibrotic tissue – and to see the implications this may have on tissue function.

Given that senescence-associated signature is increased in the absence of eosinophils, it is tempting to speculate that they may function as a negative regulator of senescence in the intestine. If it is true that senescence is increased in the absence of eosinophils, it would be interesting to see whether it is driven in response to the microbiota and/or eosinophil-independent, IL33/25 induced ECM remodelling. Regardless, the relevance of this gene signature to the villous phenotype we observed between Δdbl.GATA1 and ST2IL17rbko mice remains unclear.

Taken together, our data make a case for eosinophils contributing to the regulation of villus architecture/volume - with a significant role for cell-intrinsic IL33/25 signalling in driving this process. Eosinophil regulation of villous architecture is likely achieved through the regulation of ECM turnover and composition occurring in response to the microbiota. Neural and stromal networks (particularly contractile cells) may contribute to this process by functioning as a source for ECM-substrates/modifiers. In turn, eosinophil-mediated changes in ECM may also impact the function of stromal cells – both through the alteration of ligand bioavailability and changes in mechanical homeostasis.

Chapter 6: Assessing the impact of SI eosinophils on nutrient homeostasis

Eosinophils are enriched in the proximal intestine, where nutrient absorption takes place – particularly that of dietary lipids. This correlates with larger villus surface area in this region of the small intestine compared to the lower intestine where water and bile acids are resorbed; a region specific trait likely geared towards the maximization of dietary absorption.

In this chapter, we explore the contributions of eosinophils to nutrient homeostasis, by assessing 1) the function of eosinophils in nutrient absorption, 2) changes in eosinophil function in response to feeding.

6.1. ASSESSING THE IMPACT OF SI EOSINOPHILS ON NUTRIENT ABSORPTION

Through the work presented in the previous chapters, we have demonstrated the importance of eosinophils in the maintenance of villous surface area and integrity – in response to colonization of intestinal microbiota. We therefore reasoned that reduced villous volume in the proximal small intestine might have implications for nutrient absorption. We addressed this question in a broad sense, through evaluation of total caloric nutrition efficiency and, through assessment of lipid absorption capacity in Δdbl.GATA1 mice.

6.1.1 Eosinophil-deficiency does not impact total caloric absorption under homeostatic conditions

To examine whether eosinophil-deficiency impacts on total caloric absorption, we compared the energy assimilation of co-housed Balb/c and Δdbl.GATA1 mice using bomb calorimetry. In brief, we single housed male and female mice from these two different groups and acclimatized them for 24h prior to analysis, which includes a fixed fasting/re-feeding regime to reduce confounding variability in our analysis. In single-housing conditions, we were able to monitor the caloric intake (normal chow) of individual mice and examined their caloric intake efficiency by measuring the amount of energy in fecal pellets (collected over a period of 24 hours). The dessicated fecal pellets were then burned to completion in the bomb calorimeter, which measures the amount of energy present within the fecal samples – with higher energy in the

fecal sample positively correlating with caloric content. Furthermore, changes in body mass (for each single-housed mouse) over the course of the experiment, was also collected.

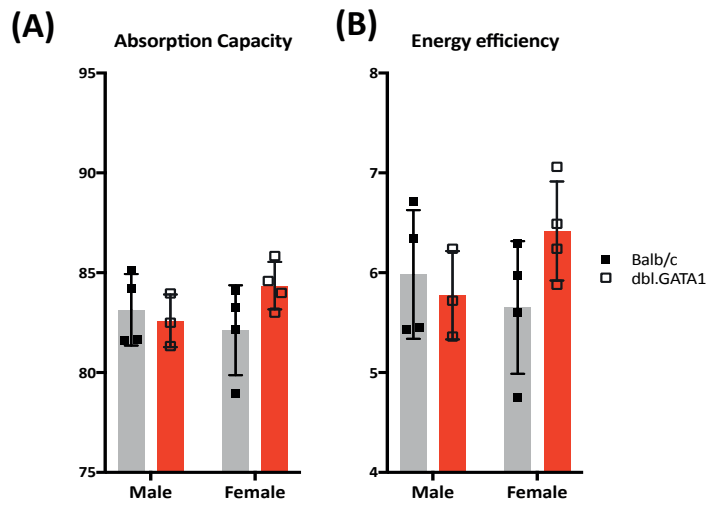

(Figure 42) Eosinophil-deficiency does not impact total caloric absorption under homeostatic conditions: (A) Absorption capacity (total caloric intake minus calories in feces (g)) from Balb/c (male, female) and dbl.GATA1 (male, female) mice over a period of 24h after acclimatization.**(B)** Energy efficiency (change in body mass from beginning to end of analysis/gross caloric intake). For measurement of calories lost in feces, pellets generated over a 24h period were collected, desiccated and burned in a bomb calorimeter to assess energy content. Error bars represent SD within group.

Caloric absorption capacity was measured by calculating the total calories consumed by each individual mouse, subtracted by total number of calories lost in the feces. In contrast, energy efficiency – which takes in consideration energy intake vs. output observed in body mass - was calculated dividing the change in body mass (in each individual mouse during the duration of the experiment) by the total calories (i.e. consumed + excreted in feces) absorbed during the same duration.

Overall, we found no differences in either caloric absorption efficiency **(Figure 42A)** nor energy efficiency **(Figure 42B)** between normal chow-fed Balb/c mice (control) and Δdbl.GATA1 mice. We also did not find any discrepancy between gender, with males and females exhibiting the same caloric absorption/energy efficiency over the course of the experiment. These results suggest that, at least under homeostatic conditions, eosinophil-deficiency (despite having significantly reduced villus area) does not have any gross impacts on total caloric absorption.

6.1.2 Dietary lipid uptake is impaired in the absence of eosinophils

Lipid absorption is a complex, multi-step process[242,243]. Lipids – which are hydrophobic – need to be emulsified by bile acids and subsequently require enzymatic digestion to monoglycerides and fatty acids in order for them to be absorbed via enterocytes. Within the enterocyte, they are synthesized into triglycerides and repackaged into chylomicrons. This step enables hydrophobic substances to be efficiently transported from the epithelium to the lacteal (lymphatics) and eventually the bloodstream.

Our previous RNA-seq analysis of the epithelial fraction from Δdbl.GATA1 mice suggest that genes involved in lipid processing (*i.e.* ketone, triacylglycerol) and lipid metabolism are decreased in the absence of eosinophils – with most targets participating in the PPAR-α pathway, which is important for fatty acid oxidization **(Figure 15)**. However, the relevance this has on nutrient homeostasis - particularly its influence on lipid absorption/utilization processes in the intestine, is unclear. To gain insight on the impact of eosinophils, we utilized triglyceride analysis as a means of comparing lipid absorption efficiency between Δdbl.GATA1 and Balb/c mice.

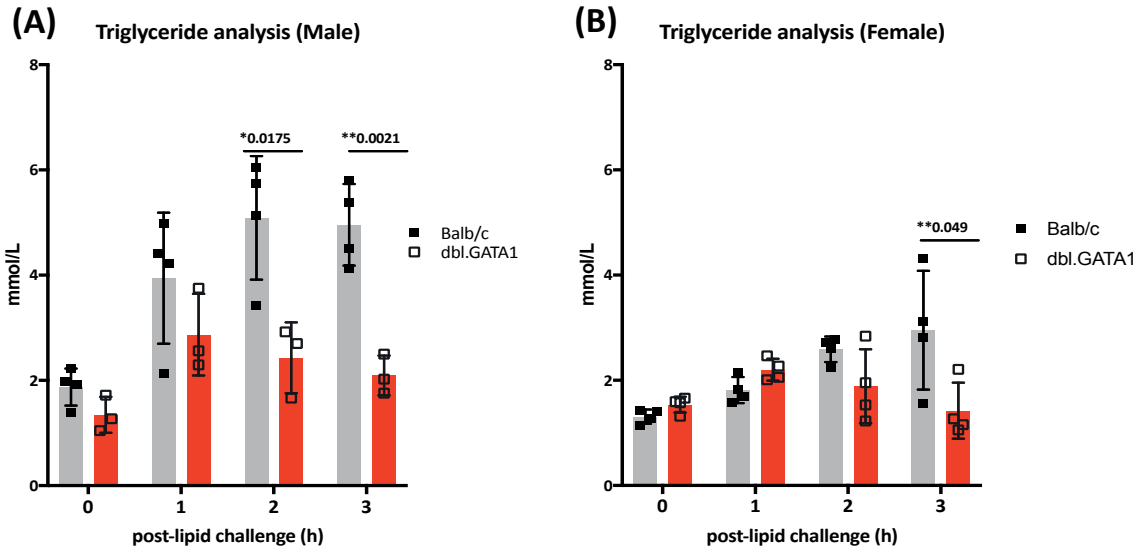

(Figure 43) Δdbl.GATA1 mice have decreased lipid absorption: Triglyceride concentrations (TG) in serum of **(A)** male and **(B)** female Balb/c, dbl.GATA1 mice challenged with olive-oil bolus (oral-gavage) after 3h-fasting period, data points corresponds to plasma TG concentrations at different time-points post-gavage. Data representative of at least 2 independent experiments (n=4-5 per group). Statistical analysis student (p-values as indicated in figure) t-test. Error bars represent SD within group.

In brief, mice were subjected to a lipid challenge (i.e. bolus of olive oil by oral gavage) 3 hours after fasting. We then collected blood samples at time point 0-3 hours post-gavage in 1-hour intervals to measure triglyceride concentrations in the blood. Such an analysis allowed us to broadly assess overall lipid absorption capacity and clearance in the mice. We also compared the 2 groups across genders to catch any gender specific differences in this process. In both male and female Δdbl.GATA1 mice, we observed decreased levels of triglyceride in the blood from 2, 3 hours post-gavage respectively – in comparison to challenged Balb/c controls **(Figure 43)**. While we observed this decrease in both male and females in the Δdbl.GATA1 group, the kinetics of triglyceride accumulation in the blood was different between genders. This data suggests that eosinophils may be required for optimal lipid absorption/processing.

6.1.3 High-fat diet does not deplete SI eosinophils

Subjecting Δdbl.GATA1 mice to a high-fat diet challenge would be a logical way of validating our observations of impaired lipid uptake in these mice. However, a previous study by Johnson et al. 2015 reported that chronic high-fat feeding resulted in depletion of small intestinal eosinophils[244]. In order to confirm whether this is occurring, we utilized flowcytometric and wholemount imaging methods to compare differences in eosinophil number and localization at 7 weeks of high fat diet challenge in the small intestine. By flowcytometry, we observed that, eosinophil populations were still present in the proximal gut of mice under high fat diet challenge **(Figure 44B)**. Using wholemount imaging, we did not notice any dramatic changes in eosinophil-localization or number after 7 weeks of HFD challenge, compared to mice on control chow **(Figure 44A).** This suggests that contrary to the Johnson et *al.* (2015) study, eosinophils were not depleted during chronic high fat diet. However, these findings do not rule out the possibility that eosinophil turnover/activation status may be altered under these conditions.

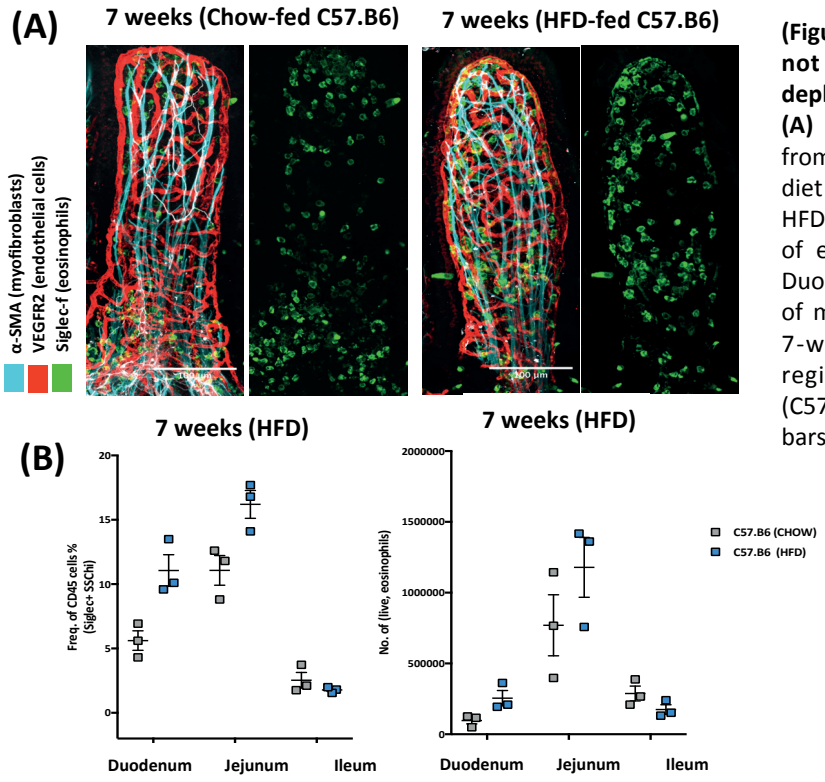

(Figure 44) High-fat diet does not result in SI eosinophil depletion:
(A) Wholemount image of villi from C57.B6 mice under chow diet (A, left) and 7 weeks post-HFD (A, right). **(B)** FACS analysis of eosinophils numbers in the Duodenum, jejunum and ileum of mice at **(B)** 3-weeks **(C)** and 7-weeks into HFD feeding regiment alongside controls (C57.B6 fed chow diet). Error bars represent SD

6.1.4 Eosinophil-deficient mice have decreased weight gain under high-fat diet

We next subjected Δdbl.GATA1 mice and Balb/c control mice to high-fat diet over the course of several weeks and monitored their fold change in weight gain from their initial weight pre-HFD. We report that Δdbl.GATA1 mice had a trend for decreased weight gain over time compared to control groups – particularly at 10 weeks of HFD challenge **(Figure 45A)**. In support of this finding, Δdbl.GATA1 mice had decreased fat mass (%) in the early to mid time-points of HFD challenge (*i.e.* 3, 6 weeks) as determined by echo MRI **(Figure 45B)**. However, this difference in fat mass between Balb/c and Δdbl.GATA1 mice under HFD challenge was lost from 14 weeks onwards, suggesting that these differences in lipid absorption is a phenomenon restricted to early stages of HFD challenge.

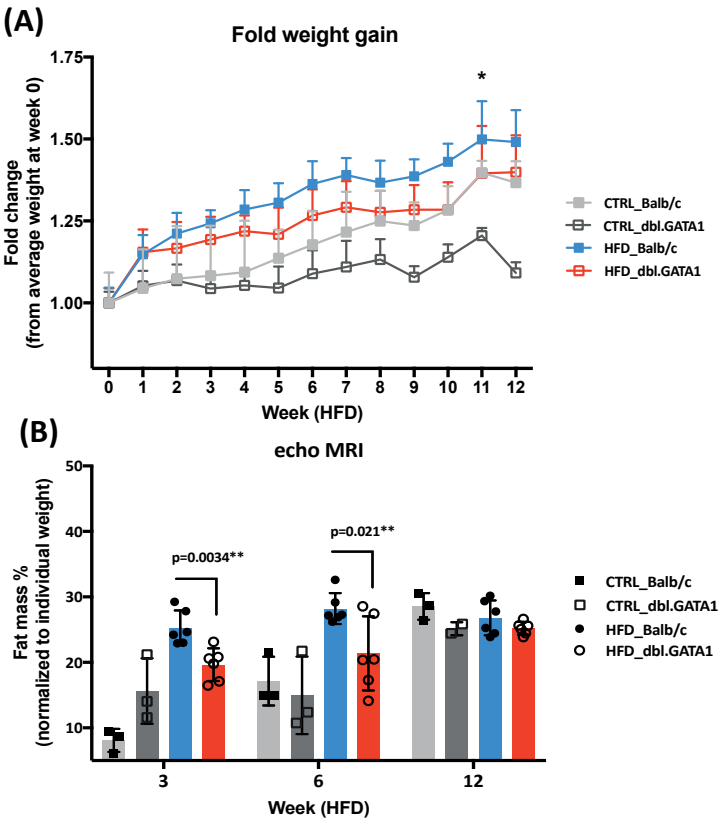

(Figure 45) Δdbl.GATA1 mice gain less weight under high-fat diet :
(A) Fold weight gain of control mice (CTRL_Balbc, CTRL_dbl.GATA1 mice on chow diet), and HFD-fed mice (HFD_Balbc, HFD_Δdbl.GATA1) from week 0 at various timepoints **(B)** Percentage fat mass from 4 groups analyzed in (A) at 3, 6 and 14 weeks post-initiation of experiment measured by echo MRI. Statistical analysis student t-test ($p<0.05$*), Error bars represent SD between group, n=3-6 mice per group.

Although we controlled for the microbiota of all groups by co-housing, we wanted to further eliminate the possibility that discrepancies in weight gain might have been due to differences in microbiota composition. In order to achieve this, we repeated the experiment with mice that were controlled for microbiota from birth. In brief, this was accomplished by mating females

(Balb/c and Δdbl.GATA1 mice) and males generated from heterozygous breedings. . The females, which were housed in the same cage, were separated for a brief period and housed with males from their respective genotype for mating purposes, and upon impregnation, were housed in the same cage again. This ensures that the homozygous litters (either Balb/c or Δdbl.GATA1) had their microbiota controlled from pre-post natal life until the weaning period.

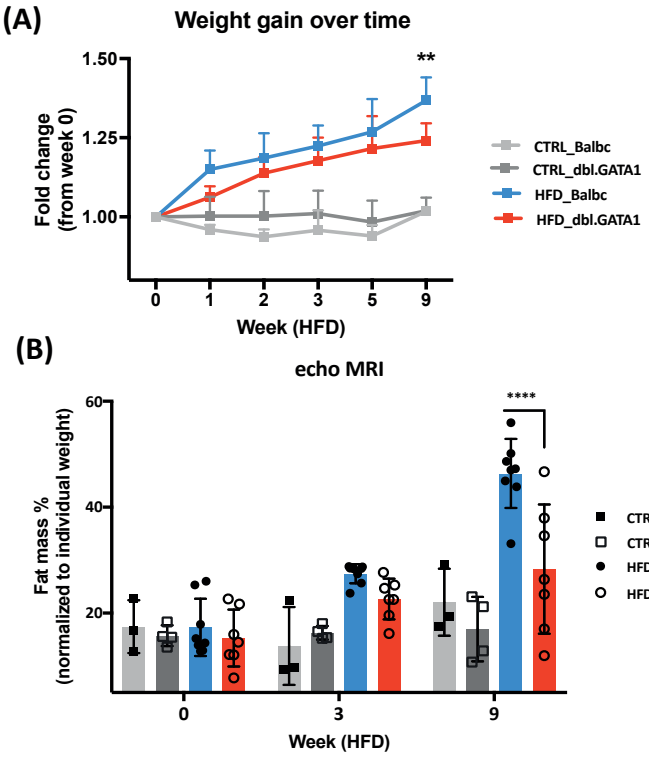

(Figure 46) Decreased weight gain in HFD-fed dbl.GATA1 mice is independent of microbiota-composition:
(A) Fold weight gain of microbiota-normalized control mice (CTRL_Balbc, CTRL_dbl.GATA1 mice on chow diet), and HFD-fed mice (HFD_Balbc, HFD_dbl.GATA1) from week 0 at various timepoints **(B)** Percentage fat mass from 4 groups analyzed in **(A)** at 0, 3 and 9 weeks post-initiation of experiment measured by echo MRI. Statistical analysis student t-test ($p<0.01$**, $p<0.0001$***). Mann-Whitney test correction was added if SD >0.05. Error bars represent SD, n=3-6 mice per group.

After the mice were weaned, we continued to co-house the mice. We observed that, similarly to the first HFD experiment, HFD-challenged Δdbl.GATA1 mice had decreased fold weight gain in comparison to the other groups **(Figure 46A)**. Furthermore, we also observed that HFD-challenged Δdbl.GATA1 mice had decreased fat mass% compared to the control groups as measured by echo MRI **(Figure 46B)**. However, we observed that this phenotype arose at a later timepoint than the first experiment (i.e. 9 weeks vs. 3 weeks post-HFD) – it is unclear whether this is due to experimental variation or a direct consequence of microbiota normalization between the groups.

Taken together, this data supports our initial observations of impaired lipid uptake/utilization in the absence of eosinophils.

6.2. POST-PRANDIAL REGULATION OF EOSINOPHIL FUNCTION AND ITS IMPLICATIONS ON INTESTINAL HOMEOSTASIS

Eosinophils are known to follow circadian cycling in the blood, with meal timing identified as the dominant synchronizer of this pattern instead of light/dark cycles[92,245]. In brief, circadian cycling describes phenomena where biological processes (e.g. cellular migration, gene transcription) undergo predictable oscillatory patterns over the course of a 24-hour period. Given that the intestine is the primary site of nutrient absorption and that eosinophils are impacting on lipid uptake we wanted to understand the impact of feeding on resident eosinophils – and explore the relationship this has on eosinophil cycling (in terms of number and activation) in this tissue.

6.2.1 Circadian rhythm, nor feeding, impact ILC2 and eosinophil numbers in the SI

Nussbaum et al. 2013, has shown that in response to feeding – intestinal ILC2s upregulated expression and release of IL-5 and IL-13 and these cytokines are known regulators of eosinophil migration, survival and activation[92]. Therefore, we devised an experiment with the purpose of addressing whether feeding regulated intestinal eosinophil numbers. In brief, we utilized wild-type C57.B6 mice and looked at the changes in eosinophil and ILC2 frequencies in the proximal and distal intestine under fed and fasted conditions. To ensure that all the mice used in the experiment were synchronized – we restricted feeding times to the dark cycle (~ 7PM) where mice are noted to be more active, and removed food during the light cycle (~7AM) as mice are known to be less active/feed less during this period. As an additional control, we utilized BMAL1-ko mice – which have asynchronous circadian rhythm due to a deletion of BMAL1 - a master regulator of various clock genes. This would allow us to separate the influence of clock-related genes on eosinophil and ILC2 cycling. We report that contrary to reported cycling of eosinophils in the blood, neither SI eosinophils nor ILC2s from C57.B6 and BMAL1ko mice - change in frequency in response to feeding **(Figure 47)**. However, this does not rule out changes in the activation status of these cells in response to feeding.

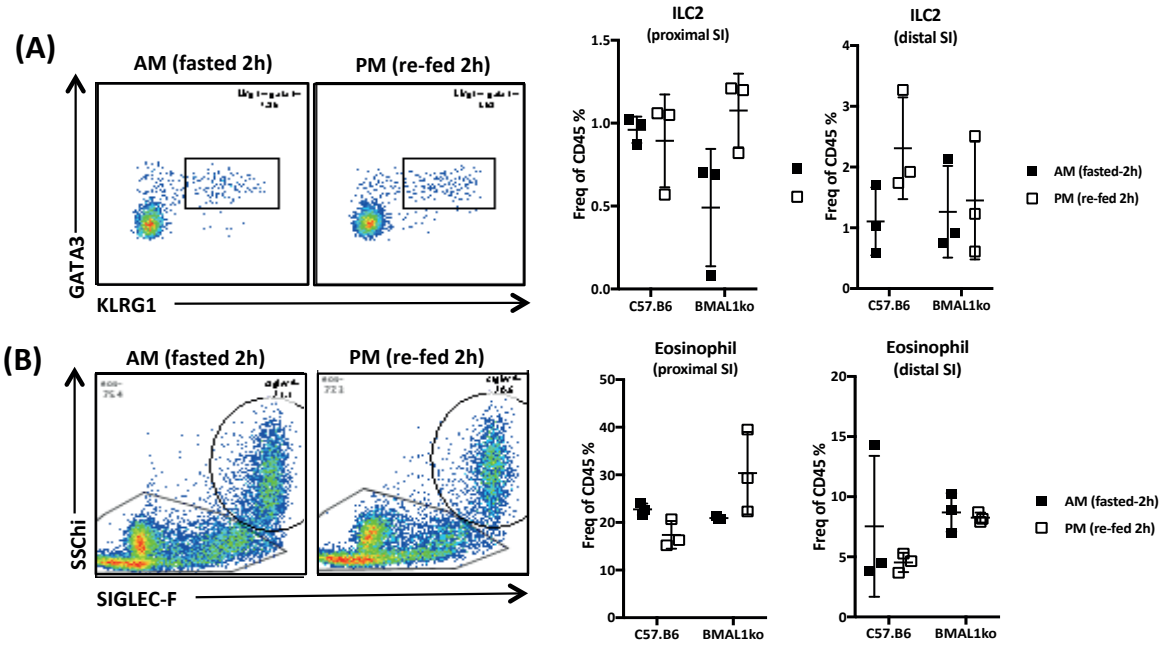

(Figure 47) SI eosinophil and ILC2s population frequency do not change in response to feeding: (A) Representative FACS plot of ILC2s from the proximal SI of fasted (AM; after 12 hours of feeding *ad-libidum*, analyzed 2h of fasting) and re-fed (PM; after 12 hours of fasting, analyzed 2h post-re feeding) C57.B6 mice; (A, bottom) Quantification of ILC2 frequency within total CD45 cells in the proximal, distal small intestine of C57.B6 and Bmal1ko mice (pre-gated on live CD45+ CD3- GATA1+ KLRG1+). **(B)** Representative FACS plot of eosinophil from the proximal SI from fasted (AM) and re-fed (PM) C57.B6 mice; (B, bottom) Quantification of eosinophil frequency within total CD45 cells in the proximal, distal small intestine of C57.B6 and Bmal1ko mice (pre-gated on live CD45+ SSChi Siglecf+). Data representative of 2 independent experiments. Error bars denote SD within group.

6.2.2 Changes in epithelial IL-33 patterning in response to feeding

Although Nussbaum et al. 2013, identified vasoactive intestinal peptide (VIP) signalling to ILC2s as a regulator of IL-5/13 release in response to feeding we reasoned that other cytokines, such as IL-33 may also play a role[92]. IL-33 is known to be a potent activator/inducer of IL-5/13 release in ILC2s and likely signals directly to intestinal eosinophils which constitutively express ST2 (IL-33 receptor). As discussed previously, IL-33 is released in response to cellular stress and damage and is widely expressed by intestinal epithelial cells under homeostatic conditions. Feeding, (especially binge feeding post-fasting), results in dynamic changes to intestinal mechanics, due to the increased luminal load, and peristaltic activity – as the bolus/chime churns and migrates down the intestinal tract.

In order to determine whether or not IL-33 is released in response to feeding, we utilized wholemount imaging to identify changes in the nuclear IL-33 pattern in the small intestinal

epithelium around the feeding period (i.e. 12-hours fasted, ad-libidum fed, 1.5 and 3 hours post-feeding) in Balb/c mice. We did not observe any dramatic changes in the pattern of nuclear IL-33 in the epithelium of mice fed *ad-libidum* compared with fasted mice **(Figure 48A vs. B).** In contrast, we saw a striking decrease in IL-33 staining 1.5h post-feeding **(Figure 48C)** – suggesting that IL-33 may indeed be released in response to feeding. At 3 hours post-feeding, nuclear IL-33 is still decreased – but looks like it is slowly rebounding compared to the I.5 hour post-feeding time point **(Figure 48D)**.

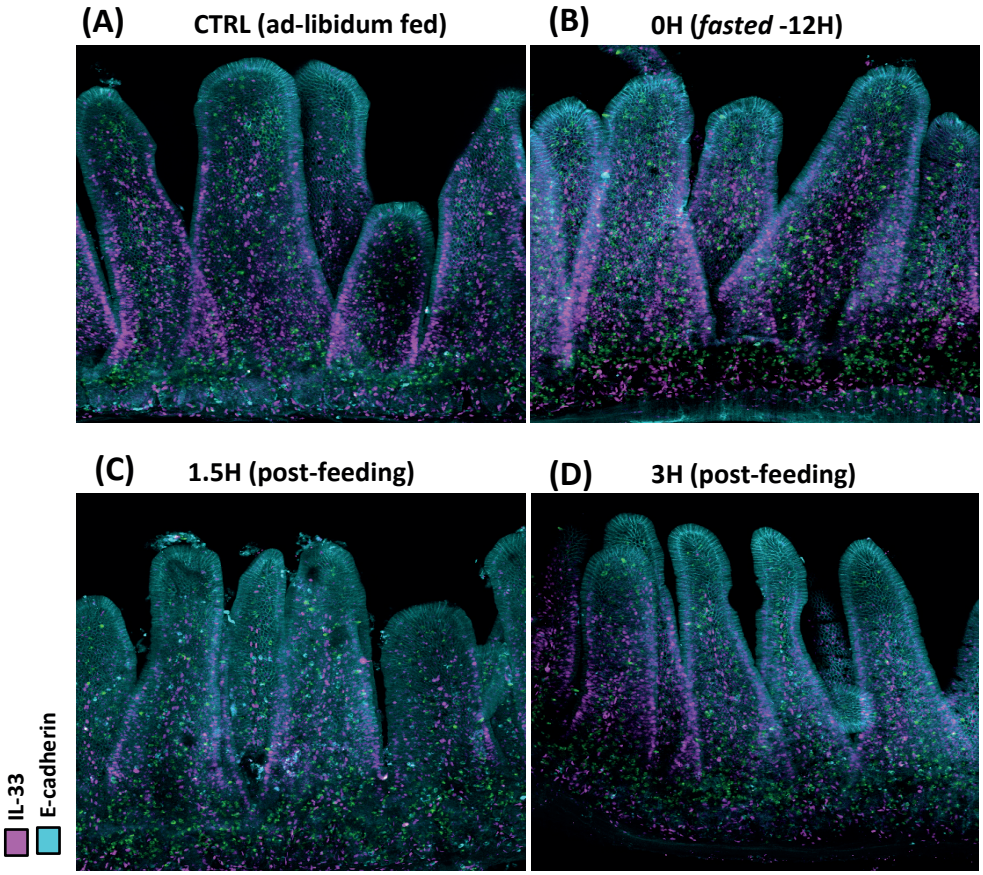

(Figure 48) Changes in epithelial IL-33 patterning in response to feeding: Representative wholemount images from Balb/c mice fed *ad-libidum* **(A)**, 12-h fasted (**B)**, 1.5h post-feeding **(C)** and 3h post-feeding **(D) –** after 12h-fasting regime.

6.2.3 Down-regulation of surface ST2 expression may correspond to active IL-33 signalling in response to feeding

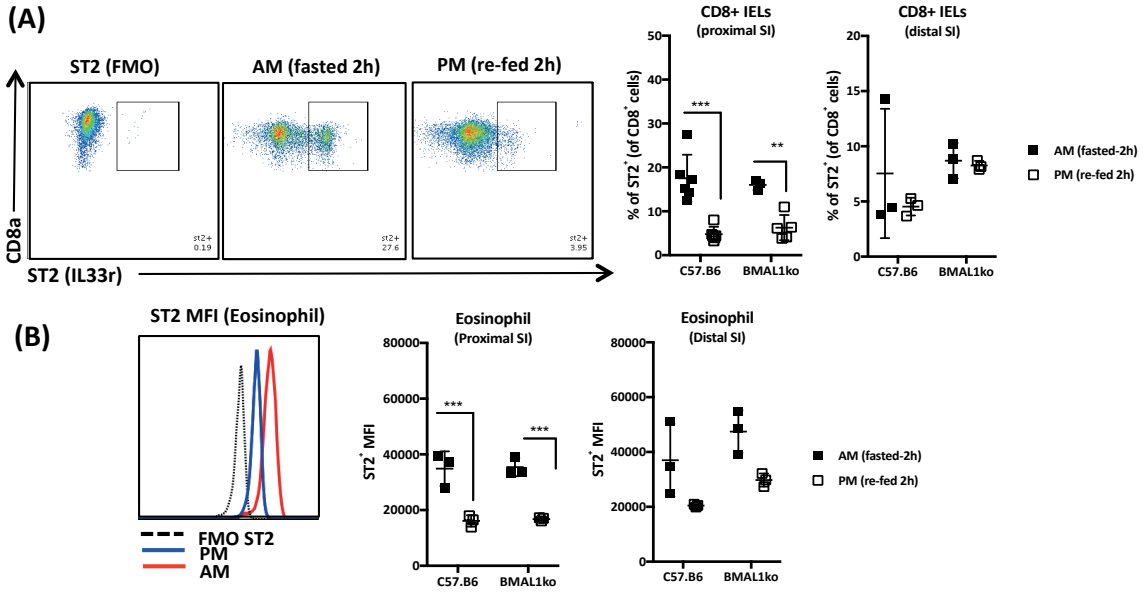

(Figure 49) Surface ST2 is downregulated in ST2+ cells in response to feeding: (A) Representative FACS plot showing gating for ST2+ cells within CD8a+ IEL populations (pre-gated live, CD45+ CD3+). Quantification of surface ST2+ CD8 IELs in the epithelial fraction of C57.B6, BMAL1ko mice at 2h-post refeeding (PM), and after 2-hours fasting (AM) from the proximal, distal small intestine. **(B)** Representative plot of ST2 MFI from SI eosinophils obtained from the lamina propria of proximal and distal small intestine at AM (red), PM(blue) time-points – plotted against FMO control (dotted line – black); quantifications of MFI from C57.B6 and BMAL1ko mice. Data pooled from 2 independent experiments (n=1-3 mice per experiment). Error bars represent SD between samples.

IL-33 binding to its receptor ST2, results in internalization of ST2 and subsequent degradation in the proteasome[246,247]. This process has been described to be one of the critical mechanisms regulating IL-33 signalling, which could induce damage and pathology if unregulated[110,219]. To corroborate our observation of IL-33 release in response to feeding, we wanted to use ST2-internalization as a proxy for active IL-33 signalling in the SI. For this experiment, we separated the epithelial layer from the lamina propria fraction. Since, CD8α+ IELs (in the epithelial fraction) and Eosinophils (in the LP fraction) are known to express high levels of ST2+ we focused on these 2 populations for our analysis. Concurrent with the release of epithelial-derived IL-33 in response to feeding, we observe decreased expression of surface ST2 at the PM (re-fed) time point compared to the AM (fasted) timepoint in both CD8α+ IELs **(Figure 49A)** and eosinophils **(Figure 49B)** in the proximal and distal intestine. This decreased is not dependent on BMAL1-

mediated circadian regulation as the same changes were observed in these mice in response to feeding. Taken together, these findings suggest that in response to feeding, epithelial-derived IL33 is released and signals to ST2+ cells. However, given that the preliminary nature of these findings, the functional significance of this active IL-33 signalling to intestinal homeostasis remains unclear.

6.3 DISCUSSION

In this chapter we investigated the function of eosinophils in nutrient homeostasis. This was explored in two ways, with the first focusing on the impact of eosinophil-deficiency on nutrient absorption. The second part, examined eosinophil responses to feeding.

Eosinophils are required for optimal intake of dietary lipids

In the first part, we studied the consequences of eosinophil deficiency on nutrient absorption. While we did not see an impact in total caloric absorption, we report that Δdbl.GATA1 mice exhibited impaired lipid uptake in response to intake of triglyceride-rich nutrients. This was supported by the decreased weight gain under high-fat diet in the absence of eosinophils. We also observed that, this reduced weight gain is independent of gender – removing the possible impact of sex-dependent hormones on this phenotype. On this note, normalization of the microbiota between Δdbl.GATA1, and Balb/c control mice – did not abolish this phenotype, suggesting that it is not necessarily due to eosinophil-dependent modulation of intestinal microbiota.

Lipid absorption and trafficking in the small intestine is a complex multi-part process that requires careful coordinated effort between enterocytes and lacteal/lymphatics. At the level of absorption, enterocytes play a major role – facilitating the processing and integration of complex lipids (broken down in the intestinal lumen) into chylomicrons. This renders hydrophobic molecules to be transported across the lamina propria and into the lacteal/lymphatics.

Based on our RNA-seq data from the epithelial fraction of Balb/c and Δdbl.GATA1 mice, there does not appear to be any defects with regards to chylomicron packaging and lipid transport into the enterocytes that could account for the decreased lipid intake in Δdbl.GATA1 mice (data not shown). However, we did see a decrease in PPAR-α signalling in intestinal epithelial layer indicating a potential decrease in fatty acid oxidization capacity in enterocytes of Δdbl.GATA1 mice **(Figure 15).** It is unclear whether this account for the decreased lipid absorption observed, as studies on PPAR- α signalling in the context of high-fat feeding is actually protective against obesity; which contradicts our observations[188,248,249]. Nonetheless, these studies often utilized mice fully deficient in PPAR- α signalling – and does not account for any tissue-specific

differences in PPAR- α function. Indeed, studies of PPAR- α signalling in the intestine do not seem to reveal metabolic defects [189,190].

Similarly, a broad analysis of lymphatic network in the villous lamina propria did not reveal any overt defects **(Figure 23)**. Instead, we see a significant downregulation of genes involved in actomyosin/muscle contraction – likely coming from contractile cells in the lamina propria **(Figure 39)**. Of these contractile cells, myofibroblasts play an important role in lipid transport. These α-SMA positive cells form a highly-branched network surrounding the lacteal. As lacteals are blind-ended, piston-like contractile activity *via* neural input is purportedly facilitating chylomicron movement from the lacteal into the underlying submucosal lymphatic enabling systemic transport of packaged lipids[27,250]. Considering the enrichment for downregulated expression of genes involved in neuron activation and function – it is tempting to speculate that this process is impaired in the absence of eosinophils. It is unclear however, whether eosinophils impact this process directly through provision of neuro-active ligands or through release of leukotrienes which result in smooth muscle contraction. Alternatively, this decreased activity could also be secondary to alterations in the ECM, which could impact the mechanical properties of the villous lamina propria – in addition to regulating bio-availability/distribution of molecules regulating this process.

Implications of IL-33 signalling on eosinophil-mediated responses to feeding

Our observations suggest that epithelial-derived IL-33 is released in response to feeding. This is supported by the downregulation of ST2 surface expression in eosinophils and CD8+ T-cells, indicating increased receptor internalization in response to ligand binding. However, the mechanism mediating this release in response to feeding remains unclear. One possibility is that IL-33 release in this context is driven by increased mechanical/peristaltic activity in the response to feeding. Alternatively, the bolus itself could cause acute epithelial stress/damage as it travels down the intestinal tract. Tissue damage is likely to occur to a greater extent in the proximal than the distal small intestine as I) the food bolus is less digested/bulkier in the proximal part, II) the villi are longer here and III) mucous is sparse in the proximal section but increases in depth in the distal regions. Interestingly this hypothetical axis of damage runs ante to the distribution of intestinal eosinophils supporting the idea that these cells may be present in the proximal small intestine to repair damage.

IL-33 has mostly been studied in the context of inflammation, and has often been alluded to as a culprit promoting epithelial barrier disruption in several disorders. However, IL-33 is also be expressed in epithelial cells at barrier sites such as the lung and the intestine under homeostatic conditions questioning the dogmatic view of this cytokine as only pathophysiologic and only being present under conditions of disorder[110,219]. Indeed, a few studies are supportive for a beneficial role of the IL33/ST2 axis in barrier maintenance [49,251]. Epithelial cells store IL-33 in their nucleus, and released in response to damage. Once out in the extracellular space, they are rapidly oxidized thereby limiting their bioactivity under steady state conditions[123]. Post-translational regulation of IL-33 can also render them inactive or decrease/ enhance their affinity for ST2 depending on the site of cleavage[110,219]. Consideration of this differential regulation of IL-33 protein could potentially explain their dual nature as a homeostasis-promoting, or damage-inducing factor.

While our findings are preliminary in nature, it is tempting to speculate that this transient release of IL-33 in response to feeding could be promoting tissue repair, or aid in intestinal adaptation to increased mechanical load. Furthermore, given the common downregulation of contraction and neural activation pathways between ST2.IL17rbko and Δdbl.GATA1 mice, it could also be possible that this crosstalk between IL33/eosinophils may also be important in regulating peristaltic tone/activity, chylomicron trafficking and satiety responses in to feeding via regulation of the enteric nervous system. Of note, we observed eosinophils to be in close interaction with glial cells and neurons in the villous lamina propria **(Figure 5D, E)**. Indeed, with the villous glia and neurons in reciprocal interaction with submucosal and muscular networks – the tissue is equipped for such a possibility.

Chapter 7: Conclusions and Perspectives

7.1 SUMMARY OF FINDINGS

In this thesis we investigated the functional significance of eosinophil residency in the small intestine under homeostatic conditions.

We identified the microbiota as a regulator of eosinophil activation and survival – with eosinophils playing an important role in the establishment of appropriate host-microbiota interactions. Eosinophils were found to primarily reside in the villous lamina propria, in close interaction with structural cells such as myofibroblasts, blood vessels, enteric neurons and glial cells making these cells a potential primary target for eosinophil-derived molecules released upon activation.

The importance of eosinophils in the establishment of host-microbiota homeostasis was demonstrated by microbiota-driven defects in villous architecture (*i.e.* shrinkage), and altered epithelial barrier integrity (*i.e.* IEC turnover, increased permeability) in the absence of eosinophils. We also report significant impairment of intestinal lipid absorption capacity in Δdbl.GATA1 mice – despite finding no obvious defects in the expression of genes that regulate enterocyte lipid transport capacity, or any overt alterations in intestinal lymphatic homeostasis.

In contrast to the obvious contribution of eosinophils to the regulation of intestinal architecture and barrier integrity, we did not find obvious defects in immune cell homeostasis in the intestinal lamina propria in the Δdbl.GATA1 mice. Eosinophils, did however, contribute to the regulation of microbiota-induced intraepithelial lymphocytes.

We established that epithelial-derived alarmins IL-33/25, released in response to injury and mechanical stress, are a major driver of eosinophil-mediated function in the small intestine and that these function by shaping the repertoire of eosinophils-derived molecules released in response to the microbiota. Nuclear IL-33, which is stored in all enterocytes in the epithelial barrier, was found to be released in response to the microbiota and to feeding – serving as an example of IL-33/eosinophil crosstalk in a physiological context, under homeostatic conditions.
Through RNA-seq analysis, we have identified significant overlap between pathways affected by IL-33/25 and eosinophil-mediated signalling. The most notable changes were in ECM-associated

processes. This indicates that eosinophils may play a critical role in the determination and regulation of ECM homeostasis, even under homeostatic conditions, and that their activation by IL-33/25 likely contributes to this. Furthermore, gene signatures altered by both eosinophils and IL-33/25 are enriched in contractile cells such as myofibroblasts, in addition to neurons – suggesting that eosinophils, under the influence of IL-33/25, may be modulating the ECM through direct/indirect actions on these targets.

7.2 WORKING MODEL OF SI EOSINOPHIL FUNCTION DURING HOMEOSTASIS

In consideration of all the findings presented here, we argue for ECM regulation as a key function of eosinophils in the small intestine.

We suggest that a major function of eosinophils in the intestine is to maintain a balance between ECM-remodeling and deposition. Positive regulation of ECM deposition is achieved with significant input from epithelial-derived alarmins IL33/25, likely released in response to the microbiota and mechanical stimulation driven by feeding responses. Simultaneously, eosinophils also seem to negatively regulate ECM deposition and turnover. The dual nature of eosinophils in this process is suggestive that eosinophils function as a cellular rheostat to control ECM dynamics according to tissue demands - whether mechanical or molecular.

Eosinophil recruitment to intestinal tissue is a developmentally regulate process, that occurs independently of the microbiota. Cells recruited in early life have often served an important function with regards to total tissue homeostasis and development. However, the significance of eosinophil recruitment in early life, and of the residency of eosinophils in the small intestine under steady state conditions, has remained an enigma in the field of immunology - given the supposed tissue-destructive role for these cells in disorders such as asthma and eosinophilic esophagitis. Based on our findings we argue that the early life recruitment of eosinophils holds a fundamental importance for tissue integrity under homeostatic conditions, as the loss of eosinophils results in significant defects in villous architecture (*i.e*. volume) and barrier integrity in response to the microbiota. The establishment of appropriate host-microbiota interactions is well known to be critical for maintaining overall organismal physiology, and our findings suggest that eosinophils play an important role in facilitating this process

Several parameters such as villous volume/morphology and intestinal mechanical activity are changed between colonized and germ-free settings. Germ-free mice exhibit thinner and longer villi, whereas colonized mice present with shorter villous exhibiting increased villous volume[201,202]. Furthermore, the intestine of GF mice has significantly decreased peristaltic activity compared to SPF-colonized mice[39,202]. Both of these parameters are heavily influenced by changes in ECM dynamics and mechanical properties within the intestinal tissue suggesting that the microbiota influences homeostatic tissue remodeling. Our work suggests that eosinophils play a role in regulating microbiota-induced alterations to villous architecture. However whether or not these cells also regulate microbiota-induced alterations to intestinal contractility remains to be determined.

Of note small intestinal eosinophils localized in the villous lamina propria were in close contact with neurons, glia and myofibroblasts indicating that cross-talk between eosinophils and various stromal cell populations is likely to occur – and possibly explaining why eosinophil deficiency lead to a dysregulation of gene networks involved in processes influencing the maintenance of neuronal plasticity, activation and development, and myocyte contraction/homeostasis. We speculate that eosinophils could be impacting these processes directly through provision of factors (*e.g.* NGF for neurite growth, leukotrienes for muscle contraction). Alternatively or simultaneously, eosinophils could also be influencing these processes indirectly via its activation of myofibroblasts (*e.g.* via IL6, TGF-β release) stimulating ECM deposition - which could alter signaling of adherent cells and the bio-availability of molecules bound to the ECM[253].

In addition to the villous defects discussed above, we also observed changes in IEC migration/restitution that did not appear to be due to cell-intrinsic changes in IEC homeostasis. IEC migration is dependent on the anchoring properties of IECs to the basal lamina matrix, and this defect is likely due to alterations in ECM composition and mechanics of the sub-epithelial ECM network in the absence of eosinophils[20,254,255]. Overall, we do not know if it's due to decreased ECM deposition or, increased ECM turnover that drives these defects. Experiments are currently on going using mass spectrometry analysis of ECM-enriched fraction from the small intestine of Δdbl.GATA1 mice, to truly assess the ECM changes resulting from eosinophil deficiency.

A role for eosinophils in regulating ECM dynamics and mechanical properties is supported by the literature[143,253,256–258]. In these publications the authors investigate a pathological role for eosinophils, reporting that they promote tissue fibrosis through promoting ECM deposition and increasing stiffness of the ECM. We argue that maybe under homeostatic conditions, the same processes eosinophils use to promote fibrosis may actually be beneficial and by regulating the 3D structure of the ECM and by allowing tissues such as the intestine to adapt to environmental stressors.

7.3 FUTURE DIRECTIONS

Validation of RNA-seq data

RNA-seq of tissues provides a wealth of data, but it is clear that it must be approached with caution, requiring validation for targets of interest. A major limitation for RNA-seq is that, while expression may be changed – it may not necessarily translate to changes at a proteonomic level. To address this limitation, we will utilize mass spectrometry analysis in order to complement our RNA-seq analysis and validate our RNA-seq targets. Since most of the genes altered in our models were ECM substrates or ECM-associated factors, we will limit our analysis to the characterization of changes in the ECM-enriched fraction of the proximal small intestine. This will be achieved by unbiased, broad analysis of the ECM-enriched fractions, in parallel to Label Free Quantification mass spectrometry methods – which in combination, would allow us to not only characterize the overall changes and composition of the ECM, but also increase our resolution in order to detect low expressed ECM-associated components. These experiments are currently ongoing.

Another limitation of our RNA-seq data is that, in complex, and heterogeneous (cellular) tissues such as the intestine – it is difficult to decipher which cell type(s) the genetic signature of interest is emanating from. Currently, there are no known cell surface markers distinguishing myofibroblasts (a likely target of eosinophil activation). Therefore, we will have to confirm genes of interest in samples enriched for stromal cells (i.e. CD45-) by a combination of QPCR and immune-blotting/imaging techniques.

IL33/25 signalling in eosinophil-mediated responses under homeostatic conditions

Due to the unavailability of single ST2 and single IL17RB knockout mice at our disposable, we were not able to confirm whether IL-33, IL-25 or both IL33/25 signalling is responsible for eosinophil-mediated homeostatic maintenance of the small intestine. We aim to address this issue, by validating our findings using a model where eosinophils are deficient for both, or either receptors in a cell-intrisic manner using cre/flox system. Alternatively, we could also conduct this experiment using mixed-BM chimeras using a similar set up as presented in Chapter 5 **(Figure 37)**. Upon identification of the relevant signalling pathway, we plan to also test the dependence of the phenotype on the microbiota using germ-free models. Furthermore, we would like to further characterize the mechanism relevant for the release of the identified cytokine in response to the microbiota.

Characterization and identification of tissue protective, eosinophil-derived molecules

The microbiota and IL33/25 signalling plays an important role in driving and mediating homeostatic function of eosinophils in the intestine. However, it is still unclear as to how the microbiota and IL33/25 signalling influence the repertoire of pre-formed molecules stored in the eosinophil cytoplasm. These questions are currently being addressed, through our collaborators (McCoy lab; University of Calgary) by mass spectrometry analysis of eosinophils derived from GF and SPF mice. It would also be of interest to do a similar analysis in eosinophils derived from either ST2/IL17RBko mice once we identify which receptor is relevant for eosinophil homeostatic function.

Elucidating the role of eosinophils in the regulation of mechanical activity in the small intestine

Many of the pathways altered in Δdbl.GATA1 were found to be involved in muscle contraction, neurogenesis/maintenance and ECM-related process, indicative of alterations in neuromuscular junctions. All these factors have the potential to influence the mechanical properties of the intestinal connective tissue. To determine whether these alterations translate into a physiological consequence, future studies will be conducted investigating potential defects in peristaltic activity of the small intestine (by organ bath studies).

Peristaltic activity will also be assessed at an individual villus level. Eosinophil-deficient mice had impaired lipid absorption, both upon lipid challenge and under high-fat diet. However, we were

unable to identify any defects in enterocytes that could account for this phenotype. Chylomicron movement from the lacteal, into the central lymphatics is facilitated by contractile activity of myofibroblast network, which branch around the lacteal. To test where this could be explained by defects in intravillus peristalsis, our collaborators (Petrova lab; University of Lausanne) are currently working on a method that would enable us to measure the contractile activity of myofibroblasts in response to lipid uptake – by two-photon microscopy.

7.4 SIGNIFICANCE OF OUR FINDINGS

The proximal intestine is a primary site for nutrient absorption but it is also a very complex system that requires delicate balance. On one hand, you need it to maintain barrier integrity because it is an immune dense place with and little protection (*e.g.* mucus barrier). This makes it a prime site for host-microbiota crosstalk, with is good for the host in terms of immune homeostasis - but dangerous if dysregulated. On the other hand, you also need to maintain a degree of permissibility in order to in order to maximize absorption of nutrients. Lastly, it's also a highly mechanical part of the small intestine within which, some of the strongest peristaltic waves are encountered, in order to maximize churning and nutrient contact with the villous epithelia. In case of high mechanical load (*i.e.* re-feeding after fasting) this could potentially lead to acute epithelial barrier damage/breech - which may in turn activate eosinophils to reinforce the barrier before the microbiota translocates to the lamina propria. Well-balanced ECM stiffness (in compressibility, structure) combined with maintenance of elasticity is necessary to tolerate dynamic changes in mechanical load. If these abilities are lost, once could imagine significant 'wear and tear' of the tissue would result. Our data reveal a previously unrecognized role for eosinophils in providing resistance against this 'wear and tear' and opens the door to many new questions related to eosinophil biology.

Our data also highlights an important role for IL33/25 signaling in maintaining tissue integrity in the small intestine in response to feeding and the microbiota, with microbial and other luminal signals (e.g. dietary) dictating the extent of release of epithelial cell-derived alarmins. For example, in the event of acute tissue damage, IL33/25-mediated eosinophil function might promote tissue homeostasis. However, if the activating signal (e.g. injury) become to intense or becomes dysregulated - IL33/25 signaling might override the negative feedback of eosinophils on the ECM, promoting excessive deposition of matrix and fibroblast expansion causing fibrosis

to occur. Of course, this inflammation/remodeling event will be resolved under healthy circumstances, but if the microbiota is imbalanced (unhealthy) it may make this healing process defective, causing chronic remodeling and inflammation to persist. Understanding how IL33/25 mediated eosinophil activation might function to promote tissue homeostasis will be key to linking environmental stressors to host adaptation at a molecular level.

Overall, while our study (on various aspects) may be preliminary in nature, we hope it will add to the already accumulating evidence for an important contribution of epithelial-derived alarmins and eosinophils in the preservation of intestinal homeostasis. Furthermore, we hope this work will change us to question the over simplistic, and negative dogma of these pathways as being 'pathophysiologic' and to acknowledge that their nature/function in this tissue is highly dependent on the given context and microenvironment.

Study of the complex, multi-faceted system of the intestine requires an equally complex, multi-disciplinary approach to unravel its inner workings. Only in understanding the functional significance of such interactions under homeostasis could we collectively understand the etiology of complex digestive diseases/disorders and develop novel treatments that are targeted, and efficient.

7.5 STUDY LIMITATIONS

The findings presented herein, suggest the importance of eosinophils in the maintenance of small intestinal tissue integrity under colonized settings through a mechanism dependent on cell-intrinsic signalling by epithelial derived alarmins. Nonetheless, these findings present limitations (both technical and/or inherent to the question addressed) that must be carefully considered - with regards to its interpretation and analysis.

Mouse models

While the Δdbl.GATA1 mouse model is currently the most cited and used eosinophil-deficient strain in the field, it is important to acknowledge that it is not entirely eosinophil-specific. The mutation inserted into this strain targets an auto-regulatory region upstream of the *Gata1* gene, in a DNAseI hypersensitive region identified in hematopoietic cells, thereby limiting the accumulation of GATA1 in cells within the hematopoietic lineage. In the context of normal hematopoiesis, eosinophils (in theory) should be specifically absent in this strain as they distinctly require high levels of this protein for their terminal differentiation. Indeed, our observations (along with other groups) report complete absence of eosinophils within Δdbl.GATA1 mice. However, while there is still controversy about whether other cells within this mouse model are affected in addition to eosinophils, we cannot entirely rule out the contributions of cells (which are potentially changed in the Δdbl.GATA1 model) such as, basophils and erythrocytes to the phenotype reported in this work, as we did not conduct a thorough examination of these populations. Hence, to solidify our findings, major findings reported in this thesis will need to be validated in alternate models of eosinophil-deficiency – such as the newly generated, epx-cre.rosa26 DTA mouse strain or other established models such as PHIL mice.

Additionally, our data on the contributions of epithelial-derived alarmins on SI eosinophil function also present with significant limitations. The ST2.IL17rbko mice utilized in our studies have a full-body deficiency in IL33/25 signalling, and as such – we cannot rule out the potential of extra-intestinal effects of this deficiency in influencing our observations. In a similar regard, while we tried to circumvent this limitation by generating mixed bone marrow chimeras – we cannot rule out the possibility that another hematopoietic lineage/subpopulation from ST2.IL17rbko mice may have competitive advantage over Δdbl.GATA1 mice, that could have

influenced the phenotype we observed. The only way to definitely assess the impact of this IL33/25 signalling on eosinophils is to do an eosinophil-specific deletion – by crossing epx-cre mice with either ST2 flox or IL17rb flox mice (if they are available). Furthermore, it still remains to be determined whether IL33 or IL25 alone mediates the tissue protective functions of eosinophils under homeostatic conditions.

RNA-seq

The limitations discussed regarding the animal models used for this work, also have significant ramifications on the interpretation of the generated RNA-seq data. The samples used to generate the RNA-seq presented in this thesis, were obtained from total IEC and epithelial-negative small intestinal tissue. Therefore, it is unclear as to which cell types were altered that could've accounted for the changes reported. Furthermore, this data would have also presented changes that are solely due to a cell intrinsic deficiency in IL33/25 signalling and possibly any unaccounted defects of the mutation present in cells from Δdbl.GATA1 mice. To add to the complexity of interpreting these results, RNA-seq data does not necessarily correlate with changes at a protein level – particularly, in the case of ECM components, which in many cases are deposited during development independent of the microbiota. To circumvent these limitations, and to validate RNA-seq datasets – targets of interest will need to be re-examined in alternate models of eosinophil deficiency ideally in a model having eosinophil-specific abrogation of IL33 and/or 25 signalling. Further validation will also need to be conducted at a protein level through mass spectrometry analysis (broad validation) or of specific targets of interest by immune-blotting methods. Particularly relevant for the changes in ECM-associated factors, only after this validation has been conducted could we make an adequate conclusion as to what changes are actually occurring in the context of eosinophil deficiency under the conditions discussed (*i.e.* homeostatic, microbiota-colonized).

Other limitations

In this thesis, we have also reported significant changes in the intestinal epithelial lymphocyte population – a finding we did not address or explore further in terms of characterization. It is advised that this phenomenon be examined further, by an in-depth characterization of these IEL populations through assessment of markers (by flowcytometry) that provide information about the activation status and survival potential of these cells. Only then can we start to gain insight

on the mechanisms that underlie the observed phenotype. Another limitation of our findings is that we failed to determine as to whether this phenotype is linked to IL33/25-dependent eosinophil regulation of tissue homeostasis. On a similar note, we also did not address whether this signalling pathway had an impact on the barrier permeability observed in Δdbl.GATA1 mice. All we can conclude is that both of these observed defects only arise in the presence of the microbiota (as both phenotypes are absent under germ-free settings), coincident with the release of epithelial-derived alarmin IL-33 – enhanced in colonized mice vs. GF mice. To truly determine the connection of theses 2 phenotypes to the observed villous phenotype, and to assess whether these phenotypes are similarly due to the loss of cell -intrinsic IL33/25 signalling in eosinophils – it is advised that an experiment be conducted comparing IEL populations and barrier permeability between control mice and mice deficient in IL33/25 signalling (preferably in an eosinophil-specific manner) under both GF and colonized settings.

Chapter 8: Materials and Methods

8.1 Materials

Mice

All mice utilized for the experiments were approved by the Service de la consummation et des affaires vétérinaires (Vaud), according to the guidelines set by the Swiss Animal Welfare Ordinance. Unless indicated, Mice were housed under Specific-Pathogen Free (SPF conditions) and are maintained on a normal 12-h light/dark period with feeding *Ad libidum* on standard-chow diet.

Table: 1 Summary of mouse strains used for thesis work

JAX/MGI strain ID	Common name	Source	PubMed ID (Reference)	Bred-in house	Purchased/ Import	Relevant experiment	Comments
3778536	Δdbl.GATA1	Jackson Laboratories	12045237	✓		Fig. 10-12, 14, 15-26, 30-33, 35-42, 44-45	All mice housed under SPF conditions (EPFL)
	Balb/c	Charles River		✓		Fig. 4-8, 10-12, 14, 15-26, 30-33, 35-42, 44-45	All mice housed under SPF conditions (EPFL)
	Balb/c	Charles River			✓	Fig. 37, 43, 47	Balb/c receipient mice for irradiation experiment; on occasion used for dbl.GATA1 mice experiments (control) Balb/c mice (purchased). For these experiments, mice were co-housed and mixed with in-house bred Balb/c to normalize for microbiota. All mice housed under SPF conditions (EPFL)
008449	Rag2-/-	Jackson Laboratories	11602643	✓		Fig. 28-29	All mice housed under SPF conditions (EPFL)
	C57.B6	Charles River			✓	Fig. 28, 29, 44	All mice housed under SPF conditions (EPFL)
	NOD.SCID	Collaborator			✓	Fig. 27	Mice for first study was from T. Petrova lab (UNIL); mice for replication study was gift from E. Oricchio lab (EPFL)
	NOD.SCID x Yc-/-	Collaborator			✓	Fig. 27	Mice for first study was from T. Petrova lab (UNIL); mice for replication study was gift from E. Oricchio lab (EPFL)
	IL4ra-/-			✓		Fig. 29	
	Balb/c (GF)	Ubern axenic/GF facility (A. Macpherson/ K McCoy lab)	10727469 12045237		✓	Fig. 7, 8, 31, 36, 38,	All GF mice were housed in axenic conditions until harvest
	dbl.GATA1 (GF)					Fig. 31, 36, 38	
4457616	ST2-/- (GF)					Fig. 38	
4457616 X 2386675	ST2-/- x IL17rb-/-	Collaborator	10727469 X 20200518		✓	Fig. 36-40	Mice were a gift from B. Marsland lab (UNIL); co-housed with Balb/c mice (EPFL-bred in house) prior to experiments for at least 2 weeks under SPF conditions (EPFL)
007668	BMAL1-/-	Collaborator	23300284		✓	Fig. 46, 48	Mice were a gift from F. Gachon lab (NRI): control C57.B6 mice were also obtained for this experiment
	IL33-/- GFP	Collaborator	28548102		✓	Fig. 35	Mice were a gift from S. Luther lab (UNIL)

Antibody list I

Table: 2 Antibodies used for cellular staining (flowcytometry)

Antibody	Fluorochrome	Clone	Source	Dilution
CCR3	PE	FAB729P	RND	1:100
CCR9/CD199	PERCP-efluor710	eBIOCW1.2	eBioscience	1:50
CD103	PE	2 E7	ebiosciences	1:200
CD103	PERCP-efluor710	2 E7	eBioscience	1:100
CD11b	apc	M1/70	ebioscience	1:200
CD11c	apc	N418	Biolegend	1:300
CD11c	PE	N418	Biolegend	1:300
CD138	BV421	281-2	BD Biosciences	1:200
CD31	PE-Cy7	390	BD Biosciences	1:300
CD335/NKP46	PE	29A1.4	Biolegend	1:200
CD34	FITC	RAM34	ebiosciences	1:200
CD3e	APC-Cy7	145-2C11	Biolegend	1:100
CD4	BV421	9K1-5	Biolegend	1:200
CD4	BV711	RM4-5	BD Biosciences	1:200
CD44	PE	IM7	ebiosciences	1:200
CD45	PE-Cy7	30.F11	Biolegend	1:500
CD45	AF700	30-F11	Biolegend	1:500
CD8a	PE-Cy7	53.6.7	Biolegend	1:200
CD8b	BV786	H35-17.2	BD Biosciences	1:200
F4/80	APC-Cy7	BM8	ebiosciences	1:400
Foxp3	apc	FJK-16α	ebioscience	1:100
Gata-3	PERCP-efluor710	TWAJ	eBioscience	1:200
GP38/Podoplanin	PE	8 1 1	Biolegend	1:200
IgA	FITC	C10-3	BD Biosciences	1:100
IL-17rb	BV605	6B7	BD Biosciences	1:100
KLRG1	Pacific Blue	2F1	BD Biosciences	1:400
LY6-C	Pacific Blue	HK1-4	Biolegend	1:400
Ly6-G	AF647	1A8	Biolegend	1:400
MHCII	AF700	M5/114-15-2	Biolegend	1:500
MHCII	FITC	M5II14-15-2	ebiosciences	1:500
Roryt	Pacific Blue	Q31-378	BD Biosciences	1:100
Siglec-f	PECF594	E20-2440	BD Biosciences	1:100
ST2	FITC	HB12	MBL lifescience	1:100
TCR-yd	gl3	bv421	BD Biosciences	1:300
viability dye	Amcyan		Life Technologies	1:500
viability dye	DAPI		Life Technologies	1:500

Antibodies List II

Table 3: Antibodies used for histological (Wholemount *WM*; Immunofluorescence *IF*; Immunohistochemistry *IHC*)

Antibody	Source	Reference no.	Provider	Dilution	Assay
VEGFR2	goat	AF644	RND	1:100	WM
lyve1	rabbit	103-PA50	rella tech GmbH	1:400	WM
IL-33	goat	AF3626	RND	1:200	WM
E-cadherin	mouse	610181	BD Biosciences	1:400	WM
GFAP	rabbit	Z0334	Dako	1:250	WM
aSMA-CY3	mouse	C6198	SIGMA	1:800	WM
α mouse IgG (AF555)	donkey	A31570	Life Technologies	1:500	WM/ IF
α rat IgG (AF647)	chicken	A21472	Life Technologies	1:500	WM/ IF
α rat IgG (AF488)	donkey	A21208	Life Technologies	1:500	WM/ IF
α goat IgG (AF647)	donkey	A21447	Life Technologies	1:500	WM/ IF
Caspase-3					IHC
Ki67					IHC
Lysozyme-1					IHC

Miscellaneous consumables

Table 4: List of key reagents used for various experimental analyses

Reagent	Reference	Provider	Information	Comments	Assay
EdU (5-ethynyl-2'-deoxyuridine)	A10044	Thermo Scientific	200µg/mice (i.p.)	Fig. 12, 37	EdU proliferation assay
Click-iT® Plus EdU Alexa Fluor® 555 Imaging Kit	C10638	Thermo Scientific	as per manufacturer instructions	Fig. 12, 37	
ProLong Gold Antifade Reagent	P36934	Invitrogen	1-2 drops per sample	Tissue mounting	Wholemount imaging
FocusClear	FC-101	CelExplorer	75µl per sample	Tissue clearing	
Insect pins	26002-20	Fine Science Tools	as per manufacturer instructions	Tissue preparation	
Sylgard 184 Silicone Elastomer Kit	761036-5EA	Dow Corning			
Secure-Seal Spacer, 20x0.12-mm	S24736	Molecular Probes		Tissue mounting	
Liberase TL	5401020001	Roche	100µg/ml	LP digestion	Flowcytometry
DNAse I	04536282001	Roche	12U/ml		
Transcription Factor Staining Buffer Set	00-5523-00	eBioscience	see methods	Intracellular staining	
TruStain Fcx (anti-mouse CD16/32)	101320	Biolegend		Fc Block	
Bactrim		Bayer	2.5ml per 250ml of H20	Treatment during irradiation (Fig. 26, 37)	Bone marrow chimera/irradiation experiment
Dafalgan		Bayer	2 packs per 250ml of H20		
DIO (VHFD) 60 kcal% fat	D12492	ResearchDiets	High-fat diet (pellet)	Fig. 43-45	High-fat diet
Control (LFD) 10 kcal% fat D12492 Match 7% Sucrose	D12450J		Control-diet (pellet)		
Olive Oil	O1514	Sigma	200µl/mice (i.g.)	Fig. 42	Triglyceride analysis
RNeasy Plus Universal Mini Kit	73404	Qiagen	as per manufacturer instructions	RNA-isolation	RNA-sequencing
RNase-Free DNase Set	79254	Qiagen	as per manufacturer instructions	RNA-isolation	
TruSeq Stranded mRNA	20020594	Illumina	as per manufacturer instructions	mRNA library preparation (IEC fraction)	
NextSeq 500/550 High Output v2 kit (75 cycles)	FC-404-2005	Illumina	as per manufacturer instructions	mRNA sequencing	
KAPA RNA HyperPrep Kit with RiboErase (HMR)	KK8560	KAPA Biosystems	as per manufacturer instructions	mRNA library preparation LP fraction)	

8.2 METHODS

8.2.1 Experimental design and statistical analysis

With the exception of mice from experiments presented in **figure 6**, all data was acquired from experiments using 8-12 week old mice. For each quantified experiment, n=3-5 mice were used per group. Graphed data sets were either pooled (*i.e.* flowcytometric analysis) or shown as representative images (*i.e.* histological, wholemount analysis). Histological and wholemount analysis were shown as representative experiments, due to inter-experiment variability – largely dependent on the fixation quality within an experiment and differences in age (while we controlled for age within an experiment, age between experiments could vary by weeks), which could impact intestinal length and consequently villous size of the area examined.

Sampling methods and statistics also varied depending on a given analysis (discussed in further detail below). In brief, for the wholemount and other histological analysis, each datapoint represents the average villous area of a given intestinal region per mouse – summarized in **figure 50**. The average was generated by quantifying the area of >30 villi from 10 field images acquired per mouse and per region. In comparison of >2 groups, a two-way ANOVA was conducted – otherwise, student t-tests were used for statistical analysis between groups (a non-parametric, Mann-whitney test was used in experiments where the standard deviation between samples in a group had a p-value >0.05). Similarly, for flowcytometric analysis, each data point represents a single mouse – and single-cell preparations were generated from regions indicated in **figure 52**. Student t-tests were used for statistical analysis between groups and a non-parametric, Mann-whitney test was used in experiments where the standard deviation between samples in a group had a p-value >0.05).

For high-fat diet experiments where weight gain was monitored (**figure 45, 46**), each data point is shown as the average fold change weight from the recorded weight at timepoint 0 (beginning of experiment). For statistical analysis between HFD Balb/c and HFD Δdbl.GATA1 mice, student t-tests were used between groups (a non-parametric, Mann-whitney test was used in experiments where the standard deviation between samples in a group had a p-value >0.05).

For RNA-seq experiments, Edge-R statistical analysis was used to determine statistical significance between control and experimental groups. Additional criteria such as FDR<0.05 and log2 fold-change of >1.5 also needed to be met to identify genes that were differentially expressed.

8.2.2 Wholemount and other histological analysis

Sample preparation for wholemount and other histological analyses

In brief, mice were lethally anaesthetized with ketasol/xylosol. Once unresponsive, the mice were perfused with 1x PBS, followed by 4% paraformaldehyde (PFA; room temperature). Tissue was then divided according to schematic explained in (**Figure 50).**

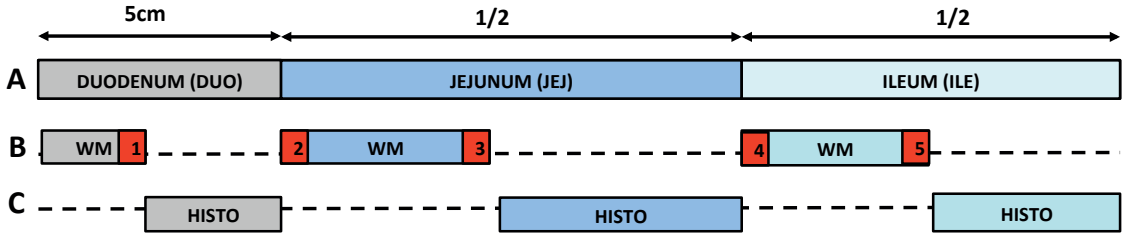

(Figure 50) Schematic of tissue collection for histology/wholemount analysis: (A) Collection of different SI regions, DUO is region 5 cm from pyloric spincter, JEJ and ILE is determined as the proximal ½ and distal ½ following the DUO, respectively. **(B)** Collection of tissues for Wholemount analysis; (1) DUO (2) Upper jejunum UPJEJ (3) Lower jejunum LOJEJ (4) Upper Ileum UPILE (5) Lower Ileum LOILE. **(C)** Collection of tissues for histological analysis (paraffin embedded; HISTO) made into 'Swiss Rolls'

Wholemount imaging

Wholemount tissue preparation was conducted according to published protocols (J. Bernier-Latmani, T. Petrova 2016 Nature Protocols). This protocol is summarized in (**Figure 50)**. Regions of interest were collected and pinned onto a silicone-lined plate using metallic (insect) pins to maximize surface area, and allow for optimal fixation. Unless mentioned otherwise, all incubations were done at 4C on an orbital shaker. Tissues were fixed overnight with wholemount fixation buffer (0.5% PFA, 15% Picric Acid saturated in 10mM of phosphate buffer (pH 7)). Samples were then washed 1xPBS 5 times, over 10 min intervals. The tissue was then subjected to a sucrose gradient for better preservation of tissue structure/morphology - where the tissues were first incubated with 10% sucrose in 1xPBS for 4hours, then switched to a solution consisting of 20% sucrose 10% glycerol in 1x PBS O/N. Samples were rinsed with 1xPBS at least twice after the O/N incubation. 1-2cm sized tissues were acquired from regions of

interest, and were pinned on a new silicone-lined plate. Prior to staining, the samples were incubated for at least 4hours with filtered blocking solution (0.5% BSA, 0.1% NaN3, 5% donkey serum, 0.3% Triton-X100 – in 500ml of PBS). Primary antibody incubation was done over 2 days. Post-incubation, the samples were washed with washing buffer (0.03% Triton-X100 in 1xPBS) repeated 5 times over 1hour intervals. Secondary antibodies were incubated O/N, and the plate was covered with aluminum foil to prevent bleaching of conjugated-fluorophores. Antibodies were diluted **(Table 2)** in wholemount blocking buffer. Post-incubation, the samples were washed with washing buffer (0.03% Triton-X100 in 1xPBS) repeated 10 times over 30 min intervals. The samples were then fixed over 2-3 days in 4% PFA. For imaging, tissue was longitudinally cut with scissors into sections approximately 1-2 villi thick (at least 10 strips were obtained per sample). The cut sections were placed on a super-frost slide (after addition of tissue spacers) and clarified with FocusClear for 30mins at room temp. This allows for better visualization of lamina propria - as the solution renders the epithelial barrier translucent. After removal of excess FocusClear solution, 1-2 drops of Prolong gold was added – followed by coverslip.

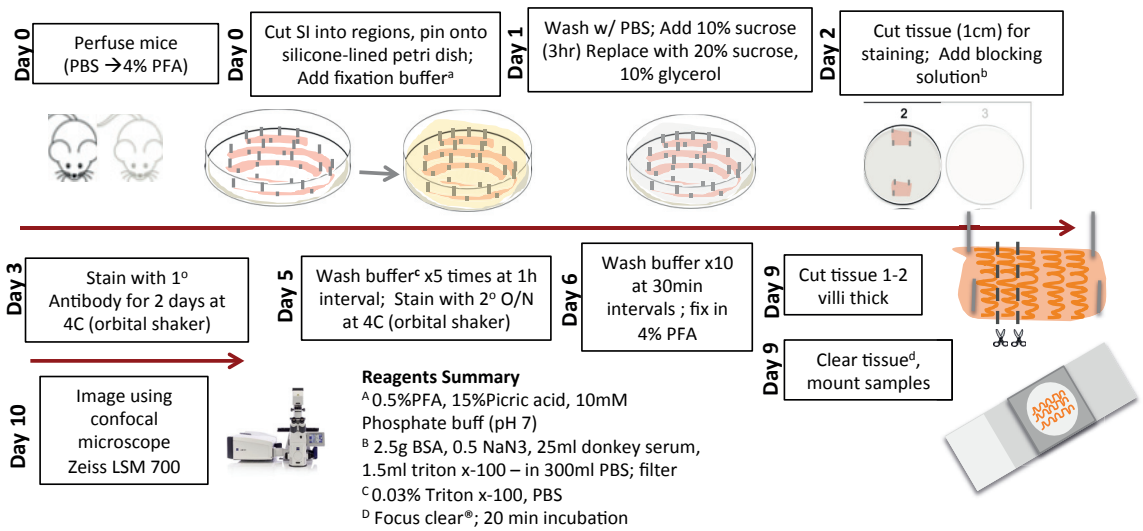

(Figure 51) Graphical representation of wholemount protocol

The samples were imaged using Zeiss LSM700 (inverted microscope). Villi used for analyses were randomly selected from different regions of the slide. Every each image has a field of area containing at least 3 villi, and 10 images were collected per mouse. Images were analysed using ImageJ/FIJI software, and surface area was traced-manually – but measured by the software. For

measurement of vessel branching **(Figure 24)**, the vessel networks were traced manually on Adobe photoshop – and analysed using Angiotool software (National Cancer Institute; NCI). All statistical tests, and graphs were generated using GraphPad Prism.

Immunofluorescence (IF)

After collection of tissue for wholemount preparation, the rest of the small intestine reserved for other histological analyses were laid flat (villi-side up) on whatmann paper to maximize surface area for fixation in 4% PFA O/N. The samples were then rolled into 'Swiss rolls' embedded into a cassette, and placed in 70% EtOH. The samples were then prepared for paraffin embedding, and placed into paraffin blocks. 0.4µm sections were sectioned using a microtome (Hyrax M25) and placed onto a super frost slide (2 sections/slide – 1 for negative staining control, 1 test sample). Briefly, prior to staining, paraffin sections samples were dewaxed and rehydrated. For antigen retrieval, the samples were incubated with Sodium Citrate Buffer (pH 6) for 5 mins at boiling point, using a standard microwave. After blocking for 1h with wholemount blocking buffer, the primary antibodies (i.e. lysozyme-1, DCAMKL1, E-cadherin) were incubated overnight at 4C. After washing with wholemount wash buffer, slides were incubated for 2 hours with secondary antibodies. Antibodies were diluted with wholemount fixation buffer. Slides were counterstained with DAPI for nuclear staining, and mounted with Prolong gold. For Click-it EdU staining, protocol was followed according to manufacturers instructions. Slides were imaged with Olympus AX70 fluorescence microscope; on occasion, with Zeiss LSM700 (inverted microscope). For analysis, at least 10 images were acquired per mouse, with at least 4 villi per field – blindly sampled from different areas of the swiss roll (jejunum). All statistical tests, and graphs were generated using GraphPad Prism.

Immunohistochemistry (IHC)

Detection of proliferation (rabbit α-Ki67, SP6, Springbio, diluted 1:100) and apoptosis (rabbit α-cleaved caspase 3, Asp175, Cell signaling, diluted 1:200) was performed using the fully automated Ventana Discovery ULTRA (Roche Diagnostics, Rotkreuz, Switzerland). All steps were performed on the machine with Ventana solutions. Briefly, dewaxed and rehydrated paraffin sections were pretreated with heat using standard condition (40 minutes) CC1 solution. The primary antibodies were incubated 1 hour at 37°C. After incubation with a rabbit Immpress HRP (Ready to use, Vector laboratories Laboratories), chromogenic revelation was performed with

ChromoMap DAB kit (Roche Diagnostics, Rotkreuz, Switzerland). Sections were counterstained with Harris hematoxyline and permanently mounted. For analysis, at least 10 images were acquired per mouse, with at least 4 villi per field – blindly sampled from different areas of the swiss roll (jejunum). All statistical tests, and graphs were generated using GraphPad Prism.

Transmission Electron microscopy (TEM)

Adult mice age-matched, sex-matched Balb/c, Δdbl.GATA1 or ST2IL17rbko (either SPF or GF) were perfused via the heart with a buffered mix of 2.5 % glutaraldehyde and 2.0 % paraformaldehyde in 0.1M phosphate buffer (pH 7.4). After 2 hours 4cm several 0.5-1cm pieces of tissue from the upper jejunum was removed from the animal and sliced transversally using a vibratome (VT1200, Leica) at a thickness of 100 micrometers. The pieces of interest were then fixed overnight in the same fixative. The next day they were washed thoroughly with cacodylate buffer (0.1M, pH 7.4), postfixed for 40 minutes in 1.0 % osmium tetroxide with 1.5% potassium ferrocyanide, and then 40 minutes in 1.0% osmium tetroxide alone. They were finally stained for 30 minutes in 1% uranyl acetate in water before being dehydrated through increasing concentrations of alcohol and then embedded in Durcupan ACM (Fluka, Switzerland) resin. The resin was hardened for 24 hours in an oven at 65°C. Regions of interest were sectioned at a thickness of 50 nm, and sections collected onto single slot grids with a pioloform support film. These were further contrasted with lead citrate and uranyl acetate solutions, and images taken using an FEI Spirit TEM with Eagle CCD camera.

8.2.3 Cell Isolation and Flowcytometric analyses

Sample preparation

Mice used for analysis were euthanized with CO_2 as per ethical guidelines followed by the animal facility at the EPFL. **Figure 51** depicts the sample collection method for cell isolation (from small intestinal tissue) for flowcytometric analysis. Our lab has published the standard protocol used in this work for SI cell isolation – a version that was modified/optimized from established protocols published by several labs.

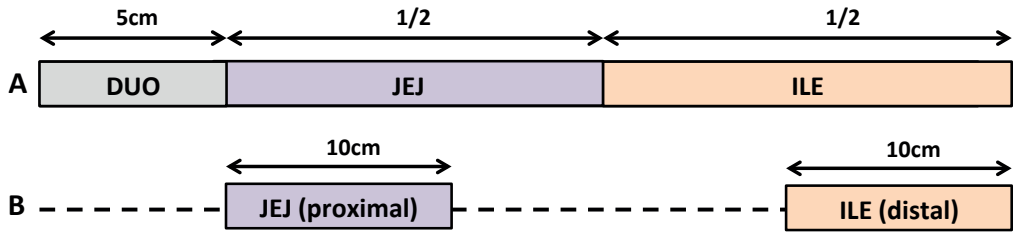

(Figure 52) Schematic of sample collection for flowcytometric analysis: (A) Duodenum (DUO) is 5cm region post-pyloric spincter. Jejunum (JEJ) and Ileum (ILE) are determined as the proximal ½ and distal ½ of small intestinal tissue downstream of the DUO, respectively. This scheme was used for experiments in *Figure 4.* (B) Following separation in (A), the JEJ and ILE were further separated. For jejunal analysis, the proximal 10cm of the tissue was used – whereas for the ileum, the distal 10cm was used.

Cell isolation of epithelial and lamina propria fraction

In brief, after the region of interest has been collected, the tissue is flushed with ice-cold 1x PBS to remove luminal contents. Attached mesenteric tissue/fat, and Peyer's Patches were also removed to prevent cellular contamination. The tissue was then opened longitudinally and cut into 1-2 cm pieces, and placed into a tube containing solution I (1xHBSS, 2% FBS, 1%P/S, 10mM HEPES) on ice until the other mice have been harvested. The tissue was then transferred onto solution II (1xHBSS, 2% FBS, 1%P/S, 10mM HEPES, 5mM EDTA; epithelial cell removal) and incubated on a rotating shaker at 37C for 30 mins. To wash off FBS and EDTA (required for optimal tissue digestion), the tissues were washed 3-times with ice-cold 1xPBS. The detachment of cells from the epithelial barrier was assisted through manual shaking of the tube containing the samples. The washes were collected, spun down and snap-frozen - labelled as 'epithelial (IEC)-fraction' used for measurement of IELs and for RNA-seq analysis – after filtering in 70µm strainer, the samples are ready for FACs staining.

Translucency of the remaining tissue is indicative that the IECs have been successfully removed – and only containing the lamina propria (along with the muscularis layer). The sample was further minced prior to digestion with Solution III (Liberase TL 100µg/ml, DNAse I 12U/ml, 10mM HEPES in RPMI solution). 1ml of Solution III was used per cm of tissue digested. The tissue was digested for 40 mins in an orbital shaker (37C). After digestion, Solution III was deactivated using solution IV (1xRPMI, 10% FBS, 10mM HEPES, 1%P/S) at a 1:1 ratio. The tissue was further dissociation using gentle, manual suction using a 5ml syringe (without needle) and the contents filtered through a 70µm cell strainer – and washed twice with solution IV. After washing, the cells were ready for FACs staining.

Staining of cells for flowcytometry

2x10^6 cells of live cells from each sample was used for FACs staining. Information reagents, dilutions can be found in **(Table 3).** In brief, samples were rinsed twice with 1xPBS prior to viability staining. Viability dye was used at a (1:500), and samples were incubated on ice for 30 mins. The samples were then washed with FACS buffer (1xPBS, 10mM HEPES, 2%FBS, 1%P/S, 2.5mM EDTA) and incubated with Fc-block cocktail (1:100) for at least 10 minutes on ice. After washing, the samples were then stained with an antibody cocktail for 30 minutes (surface staining). For intracellular staining, the samples were washed with FACS buffer twice. Prior to fixation using Transcription factor buffer kit (eBioscience; according to manufacturers instructions), the pellet was gently loosen manually, and after fixative was added – the samples were incubated for 30 mins on ice. After incubation, permebilization solution (from the kit) was added on top of the samples, followed by an additional wash using this solution. Antibodies for intracellular staining, were diluted in this permeabilization solution – and incubated O/N. Samples were then washed twice with the same solution. Once the samples were ready they were suspended in 1xPBS. Samples were analyzed using an LSRII Flowcytometer (BD Biosciences).

8.2.4 RNA-seq

Samples for RNA-seq analyses were acquired as follows: (1) epithelial-fraction from 10cm of proximal jejunum (2) 2cm of lamina propria (post-epithelial removal) from the proximal jejunum. Samples were quickly snap frozen in liquid nitrogen until RNA-extraction. RNA-extraction was conducted using QIAGEN RNA-easy universal kit – as per manufacturers

instructions, with an additional DNA-removal step using DNAseI (QIAGEN). Samples were stored at -80C until further analysis.

RNA library preparation and sequencing for intestinal epithelial-fraction

Multiplexed libraries for mRNA-seq were prepared according to manufacturer's instructions with the TruSeq stranded mRNA kit (Illumina) starting from 3000 ng of good-quality total RNAs (RNA quality scores >7.5 on the TapeStation 4200). Libraries were subsequently loaded at 1.44pM on a High Output flow cell (Illumina) and sequenced in a NextSeq 500 instrument (Illumina) according to manufacturer instructions, yielding single-end reads of 75 nucleotides.

RNA library preparation and sequencing for intestinal lamina propria -fraction

Multiplexed libraries for total RNA-seq were prepared according to manufacturer's instructions with the "RNA HyperPrep with RiboErase" kit (Kapa) starting from 200 ng of total RNAs. Since RNA quality varied among samples (scores from 4.1 to 8.3 on the TapeStation 4200), RNA fragmentation times were adjusted as recommended by the manufacturer. Libraries were subsequently pooled and loaded at 1.53pM on two High Output flow cells (Illumina) and sequenced in a NextSeq 500 instrument (Illumina) according to manufacturer instructions, yielding single-end reads of 75 nucleotides. Reads from these two runs were then pooled.

Analysis of RNA-seq data

Raw fastq files were processed using RNASik v1.4.7 with default settings (https://monashbioinformaticsplatform.github.io/RNAsik-pipe/). RNASik wraps alignment, QC metrics and quantification in the one script giving a count file. Alignment was performed using STAR v2.5.2 against iGenomes ensembl GRCm10 reference. Using the GTF from the same reference, FeatureCounts quantified reads to genes. Differential expression analysis (statistical analysis using EdgeR) was conducted with significantly up/down regulated genes defined as having log2 fold change of >1.5, FDR <0.05 over Balb/c control mice. For GSEA analysis, significantly up/down regulated data sets were analyzed using the Molecular Signature database (Broad Institute; curated gene sets - canonical pathways) based on a publication by Liberzon A. et *al.* 2015 *Cell Systems*

8.2.5 Chimera experiments

For chimera experiments, we pre-treated >10-week old mice with antibiotics in their drinking water for 2 days prior to the irradiation – in an effort to limit microbiota-induced intestinal damage.

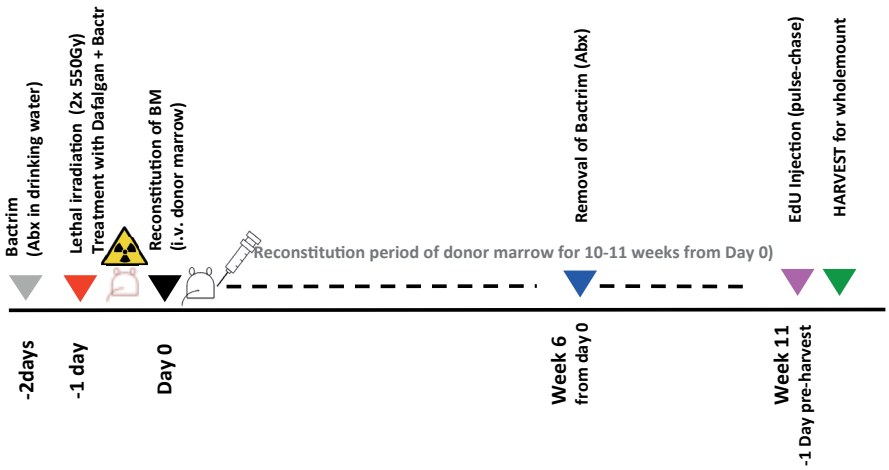

(Figure 53) Graphical summary of chimera experiments

The mice were then lethally irradiated with a total of exposure of 700 grays – split into two doses (335gy per dose), 12 hours apart. After the last dose, the hematopoietic compartment for each irradiated mouse (recipient) was reconstituted with approx. 7-10 x10^6 cells from donor mice (6-8 weeks old) after pan-Tcell depletion (a-CD90.2, Milteny Biotech Cat. 130-049-101) according to manufacturers instructions. All steps were conducted on ice, in a sterile hood. From day -2 till week 6, the mice were kept on antibiotics Bactrim and pain-reliever Dafalgan (Table 3). 24 hours prior to analysis, the mice were injected with EdU, in a temporally staggered manner to maintain accuracy for proliferation studies. The mice were analyzed 4 weeks after antibiotic removal.

8.2.6 Metabolic/nutritional analysis

Bomb Calorimetry (Indirect calorimetry)

Prior to experiment, mice were individually housed and acclimatized for 24h on Type 2IVC cages with a grid floor. On the day of analysis, 3-5 hours after fasting, the mice are given ad libidum access to food and water over the course of 24 hours. After 24 hours, mice are placed back in groups in their home cages on normal racks in the animal facility. Food consumption was assessed, by food weighting and the feces are collected (from 24 hours period) for measurement of their energy content using an IKA C200 Bomb calorimeter. Fecal pellets were dessicated and pre-weight prior to combustion.

Triglyceride Analysis

For Triglyceride (Tg) analysis, blood was collected 1 day before the experiment (T0 – baseline tg level) from the tail vein of all mice after fasting for 3 hours. On the day of the experiment, the mice were fasted for 3 hours prior to intra-gastric gavage with 200µl of olive oil (sigma). Blood was collected from the tail vein (stored in EDTA tubes) at 1,2 and 3 hours post-gavage. The samples were then snap-frozen in liquid nitrogen until analysis. Plasma concentrations of triglycerides were determined using the Cobas C111 robot (Roche Diagnostics).

High-fat diet experiment (maintenance, echo-MRI)

For HFD-experiments, mice were co-housed and their weights measures at timepoint-0 (T0) weekly until 9-15 weeks into the experiment. To measure body composition (fat vs. protein), mice were analyzed using EchoMRI-100 (EchoMRI^{TM}) every 3 weeks with the fat mass calculated and normalized based on their weight within the given time point. Weight gain over time was calculated as the fold change from the initial weight at T0. HFD and control-chow was obtained from ResearchDiets **(Table 3)**.

Circadian Rhythm experiment

Mice were entrained for 1 week to a 7am (light) /7pm (dark) cycle through restricting food intake only during the dark cycle, and removing food during the light cycle to synch the circadian rhythm of the mice used for circadian experiments **(Figure 46, 48).** In brief, mice analyzed in the light cycle had food removed at 7am, and were sacrificed at 9am (2 hours post-feeding). Mice

analyzed during the dark cycle, were re-fed at 7pm until sacrifice – at 9pm (2-hours post-feeding). Flowcytometric analyses of samples follow the methods mentioned in this section.

8.2.7 Methods from KD McCoy lab

BrdU labeling under axenic conditions

Germ-free experiments were performed either in the lamina flow hood for short term experiments up to 4 days, or in surgical isolators in the germ-free facility. For all experiments autoclavable BrdU injection kits containing a 50 mL Falcon tube, a 3mL syringe with a 18 gauge needle, aluminium foil and a 1.5mL eppendorf tube were prepared. Additionally, sterile water, sterile PBS, a gown and a drape for the hood were prepared. For intraperitoneal injection, BrdU was dissolved in sterile PBS at a concentration of 10mg/mL by vigorously vortexing. The tube containing BrdU solution was imported into the laminar flow hood and sterilily taken up with a syringe before being filtered through a 0.2µm pore filter. The filtered BrdU solution was transferred to a sterile eppendorf tube (screw cap), covered with aluminium foil to protect from exposure to light and either used for laminar flow injections or further transferred into a glas container with insulin injection needles in order to be used for injections in a surgical isolator. The solution for intraperitoneal injections were freshly prepared before each injection. Per mouse, an initial dose of 1mg BrdU was applied intraperitoneally and mice were given 0.8mg BrdU/mL supplemented drinking water for the rest of the pulse. The drinking water was prepared at 0.8-1mg BrdU/mL sterile water, covered in aluminium foil to protect against light and renewed every other day.

8.3 SUPPLEMENTARY TABLES

Table 5: GSEA analysis on **downregulated** gene data sets (total of 15 genes) from *epithelial fraction* of Δdbl.GATA1 mice, relative to Balb/c (n=5 mice/group; same dataset as Figure 15).

	Gene Set Name	# Genes in Gene Set (K)	Description	# Genes in Overlap (k)	k/K	p-value	FDR q-value
1	REACTOME_FATTY_ACID_TRIACYLGLYCEROL_AND_KETONE_BODY_METABOLISM	168	Genes involved in Fatty acid, triacylglycerol, and ketone body metabolism	7	0.0417	4.83E-14	6.42E-11
2	KEGG_PPAR_SIGNALING_PATHWAY	69	PPAR signaling pathway	5	0.0725	1.95E-11	1.30E-08
3	REACTOME_METABOLISM_OF_LIPIDS_AND_LIPOPROTEINS	478	Genes involved in Metabolism of lipids and lipoproteins	7	0.0146	7.55E-11	3.34E-08
4	REACTOME_PPARA_ACTIVATES_GENE_EXPRESSION	104	Genes involved in PPARA Activates Gene Expression	5	0.0481	1.59E-10	5.28E-08
5	KEGG_FATTY_ACID_METABOLISM	42	Fatty acid metabolism	2	0.0476	8.50E-05	2.26E-02

Gene Set Overlap Matrix **Δdbl.GATA1 vs. Balb/c (FC Log2 >0.3; FDR 0.05) - DOWNREGULATED**

Entrez Gene Id	Gene Symbol	Gene Description	1	2	3	4	5
1579	CYP4A11	cytochrome P450, family 4, subfamily A, polypeptide 11	■	■	■	■	■
51129	ANGPTL4	angiopoietin-like 4	■	■	■	■	
3158	HMGCS2	3-hydroxy-3-methylglutaryl-CoA synthase 2 (mitochondrial)	■	■	■	■	
4199	ME1	malic enzyme 1, NADP(+)-dependent, cytosolic	■	■	■	■	
33	ACADL	acyl-CoA dehydrogenase, long chain	■	■	■		■
8800	PEX11A	peroxisomal biogenesis factor 11 alpha	■		■		
788	SLC25A20	solute carrier family 25 (carnitine/acylcarnitine translocase), member 20	■		■		
373156	GSTK1	glutathione S-transferase kappa 1					
2695	GIP	gastric inhibitory polypeptide					
80301	PLEKHO2	pleckstrin homology domain containing, family O member 2					
5166	PDK4	pyruvate dehydrogenase kinase, isozyme 4					
84986	ARHGAP19	Rho GTPase activating protein 19					
10282	BET1	blocked early in transport 1 homolog (S. cerevisiae)					
116842	LEAP2	liver expressed antimicrobial peptide 2					
6038	RNASE4	ribonuclease, RNase A family, 4					

Table 6: GSEA analysis on **upregulated** gene data sets (total of 33 genes) from *epithelial fraction* of Δdbl.GATA1 mice, relative to Balb/c (n=5 mice/group; same dataset as Figure 16)

	Gene Set Name	# Genes in Gene Set (K)	Description	# Genes in Overlap (k)	k/K	p-value	FDR q-value
1	NABA_MATRISOME	1028	Ensemble of genes encoding extracellular matrix and extracellular matrix-associated proteins	11	0.0107	2.23E-12	2.96E-09
2	REACTOME_CREATION_OF_C4_AND_C2_ACTIVATORS	10	Genes involved in Creation of C4 and C2 activators	3	0.3	1.70E-08	1.13E-05
3	BIOCARTA_CLASSIC_PATHWAY	14	Classical Complement Pathway	3	0.2143	5.16E-08	2.28E-05
4	REACTOME_INITIAL_TRIGGERING_OF_COMPLEMENT	16	Genes involved in Initial triggering of complement	3	0.1875	7.93E-08	2.63E-05
5	BIOCARTA_COMP_PATHWAY	19	Complement Pathway	3	0.1579	1.37E-07	3.64E-05
6	NABA_CORE_MATRISOME	275	Ensemble of genes encoding core extracellular matrix including ECM glycoproteins, collagens and proteoglycans	5	0.0182	3.56E-07	7.89E-05
7	REACTOME_COMPLEMENT_CASCADE	32	Genes involved in Complement cascade	3	0.0938	6.98E-07	1.33E-04
8	KEGG_PRION_DISEASES	35	Prion diseases	3	0.0857	9.20E-07	1.47E-04
9	KEGG_SYSTEMIC_LUPUS_ERYTHEMATOSUS	140	Systemic lupus erythematosus	4	0.0286	9.93E-07	1.47E-04
10	NABA_MATRISOME_ASSOCIATED	753	Ensemble of genes encoding ECM-associated proteins including ECM-affilaited proteins, ECM regulators and secreted factors	6	0.008	2.58E-06	3.42E-04

Gene/Gene Set Overlap Matrix **Δdbl.GATA1 vs. Balb/c (FC Log2 >0.3; FDR 0.05) - DOWNREGULATED**

Entrez Gene Id	Gene Symbol	Gene Description	1	2	3	4	5	6	7	8	9	10
712	C1QA	complement component 1, q subcomponent, A chain	■	■	■	■	■		■	■	■	■
713	C1QB	complement component 1, q subcomponent, B chain	■	■	■	■	■		■	■	■	■
714	C1QC	complement component 1, q subcomponent, C chain	■	■	■	■	■		■	■	■	■
1277	COL1A1	collagen, type I, alpha 1	■					■				
3371	TNC	tenascin C	■					■				
10418	SPON1	spondin 1, extracellular matrix protein	■					■				
8404	SPARCL1	SPARC-like 1 (hevin)	■					■				
633	BGN	biglycan	■					■				
4313	MMP2	matrix metallopeptidase 2 (gelatinase A, 72kDa gelatinase, 72kDa type IV collagenase)	■									
4322	MMP13	matrix metallopeptidase 13 (collagenase 3)	■									
27299	ADAMDEC1	ADAM-like, decysin 1	■									
2212	FCGR2A	Fc fragment of IgG, low affinity IIa, receptor (CD32)										
5156	PDGFRA	platelet-derived growth factor receptor, alpha polypeptide										
10398	MYL9	myosin, light chain 9, regulatory										
1436	CSF1R	colony stimulating factor 1 receptor										
59	ACTA2	actin, alpha 2, smooth muscle, aorta										
1524	CX3CR1	chemokine (C-X3-C motif) receptor 1										
51676	ASB2	ankyrin repeat and SOCS box containing 2										
1910	EDNRB	endothelin receptor type B										
54947	LPCAT2	lysophosphatidylcholine acyltransferase 2										
348	APOE	apolipoprotein E										
1776	DNASE1L3	deoxyribonuclease I-like 3										
4481	MSR1	macrophage scavenger receptor 1										
7940	LST1	leukocyte specific transcript 1										
79772	MCTP1	multiple C2 domains, transmembrane 1										

Table 7: GSEA analysis on **downregulated** gene data sets (294 genes) from *lamina propria* fraction of dbl.GATA1 mice, relative to Balb/c (n=5 mice/group; same dataset as Figure 32)

	Gene Set Name	# Genes in Gene Set (K)	Description	# Genes in Overlap (k)	k/K	p-value	FDR q-value
1	REACTOME_NEURONAL_SYSTEM	279	Genes involved in Neuronal System	21	0.0753	1.93E-16	2.57E-13
2	KEGG_NEUROACTIVE_LIGAND_RECEPTOR_INTERACTION	272	Neuroactive ligand-receptor interaction	16	0.0588	3.30E-11	2.19E-08
3	REACTOME_VOLTAGE_GATED_POTASSIUM_CHANNELS	43	Genes involved in Voltage gated Potassium channels	8	0.186	3.05E-10	1.35E-07
4	REACTOME_POTASSIUM_CHANNELS	98	Genes involved in Potassium Channels	10	0.102	8.40E-10	2.79E-07
5	KEGG_CALCIUM_SIGNALING_PATHWAY	178	Calcium signaling pathway	12	0.0674	2.11E-09	5.62E-07
6	KEGG_ARRHYTHMOGENIC_RIGHT_VENTRICULAR_CARDIOMYOPATHY_ARVC	76	Arrhythmogenic right ventricular cardiomyopathy (ARVC)	8	0.1053	3.30E-08	7.31E-06
7	REACTOME_TRANSMISSION_ACROSS_CHEMICAL_SYNAPSES	186	Genes involved in Transmission across Chemical Synapses	11	0.0591	3.87E-08	7.34E-06
8	NABA_MATRISOME	1028	Ensemble of genes encoding extracellular matrix and extracellular matrix-associated proteins	24	0.0233	6.68E-08	1.11E-05
9	KEGG_DILATED_CARDIOMYOPATHY	92	Dilated cardiomyopathy	8	0.087	1.49E-07	2.20E-05
10	REACTOME_GPCR_LIGAND_BINDING	408	Genes involved in GPCR ligand binding	14	0.0343	4.84E-07	6.43E-05

Gene/Gene Set Overlap Matrix (1/5) **ΔdbI.GATA1 vs. Balb/c (FC Log2 >1; FDR 0.05) - DOWNREGULATED**

Entrez Gene Id	Gene Symbol	Gene Description	1	2	3	4	5	6	7	8	9	10
2890	GRIA1	glutamate receptor, ionotropic, AMPA 1										
2898	GRIK2	glutamate receptor, ionotropic, kainate 2										
1136	CHRNA3	cholinergic receptor, nicotinic, alpha 3										
3785	KCNQ2	potassium voltage-gated channel, KQT-like subfamily, member 2										
3786	KCNQ3	potassium voltage-gated channel, KQT-like subfamily, member 3										
3736	KCNA1	potassium voltage-gated channel, shaker-related subfamily, member 1 (episodic ataxia with myokymia)										
3737	KCNA2	potassium voltage-gated channel, shaker-related subfamily, member 2										
3742	KCNA6	potassium voltage-gated channel, shaker-related subfamily, member 6										
3751	KCND2	potassium voltage-gated channel, Shal-related subfamily, member 2										
3754	KCNF1	potassium voltage-gated channel, subfamily F, member 1										
9312	KCNB2	potassium voltage-gated channel, Shab-related subfamily, member 2										
3768	KCNJ12	potassium inwardly-rectifying channel, subfamily J, member 12										
6833	ABCC8	ATP-binding cassette, sub-family C (CFTR/MRP), member 8										
107	ADCY1	adenylate cyclase 1 (brain)										
774	CACNA1B	calcium channel, voltage-dependent, N type, alpha 1B subunit										
55799	CACNA2D3	calcium channel, voltage-dependent, alpha 2/delta subunit 3										
88	ACTN2	actinin, alpha 2										
80852	GRIP2	glutamate receptor interacting protein 2										
43	ACHE	acetylcholinesterase										
6854	SYN2	synapsin II										
127833	SYT2	synaptotagmin II										
5021	OXTR	oxytocin receptor										
3356	HTR2A	5-hydroxytryptamine (serotonin) receptor 2A										
148	ADRA1A	adrenergic, alpha-1A-, receptor										
155	ADRB3	adrenergic, beta-3-, receptor										
22953	P2RX2	purinergic receptor P2X, ligand-gated ion channel, 2										
2587	GALR1	galanin receptor 1										
4985	OPRD1	opioid receptor, delta 1										
4987	OPRL1	opiate receptor-like 1										
1813	DRD2	dopamine receptor D2										
3061	HCRTR1	hypocretin (orexin) receptor 1										
117	ADCYAP1R1	adenylate cyclase activating polypeptide 1 (pituitary) receptor type I										
2917	GRM7	glutamate receptor, metabotropic 7										
1132	CHRM4	cholinergic receptor, muscarinic 4										
6262	RYR2	ryanodine receptor 2 (cardiac)										
6543	SLC8A2	solute carrier family 8 (sodium/calcium exchanger), member 2										
492	ATP2B3	ATPase, Ca++ transporting, plasma membrane 3										
4842	NOS1	nitric oxide synthase 1 (neuronal)										
6263	RYR3	ryanodine receptor 3										
9254	CACNA2D2	calcium channel, voltage-dependent, alpha 2/delta subunit 2										
3679	ITGA7	integrin, alpha 7										
6445	SGCG	sarcoglycan, gamma (35kDa dystrophin-associated glycoprotein)										
1496	CTNNA2	catenin (cadherin-associated protein), alpha 2										
29119	CTNNA3	catenin (cadherin-associated protein), alpha 3										

Gene/Gene Set Overlap Matrix (2/4) **Δdbl.GATA1 vs. Balb/c (FC Log2 >1; FDR 0.05) - DOWNREGULATED**

Entrez Gene Id	Gene Symbol	Gene Description	1	2	3	4	5	6	7	8	9	10
6585	SLIT1	slit homolog 1 (Drosophila)										
1463	NCAN	neurocan										
7148	TNXB	tenascin XB										
1301	COL11A1	collagen, type XI, alpha 1										
127731	VWA5B1	von Willebrand factor A domain containing 5B1										
2006	ELN	elastin										
256158	HMCN2	hemicentin 2										
4745	NELL1	NEL-like 1 (chicken)										
4753	NELL2	NEL-like 2 (chicken)										
1296	COL8A2	collagen, type VIII, alpha 2										
9806	SPOCK2	sparc/osteonectin, cwcv and kazal-like domains proteoglycan (testican) 2										
4902	NRTN	neurturin										
5055	SERPINB2	serpin peptidase inhibitor, clade B (ovalbumin), member 2										
2259	FGF14	fibroblast growth factor 14										
4803	NGF	nerve growth factor (beta polypeptide)										
7093	TLL2	tolloid-like 2										
64386	MMP25	matrix metallopeptidase 25										
283208	P4HA3	prolyl 4-hydroxylase, alpha polypeptide III										
57188	ADAMTSL3	ADAMTS-like 3										
80332	ADAM33	ADAM metallopeptidase domain 33										
8646	CHRD	chordin										
10718	NRG3	neuregulin 3										
2662	GDF10	growth differentiation factor 10										
114794	ELFN2	extracellular leucine-rich repeat and fibronectin type III domain containing 2										
4624	MYH6	myosin, heavy chain 6, cardiac muscle, alpha										
7139	TNNT2	troponin T type 2 (cardiac)										
3579	CXCR2	chemokine (C-X-C motif) receptor 2										
1232	CCR3	chemokine (C-C motif) receptor 3										
51083	GAL	galanin prepropeptide										
85397	RGS8	regulator of G-protein signaling 8										
1607	DGKB	diacylglycerol kinase, beta 90kDa										
1608	DGKG	diacylglycerol kinase, gamma 90kDa										
9162	DGKI	diacylglycerol kinase, iota										
5143	PDE4C	phosphodiesterase 4C, cAMP-specific										
7111	TMOD1	tropomodulin 1										
6331	SCN5A	sodium channel, voltage-gated, type V, alpha subunit										
2674	GFRA1	GDNF family receptor alpha 1										
56963	RGMA	RGM domain family, member A										
1400	CRMP1	collapsin response mediator protein 1										
1675	CFD	complement factor D (adipsin)										
2153	F5	coagulation factor V (proaccelerin, labile factor)										
29106	SCG3	secretogranin III										
2623	GATA1	GATA binding protein 1 (globin transcription factor 1)										
6517	SLC2A4	solute carrier family 2 (facilitated glucose transporter), member 4										
5346	PLIN1	perilipin 1										
6528	SLC5A5	solute carrier family 5 (sodium iodide symporter), member 5										
1621	DBH	dopamine beta-hydroxylase (dopamine beta-monooxygenase)										
1734	DIO2	deiodinase, iodothyronine, type II										
123745	PLA2G4E	phospholipase A2, group IVE										
9899	SV2B	synaptic vesicle glycoprotein 2B										
9900	SV2A	synaptic vesicle glycoprotein 2A										
5522	PPP2R2C	protein phosphatase 2, regulatory subunit B, gamma										
5865	RAB3B	RAB3B, member RAS oncogene family										
5602	MAPK10	mitogen-activated protein kinase 10										
23542	MAPK8IP2	mitogen-activated protein kinase 8 interacting protein 2										
353189	SLCO4C1	solute carrier organic anion transporter family, member 4C1										
222962	SLC29A4	solute carrier family 29 (nucleoside transporters), member 4										
57419	SLC24A3	solute carrier family 24 (sodium/potassium/calcium exchanger), member 3										
116085	SLC22A12	solute carrier family 22 (organic anion/urate transporter), member 12										
3945	LDHB	lactate dehydrogenase B										
3948	LDHC	lactate dehydrogenase C										
84532	ACSS1	acyl-CoA synthetase short-chain family member 1										
1363	CPE	carboxypeptidase E										
5630	PRPH	peripherin										
166012	CHST13	carbohydrate (chondroitin 4) sulfotransferase 13										
23017	FAIM2	Fas apoptotic inhibitory molecule 2										
6258	RXRG	retinoid X receptor, gamma										
5803	PTPRZ1	protein tyrosine phosphatase, receptor-type, Z polypeptide 1										
23114	NFASC	neurofascin										
9369	NRXN3	neurexin 3										
9378	NRXN1	neurexin 1										
9379	NRXN2	neurexin 2										
246	ALOX15	arachidonate 15-lipoxygenase										
956	ENTPD3	ectonucleoside triphosphate diphosphohydrolase 3										
205	AK4	adenylate kinase 4										
7704	ZBTB16	zinc finger and BTB domain containing 16										
5798	PTPRN	protein tyrosine phosphatase, receptor type, N										
9951	HS3ST4	heparan sulfate (glucosamine) 3-O-sulfotransferase 4										
4916	NTRK3	neurotrophic tyrosine kinase, receptor, type 3										
5596	MAPK4	mitogen-activated protein kinase 4										

Gene/Gene Set Overlap Matrix (3/4) **Δdbl.GATA1 vs. Balb/c (FC Log2 >1; FDR 0.05) - DOWNREGULATED**

Entrez Gene Id	Gene Symbol	Gene Description	1	2	3	4	5	6	7	8	9	10
5662	PSD	pleckstrin and Sec7 domain containing										
84448	ABLIM2	actin binding LIM protein family, member 2										
25830	SULT4A1	sulfotransferase family 4A, member 1										
8329	HIST1H2AI	histone cluster 1, H2ai										
92369	SPSB4	splA/ryanodine receptor domain and SOCS box containing 4										
1780	DYNC1I1	dynein, cytoplasmic 1, intermediate chain 1										
442117	GALNTL6	UDP-N-acetyl-alpha-D-galactosamine:polypeptide N-acetylgalactosaminyltransferase-like 6										
23345	SYNE1	spectrin repeat containing, nuclear envelope 1										
1261	CNGA3	cyclic nucleotide gated channel alpha 3										
92737	DNER	delta/notch-like EGF repeat containing										
170261	ZCCHC12	zinc finger, CCHC domain containing 12										
575	BAI1	brain-specific angiogenesis inhibitor 1										
9464	HAND2	heart and neural crest derivatives expressed 2										
203447	NRK	Nik related kinase										
23426	GRIP1	glutamate receptor interacting protein 1										
8288	EPX	eosinophil peroxidase										
64344	HIF3A	hypoxia inducible factor 3, alpha subunit										
761	CA3	carbonic anhydrase III, muscle specific										
1053	CEBPE	CCAAT/enhancer binding protein (C/EBP), epsilon										
10687	PNMA2	paraneoplastic antigen MA2										
10815	CPLX1	complexin 1										
11149	BVES	blood vessel epicardial substance										
11170	FAM107A	family with sequence similarity 107, member A										
11189	CELF3	CUGBP, Elav-like family member 3										
11248	NXPH3	neurexophilin 3										
112609	MRAP2	melanocortin 2 receptor accessory protein 2										
11281	POU6F2	POU class 6 homeobox 2										
114783	LMTK3	lemur tyrosine kinase 3										
115572	FAM46B	family with sequence similarity 46, member B										
119	ADD2	adducin 2 (beta)										
124925	SEZ6	seizure related 6 homolog (mouse)										
128439	SNHG11	small nucleolar RNA host gene 11 (non-protein coding)										
135138	PACRG	PARK2 co-regulated										
139728	PNCK	pregnancy up-regulated non-ubiquitously expressed CaM kinase										
143425	SYT9	synaptotagmin IX										
148281	SYT6	synaptotagmin VI										
148753	FAM163A	family with sequence similarity 163, member A										
150726	FBXO41	F-box protein 41										
154215	NKAIN2	Na+/K+ transporting ATPase interacting 2										
160777	CCDC60	coiled-coil domain containing 60										
161357	MDGA2	MAM domain containing glycosylphosphatidylinositol anchor 2										
164684	WBP2NL	WBP2 N-terminal like										
165186	FAM179A	family with sequence similarity 179, member A										
1747	DLX3	distal-less homeobox 3										
1760	DMPK	dystrophia myotonica-protein kinase										
1767	DNAH5	dynein, axonemal, heavy chain 5										
1804	DPP6	dipeptidyl-peptidase 6										
1917	EEF1A2	eukaryotic translation elongation factor 1 alpha 2										
1952	CELSR2	cadherin, EGF LAG seven-pass G-type receptor 2 (flamingo homolog, Drosophila)										
1995	ELAVL3	ELAV (embryonic lethal, abnormal vision, Drosophila)-like 3 (Hu antigen C)										
201780	SLC10A4	solute carrier family 10 (sodium/bile acid cotransporter family), member 4										
202374	STK32A	serine/threonine kinase 32A										
220108	FAM124A	family with sequence similarity 124A										
220296	HEPACAM	hepatic and glial cell adhesion molecule										
221662	RBM24	RNA binding motif protein 24										
222183	SRRM3	serine/arginine repetitive matrix 3										
222865	TMEM130	transmembrane protein 130										
22844	FRMPD1	FERM and PDZ domain containing 1										
22866	CNKSR2	connector enhancer of kinase suppressor of Ras 2										
22895	RPH3A	rabphilin 3A homolog (mouse)										
22997	IGSF9B	immunoglobulin superfamily, member 9B										
23040	MYT1L	myelin transcription factor 1-like										
23281	MTUS2	microtubule associated tumor suppressor candidate 2										
23336	SYNM	synemin, intermediate filament protein										
23544	SEZ6L	seizure related 6 homolog (mouse)-like										
23762	OSBP2	oxysterol binding protein 2										
238	ALK	anaplastic lymphoma receptor tyrosine kinase										
246176	GAS2L2	growth arrest-specific 2 like 2										
255426	RASGEF1C	RasGEF domain family, member 1C										
255928	SYT14	synaptotagmin XIV										
257240	KLHL34	kelch-like 34 (Drosophila)										
25789	TMEM59L	transmembrane protein 59-like										
26059	ERC2	ELKS/RAB6-interacting/CAST family member 2										
266743	NPAS4	neuronal PAS domain protein 4										
27344	PCSK1N	proprotein convertase subtilisin/kexin type 1 inhibitor										
27445	PCLO	piccolo (presynaptic cytomatrix protein)										
282973	JAKMIP3	Janus kinase and microtubule interacting protein 3										
2843	GPR20	G protein-coupled receptor 20										

Gene/Gene Set Overlap Matrix (4/4) **Δdbl.GATA1 vs. Balb/c (FC Log2 >1; FDR 0.05) - DOWNREGULATED**

Entrez Gene Id	Gene Symbol	Gene Description	1	2	3	4	5	6	7	8	9	10
284434	NWD1	NACHT and WD repeat domain containing 1										
284615	ANKRD34A	ankyrin repeat domain 34A										
285175	UNC80	unc-80 homolog (C. elegans)										
285755	PPIL6	peptidylprolyl isomerase (cyclophilin)-like 6										
29944	PNMA3	paraneoplastic antigen MA3										
30819	KCNIP2	Kv channel interacting protein 2										
340371	NRBP2	nuclear receptor binding protein 2										
342346	C16orf96	chromosome 16 open reading frame 96										
342357	ZKSCAN2	zinc finger with KRAB and SCAN domains 2										
347404	LANCL3	LanC lantibiotic synthetase component C-like 3 (bacterial)										
347730	LRRTM1	leucine rich repeat transmembrane neuronal 1										
349149	GJC3	gap junction protein, gamma 3, 30.2kDa										
375323	LHFPL4	lipoma HMGIC fusion partner-like 4										
379	ARL4D	ADP-ribosylation factor-like 4D										
388015	RTL1	retrotransposon-like 1										
388591	RNF207	ring finger protein 207										
388662	SLC6A17	solute carrier family 6, member 17										
390205	LRRC10B	leucine rich repeat containing 10B										
399693	MGC50722	uncharacterized MGC50722										
440730	TRIM67	tripartite motif containing 67										
450091	CHD5	Coronary heart disease, susceptibility to, 5										
460	ASTN1	astrotactin 1										
4884	NPTX1	neuronal pentraxin I										
50651	SLC45A1	solute carrier family 45, member 1										
50861	STMN3	stathmin-like 3										
51412	ACTL6B	actin-like 6B										
51440	HPCAL4	hippocalcin like 4										
5325	PLAGL1	pleiomorphic adenoma gene-like 1										
53353	LRP1B	low density lipoprotein receptor-related protein 1B										
53942	CNTN5	contactin 5										
54212	SNTG1	syntrophin, gamma 1										
547	KIF1A	kinesin family member 1A										
54715	RBFOX1	RNA binding protein, fox-1 homolog (C. elegans) 1										
55118	CRTAC1	cartilage acidic protein 1										
55228	PNMAL1	PNMA-like 1										
55530	SVOP	SV2 related protein homolog (rat)										
56341	PRMT8	protein arginine methyltransferase 8										
57110	HRASLS	HRAS-like suppressor										
57158	JPH2	junctophilin 2										
57214	KIAA1199	KIAA1199										
57582	KCNT1	potassium channel, subfamily T, member 1										
577	BAI3	brain-specific angiogenesis inhibitor 3										
57709	SLC7A14	solute carrier family 7 (orphan transporter), member 14										
579	NKX3-2	NK3 homeobox 2										
60677	CELF6	CUGBP, Elav-like family member 6										
64091	POPDC2	popeye domain containing 2										
64122	FN3K	fructosamine 3 kinase										
64130	LIN7B	lin-7 homolog B (C. elegans)										
645369	TMEM200C	transmembrane protein 200C										
65009	NDRG4	NDRG family member 4										
65268	WNK2	WNK lysine deficient protein kinase 2										
6620	SNCB	synuclein, beta										
6769	STAC	SH3 and cysteine rich domain										
6860	SYT4	synaptotagmin IV										
7275	TUB	tubby homolog (mouse)										
729085	FAM198A	family with sequence similarity 198, member A										
729359	PLIN4	perilipin 4										
7732	RNF112	ring finger protein 112										
78986	DUSP26	dual specificity phosphatase 26 (putative)										
794	CALB2	calbindin 2										
79605	PGBD5	piggyBac transposable element derived 5										
79957	PAQR6	progestin and adipoQ receptor family member VI										
80023	NRSN2	neurensin 2										
80059	LRRTM4	leucine rich repeat transmembrane neuronal 4										
80731	THSD7B	thrombospondin, type I, domain containing 7B										
81543	LRRC3	leucine rich repeat containing 3										
81551	STMN4	stathmin-like 4										
8328	GFI1B	growth factor independent 1B transcription repressor										
83394	PITPNM3	PITPNM family member 3										
83851	SYT16	synaptotagmin XVI										
8447	DOC2B	double C2-like domains, beta										
84530	SRRM4	serine/arginine repetitive matrix 4										
84630	TTBK1	tau tubulin kinase 1										
84665	MYPN	myopalladin										
84940	CORO6	coronin 6										
85300	ATCAY	ataxia, cerebellar, Cayman type										
85442	KNDC1	kinase non-catalytic C-lobe domain (KIND) containing 1										
85455	DISP2	dispatched homolog 2 (Drosophila)										
8736	MYOM1	myomesin 1, 185kDa										
8929	PHOX2B	paired-like homeobox 2b										
9118	INA	internexin neuronal intermediate filament protein, alpha										
9145	SYNGR1	synaptogyrin 1										
91608	RASL10B	RAS-like, family 10, member B										
91662	NLRP12	NLR family, pyrin domain containing 12										
92235	DUSP27	dual specificity phosphatase 27 (putative)										
93099	DMKN	dermokine										
9381	OTOF	otoferlin										
94030	LRRC4B	leucine rich repeat containing 4B										
9472	AKAP6	A kinase (PRKA) anchor protein 6										
9671	WSCD2	WSC domain containing 2										
9832	JAKMIP2	janus kinase and microtubule interacting protein 2										
9881	TRANK1	tetratricopeptide repeat and ankyrin repeat containing 1										

Table 8: GSEA analysis on **upregulated** gene data sets (183 genes) from *lamina propria* fraction of dbl.GATA1 mice, relative to Balb/c (n=5 mice/group; same dataset as Figure 33)

	Gene Set Name	# Genes in Gene Set (K)	Description	# Genes in Overlap (k)	k/K	p-value	FDR q-value
1	NABA_MATRISOME	1028	Ensemble of genes encoding extracellular matrix and extracellular matrix-associated proteins	55	0.0535	6.74E-46	8.96E-43
2	NABA_MATRISOME_ASSOCIATED	753	Ensemble of genes encoding ECM-associated proteins including ECM-affilaited proteins, ECM regulators and secreted factors	39	0.0518	1.02E-31	6.78E-29
3	REACTOME_GPCR_LIGAND_BINDING	408	Genes involved in GPCR ligand binding	21	0.0515	2.55E-17	8.92E-15
4	REACTOME_CLASS_A1_RHODOPSIN_LIKE_RECEPTORS	305	Genes involved in Class A/1 (Rhodopsin-like receptors)	19	0.0623	2.68E-17	8.92E-15
5	NABA_SECRETED_FACTORS	344	Genes encoding secreted soluble factors	19	0.0552	2.47E-16	6.56E-14
6	KEGG_CYTOKINE_CYTOKINE_RECEPTOR_INTERACTION	267	Cytokine-cytokine receptor interaction	17	0.0637	9.38E-16	1.96E-13
7	REACTOME_IMMUNE_SYSTEM	933	Genes involved in Immune System	27	0.0289	1.03E-15	1.96E-13
8	NABA_CORE_MATRISOME	275	Ensemble of genes encoding core extracellular matrix including ECM glycoproteins, collagens and proteoglycans	16	0.0582	2.75E-14	4.57E-12
9	REACTOME_PEPTIDE_LIGAND_BINDING_RECEPTORS	188	Genes involved in Peptide ligand-binding receptors	14	0.0745	4.01E-14	5.92E-12
10	KEGG_COMPLEMENT_AND_COAGULATION_CASCADES	69	Complement and coagulation cascades	9	0.1304	9.53E-12	1.27E-09

Gene/Gene Set Overlap Matrix (1/3) **Δdbl.GATA1 vs. Balb/c (FC Log2 >1; FDR 0.05) - UPREGULATED**

Entrez Gene Id	Gene Symbol	Gene Description	1	2	3	4	5	6	7	8	9	10
3576	IL8	interleukin 8										
4283	CXCL9	chemokine (C-X-C motif) ligand 9										
6356	CCL11	chemokine (C-C motif) ligand 11										
183	AGT	angiotensinogen (serpin peptidase inhibitor, clade A, member 8)										
54361	WNT4	wingless-type MMTV integration site family, member 4										
6369	CCL24	chemokine (C-C motif) ligand 24										
9547	CXCL14	chemokine (C-X-C motif) ligand 14										
356	FASLG	Fas ligand (TNF superfamily, member 6)										
650	BMP2	bone morphogenetic protein 2										
8995	TNFSF18	tumor necrosis factor (ligand) superfamily, member 18										
2254	FGF9	fibroblast growth factor 9 (glia-activating factor)										
2255	FGF10	fibroblast growth factor 10										
2252	FGF7	fibroblast growth factor 7										
64399	HHIP	hedgehog interacting protein										
653	BMP5	bone morphogenetic protein 5										
4908	NTF3	neurotrophin 3										
10468	FST	follistatin										
3084	NRG1	neuregulin 1										
2487	FRZB	frizzled-related protein										
80274	SCUBE1	signal peptide, CUB domain, EGF-like 1										
712	C1QA	complement component 1, q subcomponent, A chain										
713	C1QB	complement component 1, q subcomponent, B chain										
714	C1QC	complement component 1, q subcomponent, C chain										
1520	CTSS	cathepsin S										
1075	CTSC	cathepsin C										
3958	LGALS3	lectin, galactoside-binding, soluble, 3										
5328	PLAU	plasminogen activator, urokinase										
4318	MMP9	matrix metallopeptidase 9 (gelatinase B, 92kDa gelatinase, 92kDa type IV collagenase)										
4322	MMP13	matrix metallopeptidase 13 (collagenase 3)										
4321	MMP12	matrix metallopeptidase 12 (macrophage elastase)										
4319	MMP10	matrix metallopeptidase 10 (stromelysin 2)										
9508	ADAMTS3	ADAM metallopeptidase with thrombospondin type 1 motif, 3										
5046	PCSK6	proprotein convertase subtilisin/kexin type 6										
10863	ADAM28	ADAM metallopeptidase domain 28										
170692	ADAMTS18	ADAM metallopeptidase with thrombospondin type 1 motif, 18										
27299	ADAMDEC1	ADAM-like, decysin 1										
10462	CLEC10A	C-type lectin domain family 10, member A										
51266	CLEC1B	C-type lectin domain family 1, member B										
93978	CLEC6A	C-type lectin domain family 6, member A										
284217	LAMA1	laminin, alpha 1										
6696	SPP1	secreted phosphoprotein 1										
255743	NPNT	nephronectin										
1758	DMP1	dentin matrix acidic phosphoprotein 1										
22915	MMRN1	multimerin 1										
3486	IGFBP3	insulin-like growth factor binding protein 3										
10418	SPON1	spondin 1, extracellular matrix protein										
10516	FBLN5	fibulin 5										
163479	FNDC7	fibronectin type III domain containing 7										
2202	EFEMP1	EGF containing fibulin-like extracellular matrix protein 1										
27286	SRPX2	sushi-repeat containing protein, X-linked 2										
285313	IGSF10	immunoglobulin superfamily, member 10										
80781	COL18A1	collagen, type XVIII, alpha 1										
7373	COL14A1	collagen, type XIV, alpha 1										
1462	VCAN	versican										
633	BGN	biglycan										

Gene/Gene Set Overlap Matrix (2/3) **Δdbl.GATA1 vs. Balb/c (FC Log2 >1; FDR 0.05) - UPREGULATED**

Entrez Gene Id	Gene Symbol	Gene Description	1	2	3	4	5	6	7	8	9	10
729230	CCR2	chemokine (C-C motif) receptor 2										
1234	CCR5	chemokine (C-C motif) receptor 5										
1230	CCR1	chemokine (C-C motif) receptor 1										
2829	XCR1	chemokine (C motif) receptor 1										
1524	CX3CR1	chemokine (C-X3-C motif) receptor 1										
719	C3AR1	complement component 3a receptor 1										
728	C5AR1	complement component 5a receptor 1										
2149	F2R	coagulation factor II (thrombin) receptor										
10316	NMUR1	neuromedin U receptor 1										
1910	EDNRB	endothelin receptor type B										
53829	P2RY13	purinergic receptor P2Y, G-protein coupled, 13										
3351	HTR1B	5-hydroxytryptamine (serotonin) receptor 1B										
64805	P2RY12	purinergic receptor P2Y, G-protein coupled, 12										
10800	CYSLTR1	cysteinyl leukotriene receptor 1										
3269	HRH1	histamine receptor H1										
9340	GLP2R	glucagon-like peptide 2 receptor										
7850	IL1R2	interleukin 1 receptor, type II										
1436	CSF1R	colony stimulating factor 1 receptor										
3595	IL12RB2	interleukin 12 receptor, beta 2										
10913	EDAR	ectodysplasin A receptor										
729	C6	complement component 6										
5627	PROS1	protein S (alpha)										
5641	LGMN	legumain										
51284	TLR7	toll-like receptor 7										
51311	TLR8	toll-like receptor 8										
9636	ISG15	ISG15 ubiquitin-like modifier										
81030	ZBP1	Z-DNA binding protein 1										
3824	KLRD1	killer cell lectin-like receptor subfamily D, member 1										
7305	TYROBP	TYRO protein tyrosine kinase binding protein										
22914	KLRK1	killer cell lectin-like receptor subfamily K, member 1										
8519	IFITM1	interferon induced transmembrane protein 1 (9-27)										
10666	CD226	CD226 molecule										
11006	LILRB4	leukocyte immunoglobulin-like receptor, subfamily B (with TM and ITIM domains), member 4										
131450	CD200R1	CD200 receptor 1										
2209	FCGR1A	Fc fragment of IgG, high affinity Ia, receptor (CD64)										
1536	CYBB	cytochrome b-245, beta polypeptide										
4940	OAS3	2'-5'-oligoadenylate synthetase 3, 100kDa										
3437	IFIT3	interferon-induced protein with tetratricopeptide repeats 3										
388646	GBP7	guanylate binding protein 7										
5321	PLA2G4A	phospholipase A2, group IVA (cytosolic, calcium-dependent)										
5743	PTGS2	prostaglandin-endoperoxide synthase 2 (prostaglandin G/H synthase and cyclooxygenase)										
5023	P2RX1	purinergic receptor P2X, ligand-gated ion channel, 1										
8516	ITGA8	integrin, alpha 8										
860	RUNX2	runt-related transcription factor 2										
8613	PPAP2B	phosphatidic acid phosphatase type 2B										
54947	LPCAT2	lysophosphatidylcholine acyltransferase 2										
7941	PLA2G7	phospholipase A2, group VII (platelet-activating factor acetylhydrolase, plasma)										
2207	FCER1G	Fc fragment of IgE, high affinity I, receptor for; gamma polypeptide										
3002	GZMB	granzyme B (granzyme 2, cytotoxic T-lymphocyte-associated serine esterase 1)										
7018	TF	transferrin										
2212	FCGR2A	Fc fragment of IgG, low affinity IIa, receptor (CD32)										
27306	HPGDS	hematopoietic prostaglandin D synthase										
9536	PTGES	prostaglandin E synthase										
2760	GM2A	GM2 ganglioside activator										
968	CD68	CD68 molecule										
4023	LPL	lipoprotein lipase										
348	APOE	apolipoprotein E										
3290	HSD11B1	hydroxysteroid (11-beta) dehydrogenase 1										
3682	ITGAE	integrin, alpha E (antigen CD103, human mucosal lymphocyte antigen 1; alpha polypeptide)										
8633	UNC5C	unc-5 homolog C (C. elegans)										
7903	ST8SIA4	ST8 alpha-N-acetyl-neuraminide alpha-2,8-sialyltransferase 4										
64711	HS3ST6	heparan sulfate (glucosamine) 3-O-sulfotransferase 6										
3766	KCNJ10	potassium inwardly-rectifying channel, subfamily J, member 10										
3773	KCNJ16	potassium inwardly-rectifying channel, subfamily J, member 16										
486	FXYD2	FXYD domain containing ion transport regulator 2										
3101	HK3	hexokinase 3 (white cell)										
80896	NPL	N-acetylneuraminate pyruvate lyase (dihydrodipicolinate synthase)										
220	ALDH1A3	aldehyde dehydrogenase 1 family, member A3										
1339	COX6A2	cytochrome c oxidase subunit VIa polypeptide 2										
54363	HAO1	hydroxyacid oxidase (glycolate oxidase) 1										
8942	KYNU	kynureninase										
56158	TEX12	testis expressed 12										
9615	GDA	guanine deaminase										
157506	RDH10	retinol dehydrogenase 10 (all-trans)										
3039	HBA1	hemoglobin, alpha 1										
100131451	TLR12P	toll-like receptor 12, pseudogene										
10110	SGK2	serum/glucocorticoid regulated kinase 2										
10561	IFI44	interferon-induced protein 44										

Gene/Gene Set Overlap Matrix (3/3) **Δdbl.GATA1 vs. Balb/c (FC Log2 >1; FDR 0.05) - UPREGULATED**

Entrez Gene Id	Gene Symbol	Gene Description	1	2	3	4	5	6	7	8	9	10
10630	PDPN	podoplanin										
10748	KLRAP1	killer cell lectin-like receptor subfamily A pseudogene 1										
10964	IFI44L	interferon-induced protein 44-like										
115761	ARL11	ADP-ribosylation factor-like 11										
124842	TMEM132E	transmembrane protein 132E										
130733	TMEM178	transmembrane protein 178										
140738	TMEM37	transmembrane protein 37										
1776	DNASE1L3	deoxyribonuclease I-like 3										
203859	ANO5	anoctamin 5										
2123	EVI2A	ecotropic viral integration site 2A										
219972	MPEG1	macrophage expressed 1										
221303	FAM162B	family with sequence similarity 162, member B										
2300	FOXL1	forkhead box L1										
23284	LPHN3	latrophilin 3										
2615	LRRC32	leucine rich repeat containing 32										
2813	GP2	glycoprotein 2 (zymogen granule membrane)										
283150	FOXR1	forkhead box R1										
283659	PRTG	protogenin										
2857	GPR34	G protein-coupled receptor 34										
29953	TRHDE	thyrotropin-releasing hormone degrading enzyme										
3428	IFI16	interferon, gamma-inducible protein 16										
353514	LILRA5	leukocyte immunoglobulin-like receptor, subfamily A (with TM domain), member 5										
3903	LAIR1	leukocyte-associated immunoglobulin-like receptor 1										
4061	LY6E	lymphocyte antigen 6 complex, locus E										
441168	FAM26F	family with sequence similarity 26, member F										
4481	MSR1	macrophage scavenger receptor 1										
497189	TIFAB	TRAF-interacting protein with forkhead-associated domain, family member B										
51450	PRRX2	paired related homeobox 2										
54491	FAM105A	family with sequence similarity 105, member A										
55885	LMO3	LIM domain only 3 (rhombotin-like 2)										
57491	AHRR	aryl-hydrocarbon receptor repressor										
58475	MS4A7	membrane-spanning 4-domains, subfamily A, member 7										
5918	RARRES1	retinoic acid receptor responder (tazarotene induced) 1										
5919	RARRES2	retinoic acid receptor responder (tazarotene induced) 2										
6039	RNASE6	ribonuclease, RNase A family, k6										
6299	SALL1	sal-like 1 (Drosophila)										
64231	MS4A6A	membrane-spanning 4-domains, subfamily A, member 6A										
646480	FABP9	fatty acid binding protein 9, testis										
64881	PCDH20	protocadherin 20										
6781	STC1	stanniocalcin 1										
6943	TCF21	transcription factor 21										
7940	LST1	leukocyte specific transcript 1										
84189	SLITRK6	SLIT and NTRK-like family, member 6										
84868	HAVCR2	hepatitis A virus cellular receptor 2										
8796	SCEL	sciellin										
8808	IL1RL2	interleukin 1 receptor-like 2										
8989	TRPA1	transient receptor potential cation channel, subfamily A, member 1										
9173	IL1RL1	interleukin 1 receptor-like 1										
91937	TIMD4	T-cell immunoglobulin and mucin domain containing 4										
9242	MSC	musculin										

Table 9: GSEA analysis on **downregulated** gene data sets (total of 565 genes) from *lamina propria* fraction of ST2.IL17rbko mice, relative to Balb/c (n=4-5 mice/group; same dataset as Figure 38)

	Gene Set Name	# Genes in Gene Set (K)	Description	# Genes in Overlap (k)	k/K	p-value	FDR q-value
1	REACTOME_NEURONAL_SYSTEM	279	Genes involved in Neuronal System	38	0.1362	5.64E-28	7.50E-25
2	NABA_MATRISOME	1028	Ensemble of genes encoding extracellular matrix and extracellular matrix-associated proteins	55	0.0535	1.02E-19	6.78E-17
3	REACTOME_POTASSIUM_CHANNELS	98	Genes involved in Potassium Channels	19	0.1939	1.32E-17	5.27E-15
4	NABA_CORE_MATRISOME	275	Ensemble of genes encoding core extracellular matrix including ECM glycoproteins, collagens and proteoglycans	28	0.1018	1.59E-17	5.27E-15
5	KEGG_CALCIUM_SIGNALING_PATHWAY	178	Calcium signaling pathway	22	0.1236	7.87E-16	2.09E-13
6	REACTOME_VOLTAGE_GATED_POTASSIUM_CHANNELS	43	Genes involved in Voltage gated Potassium channels	13	0.3023	3.34E-15	7.40E-13
7	REACTOME_TRANSMISSION_ACROSS_CHEMICAL_SYNAPSES	186	Genes involved in Transmission across Chemical Synapses	21	0.1129	2.24E-14	4.25E-12
8	KEGG_NEUROACTIVE_LIGAND_RECEPTOR_INTERACTION	272	Neuroactive ligand-receptor interaction	24	0.0882	7.91E-14	1.31E-11
9	NABA_ECM_GLYCOPROTEINS	196	Genes encoding structural ECM glycoproteins	20	0.102	6.36E-13	9.39E-11
10	REACTOME_AXON_GUIDANCE	251	Genes involved in Axon guidance	19	0.0757	4.32E-10	5.74E-08

Gene/Gene Set Overlap Matrix (1/7) **ST2.IL17rbko vs. Balb/c (FC log2>1; FDR 0.05) - DOWNREGULATED**

Entrez Gene Id	Gene Symbol	Gene Description	1	2	3	4	5	6	7	8	9	10
3785	KCNQ2	potassium voltage-gated channel, KQT-like subfamily, member 2										
3786	KCNQ3	potassium voltage-gated channel, KQT-like subfamily, member 3										
3745	KCNB1	potassium voltage-gated channel, Shab-related subfamily, member 1										
3736	KCNA1	potassium voltage-gated channel, shaker-related subfamily, member 1 (episodic ataxia with myokymia)										
3737	KCNA2	potassium voltage-gated channel, shaker-related subfamily, member 2										
3739	KCNA4	potassium voltage-gated channel, shaker-related subfamily, member 4										
3742	KCNA6	potassium voltage-gated channel, shaker-related subfamily, member 6										
3746	KCNC1	potassium voltage-gated channel, Shaw-related subfamily, member 1										
3752	KCND3	potassium voltage-gated channel, Shal-related subfamily, member 3										
3754	KCNF1	potassium voltage-gated channel, subfamily F, member 1										
3757	KCNH2	potassium voltage-gated channel, subfamily H (eag-related), member 2										
93107	KCNG4	potassium voltage-gated channel, subfamily G, member 4										
9312	KCNB2	potassium voltage-gated channel, Shab-related subfamily, member 2										
2788	GNG7	guanine nucleotide binding protein (G protein), gamma 7										
3760	KCNJ3	potassium inwardly-rectifying channel, subfamily J, member 3										
3768	KCNJ12	potassium inwardly-rectifying channel, subfamily J, member 12										
10060	ABCC9	ATP-binding cassette, sub-family C (CFTR/MRP), member 9										
10021	HCN4	hyperpolarization activated cyclic nucleotide-gated potassium channel 4										
3782	KCNN3	potassium intermediate/small conductance calcium-activated channel, subfamily N, member 3										
107	ADCY1	adenylate cyclase 1 (brain)										
815	CAMK2A	calcium/calmodulin-dependent protein kinase II alpha										
774	CACNA1B	calcium channel, voltage-dependent, N type, alpha 1B subunit										
2562	GABRB3	gamma-aminobutyric acid (GABA) A receptor, beta 3										
2890	GRIA1	glutamate receptor, ionotropic, AMPA 1										
1136	CHRNA3	cholinergic receptor, nicotinic, alpha 3										
1138	CHRNA5	cholinergic receptor, nicotinic, alpha 5										
1143	CHRNB4	cholinergic receptor, nicotinic, beta 4										
2898	GRIK2	glutamate receptor, ionotropic, kainate 2										
783	CACNB2	calcium channel, voltage-dependent, beta 2 subunit										
23229	ARHGEF9	Cdc42 guanine nucleotide exchange factor (GEF) 9										
27092	CACNG4	calcium channel, voltage-dependent, gamma subunit 4										
4747	NEFL	neurofilament, light polypeptide										
55799	CACNA2D3	calcium channel, voltage-dependent, alpha 2/delta subunit 3										
6616	SNAP25	synaptosomal-associated protein, 25kDa										
6857	SYT1	synaptotagmin I										
6854	SYN2	synapsin II										
43	ACHE	acetylcholinesterase										
127833	SYT2	synaptotagmin II										
6585	SLIT1	slit homolog 1 (Drosophila)										
9353	SLIT2	slit homolog 2 (Drosophila)										
6586	SLIT3	slit homolog 3 (Drosophila)										
9370	ADIPOQ	adiponectin, C1Q and collagen domain containing										
7058	THBS2	thrombospondin 2										
7143	TNR	tenascin R (restrictin, janusin)										
7148	TNXB	tenascin XB										
26577	PCOLCE2	procollagen C-endopeptidase enhancer 2										
3485	IGFBP2	insulin-like growth factor binding protein 2, 36kDa										
3488	IGFBP5	insulin-like growth factor binding protein 5										
10631	POSTN	periostin, osteoblast specific factor										
127731	VWA5B1	von Willebrand factor A domain containing 5B1										
163175	LGI4	leucine-rich repeat LGI family, member 4										
2192	FBLN1	fibulin 1										
256158	HMCN2	hemicentin 2										
4745	NELL1	NEL-like 1 (chicken)										
4753	NELL2	NEL-like 2 (chicken)										
55203	LGI2	leucine-rich repeat LGI family, member 2										
84624	FNDC1	fibronectin type III domain containing 1										

Gene/Gene Set Overlap Matrix (2/7) **ST2.IL17rbko vs. Balb/c (FC log2>1; FDR 0.05) - DOWNREGULATED**

Entrez Gene Id	Gene Symbol	Gene Description	1	2	3	4	5	6	7	8	9	10
9211	LGI1	leucine-rich, glioma inactivated 1										
1463	NCAN	neurocan										
1301	COL11A1	collagen, type XI, alpha 1										
1295	COL8A1	collagen, type VIII, alpha 1										
1296	COL8A2	collagen, type VIII, alpha 2										
1310	COL19A1	collagen, type XIX, alpha 1										
26254	OPTC	opticin										
50859	SPOCK3	sparc/osteonectin, cwcv and kazal-like domains proteoglycan (testican) 3										
9806	SPOCK2	sparc/osteonectin, cwcv and kazal-like domains proteoglycan (testican) 2										
5365	PLXNB3	plexin B3										
9048	ARTN	artemin										
7483	WNT9A	wingless-type MMTV integration site family, member 9A										
4803	NGF	nerve growth factor (beta polypeptide)										
2258	FGF13	fibroblast growth factor 13										
2259	FGF14	fibroblast growth factor 14										
10500	SEMA6C	sema domain, transmembrane domain (TM), and cytoplasmic domain, (semaphorin) 6C										
6285	S100B	S100 calcium binding protein B										
10718	NRG3	neuregulin 3										
5764	PTN	pleiotrophin										
392255	GDF6	growth differentiation factor 6										
147381	CBLN2	cerebellin 2 precursor										
2662	GDF10	growth differentiation factor 10										
57758	SCUBE2	signal peptide, CUB domain, EGF-like 2										
84466	MEGF10	multiple EGF-like-domains 10										
2719	GPC3	glypican 3										
283463	MUC19	mucin 19, oligomeric										
10584	COLEC10	collectin sub-family member 10 (C-type lectin)										
10882	C1QL1	complement component 1, q subcomponent-like 1										
114899	C1QTNF3	C1q and tumor necrosis factor related protein 3										
158326	FREM1	FRAS1 related extracellular matrix 1										
283208	P4HA3	prolyl 4-hydroxylase, alpha polypeptide III										
11095	ADAMTS8	ADAM metallopeptidase with thrombospondin type 1 motif, 8										
171019	ADAMTS19	ADAM metallopeptidase with thrombospondin type 1 motif, 19										
4185	ADAM11	ADAM metallopeptidase domain 11										
57188	ADAMTSL3	ADAMTS-like 3										
80332	ADAM33	ADAM metallopeptidase domain 33										
4923	NTSR1	neurotensin receptor 1 (high affinity)										
5021	OXTR	oxytocin receptor										
6865	TACR2	tachykinin receptor 2										
886	CCKAR	cholecystokinin A receptor										
148	ADRA1A	adrenergic, alpha-1A-, receptor										
5737	PTGFR	prostaglandin F receptor (FP)										
155	ADRB3	adrenergic, beta-3-, receptor										
22953	P2RX2	purinergic receptor P2X, ligand-gated ion channel, 2										
491	ATP2B2	ATPase, Ca++ transporting, plasma membrane 2										
492	ATP2B3	ATPase, Ca++ transporting, plasma membrane 3										
6543	SLC8A2	solute carrier family 8 (sodium/calcium exchanger), member 2										
775	CACNA1C	calcium channel, voltage-dependent, L type, alpha 1C subunit										
6262	RYR2	ryanodine receptor 2 (cardiac)										
4638	MYLK	myosin light chain kinase										
777	CACNA1E	calcium channel, voltage-dependent, R type, alpha 1E subunit										
4842	NOS1	nitric oxide synthase 1 (neuronal)										
2066	ERBB4	v-erb-a erythroblastic leukemia viral oncogene homolog 4 (avian)										
6263	RYR3	ryanodine receptor 3										
493	ATP2B4	ATPase, Ca++ transporting, plasma membrane 4										
4986	OPRK1	opioid receptor, kappa 1										
2587	GALR1	galanin receptor 1										
4887	NPY2R	neuropeptide Y receptor Y2										
4985	OPRD1	opioid receptor, delta 1										
4987	OPRL1	opiate receptor-like 1										
151	ADRA2B	adrenergic, alpha-2B-, receptor										
1268	CNR1	cannabinoid receptor 1 (brain)										
117	ADCYAP1R1	adenylate cyclase activating polypeptide 1 (pituitary) receptor type I										
2917	GRM7	glutamate receptor, metabotropic 7										
1132	CHRM4	cholinergic receptor, muscarinic 4										
4629	MYH11	myosin, heavy chain 11, smooth muscle										
4897	NRCAM	neuronal cell adhesion molecule										
6326	SCN2A	sodium channel, voltage-gated, type II, alpha subunit										
6331	SCN5A	sodium channel, voltage-gated, type V, alpha subunit										
6900	CNTN2	contactin 2 (axonal)										
2674	GFRA1	GDNF family receptor alpha 1										
56963	RGMA	RGM domain family, member A										
7223	TRPC4	transient receptor potential cation channel, subfamily C, member 4										
10570	DPYSL4	dihydropyrimidinase-like 4										
1400	CRMP1	collapsin response mediator protein 1										
10874	NMU	neuromedin U										
4852	NPY	neuropeptide Y										
51083	GAL	galanin prepropeptide										

Gene/Gene Set Overlap Matrix (3/7) ST2.IL17rbko vs. Balb/c (FC log2>1; FDR 0.05) - DOWNREGULATED

Entrez Gene Id	Gene Symbol	Gene Description	1	2	3	4	5	6	7	8	9	10
7432	VIP	vasoactive intestinal peptide										
797	CALCB	calcitonin-related polypeptide beta										
6517	SLC2A4	solute carrier family 2 (facilitated glucose transporter), member 4										
5346	PLIN1	perilipin 1										
477	ATP1A2	ATPase, Na+/K+ transporting, alpha 2 polypeptide										
5575	PRKAR1B	protein kinase, cAMP-dependent, regulatory, type I, beta										
3359	HTR3A	5-hydroxytryptamine (serotonin) receptor 3A										
23460	ABCA6	ATP-binding cassette, sub-family A (ABC1), member 6										
64137	ABCG4	ATP-binding cassette, sub-family G (WHITE), member 4										
10351	ABCA8	ATP-binding cassette, sub-family A (ABC1), member 8										
364	AQP7	aquaporin 7										
154091	SLC2A12	solute carrier family 2 (facilitated glucose transporter), member 12										
6528	SLC5A5	solute carrier family 5 (sodium iodide symporter), member 5										
55117	SLC6A15	solute carrier family 6 (neutral amino acid transporter), member 15										
284111	SLC13A5	solute carrier family 13 (sodium-dependent citrate transporter), member 5										
57419	SLC24A3	solute carrier family 24 (sodium/potassium/calcium exchanger), member 3										
222962	SLC29A4	solute carrier family 29 (nucleoside transporters), member 4										
7169	TPM2	tropomyosin 2 (beta)										
7139	TNNT2	troponin T type 2 (cardiac)										
59284	CACNG7	calcium channel, voltage-dependent, gamma subunit 7										
125965	COX6B2	cytochrome c oxidase subunit VIb polypeptide 2 (testis)										
4632	MYL1	myosin, light chain 1, alkali; skeletal, fast										
7111	TMOD1	tropomodulin 1										
7138	TNNT1	troponin T type 1 (skeletal, slow)										
59	ACTA2	actin, alpha 2, smooth muscle, aorta										
3679	ITGA7	integrin, alpha 7										
1496	CTNNA2	catenin (cadherin-associated protein), alpha 2										
29119	CTNNA3	catenin (cadherin-associated protein), alpha 3										
85397	RGS8	regulator of G-protein signaling 8										
1607	DGKB	diacylglycerol kinase, beta 90kDa										
9162	DGKI	diacylglycerol kinase, iota										
5143	PDE4C	phosphodiesterase 4C, cAMP-specific										
26575	RGS17	regulator of G-protein signaling 17										
5602	MAPK10	mitogen-activated protein kinase 10										
123745	PLA2G4E	phospholipase A2, group IVE										
23542	MAPK8IP2	mitogen-activated protein kinase 8 interacting protein 2										
4137	MAPT	microtubule-associated protein tau										
3306	HSPA2	heat shock 70kDa protein 2										
1946	EFNA5	ephrin-A5										
2044	EPHA5	EPH receptor A5										
2046	EPHA8	EPH receptor A8										
285220	EPHA6	EPH receptor A6										
84448	ABLIM2	actin binding LIM protein family, member 2										
4741	NEFM	neurofilament, medium polypeptide										
4744	NEFH	neurofilament, heavy polypeptide										
5630	PRPH	peripherin										
4685	NCAM2	neural cell adhesion molecule 2										
26047	CNTNAP2	contactin associated protein-like 2										
54413	NLGN3	neuroligin 3										
9369	NRXN3	neurexin 3										
9378	NRXN1	neurexin 1										
9379	NRXN2	neurexin 2										
9900	SV2A	synaptic vesicle glycoprotein 2A										
6258	RXRG	retinoid X receptor, gamma										
1363	CPE	carboxypeptidase E										
5126	PCSK2	proprotein convertase subtilisin/kexin type 2										
222537	HS3ST5	heparan sulfate (glucosamine) 3-O-sulfotransferase 5										
64579	NDST4	N-deacetylase/N-sulfotransferase (heparan glucosaminyl) 4										
1675	CFD	complement factor D (adipsin)										
29106	SCG3	secretogranin III										
3798	KIF5A	kinesin family member 5A										
1795	DOCK3	dedicator of cytokinesis 3										
5521	PPP2R2B	protein phosphatase 2, regulatory subunit B, beta										
5522	PPP2R2C	protein phosphatase 2, regulatory subunit B, gamma										
5865	RAB3B	RAB3B, member RAS oncogene family										
4804	NGFR	nerve growth factor receptor										
80319	CXXC4	CXXC finger protein 4										
27123	DKK2	dickkopf homolog 2 (Xenopus laevis)										
85409	NKD2	naked cuticle homolog 2 (Drosophila)										
23017	FAIM2	Fas apoptotic inhibitory molecule 2										
23413	NCS1	neuronal calcium sensor 1										
2670	GFAP	glial fibrillary acidic protein										
8936	WASF1	WAS protein family, member 1										
10810	WASF3	WAS protein family, member 3										
1621	DBH	dopamine beta-hydroxylase (dopamine beta-monooxygenase)										
4916	NTRK3	neurotrophic tyrosine kinase, receptor, type 3										
5979	RET	ret proto-oncogene										
3945	LDHB	lactate dehydrogenase B										
5166	PDK4	pyruvate dehydrogenase kinase, isozyme 4										
137872	ADHFE1	alcohol dehydrogenase, iron containing, 1										

Gene/Gene Set Overlap Matrix (4/7) **ST2.IL17rbko vs. Balb/c (FC log2>1; FDR 0.05) - DOWNREGULATED**

Entrez Gene Id	Gene Symbol	Gene Description	1	2	3	4	5	6	7	8	9	10
80339	PNPLA3	patatin-like phospholipase domain containing 3										
730	C7	complement component 7										
113451	ADC	arginine decarboxylase										
23426	GRIP1	glutamate receptor interacting protein 1										
9421	HAND1	heart and neural crest derivatives expressed 1										
9464	HAND2	heart and neural crest derivatives expressed 2										
273	AMPH	amphiphysin										
658	BMPR1B	bone morphogenetic protein receptor, type IB										
64388	GREM2	gremlin 2										
5740	PTGIS	prostaglandin I2 (prostacyclin) synthase										
2686	GGT7	gamma-glutamyltransferase 7										
956	ENTPD3	ectonucleoside triphosphate diphosphohydrolase 3										
2766	GMPR	guanosine monophosphate reductase										
205	AK4	adenylate kinase 4										
966	CD59	CD59 molecule, complement regulatory protein										
2596	GAP43	growth associated protein 43										
635	BHMT	betaine--homocysteine S-methyltransferase										
5662	PSD	pleckstrin and Sec7 domain containing										
2026	ENO2	enolase 2 (gamma, neuronal)										
56603	CYP26B1	cytochrome P450, family 26, subfamily B, polypeptide 1										
25830	SULT4A1	sulfotransferase family 4A, member 1										
316	AOX1	aldehyde oxidase 1										
10157	AASS	aminoadipate-semialdehyde synthase										
5798	PTPRN	protein tyrosine phosphatase, receptor type, N										
64409	WBSCR17	Williams-Beuren syndrome chromosome region 17										
5803	PTPRZ1	protein tyrosine phosphatase, receptor-type, Z polypeptide 1										
7345	UCHL1	ubiquitin carboxyl-terminal esterase L1 (ubiquitin thiolesterase)										
2861	GPR37	G protein-coupled receptor 37 (endothelin receptor type B-like)										
5596	MAPK4	mitogen-activated protein kinase 4										
10381	TUBB3	tubulin, beta 3 class III										
1780	DYNC1I1	dynein, cytoplasmic 1, intermediate chain 1										
26232	FBXO2	F-box protein 2										
1261	CNGA3	cyclic nucleotide gated channel alpha 3										
8120	AP3B2	adaptor-related protein complex 3, beta 2 subunit										
1008	CDH10	cadherin 10, type 2 (T2-cadherin)										
92737	DNER	delta/notch-like EGF repeat containing										
170261	ZCCHC12	zinc finger, CCHC domain containing 12										
575	BAI1	brain-specific angiogenesis inhibitor 1										
50507	NOX4	NADPH oxidase 4										
203447	NRK	Nik related kinase										
3196	TLX2	T-cell leukemia homeobox 2										
56776	FMN2	formin 2										
761	CA3	carbonic anhydrase III, muscle specific										
100505381	MMD2	Miyoshi muscular dystrophy 2										
1038	CDR1	cerebellar degeneration-related protein 1, 34kDa										
1047	CLGN	calmegin										
10650	SLMO1	slowmo homolog 1 (Drosophila)										
10687	PNMA2	paraneoplastic antigen MA2										
10752	CHL1	cell adhesion molecule with homology to L1CAM (close homolog of L1)										
11075	STMN2	stathmin-like 2										
11247	NXPH4	neurexophilin 4										
11248	NXPH3	neurexophilin 3										
112609	MRAP2	melanocortin 2 receptor accessory protein 2										
11281	POU6F2	POU class 6 homeobox 2										
114783	LMTK3	lemur tyrosine kinase 3										
114786	XKR4	XK, Kell blood group complex subunit-related family, member 4										
114798	SLITRK1	SLIT and NTRK-like family, member 1										
114801	TMEM200A	transmembrane protein 200A										
114815	SORCS1	sortilin-related VPS10 domain containing receptor 1										
114928	GPRASP2	G protein-coupled receptor associated sorting protein 2										
115827	RAB3C	RAB3C, member RAS oncogene family										
116173	CMTM5	CKLF-like MARVEL transmembrane domain containing 5										
116496	FAM129A	family with sequence similarity 129, member A										
116535	MRGPRF	MAS-related GPR, member F										
118812	MORN4	MORN repeat containing 4										
119	ADD2	adducin 2 (beta)										
120114	FAT3	FAT tumor suppressor homolog 3 (Drosophila)										
124925	SEZ6	seizure related 6 homolog (mouse)										
126075	CCDC159	coiled-coil domain containing 159										
126206	NLRP5	NLR family, pyrin domain containing 5										
126393	HSPB6	heat shock protein, alpha-crystallin-related, B6										
127254	C1orf173	chromosome 1 open reading frame 173										
128414	NKAIN4	Na+/K+ transporting ATPase interacting 4										
128439	SNHG11	small nucleolar RNA host gene 11 (non-protein coding)										
130497	OSR1	odd-skipped related 1 (Drosophila)										
132014	IL17RE	interleukin 17 receptor E										
135138	PACRG	PARK2 co-regulated										
1381	CRABP1	cellular retinoic acid binding protein 1										
139728	PNCK	pregnancy up-regulated non-ubiquitously expressed CaM kinase										
143425	SYT9	synaptotagmin IX										

Gene/Gene Set Overlap Matrix (5/7) **ST2.IL17rbko vs. Balb/c (FC log2>1; FDR 0.05) - DOWNREGULATED**

Entrez Gene Id	Gene Symbol	Gene Description	1	2	3	4	5	6	7	8	9	10
145270	PRIMA1	proline rich membrane anchor 1										
146330	FBXL16	F-box and leucine-rich repeat protein 16										
147906	DACT3	dapper, antagonist of beta-catenin, homolog 3 (Xenopus laevis)										
148252	DIRAS1	DIRAS family, GTP-binding RAS-like 1										
148281	SYT6	synaptotagmin VI										
148753	FAM163A	family with sequence similarity 163, member A										
149111	CNIH3	cornichon homolog 3 (Drosophila)										
149297	FAM78B	family with sequence similarity 78, member B										
150726	FBXO41	F-box protein 41										
152404	IGSF11	immunoglobulin superfamily, member 11										
154215	NKAIN2	Na+/K+ transporting ATPase interacting 2										
157807	CLVS1	clavesin 1										
158038	LINGO2	leucine rich repeat and Ig domain containing 2										
160777	CCDC60	coiled-coil domain containing 60										
161753	ODF3L1	outer dense fiber of sperm tails 3-like 1										
164832	LONRF2	LON peptidase N-terminal domain and ring finger 2										
165186	FAM179A	family with sequence similarity 179, member A										
165215	FAM171B	family with sequence similarity 171, member B										
167410	LIX1	Lix1 homolog (chicken)										
169166	SNX31	sorting nexin 31										
1746	DLX2	distal-less homeobox 2										
1747	DLX3	distal-less homeobox 3										
1760	DMPK	dystrophia myotonica-protein kinase										
1767	DNAH5	dynein, axonemal, heavy chain 5										
1804	DPP6	dipeptidyl-peptidase 6										
1917	EEF1A2	eukaryotic translation elongation factor 1 alpha 2										
1995	ELAVL3	ELAV (embryonic lethal, abnormal vision, Drosophila)-like 3 (Hu antigen C)										
1996	ELAVL4	ELAV (embryonic lethal, abnormal vision, Drosophila)-like 4 (Hu antigen D)										
200844	C3orf67	chromosome 3 open reading frame 67										
201780	SLC10A4	solute carrier family 10 (sodium/bile acid cotransporter family), member 4										
202374	STK32A	serine/threonine kinase 32A										
220108	FAM124A	family with sequence similarity 124A										
221476	PI16	peptidase inhibitor 16										
221662	RBM24	RNA binding motif protein 24										
222183	SRRM3	serine/arginine repetitive matrix 3										
222553	SLC35F1	solute carrier family 35, member F1										
222865	TMEM130	transmembrane protein 130										
22866	CNKSR2	connector enhancer of kinase suppressor of Ras 2										
22895	RPH3A	rabphilin 3A homolog (mouse)										
23034	SAMD4A	sterile alpha motif domain containing 4A										
23040	MYT1L	myelin transcription factor 1-like										
23072	HECW1	HECT, C2 and WW domain containing E3 ubiquitin protein ligase 1										
23148	NACAD	NAC alpha domain containing										
23208	SYT11	synaptotagmin XI										
23251	KIAA1024	KIAA1024										
23281	MTUS2	microtubule associated tumor suppressor candidate 2										
23336	SYNM	synemin, intermediate filament protein										
23349	KIAA1045	KIAA1045										
23544	SEZ6L	seizure related 6 homolog (mouse)-like										
23704	KCNE4	potassium voltage-gated channel, Isk-related family, member 4										
23762	OSBP2	oxysterol binding protein 2										
238	ALK	anaplastic lymphoma receptor tyrosine kinase										
24147	FJX1	four jointed box 1 (Drosophila)										
246176	GAS2L2	growth arrest-specific 2 like 2										
253152	EPHX4	epoxide hydrolase 4										
255928	SYT14	synaptotagmin XIV										
257019	FRMD3	FERM domain containing 3										
257240	KLHL34	kelch-like 34 (Drosophila)										
25789	TMEM59L	transmembrane protein 59-like										
25817	FAM19A5	family with sequence similarity 19 (chemokine (C-C motif)-like), member A5										
259232	NALCN	sodium leak channel, non-selective										
26032	SUSD5	sushi domain containing 5										
26050	SLITRK5	SLIT and NTRK-like family, member 5										
26059	ERC2	ELKS/RAB6-interacting/CAST family member 2										
26353	HSPB8	heat shock 22kDa protein 8										
266743	NPAS4	neuronal PAS domain protein 4										
27022	FOXD3	forkhead box D3										
27254	CSDC2	cold shock domain containing C2, RNA binding										
27344	PCSK1N	proprotein convertase subtilisin/kexin type 1 inhibitor										
27445	PCLO	piccolo (presynaptic cytomatrix protein)										
282973	JAKMIP3	Janus kinase and microtubule interacting protein 3										
28316	CDH20	cadherin 20, type 2										
283455	KSR2	kinase suppressor of ras 2										
2843	GPR20	G protein-coupled receptor 20										
284339	TMEM145	transmembrane protein 145										
28513	CDH19	cadherin 19, type 2										
285175	UNC80	unc-80 homolog (C. elegans)										
286133	SCARA5	scavenger receptor class A, member 5 (putative)										
29114	TAGLN3	transgelin 3										
29118	DDX25	DEAD (Asp-Glu-Ala-Asp) box polypeptide 25										

Gene/Gene Set Overlap Matrix (6/7)		ST2.IL17rbko vs. Balb/c (FC log2>1; FDR 0.05) - DOWNREGULATED										
Entrez Gene Id	Gene Symbol	Gene Description	1	2	3	4	5	6	7	8	9	10
2974	GUCY1B2	guanylate cyclase 1, soluble, beta 2										
29944	PNMA3	paraneoplastic antigen MA3										
30819	KCNIP2	Kv channel interacting protein 2										
30820	KCNIP1	Kv channel interacting protein 1										
339416	ANKRD45	ankyrin repeat domain 45										
339983	NAT8L	N-acetyltransferase 8-like (GCN5-related, putative)										
340146	SLC35D3	solute carrier family 35, member D3										
340371	NRBP2	nuclear receptor binding protein 2										
342346	C16orf96	chromosome 16 open reading frame 96										
342357	ZKSCAN2	zinc finger with KRAB and SCAN domains 2										
343450	KCNT2	potassium channel, subfamily T, member 2										
344758	GPR149	G protein-coupled receptor 149										
347	APOD	apolipoprotein D										
347730	LRRTM1	leucine rich repeat transmembrane neuronal 1										
347731	LRRTM3	leucine rich repeat transmembrane neuronal 3										
348093	RBPMS2	RNA binding protein with multiple splicing 2										
349149	GJC3	gap junction protein, gamma 3, 30.2kDa										
374897	SBSN	suprabasin										
375323	LHFPL4	lipoma HMGIC fusion partner-like 4										
377007	KLHL30	kelch-like 30 (Drosophila)										
379	ARL4D	ADP-ribosylation factor-like 4D										
3800	KIF5C	kinesin family member 5C										
387758	FIBIN	fin bud initiation factor homolog (zebrafish)										
388015	RTL1	retrotransposon-like 1										
388021	TMEM179	transmembrane protein 179										
388591	RNF207	ring finger protein 207										
388662	SLC6A17	solute carrier family 6, member 17										
389075	RESP18	regulated endocrine-specific protein 18 homolog (rat)										
390205	LRRC10B	leucine rich repeat containing 10B										
399693	MGC50722	uncharacterized MGC50722										
400224	PLEKHD1	pleckstrin homology domain containing, family D (with coiled-coil domains) member 1										
402665	IGLON5	IgLON family member 5										
4045	LSAMP	limbic system-associated membrane protein										
4062	LY6H	lymphocyte antigen 6 complex, locus H										
407738	FAM19A1	family with sequence similarity 19 (chemokine (C-C motif)-like), member A1										
440730	TRIM67	tripartite motif containing 67										
450091	CHD5	Coronary heart disease, susceptibility to, 5										
460	ASTN1	astrotactin 1										
4884	NPTX1	neuronal pentraxin I										
50512	PODXL2	podocalyxin-like 2										
50651	SLC45A1	solute carrier family 45, member 1										
50861	STMN3	stathmin-like 3										
5101	PCDH9	protocadherin 9										
51209	RAB9B	RAB9B, member RAS oncogene family										
5121	PCP4	Purkinje cell protein 4										
51286	CEND1	cell cycle exit and neuronal differentiation 1										
51310	SLC22A17	solute carrier family 22, member 17										
51412	ACTL6B	actin-like 6B										
51440	HPCAL4	hippocalcin like 4										
51560	RAB6B	RAB6B, member RAS oncogene family										
51617	HMP19	HMP19 protein										
51673	TPPP3	tubulin polymerization-promoting protein family member 3										
51754	TMEM8B	transmembrane protein 8B										
5239	PGM5	phosphoglucomutase 5										
5325	PLAGL1	pleiomorphic adenoma gene-like 1										
5334	PLCL1	phospholipase C-like 1										
53826	FXYD6	FXYD domain containing ion transport regulator 6										
53942	CNTN5	contactin 5										
54221	SNTG2	syntrophin, gamma 2										
54329	GPR85	G protein-coupled receptor 85										
54332	GDAP1	ganglioside-induced differentiation-associated protein 1										
54511	HMGCLL1	3-hydroxymethyl-3-methylglutaryl-CoA lyase-like 1										
547	KIF1A	kinesin family member 1A										
54715	RBFOX1	RNA binding protein, fox-1 homolog (C. elegans) 1										
54769	DIRAS2	DIRAS family, GTP-binding RAS-like 2										
54796	BNC2	basonuclin 2										
55083	KIF26B	kinesin family member 26B										
55118	CRTAC1	cartilage acidic protein 1										
55228	PNMAL1	PNMA-like 1										
56146	PCDHA2	protocadherin alpha 2										
56341	PRMT8	protein arginine methyltransferase 8										
56704	JPH1	junctophilin 1										
56853	CELF4	CUGBP, Elav-like family member 4										
57094	CPA6	carboxypeptidase A6										
57110	HRASLS	HRAS-like suppressor										
57156	TMEM63C	transmembrane protein 63C										
57158	JPH2	junctophilin 2										
57214	KIAA1199	KIAA1199										
57338	JPH3	junctophilin 3										
57408	LRTM1	leucine-rich repeats and transmembrane domains 1										
57469	PNMAL2	PNMA-like 2										
57497	LRFN2	leucine rich repeat and fibronectin type III domain containing 2										
57540	PTCHD2	patched domain containing 2										
57582	KCNT1	potassium channel, subfamily T, member 1										
57611	ISLR2	immunoglobulin superfamily containing leucine-rich repeat 2										
57622	LRFN1	leucine rich repeat and fibronectin type III domain containing 1										
57633	LRRN1	leucine rich repeat neuronal 1										
57687	VAT1L	vesicle amine transport protein 1 homolog (T. californica)-like										
577	BAI3	brain-specific angiogenesis inhibitor 3										
57709	SLC7A14	solute carrier family 7 (orphan transporter), member 14										
57822	GRHL3	grainyhead-like 3 (Drosophila)										
579	NKX3-2	NK3 homeobox 2										
58473	PLEKHB1	pleckstrin homology domain containing, family B (evectins) member 1										
58512	DLGAP3	discs, large (Drosophila) homolog-associated protein 3										
59353	TMEM35	transmembrane protein 35										
60677	CELF6	CUGBP, Elav-like family member 6										
6335	SCN9A	sodium channel, voltage-gated, type IX, alpha subunit										
64091	POPDC2	popeye domain containing 2										
64122	FN3K	fructosamine 3 kinase										

Gene/Gene Set Overlap Matrix (7/7)		ST2.IL17rbko vs. Balb/c (FC log2>1; FDR 0.05) - DOWNREGULATED										
Entrez Gene Id	Gene Symbol	Gene Description	1	2	3	4	5	6	7	8	9	10
64130	LIN7B	lin-7 homolog B (C. elegans)										
64168	NECAB1	N-terminal EF-hand calcium binding protein 1										
64377	CHST8	carbohydrate (N-acetylgalactosamine 4-0) sulfotransferase 8										
644139	PIRT	phosphoinositide-interacting regulator of transient receptor potential channels										
644353	ZCCHC18	zinc finger, CCHC domain containing 18										
645369	TMEM200C	transmembrane protein 200C										
65009	NDRG4	NDRG family member 4										
6525	SMTN	smoothelin										
654790	PCP4L1	Purkinje cell protein 4 like 1										
65997	RASL11B	RAS-like, family 11, member B										
6620	SNCB	synuclein, beta										
6623	SNCG	synuclein, gamma (breast cancer-specific protein 1)										
6663	SOX10	SRY (sex determining region Y)-box 10										
6855	SYP	synaptophysin										
6860	SYT4	synaptotagmin IV										
7216	TRO	trophinin										
7275	TUB	tubby homolog (mouse)										
728215	FAM155A	family with sequence similarity 155, member A										
729085	FAM198A	family with sequence similarity 198, member A										
729359	PLIN4	perilipin 4										
730112	FAM166B	family with sequence similarity 166, member B										
730130	TMEM229A	transmembrane protein 229A										
7732	RNF112	ring finger protein 112										
7857	SCG2	secretogranin II										
78986	DUSP26	dual specificity phosphatase 26 (putative)										
79006	METRN	meteorin, glial cell differentiation regulator										
794	CALB2	calbindin 2										
79605	PGBD5	piggyBac transposable element derived 5										
79745	CLIP4	CAP-GLY domain containing linker protein family, member 4										
79776	ZFHX4	zinc finger homeobox 4										
79937	CNTNAP3	contactin associated protein-like 3										
79957	PAQR6	progestin and adipoQ receptor family member VI										
80023	NRSN2	neurensin 2										
80034	CSRNP3	cysteine-serine-rich nuclear protein 3										
80059	LRRTM4	leucine rich repeat transmembrane neuronal 4										
80206	FHOD3	formin homology 2 domain containing 3										
80725	SRCIN1	SRC kinase signaling inhibitor 1										
80731	THSD7B	thrombospondin, type I, domain containing 7B										
81543	LRRC3	leucine rich repeat containing 3										
81551	STMN4	stathmin-like 4										
8193	DPF1	D4, zinc and double PHD fingers family 1										
827	CAPN6	calpain 6										
83394	PITPNM3	PITPNM family member 3										
83473	KATNAL2	katanin p60 subunit A-like 2										
83482	SCRT1	scratch homolog 1, zinc finger protein (Drosophila)										
84216	TMEM117	transmembrane protein 117										
84253	GARNL3	GTPase activating Rap/RanGAP domain-like 3										
84443	FRMPD3	FERM and PDZ domain containing 3										
8447	DOC2B	double C2-like domains, beta										
845	CASQ2	calsequestrin 2 (cardiac muscle)										
84502	JPH4	junctophilin 4										
84530	SRRM4	serine/arginine repetitive matrix 4										
84630	TTBK1	tau tubulin kinase 1										
84707	BEX2	brain expressed X-linked 2										
84940	CORO6	coronin 6										
8499	PPFIA2	protein tyrosine phosphatase, receptor type, f polypeptide (PTPRF), interacting protein (liprin), alpha 2										
85300	ATCAY	ataxia, cerebellar, Cayman type										
8541	PPFIA3	protein tyrosine phosphatase, receptor type, f polypeptide (PTPRF), interacting protein (liprin), alpha 3										
85442	KNDC1	kinase non-catalytic C-lobe domain (KIND) containing 1										
85455	DISP2	dispatched homolog 2 (Drosophila)										
85478	CCDC65	coiled-coil domain containing 65										
8618	CADPS	Ca++-dependent secretion activator										
8736	MYOM1	myomesin 1, 185kDa										
8929	PHOX2B	paired-like homeobox 2b										
89927	C16orf45	chromosome 16 open reading frame 45										
89944	GLB1L2	galactosidase, beta 1-like 2										
9118	INA	internexin neuronal intermediate filament protein, alpha										
9143	SYNGR3	synaptogyrin 3										
9145	SYNGR1	synaptogyrin 1										
91608	RASL10B	RAS-like, family 10, member B										
9173	IL1RL1	interleukin 1 receptor-like 1										
91752	ZNF804A	zinc finger protein 804A										
92235	DUSP27	dual specificity phosphatase 27 (putative)										
9228	DLGAP2	discs, large (Drosophila) homolog-associated protein 2										
92691	TMEM169	transmembrane protein 169										
9283	GPR37L1	G protein-coupled receptor 37 like 1										
93099	DMKN	dermokine										
93166	PRDM6	PR domain containing 6										
93233	CCDC114	coiled-coil domain containing 114										
9381	OTOF	otoferlin										
93986	FOXP2	forkhead box P2										
94030	LRRC4B	leucine rich repeat containing 4B										
9472	AKAP6	A kinase (PRKA) anchor protein 6										
9625	AATK	apoptosis-associated tyrosine kinase										
9638	FEZ1	fasciculation and elongation protein zeta 1 (zygin I)										
9671	WSCD2	WSC domain containing 2										
9715	FAM131B	family with sequence similarity 131, member B										
9746	CLSTN3	calsyntenin 3										
9758	FRMPD4	FERM and PDZ domain containing 4										
9805	SCRN1	secernin 1										
9832	JAKMIP2	janus kinase and microtubule interacting protein 2										

Table 10: GSEA analysis on **upregulated** gene (total of 24 genes) data sets from *lamina propria* fraction of ST2.IL17rbko mice, relative to Balb/c (n=4-5 mice/group) no enrichment from curated gene sets

Gene/Gene Set Overlap Matrix **ST2IL17rbko vs. Balb/c (FC log2>1; FC 0.05) - UPREGULATED**

Entrez Gene Id	Gene Symbol	Gene Description
2641	GCG	glucagon
7166	TPH1	tryptophan hydroxylase 1
9060	PAPSS2	3'-phosphoadenosine 5'-phosphosulfate synthase 2
885	CCK	cholecystokinin
2695	GIP	gastric inhibitory polypeptide
1114	CHGB	chromogranin B (secretogranin 1)
1113	CHGA	chromogranin A (parathyroid secretory protein 1)
4489	MT1A	metallothionein 1A
6555	SLC10A2	solute carrier family 10 (sodium/bile acid cotransporter family), member 2
2252	FGF7	fibroblast growth factor 7
4502	MT2A	metallothionein 2A
795	S100G	S100 calcium binding protein G
174	AFP	alpha-fetoprotein
3773	KCNJ16	potassium inwardly-rectifying channel, subfamily J, member 16
54363	HAO1	hydroxyacid oxidase (glycolate oxidase) 1
23316	CUX2	cut-like homeobox 2
3336	HSPE1	heat shock 10kDa protein 1 (chaperonin 10)
23568	ARL2BP	ADP-ribosylation factor-like 2 binding protein
4009	LMX1A	LIM homeobox transcription factor 1, alpha
8989	TRPA1	transient receptor potential cation channel, subfamily A, member 1
926	CD8B	CD8b molecule
84842	HPDL	4-hydroxyphenylpyruvate dioxygenase-like
139378	GPR112	G protein-coupled receptor 112
56158	TEX12	testis expressed 12

Table 11: GSEA analysis on <u>commonly</u> **downregulated** (total of 370 genes) gene data sets between Δdbl.GATA1 and ST2.IL17rbko mice (*lamina propria fraction*; data set from table 7 vs. 9)

	Gene Set Name	# Genes in Gene Set (K)	Description	# Genes in Overlap (k)	k/K	p-value	FDR q-value
1	REACTOME_NEURONAL_SYSTEM	279	Genes involved in Neuronal System	17	0.0609	7.48E-14	9.94E-11
2	KEGG_NEUROACTIVE_LIGAND_RECEPTOR_INTERACTION	272	Neuroactive ligand-receptor interaction	13	0.0478	1.35E-09	6.20E-07
3	KEGG_CALCIUM_SIGNALING_PATHWAY	178	Calcium signaling pathway	11	0.0618	1.77E-09	6.20E-07
4	REACTOME_VOLTAGE_GATED_POTASSIUM_CHANNELS	43	Genes involved in Voltage gated Potassium channels	7	0.1628	1.87E-09	6.20E-07
5	REACTOME_POTASSIUM_CHANNELS	98	Genes involved in Potassium Channels	8	0.0816	3.48E-08	9.25E-06
6	REACTOME_TRANSMISSION_ACROSS_CHEMICAL_SYNAPSES	186	Genes involved in Transmission across Chemical Synapses	9	0.0484	4.39E-07	9.71E-05
7	NABA_CORE_MATRISOME	275	Ensemble of genes encoding core extracellular matrix including ECM glycoproteins, collagens and proteoglycans	10	0.0364	1.36E-06	2.59E-04
8	NABA_MATRISOME	1028	Ensemble of genes encoding extracellular matrix and extracellular matrix-associated proteins	17	0.0165	1.75E-05	2.90E-03
9	REACTOME_DEVELOPMENTAL_BIOLOGY	396	Genes involved in Developmental Biology	10	0.0253	3.27E-05	4.83E-03
10	KEGG_ARRHYTHMOGENIC_RIGHT_VENTRICULAR_CARDIOMYOPATHY_ARVC	76	Arrhythmogenic right ventricular cardiomyopathy (ARVC)	5	0.0658	3.99E-05	4.88E-03

Gene/Gene Set Overlap Matrix (1/4) **Commonly downregulated genes between Δdbl.GATA1, ST2IL17.rbko (FC log2 >1; FDR 0.05 over Balb/c)**

Entrez Gene Id	Gene Symbol	Gene Description	1	2	3	4	5	6	7	8	9	10
2890	GRIA1	glutamate receptor, ionotropic, AMPA 1	■	■				■				
2898	GRIK2	glutamate receptor, ionotropic, kainate 2	■	■				■				
1136	CHRNA3	cholinergic receptor, nicotinic, alpha 3	■	■				■				
107	ADCY1	adenylate cyclase 1 (brain)	■		■			■				
774	CACNA1B	calcium channel, voltage-dependent, N type, alpha 1B subunit	■		■			■				
3785	KCNQ2	potassium voltage-gated channel, KQT-like subfamily, member 2	■			■	■				■	
3786	KCNQ3	potassium voltage-gated channel, KQT-like subfamily, member 3	■			■	■				■	
3736	KCNA1	potassium voltage-gated channel, shaker-related subfamily, member 1 (episodic ataxia with myokymia)	■			■	■					
3737	KCNA2	potassium voltage-gated channel, shaker-related subfamily, member 2	■			■	■					
3742	KCNA6	potassium voltage-gated channel, shaker-related subfamily, member 6	■			■	■					
3754	KCNF1	potassium voltage-gated channel, subfamily F, member 1	■			■	■					
9312	KCNB2	potassium voltage-gated channel, Shab-related subfamily, member 2	■			■	■					
3768	KCNJ12	potassium inwardly-rectifying channel, subfamily J, member 12	■				■	■				
55799	CACNA2D3	calcium channel, voltage-dependent, alpha 2/delta subunit 3	■					■				■
43	ACHE	acetylcholinesterase	■					■				
6854	SYN2	synapsin II	■					■				
127833	SYT2	synaptotagmin II	■									
5021	OXTR	oxytocin receptor		■	■							
155	ADRB3	adrenergic, beta-3-, receptor		■	■							
148	ADRA1A	adrenergic, alpha-1A-, receptor		■	■							
22953	P2RX2	purinergic receptor P2X, ligand-gated ion channel, 2		■	■							
2587	GALR1	galanin receptor 1		■								
4985	OPRD1	opioid receptor, delta 1		■								
4987	OPRL1	opiate receptor-like 1		■								
117	ADCYAP1R1	adenylate cyclase activating polypeptide 1 (pituitary) receptor type I		■								
2917	GRM7	glutamate receptor, metabotropic 7		■								
1132	CHRM4	cholinergic receptor, muscarinic 4		■								
6262	RYR2	ryanodine receptor 2 (cardiac)			■							■
4842	NOS1	nitric oxide synthase 1 (neuronal)			■							
6543	SLC8A2	solute carrier family 8 (sodium/calcium exchanger), member 2			■							
492	ATP2B3	ATPase, Ca++ transporting, plasma membrane 3			■							
6263	RYR3	ryanodine receptor 3			■							
6585	SLIT1	slit homolog 1 (Drosophila)							■	■	■	
1463	NCAN	neurocan							■	■	■	
7148	TNXB	tenascin XB							■	■		
127731	VWA5B1	von Willebrand factor A domain containing 5B1							■	■		
256158	HMCN2	hemicentin 2							■	■		
4745	NELL1	NEL-like 1 (chicken)							■	■		
4753	NELL2	NEL-like 2 (chicken)							■	■		
1301	COL11A1	collagen, type XI, alpha 1							■	■		
9806	SPOCK2	sparc/osteonectin, cwcv and kazal-like domains proteoglycan (testican) 2							■	■		
1296	COL8A2	collagen, type VIII, alpha 2							■	■		
2259	FGF14	fibroblast growth factor 14								■		
4803	NGF	nerve growth factor (beta polypeptide)								■		
283208	P4HA3	prolyl 4-hydroxylase, alpha polypeptide III								■		
10718	NRG3	neuregulin 3								■		
2662	GDF10	growth differentiation factor 10								■		
57188	ADAMTSL3	ADAMTS-like 3								■		
80332	ADAM33	ADAM metallopeptidase domain 33								■		
6331	SCN5A	sodium channel, voltage-gated, type V, alpha subunit									■	
2674	GFRA1	GDNF family receptor alpha 1									■	
56963	RGMA	RGM domain family, member A									■	
1400	CRMP1	collapsin response mediator protein 1									■	
6517	SLC2A4	solute carrier family 2 (facilitated glucose transporter), member 4									■	

Gene/Gene Set Overlap Matrix (2/4) **Commonly downregulated genes between Δdbl.GATA1, ST2IL17.rbko (FC log2 >1; FDR 0.05 over Balb/c)**

Entrez Gene Id	Gene Symbol	Gene Description	1	2	3	4	5	6	7	8	9	10
5346	PLIN1	perilipin 1										
3679	ITGA7	integrin, alpha 7										
1496	CTNNA2	catenin (cadherin-associated protein), alpha 2										
29119	CTNNA3	catenin (cadherin-associated protein), alpha 3										
7139	TNNT2	troponin T type 2 (cardiac)										
51083	GAL	galanin prepropeptide										
85397	RGS8	regulator of G-protein signaling 8										
1607	DGKB	diacylglycerol kinase, beta 90kDa										
9162	DGKI	diacylglycerol kinase, iota										
5143	PDE4C	phosphodiesterase 4C, cAMP-specific										
123745	PLA2G4E	phospholipase A2, group IVE										
5602	MAPK10	mitogen-activated protein kinase 10										
23542	MAPK8IP2	mitogen-activated protein kinase 8 interacting protein 2										
9900	SV2A	synaptic vesicle glycoprotein 2A										
1363	CPE	carboxypeptidase E										
5630	PRPH	peripherin										
6528	SLC5A5	solute carrier family 5 (sodium iodide symporter), member 5										
1621	DBH	dopamine beta-hydroxylase (dopamine beta-monooxygenase)										
23017	FAIM2	Fas apoptotic inhibitory molecule 2										
6258	RXRG	retinoid X receptor, gamma										
5522	PPP2R2C	protein phosphatase 2, regulatory subunit B, gamma										
5865	RAB3B	RAB3B, member RAS oncogene family										
57419	SLC24A3	solute carrier family 24 (sodium/potassium/calcium exchanger), member 3										
222962	SLC29A4	solute carrier family 29 (nucleoside transporters), member 4										
7111	TMOD1	tropomodulin 1										
956	ENTPD3	ectonucleoside triphosphate diphosphohydrolase 3										
205	AK4	adenylate kinase 4										
1675	CFD	complement factor D (adipsin)										
29106	SCG3	secretogranin III										
5798	PTPRN	protein tyrosine phosphatase, receptor type, N										
4916	NTRK3	neurotrophic tyrosine kinase, receptor, type 3										
9369	NRXN3	neurexin 3										
9378	NRXN1	neurexin 1										
9379	NRXN2	neurexin 2										
5803	PTPRZ1	protein tyrosine phosphatase, receptor-type, Z polypeptide 1										
5596	MAPK4	mitogen-activated protein kinase 4										
84448	ABLIM2	actin binding LIM protein family, member 2										
5662	PSD	pleckstrin and Sec7 domain containing										
1780	DYNC1I1	dynein, cytoplasmic 1, intermediate chain 1										
1261	CNGA3	cyclic nucleotide gated channel alpha 3										
3945	LDHB	lactate dehydrogenase B										
25830	SULT4A1	sulfotransferase family 4A, member 1										
92737	DNER	delta/notch-like EGF repeat containing										
170261	ZCCHC12	zinc finger, CCHC domain containing 12										
575	BAI1	brain-specific angiogenesis inhibitor 1										
9464	HAND2	heart and neural crest derivatives expressed 2										
203447	NRK	Nik related kinase										
23426	GRIP1	glutamate receptor interacting protein 1										
761	CA3	carbonic anhydrase III, muscle specific										
10687	PNMA2	paraneoplastic antigen MA2										
11248	NXPH3	neurexophilin 3										
112609	MRAP2	melanocortin 2 receptor accessory protein 2										
11281	POU6F2	POU class 6 homeobox 2										
114783	LMTK3	lemur tyrosine kinase 3										
119	ADD2	adducin 2 (beta)										
124925	SEZ6	seizure related 6 homolog (mouse)										
128439	SNHG11	small nucleolar RNA host gene 11 (non-protein coding)										
135138	PACRG	PARK2 co-regulated										
139728	PNCK	pregnancy up-regulated non-ubiquitously expressed CaM kinase										
143425	SYT9	synaptotagmin IX										
148281	SYT6	synaptotagmin VI										
148753	FAM163A	family with sequence similarity 163, member A										
150726	FBXO41	F-box protein 41										
154215	NKAIN2	Na+/K+ transporting ATPase interacting 2										
160777	CCDC60	coiled-coil domain containing 60										
165186	FAM179A	family with sequence similarity 179, member A										
1747	DLX3	distal-less homeobox 3										
1760	DMPK	dystrophia myotonica-protein kinase										
1767	DNAH5	dynein, axonemal, heavy chain 5										
1804	DPP6	dipeptidyl-peptidase 6										
1917	EEF1A2	eukaryotic translation elongation factor 1 alpha 2										
1995	ELAVL3	ELAV (embryonic lethal, abnormal vision, Drosophila)-like 3 (Hu antigen C)										
201780	SLC10A4	solute carrier family 10 (sodium/bile acid cotransporter family), member 4										
202374	STK32A	serine/threonine kinase 32A										
220108	FAM124A	family with sequence similarity 124A										
221662	RBM24	RNA binding motif protein 24										
222183	SRRM3	serine/arginine repetitive matrix 3										
222865	TMEM130	transmembrane protein 130										
22866	CNKSR2	connector enhancer of kinase suppressor of Ras 2										
22895	RPH3A	rabphilin 3A homolog (mouse)										

Gene/Gene Set Overlap Matrix (3/4)		Commonly downregulated genes between Δdbl.GATA1, ST2IL17.rbko (FC log2 >1; FDR 0.05 over Balb/c)										
Entrez Gene Id	Gene Symbol	Gene Description	1	2	3	4	5	6	7	8	9	10
23040	MYT1L	myelin transcription factor 1-like										
23281	MTUS2	microtubule associated tumor suppressor candidate 2										
23336	SYNM	synemin, intermediate filament protein										
23544	SEZ6L	seizure related 6 homolog (mouse)-like										
23762	OSBP2	oxysterol binding protein 2										
238	ALK	anaplastic lymphoma receptor tyrosine kinase										
246176	GAS2L2	growth arrest-specific 2 like 2										
255928	SYT14	synaptotagmin XIV										
257240	KLHL34	kelch-like 34 (Drosophila)										
25789	TMEM59L	transmembrane protein 59-like										
26059	ERC2	ELKS/RAB6-interacting/CAST family member 2										
266743	NPAS4	neuronal PAS domain protein 4										
27344	PCSK1N	proprotein convertase subtilisin/kexin type 1 inhibitor										
27445	PCLO	piccolo (presynaptic cytomatrix protein)										
282973	JAKMIP3	Janus kinase and microtubule interacting protein 3										
2843	GPR20	G protein-coupled receptor 20										
285175	UNC80	unc-80 homolog (C. elegans)										
29944	PNMA3	paraneoplastic antigen MA3										
30819	KCNIP2	Kv channel interacting protein 2										
340371	NRBP2	nuclear receptor binding protein 2										
342346	C16orf96	chromosome 16 open reading frame 96										
342357	ZKSCAN2	zinc finger with KRAB and SCAN domains 2										
347730	LRRTM1	leucine rich repeat transmembrane neuronal 1										
349149	GJC3	gap junction protein, gamma 3, 30.2kDa										
375323	LHFPL4	lipoma HMGIC fusion partner-like 4										
379	ARL4D	ADP-ribosylation factor-like 4D										
388015	RTL1	retrotransposon-like 1										
388591	RNF207	ring finger protein 207										
388662	SLC6A17	solute carrier family 6, member 17										
390205	LRRC10B	leucine rich repeat containing 10B										
399693	MGC50722	uncharacterized MGC50722										
440730	TRIM67	tripartite motif containing 67										
450091	CHD5	Coronary heart disease, susceptibility to, 5										
460	ASTN1	astrotactin 1										
4884	NPTX1	neuronal pentraxin I										
50651	SLC45A1	solute carrier family 45, member 1										
50861	STMN3	stathmin-like 3										
51412	ACTL6B	actin-like 6B										
51440	HPCAL4	hippocalcin like 4										
5325	PLAGL1	pleiomorphic adenoma gene-like 1										
53942	CNTN5	contactin 5										
547	KIF1A	kinesin family member 1A										
54715	RBFOX1	RNA binding protein, fox-1 homolog (C. elegans) 1										
55118	CRTAC1	cartilage acidic protein 1										
55228	PNMAL1	PNMA-like 1										
56341	PRMT8	protein arginine methyltransferase 8										
57110	HRASLS	HRAS-like suppressor										
57158	JPH2	junctophilin 2										
57214	KIAA1199	KIAA1199										
57582	KCNT1	potassium channel, subfamily T, member 1										
577	BAI3	brain-specific angiogenesis inhibitor 3										
57709	SLC7A14	solute carrier family 7 (orphan transporter), member 14										
579	NKX3-2	NK3 homeobox 2										
60677	CELF6	CUGBP, Elav-like family member 6										
64091	POPDC2	popeye domain containing 2										
64122	FN3K	fructosamine 3 kinase										
64130	LIN7B	lin-7 homolog B (C. elegans)										
645369	TMEM200C	transmembrane protein 200C										
65009	NDRG4	NDRG family member 4										
6620	SNCB	synuclein, beta										
6860	SYT4	synaptotagmin IV										
7275	TUB	tubby homolog (mouse)										
729085	FAM198A	family with sequence similarity 198, member A										
729359	PLIN4	perilipin 4										
7732	RNF112	ring finger protein 112										
78986	DUSP26	dual specificity phosphatase 26 (putative)										
794	CALB2	calbindin 2										
79605	PGBD5	piggyBac transposable element derived 5										
79957	PAQR6	progestin and adipoQ receptor family member VI										
80023	NRSN2	neurensin 2										
80059	LRRTM4	leucine rich repeat transmembrane neuronal 4										
80731	THSD7B	thrombospondin, type I, domain containing 7B										
81543	LRRC3	leucine rich repeat containing 3										
81551	STMN4	stathmin-like 4										
83394	PITPNM3	PITPNM family member 3										
8447	DOC2B	double C2-like domains, beta										
84530	SRRM4	serine/arginine repetitive matrix 4										
84630	TTBK1	tau tubulin kinase 1										
84940	CORO6	coronin 6										

Gene/Gene Set Overlap Matrix (4/4) **Commonly downregulated genes between Δdbl.GATA1, ST2IL17.rbko (FC log2 >1; FDR 0.05 over Balb/c)**

Entrez Gene Id	Gene Symbol	Gene Description	1	2	3	4	5	6	7	8	9	10
85300	ATCAY	ataxia, cerebellar, Cayman type										
85442	KNDC1	kinase non-catalytic C-lobe domain (KIND) containing 1										
85455	DISP2	dispatched homolog 2 (Drosophila)										
8736	MYOM1	myomesin 1, 185kDa										
8929	PHOX2B	paired-like homeobox 2b										
9118	INA	internexin neuronal intermediate filament protein, alpha										
9145	SYNGR1	synaptogyrin 1										
91608	RASL10B	RAS-like, family 10, member B										
92235	DUSP27	dual specificity phosphatase 27 (putative)										
93099	DMKN	dermokine										
9381	OTOF	otoferlin										
94030	LRRC4B	leucine rich repeat containing 4B										
9472	AKAP6	A kinase (PRKA) anchor protein 6										
9671	WSCD2	WSC domain containing 2										
9832	JAKMIP2	janus kinase and microtubule interacting protein 2										

Table 12: GSEA analysis on genes **only downregulated** (total of 370 genes) in ST2.IL17rbko mice (*lamina propria fraction;* data set from table 7 vs. 9)

	Gene Set Name	# Genes in Gene Set (K)	Description	# Genes in Overlap (k)	k/K	p-value	FDR q-value
1	NABA_MATRISOME	1028	Ensemble of genes encoding extracellular matrix and extracellular matrix-associated proteins	38	0.037	4.20E-16	5.58E-13
2	REACTOME_NEURONAL_SYSTEM	279	Genes involved in Neuronal System	21	0.0753	2.97E-15	1.97E-12
3	NABA_CORE_MATRISOME	275	Ensemble of genes encoding core extracellular matrix including ECM glycoproteins, collagens and proteoglycans	18	0.0655	3.12E-12	1.38E-09
4	REACTOME_POTASSIUM_CHANNELS	98	Genes involved in Potassium Channels	11	0.1122	1.78E-10	5.91E-08
5	NABA_ECM_GLYCOPROTEINS	196	Genes encoding structural ECM glycoproteins	14	0.0714	2.64E-10	7.01E-08
6	REACTOME_TRANSMISSION_ACROSS_CHEMICAL_SYNAPSES	186	Genes involved in Transmission across Chemical Synapses	12	0.0645	1.59E-08	3.51E-06
7	KEGG_CALCIUM_SIGNALING_PATHWAY	178	Calcium signaling pathway	11	0.0618	9.81E-08	1.86E-05
8	REACTOME_TRANSMEMBRANE_TRANSPORT_OF_SMALL_MOLECULES	413	Genes involved in Transmembrane transport of small molecules	15	0.0363	5.20E-07	8.65E-05
9	REACTOME_VOLTAGE_GATED_POTASSIUM_CHANNELS	43	Genes involved in Voltage gated Potassium channels	6	0.1395	7.21E-07	1.07E-04
10	REACTOME_NEUROTRANSMITTER_RECEPTOR_BINDING_AND_DOWNSTREAM_TRANSMISSION_IN_THE_POSTSYNAPTIC_CELL	137	Genes involved in Neurotransmitter Receptor Binding And Downstream Transmission In The Postsynaptic Cell	9	0.0657	8.67E-07	1.15E-04

Gene/Gene Set Overlap Matrix (1/5) **Downregulated genes only in ST2IL17rbko (FC log2 >1; FDR 0.05)**

Entrez Gene Id	Gene Symbol	Gene Description	1	2	3	4	5	6	7	8	9	10
9353	SLIT2	slit homolog 2 (Drosophila)										
6586	SLIT3	slit homolog 3 (Drosophila)										
9370	ADIPOQ	adiponectin, C1Q and collagen domain containing										
3485	IGFBP2	insulin-like growth factor binding protein 2, 36kDa										
3488	IGFBP5	insulin-like growth factor binding protein 5										
26577	PCOLCE2	procollagen C-endopeptidase enhancer 2										
7058	THBS2	thrombospondin 2										
7143	TNR	tenascin R (restrictin, janusin)										
10631	POSTN	periostin, osteoblast specific factor										
163175	LGI4	leucine-rich repeat LGI family, member 4										
2192	FBLN1	fibulin 1										
55203	LGI2	leucine-rich repeat LGI family, member 2										
84624	FNDC1	fibronectin type III domain containing 1										
9211	LGI1	leucine-rich, glioma inactivated 1										
1295	COL8A1	collagen, type VIII, alpha 1										
1310	COL19A1	collagen, type XIX, alpha 1										
26254	OPTC	opticin										
50859	SPOCK3	sparc/osteonectin, cwcv and kazal-like domains proteoglycan (testican) 3										
7483	WNT9A	wingless-type MMTV integration site family, member 9A										
5365	PLXNB3	plexin B3										
9048	ARTN	artemin										
10500	SEMA6C	sema domain, transmembrane domain (TM), and cytoplasmic domain, (semaphorin) 6C										
2719	GPC3	glypican 3										
283463	MUC19	mucin 19, oligomeric										
10584	COLEC10	collectin sub-family member 10 (C-type lectin)										
10882	C1QL1	complement component 1, q subcomponent-like 1										
114899	C1QTNF3	C1q and tumor necrosis factor related protein 3										
158326	FREM1	FRAS1 related extracellular matrix 1										
2258	FGF13	fibroblast growth factor 13										
6285	S100B	S100 calcium binding protein B										
392255	GDF6	growth differentiation factor 6										
5764	PTN	pleiotrophin										
147381	CBLN2	cerebellin 2 precursor										
57758	SCUBE2	signal peptide, CUB domain, EGF-like 2										
84466	MEGF10	multiple EGF-like-domains 10										
11095	ADAMTS8	ADAM metallopeptidase with thrombospondin type 1 motif, 8										
171019	ADAMTS19	ADAM metallopeptidase with thrombospondin type 1 motif, 19										
4185	ADAM11	ADAM metallopeptidase domain 11										
2788	GNG7	guanine nucleotide binding protein (G protein), gamma 7										
3760	KCNJ3	potassium inwardly-rectifying channel, subfamily J, member 3										
10060	ABCC9	ATP-binding cassette, sub-family C (CFTR/MRP), member 9										
3745	KCNB1	potassium voltage-gated channel, Shab-related subfamily, member 1										
3739	KCNA4	potassium voltage-gated channel, shaker-related subfamily, member 4										
3746	KCNC1	potassium voltage-gated channel, Shaw-related subfamily, member 1										
3752	KCND3	potassium voltage-gated channel, Shal-related subfamily, member 3										
3757	KCNH2	potassium voltage-gated channel, subfamily H (eag-related), member 2										
93107	KCNG4	potassium voltage-gated channel, subfamily G, member 4										
10021	HCN4	hyperpolarization activated cyclic nucleotide-gated potassium channel 4										
3782	KCNN3	potassium intermediate/small conductance calcium-activated channel, subfamily N, member 3										
815	CAMK2A	calcium/calmodulin-dependent protein kinase II alpha										
2562	GABRB3	gamma-aminobutyric acid (GABA) A receptor, beta 3										
23229	ARHGEF9	Cdc42 guanine nucleotide exchange factor (GEF) 9										
27092	CACNG4	calcium channel, voltage-dependent, gamma subunit 4										
1138	CHRNA5	cholinergic receptor, nicotinic, alpha 5										

Gene/Gene Set Overlap Matrix (2/5)		Downregulated genes only in ST2IL17rbko (FC log2 >1; FDR 0.05)										
Entrez Gene Id	Gene Symbol	Gene Description	1	2	3	4	5	6	7	8	9	10
1143	CHRNB4	cholinergic receptor, nicotinic, beta 4										
4747	NEFL	neurofilament, light polypeptide										
783	CACNB2	calcium channel, voltage-dependent, beta 2 subunit										
6616	SNAP25	synaptosomal-associated protein, 25kDa										
6857	SYT1	synaptotagmin I										
491	ATP2B2	ATPase, Ca++ transporting, plasma membrane 2										
4638	MYLK	myosin light chain kinase										
775	CACNA1C	calcium channel, voltage-dependent, L type, alpha 1C subunit										
4923	NTSR1	neurotensin receptor 1 (high affinity)										
6865	TACR2	tachykinin receptor 2										
886	CCKAR	cholecystokinin A receptor										
5737	PTGFR	prostaglandin F receptor (FP)										
777	CACNA1E	calcium channel, voltage-dependent, R type, alpha 1E subunit										
2066	ERBB4	v-erb-a erythroblastic leukemia viral oncogene homolog 4 (avian)										
493	ATP2B4	ATPase, Ca++ transporting, plasma membrane 4										
477	ATP1A2	ATPase, Na+/K+ transporting, alpha 2 polypeptide										
3359	HTR3A	5-hydroxytryptamine (serotonin) receptor 3A										
23460	ABCA6	ATP-binding cassette, sub-family A (ABC1), member 6										
64137	ABCG4	ATP-binding cassette, sub-family G (WHITE), member 4										
10351	ABCA8	ATP-binding cassette, sub-family A (ABC1), member 8										
5575	PRKAR1B	protein kinase, cAMP-dependent, regulatory, type I, beta										
364	AQP7	aquaporin 7										
55117	SLC6A15	solute carrier family 6 (neutral amino acid transporter), member 15										
154091	SLC2A12	solute carrier family 2 (facilitated glucose transporter), member 12										
284111	SLC13A5	solute carrier family 13 (sodium-dependent citrate transporter), member 5										
7169	TPM2	tropomyosin 2 (beta)										
4629	MYH11	myosin, heavy chain 11, smooth muscle										
59	ACTA2	actin, alpha 2, smooth muscle, aorta										
4632	MYL1	myosin, light chain 1, alkali; skeletal, fast										
7138	TNNT1	troponin T type 1 (skeletal, slow)										
59284	CACNG7	calcium channel, voltage-dependent, gamma subunit 7										
125965	COX6B2	cytochrome c oxidase subunit VIb polypeptide 2 (testis)										
4986	OPRK1	opioid receptor, kappa 1										
4887	NPY2R	neuropeptide Y receptor Y2										
151	ADRA2B	adrenergic, alpha-2B-, receptor										
1268	CNR1	cannabinoid receptor 1 (brain)										
10874	NMU	neuromedin U										
4852	NPY	neuropeptide Y										
7432	VIP	vasoactive intestinal peptide										
797	CALCB	calcitonin-related polypeptide beta										
6900	CNTN2	contactin 2 (axonal)										
4897	NRCAM	neuronal cell adhesion molecule										
7223	TRPC4	transient receptor potential cation channel, subfamily C, member 4										
6326	SCN2A	sodium channel, voltage-gated, type II, alpha subunit										
10570	DPYSL4	dihydropyrimidinase-like 4										
1946	EFNA5	ephrin-A5										
2044	EPHA5	EPH receptor A5										
2046	EPHA8	EPH receptor A8										
285220	EPHA6	EPH receptor A6										
26575	RGS17	regulator of G-protein signaling 17										
4137	MAPT	microtubule-associated protein tau										
3306	HSPA2	heat shock 70kDa protein 2										
222537	HS3ST5	heparan sulfate (glucosamine) 3-O-sulfotransferase 5										
64579	NDST4	N-deacetylase/N-sulfotransferase (heparan glucosaminyl) 4										
80319	CXXC4	CXXC finger protein 4										
27123	DKK2	dickkopf homolog 2 (Xenopus laevis)										
85409	NKD2	naked cuticle homolog 2 (Drosophila)										
2670	GFAP	glial fibrillary acidic protein										
4685	NCAM2	neural cell adhesion molecule 2										
26047	CNTNAP2	contactin associated protein-like 2										
54413	NLGN3	neuroligin 3										
4741	NEFM	neurofilament, medium polypeptide										
4744	NEFH	neurofilament, heavy polypeptide										
8936	WASF1	WAS protein family, member 1										
10810	WASF3	WAS protein family, member 3										
5126	PCSK2	proprotein convertase subtilisin/kexin type 2										
658	BMPR1B	bone morphogenetic protein receptor, type IB										
64388	GREM2	gremlin 2										
2596	GAP43	growth associated protein 43										
730	C7	complement component 7										
273	AMPH	amphiphysin										
5521	PPP2R2B	protein phosphatase 2, regulatory subunit B, beta										
4804	NGFR	nerve growth factor receptor										
5166	PDK4	pyruvate dehydrogenase kinase, isozyme 4										
137872	ADHFE1	alcohol dehydrogenase, iron containing, 1										
5740	PTGIS	prostaglandin I2 (prostacyclin) synthase										
56603	CYP26B1	cytochrome P450, family 26, subfamily B, polypeptide 1										
9421	HAND1	heart and neural crest derivatives expressed 1										
2686	GGT7	gamma-glutamyltransferase 7										
64409	WBSCR17	Williams-Beuren syndrome chromosome region 17										

Gene/Gene Set Overlap Matrix (3/5) **Downregulated genes only in ST2IL17rbko (FC log2 >1; FDR 0.05)**

Entrez Gene Id	Gene Symbol	Gene Description	1	2	3	4	5	6	7	8	9	10
3798	KIF5A	kinesin family member 5A										
1795	DOCK3	dedicator of cytokinesis 3										
7345	UCHL1	ubiquitin carboxyl-terminal esterase L1 (ubiquitin thiolesterase)										
2861	GPR37	G protein-coupled receptor 37 (endothelin receptor type B-like)										
966	CD59	CD59 molecule, complement regulatory protein										
2026	ENO2	enolase 2 (gamma, neuronal)										
5979	RET	ret proto-oncogene										
113451	ADC	arginine decarboxylase										
10157	AASS	aminoadipate-semialdehyde synthase										
635	BHMT	betaine--homocysteine S-methyltransferase										
10381	TUBB3	tubulin, beta 3 class III										
26232	FBXO2	F-box protein 2										
80339	PNPLA3	patatin-like phospholipase domain containing 3										
2766	GMPR	guanosine monophosphate reductase										
8120	AP3B2	adaptor-related protein complex 3, beta 2 subunit										
1008	CDH10	cadherin 10, type 2 (T2-cadherin)										
316	AOX1	aldehyde oxidase 1										
23413	NCS1	neuronal calcium sensor 1										
50507	NOX4	NADPH oxidase 4										
3196	TLX2	T-cell leukemia homeobox 2										
56776	FMN2	formin 2										
100505381	MMD2	Miyoshi muscular dystrophy 2										
1038	CDR1	cerebellar degeneration-related protein 1, 34kDa										
1047	CLGN	calmegin										
10650	SLMO1	slowmo homolog 1 (Drosophila)										
10752	CHL1	cell adhesion molecule with homology to L1CAM (close homolog of L1)										
11075	STMN2	stathmin-like 2										
11247	NXPH4	neurexophilin 4										
114786	XKR4	XK, Kell blood group complex subunit-related family, member 4										
114798	SLITRK1	SLIT and NTRK-like family, member 1										
114801	TMEM200A	transmembrane protein 200A										
114815	SORCS1	sortilin-related VPS10 domain containing receptor 1										
114928	GPRASP2	G protein-coupled receptor associated sorting protein 2										
115827	RAB3C	RAB3C, member RAS oncogene family										
116173	CMTM5	CKLF-like MARVEL transmembrane domain containing 5										
116496	FAM129A	family with sequence similarity 129, member A										
116535	MRGPRF	MAS-related GPR, member F										
118812	MORN4	MORN repeat containing 4										
120114	FAT3	FAT tumor suppressor homolog 3 (Drosophila)										
126075	CCDC159	coiled-coil domain containing 159										
126206	NLRP5	NLR family, pyrin domain containing 5										
126393	HSPB6	heat shock protein, alpha-crystallin-related, B6										
127254	C1orf173	chromosome 1 open reading frame 173										
128414	NKAIN4	Na+/K+ transporting ATPase interacting 4										
130497	OSR1	odd-skipped related 1 (Drosophila)										
132014	IL17RE	interleukin 17 receptor E										
1381	CRABP1	cellular retinoic acid binding protein 1										
145270	PRIMA1	proline rich membrane anchor 1										
146330	FBXL16	F-box and leucine-rich repeat protein 16										
147906	DACT3	dapper, antagonist of beta-catenin, homolog 3 (Xenopus laevis)										
148252	DIRAS1	DIRAS family, GTP-binding RAS-like 1										
149111	CNIH3	cornichon homolog 3 (Drosophila)										
149297	FAM78B	family with sequence similarity 78, member B										
152404	IGSF11	immunoglobulin superfamily, member 11										
157807	CLVS1	clavesin 1										
158038	LINGO2	leucine rich repeat and Ig domain containing 2										
161753	ODF3L1	outer dense fiber of sperm tails 3-like 1										
164832	LONRF2	LON peptidase N-terminal domain and ring finger 2										
165215	FAM171B	family with sequence similarity 171, member B										
167410	LIX1	Lix1 homolog (chicken)										
169166	SNX31	sorting nexin 31										
1746	DLX2	distal-less homeobox 2										
1996	ELAVL4	ELAV (embryonic lethal, abnormal vision, Drosophila)-like 4 (Hu antigen D)										
200844	C3orf67	chromosome 3 open reading frame 67										
221476	PI16	peptidase inhibitor 16										
222553	SLC35F1	solute carrier family 35, member F1										
23034	SAMD4A	sterile alpha motif domain containing 4A										
23072	HECW1	HECT, C2 and WW domain containing E3 ubiquitin protein ligase 1										
23148	NACAD	NAC alpha domain containing										
23208	SYT11	synaptotagmin XI										
23251	KIAA1024	KIAA1024										
23349	KIAA1045	KIAA1045										
23704	KCNE4	potassium voltage-gated channel, Isk-related family, member 4										
24147	FJX1	four jointed box 1 (Drosophila)										
253152	EPHX4	epoxide hydrolase 4										
257019	FRMD3	FERM domain containing 3										
25817	FAM19A5	family with sequence similarity 19 (chemokine (C-C motif)-like), member A5										
259232	NALCN	sodium leak channel, non-selective										
26032	SUSD5	sushi domain containing 5										
26050	SLITRK5	SLIT and NTRK-like family, member 5										

Gene/Gene Set Overlap Matrix (4/5) Downregulated genes only in ST2IL17rbko (FC log2 >1; FDR 0.05)

Entrez Gene Id	Gene Symbol	Gene Description	1	2	3	4	5	6	7	8	9	10
26353	HSPB8	heat shock 22kDa protein 8										
27022	FOXD3	forkhead box D3										
27254	CSDC2	cold shock domain containing C2, RNA binding										
28316	CDH20	cadherin 20, type 2										
283455	KSR2	kinase suppressor of ras 2										
284339	TMEM145	transmembrane protein 145										
28513	CDH19	cadherin 19, type 2										
286133	SCARA5	scavenger receptor class A, member 5 (putative)										
29114	TAGLN3	transgelin 3										
29118	DDX25	DEAD (Asp-Glu-Ala-Asp) box polypeptide 25										
2974	GUCY1B2	guanylate cyclase 1, soluble, beta 2										
30820	KCNIP1	Kv channel interacting protein 1										
339416	ANKRD45	ankyrin repeat domain 45										
339983	NAT8L	N-acetyltransferase 8-like (GCN5-related, putative)										
340146	SLC35D3	solute carrier family 35, member D3										
343450	KCNT2	potassium channel, subfamily T, member 2										
344758	GPR149	G protein-coupled receptor 149										
347	APOD	apolipoprotein D										
347731	LRRTM3	leucine rich repeat transmembrane neuronal 3										
348093	RBPMS2	RNA binding protein with multiple splicing 2										
374897	SBSN	suprabasin										
377007	KLHL30	kelch-like 30 (Drosophila)										
3800	KIF5C	kinesin family member 5C										
387758	FIBIN	fin bud initiation factor homolog (zebrafish)										
388021	TMEM179	transmembrane protein 179										
389075	RESP18	regulated endocrine-specific protein 18 homolog (rat)										
400224	PLEKHD1	pleckstrin homology domain containing, family D (with coiled-coil domains) member 1										
402665	IGLON5	IgLON family member 5										
4045	LSAMP	limbic system-associated membrane protein										
4062	LY6H	lymphocyte antigen 6 complex, locus H										
407738	FAM19A1	family with sequence similarity 19 (chemokine (C-C motif)-like), member A1										
50512	PODXL2	podocalyxin-like 2										
5101	PCDH9	protocadherin 9										
51209	RAB9B	RAB9B, member RAS oncogene family										
5121	PCP4	Purkinje cell protein 4										
51286	CEND1	cell cycle exit and neuronal differentiation 1										
51310	SLC22A17	solute carrier family 22, member 17										
51560	RAB6B	RAB6B, member RAS oncogene family										
51617	HMP19	HMP19 protein										
51673	TPPP3	tubulin polymerization-promoting protein family member 3										
51754	TMEM8B	transmembrane protein 8B										
5239	PGM5	phosphoglucomutase 5										
5334	PLCL1	phospholipase C-like 1										
53826	FXYD6	FXYD domain containing ion transport regulator 6										
54221	SNTG2	syntrophin, gamma 2										
54329	GPR85	G protein-coupled receptor 85										
54332	GDAP1	ganglioside-induced differentiation-associated protein 1										
54511	HMGCLL1	3-hydroxymethyl-3-methylglutaryl-CoA lyase-like 1										
54769	DIRAS2	DIRAS family, GTP-binding RAS-like 2										
54796	BNC2	basonuclin 2										
55083	KIF26B	kinesin family member 26B										
56146	PCDHA2	protocadherin alpha 2										
56704	JPH1	junctophilin 1										
56853	CELF4	CUGBP, Elav-like family member 4										
57094	CPA6	carboxypeptidase A6										
57156	TMEM63C	transmembrane protein 63C										
57338	JPH3	junctophilin 3										
57408	LRTM1	leucine-rich repeats and transmembrane domains 1										
57469	PNMAL2	PNMA-like 2										
57497	LRFN2	leucine rich repeat and fibronectin type III domain containing 2										
57540	PTCHD2	patched domain containing 2										
57611	ISLR2	immunoglobulin superfamily containing leucine-rich repeat 2										
57622	LRFN1	leucine rich repeat and fibronectin type III domain containing 1										
57633	LRRN1	leucine rich repeat neuronal 1										
57687	VAT1L	vesicle amine transport protein 1 homolog (T. californica)-like										
57822	GRHL3	grainyhead-like 3 (Drosophila)										
58473	PLEKHB1	pleckstrin homology domain containing, family B (evectins) member 1										
58512	DLGAP3	discs, large (Drosophila) homolog-associated protein 3										
59353	TMEM35	transmembrane protein 35										
6335	SCN9A	sodium channel, voltage-gated, type IX, alpha subunit										
64168	NECAB1	N-terminal EF-hand calcium binding protein 1										
64377	CHST8	carbohydrate (N-acetylgalactosamine 4-0) sulfotransferase 8										
644139	PIRT	phosphoinositide-interacting regulator of transient receptor potential channels										
644353	ZCCHC18	zinc finger, CCHC domain containing 18										
6525	SMTN	smoothelin										
654790	PCP4L1	Purkinje cell protein 4 like 1										
65997	RASL11B	RAS-like, family 11, member B										
6623	SNCG	synuclein, gamma (breast cancer-specific protein 1)										
6663	SOX10	SRY (sex determining region Y)-box 10										
6855	SYP	synaptophysin										

Gene/Gene Set Overlap Matrix (5/5) **Downregulated genes only in ST2IL17rbko (FC log2 >1; FDR 0.05)**

Entrez Gene Id	Gene Symbol	Gene Description	1	2	3	4	5	6	7	8	9	10
7216	TRO	trophinin										
728215	FAM155A	family with sequence similarity 155, member A										
730112	FAM166B	family with sequence similarity 166, member B										
730130	TMEM229A	transmembrane protein 229A										
7857	SCG2	secretogranin II										
79006	METRN	meteorin, glial cell differentiation regulator										
79745	CLIP4	CAP-GLY domain containing linker protein family, member 4										
79776	ZFHX4	zinc finger homeobox 4										
79937	CNTNAP3	contactin associated protein-like 3										
80034	CSRNP3	cysteine-serine-rich nuclear protein 3										
80206	FHOD3	formin homology 2 domain containing 3										
80725	SRCIN1	SRC kinase signaling inhibitor 1										
8193	DPF1	D4, zinc and double PHD fingers family 1										
827	CAPN6	calpain 6										
83473	KATNAL2	katanin p60 subunit A-like 2										
83482	SCRT1	scratch homolog 1, zinc finger protein (Drosophila)										
84216	TMEM117	transmembrane protein 117										
84253	GARNL3	GTPase activating Rap/RanGAP domain-like 3										
84443	FRMPD3	FERM and PDZ domain containing 3										
845	CASQ2	calsequestrin 2 (cardiac muscle)										
84502	JPH4	junctophilin 4										
84707	BEX2	brain expressed X-linked 2										
8499	PPFIA2	protein tyrosine phosphatase, receptor type, f polypeptide (PTPRF), interacting protein (liprin), alpha 2										
8541	PPFIA3	protein tyrosine phosphatase, receptor type, f polypeptide (PTPRF), interacting protein (liprin), alpha 3										
85478	CCDC65	coiled-coil domain containing 65										
8618	CADPS	Ca++-dependent secretion activator										
89927	C16orf45	chromosome 16 open reading frame 45										
89944	GLB1L2	galactosidase, beta 1-like 2										
9143	SYNGR3	synaptogyrin 3										
9173	IL1RL1	interleukin 1 receptor-like 1										
91752	ZNF804A	zinc finger protein 804A										
9228	DLGAP2	discs, large (Drosophila) homolog-associated protein 2										
92691	TMEM169	transmembrane protein 169										
9283	GPR37L1	G protein-coupled receptor 37 like 1										
93166	PRDM6	PR domain containing 6										
93233	CCDC114	coiled-coil domain containing 114										
93986	FOXP2	forkhead box P2										
9625	AATK	apoptosis-associated tyrosine kinase										
9638	FEZ1	fasciculation and elongation protein zeta 1 (zygin I)										
9715	FAM131B	family with sequence similarity 131, member B										
9746	CLSTN3	calsyntenin 3										
9758	FRMPD4	FERM and PDZ domain containing 4										
9805	SCRN1	secernin 1										

Table 13: GSEA analysis on **downregulated** (total of 73 genes) gene data sets only Δdbl.GATA1mice (*lamina propria fraction*; data set from table 7 vs. 9); no enrichment from curated gene sets

Entrez Gene Id	Gene Symbol	Gene Description
114794	ELFN2	extracellular leucine-rich repeat and fibronectin type III domain containing 2
88	ACTN2	actinin, alpha 2
246	ALOX15	arachidonate 15-lipoxygenase
6833	ABCC8	ATP-binding cassette, sub-family C (CFTR/MRP), member 8
9254	CACNA2D2	calcium channel, voltage-dependent, alpha 2/delta subunit 2
255426	RASGEF1C	RasGEF domain family, member 1C
353189	SLCO4C1	solute carrier organic anion transporter family, member 4C1
1813	DRD2	dopamine receptor D2
4902	NRTN	neurturin
55530	SVOP	SV2 related protein homolog (rat)
10815	CPLX1	complexin 1
5055	SERPINB2	serpin peptidase inhibitor, clade B (ovalbumin), member 2
3751	KCND2	potassium voltage-gated channel, Shal-related subfamily, member 2
54212	SNTG1	syntrophin, gamma 1
220296	HEPACAM	hepatic and glial cell adhesion molecule
84665	MYPN	myopalladin
7704	ZBTB16	zinc finger and BTB domain containing 16
3061	HCRTR1	hypocretin (orexin) receptor 1
83851	SYT16	synaptotagmin XVI
8646	CHRD	chordin
7093	TLL2	tolloid-like 2
9899	SV2B	synaptic vesicle glycoprotein 2B
22844	FRMPD1	FERM and PDZ domain containing 1
1608	DGKG	diacylglycerol kinase, gamma 90kDa
9951	HS3ST4	heparan sulfate (glucosamine) 3-O-sulfotransferase 4
84532	ACSS1	acyl-CoA synthetase short-chain family member 1
11189	CELF3	CUGBP, Elav-like family member 3
92369	SPSB4	splA/ryanodine receptor domain and SOCS box containing 4
11149	BVES	blood vessel epicardial substance
64386	MMP25	matrix metallopeptidase 25
115572	FAM46B	family with sequence similarity 46, member B
6769	STAC	SH3 and cysteine rich domain
2623	GATA1	GATA binding protein 1 (globin transcription factor 1)
8288	EPX	eosinophil peroxidase
2153	F5	coagulation factor V (proaccelerin, labile factor)
1734	DIO2	deiodinase, iodothyronine, type II
11170	FAM107A	family with sequence similarity 107, member A
23345	SYNE1	spectrin repeat containing, nuclear envelope 1
1053	CEBPE	CCAAT/enhancer binding protein (C/EBP), epsilon
8328	GFI1B	growth factor independent 1B transcription repressor
65268	WNK2	WNK lysine deficient protein kinase 2
64344	HIF3A	hypoxia inducible factor 3, alpha subunit
23114	NFASC	neurofascin
1232	CCR3	chemokine (C-C motif) receptor 3
4624	MYH6	myosin, heavy chain 6, cardiac muscle, alpha
3579	CXCR2	chemokine (C-X-C motif) receptor 2
3356	HTR2A	5-hydroxytryptamine (serotonin) receptor 2A
3948	LDHC	lactate dehydrogenase C
1952	CELSR2	cadherin, EGF LAG seven-pass G-type receptor 2 (flamingo homolog, Drosophila)
80852	GRIP2	glutamate receptor interacting protein 2
164684	WBP2NL	WBP2 N-terminal like
91662	NLRP12	NLR family, pyrin domain containing 12
8329	HIST1H2AI	histone cluster 1, H2ai
6445	SGCG	sarcoglycan, gamma (35kDa dystrophin-associated glycoprotein)
2006	ELN	elastin
347404	LANCL3	LanC lantibiotic synthetase component C-like 3 (bacterial)
116085	SLC22A12	solute carrier family 22 (organic anion/urate transporter), member 12
442117	GALNTL6	UDP-N-acetyl-alpha-D-galactosamine:polypeptide N-acetylgalactosaminyltransferase-like 6
9881	TRANK1	tetratricopeptide repeat and ankyrin repeat containing 1
53353	LRP1B	low density lipoprotein receptor-related protein 1B
166012	CHST13	carbohydrate (chondroitin 4) sulfotransferase 13
285755	PPIL6	peptidylprolyl isomerase (cyclophilin)-like 6
22997	IGSF9B	immunoglobulin superfamily, member 9B
284615	ANKRD34A	ankyrin repeat domain 34A
284434	NWD1	NACHT and WD repeat domain containing 1
161357	MDGA2	MAM domain containing glycosylphosphatidylinositol anchor 2

BIBLIOGRAPHY

1. Mowat, A. M. & Agace, W. W. Regional specialization within the intestinal immune system. *Nat. Rev. Immunol.* **14,** 667–685 (2014).
2. Agace, W. W. & McCoy, K. D. Regionalized Development and Maintenance of the Intestinal Adaptive Immune Landscape. *Immunity* **46,** 532–548 (2017).
3. Kunze, W. A. A. & Furness, J. B. The Enteric Nervous System and Regulation of Intestinal Motility. *Annu. Rev. Physiol.* **61,** 117–142 (1999).
4. Obermayr, F. & Seitz, G. Recent developments in cell-based ENS regeneration – a short review. *Innov. Surg. Sci.* **3,** 93–99 (2018).
5. Walton, K. D., Mishkind, D., Riddle, M. R., Tabin, C. J. & Gumucio, D. L. Blueprint for an intestinal villus: Species-specific assembly required. *Wiley Interdiscip. Rev. Dev. Biol.* **7,** e317 (2018).
6. Walton, K. D. *et al.* Hedgehog-responsive mesenchymal clusters direct patterning and emergence of intestinal villi. *Proc. Natl. Acad. Sci.* **109,** 15817–15822 (2012).
7. Bernier-Latmani, J. & Petrova, T. V. High-resolution 3D analysis of mouse small-intestinal stroma. *Nat. Protoc.* **11,** 1617–1629 (2016).
8. Mahadevan, V. Anatomy of the small intestine. *Surg. - Oxf. Int. Ed.* **32,** 391–395 (2014).
9. Ehrlein, H. J. & Schemann, M. Gastrointestinal Motility. 26
10. Lentle, R. G., Reynolds, G. W. & Janssen, P. W. M. Gastrointestinal tone; its genesis and contribution to the physical processes of digestion. *Neurogastroenterol. Motil.* **25,** 931–942
11. von Moltke, J., Ji, M., Liang, H.-E. & Locksley, R. M. Tuft-cell-derived IL-25 regulates an intestinal ILC2–epithelial response circuit. *Nature* **529,** 221–225 (2016).
12. Gerbe, F. *et al.* Intestinal epithelial tuft cells initiate type 2 mucosal immunity to helminth parasites. *Nature* **529,** 226–230 (2016).
13. Cheroutre, H., Lambolez, F. & Mucida, D. The light and dark sides of intestinal intraepithelial lymphocytes. *Nat. Rev. Immunol.* **11,** 445–456 (2011).
14. Konjar, Š., Ferreira, C., Blankenhaus, B. & Veldhoen, M. Intestinal Barrier Interactions with Specialized CD8 T Cells. *Front. Immunol.* **8,** (2017).
15. van Heel, D. A. Interleukin 15: its role in intestinal inflammation. *Gut* **55,** 444–445 (2006).
16. Campbell, D. J. & Butcher, E. C. Intestinal attraction: CCL25 functions in effector lymphocyte recruitment to the small intestine. *J. Clin. Invest.* **110,** 1079–1081 (2002).
17. SAVAGE, D. C. & SIEGEL, J. E. Transit Time of Epithelial Cells in the Small Intestines of Germfree Mice and Ex-Germfree Mice Associated with Indigenous Microorganisms. *APPL Env. MICROBIOL* **42,** 6 (1981).
18. Dignass, A. U. Mechanisms and modulation of intestinal epithelial repair. *Inflamm. Bowel Dis.* **7,** 68–77 (2001).

19. Kuhn, K. A., Manieri, N. A., Liu, T.-C. & Stappenbeck, T. S. IL-6 stimulates intestinal epithelial proliferation and repair after injury. *PloS One* **9,** e114195 (2014).
20. Heath, J. EPITHELIAL CELL MIGRATION IN THE INTESTINE. *Cell Biol. Int.* **20,** 139–146 (1996).
21. Andersson-Rolf, A., Zilbauer, M., Koo, B.-K. & Clevers, H. Stem Cells in Repair of Gastrointestinal Epithelia. *Physiology* **32,** 278–289 (2017).
22. Furuya, S. & Furuya, K. Subepithelial fibroblasts in intestinal villi: roles in intercellular communication. *Int. Rev. Cytol.* **264,** 165–223 (2007).
23. Furuya, K., Sokabe, M. & Furuya, S. Characteristics of subepithelial fibroblasts as a mechano-sensor in the intestine: cell-shape-dependent ATP release and P2Y1 signaling. *J Cell Sci* **118,** 3289–3304 (2005).
24. Nowarski, R., Jackson, R. & Flavell, R. A. The Stromal Intervention: Regulation of Immunity and Inflammation at the Epithelial-Mesenchymal Barrier. *Cell* **168,** 362–375 (2017).
25. Messina, V. *et al.* Gut Mesenchymal Stromal Cells in Immunity. *Stem Cells International* (2017). doi:10.1155/2017/8482326
26. Owens, B. M. J. & Simmons, A. Intestinal stromal cells in mucosal immunity and homeostasis. *Mucosal Immunol.* **6,** 224–234 (2013).
27. Choe, K. *et al.* Intravital imaging of intestinal lacteals unveils lipid drainage through contractility. *J. Clin. Invest.* **125,** 4042–4052
28. Bonnans, C., Chou, J. & Werb, Z. Remodelling the extracellular matrix in development and disease. *Nat. Rev. Mol. Cell Biol.* **15,** 786–801 (2014).
29. Hynes, R. O. & Naba, A. Overview of the Matrisome—An Inventory of Extracellular Matrix Constituents and Functions. *Cold Spring Harb. Perspect. Biol.* **4,** (2012).
30. Humphrey, J. D., Dufresne, E. R. & Schwartz, M. A. Mechanotransduction and extracellular matrix homeostasis. *Nat. Rev. Mol. Cell Biol.* **15,** 802–812 (2014).
31. Alcaraz, L. B. *et al.* Tenascin-X promotes epithelial-to-mesenchymal transition by activating latent TGF-β. *J. Cell Biol.* **205,** 409–428 (2014).
32. Robertson, I. B. & Rifkin, D. B. Regulation of the Bioavailability of TGF-β and TGF-β-Related Proteins. *Cold Spring Harb. Perspect. Biol.* **8,** a021907 (2016).
33. Wohl, A. P., Troilo, H., Collins, R. F., Baldock, C. & Sengle, G. Extracellular Regulation of Bone Morphogenetic Protein Activity by the Microfibril Component Fibrillin-1. *J. Biol. Chem.* **291,** 12732–12746 (2016).
34. Page-McCaw, A., Ewald, A. J. & Werb, Z. Matrix metalloproteinases and the regulation of tissue remodelling. *Nat. Rev. Mol. Cell Biol.* **8,** 221–233 (2007).
35. Barros, C. S., Franco, S. J. & Müller, U. Extracellular Matrix: Functions in the Nervous System. *Cold Spring Harb. Perspect. Biol.* **3,** (2011).

36. Schwartz, M. A. Integrins and Extracellular Matrix in Mechanotransduction. *Cold Spring Harb. Perspect. Biol.* **2,** (2010).
37. Shi, Y. *et al.* How mesenchymal stem cells interact with tissue immune responses. *Trends Immunol.* **33,** 136–143 (2012).
38. Veiga-Fernandes, H. & Mucida, D. Neuro-Immune Interactions at Barrier Surfaces. *Cell* **165,** 801–811 (2016).
39. Muller, P. A. *et al.* Crosstalk between Muscularis Macrophages and Enteric Neurons Regulates Gastrointestinal Motility. *Cell* **158,** 300–313 (2014).
40. De Schepper, S., Stakenborg, N., Matteoli, G., Verheijden, S. & Boeckxstaens, G. E. Muscularis macrophages: Key players in intestinal homeostasis and disease. *Cell. Immunol.* (2017). doi:10.1016/j.cellimm.2017.12.009
41. Lozupone, C. A., Stombaugh, J. I., Gordon, J. I., Jansson, J. K. & Knight, R. Diversity, stability and resilience of the human gut microbiota. *Nature* **489,** 220–230 (2012).
42. Littman, D. R. & Pamer, E. G. Role of the commensal microbiota in normal and pathogenic host immune responses. *Cell Host Microbe* **10,** 311–323 (2011).
43. Tanoue, T., Umesaki, Y. & Honda, K. Immune responses to gut microbiota-commensals and pathogens. *Gut Microbes* **1,** 224–233 (2010).
44. Spencer, S. P. & Belkaid, Y. Dietary and commensal derived nutrients: Shaping mucosal and systemic immunity. *Curr. Opin. Immunol.* **24,** 379–384 (2012).
45. Hooper, L. V., Littman, D. R. & Macpherson, A. J. Interactions Between the Microbiota and the Immune System. *Science* **336,** 1268–1273 (2012).
46. Round, J. L. & Mazmanian, S. K. The gut microbiome shapes intestinal immune responses during health and disease. *Nat. Rev. Immunol.* **9,** 313–323 (2009).
47. Makki, K., Deehan, E. C., Walter, J. & Bäckhed, F. The Impact of Dietary Fiber on Gut Microbiota in Host Health and Disease. *Cell Host Microbe* **23,** 705–715 (2018).
48. Ivanov, I. I., Diehl, G. E. & Littman, D. R. Lymphoid tissue inducer cells in intestinal immunity. *Curr. Top. Microbiol. Immunol.* **308,** 59–82 (2006).
49. Mahapatro, M. *et al.* Programming of Intestinal Epithelial Differentiation by IL-33 Derived from Pericryptal Fibroblasts in Response to Systemic Infection. *Cell Rep.* **15,** 1743–1756 (2016).
50. Stzepourginski, I. *et al.* CD34+ mesenchymal cells are a major component of the intestinal stem cells niche at homeostasis and after injury. *Proc. Natl. Acad. Sci.* **114,** E506–E513 (2017).
51. Rieder, F. The Gut Microbiome in Intestinal Fibrosis: Environmental Protector or Provocateur? *Sci. Transl. Med.* **5,** (2013).
52. Ni, J., Wu, G. D., Albenberg, L. & Tomov, V. T. Gut microbiota and IBD: causation or correlation? *Nat. Rev. Gastroenterol. Hepatol.* **14,** 573–584 (2017).

53. Quigley, E. M. M. Microflora Modulation of Motility. *J. Neurogastroenterol. Motil.* **17,** 140–147 (2011).
54. Kabouridis, P. S. *et al.* Microbiota Controls the Homeostasis of Glial Cells in the Gut Lamina Propria. *Neuron* **85,** 289–295 (2015).
55. Matthews, A. N. *et al.* Eotaxin is required for the baseline level of tissue eosinophils. *Proc. Natl. Acad. Sci.* **95,** 6273–6278 (1998).
56. Kato, M. *et al.* Eosinophil infiltration and degranulation in normal human tissue. *Anat. Rec.* **252,** 418–425 (1998).
57. Weller, P. F. & Spencer, L. A. Functions of tissue-resident eosinophils. *Nat. Rev. Immunol.* **17,** 746–760 (2017).
58. Rothenberg, M. E. & Hogan, S. P. The eosinophil. *Annu. Rev. Immunol.* **24,** 147–174 (2006).
59. Rosenberg, H. F., Dyer, K. D. & Foster, P. S. Eosinophils: changing perspectives in health and disease. *Nat. Rev. Immunol.* **13,** 9–22 (2013).
60. Huang, L. & Appleton, J. A. Eosinophils in Helminth Infection: Defenders and Dupes. *Trends Parasitol.* **32,** 798–807 (2016).
61. Furuta, G. T. & Katzka, D. A. Eosinophilic Esophagitis. *N. Engl. J. Med.* **373,** 1640–1648 (2015).
62. McBrien, C. N. & Menzies-Gow, A. The Biology of Eosinophils and Their Role in Asthma. *Front. Med.* **4,** (2017).
63. Akuthota, P. & Weller, P. F. Eosinophils and Disease Pathogenesis. *Semin. Hematol.* **49,** 113–119 (2012).
64. Buonomo, E. L. *et al.* Microbiota-regulated IL-25 increases eosinophil number to provide 1 protection during Clostridium difficile infection. *Cell Rep.* **16,** 432–443 (2016).
65. Goh, Y. P. S. *et al.* Eosinophils secrete IL-4 to facilitate liver regeneration. *Proc. Natl. Acad. Sci. U. S. A.* **110,** 9914–9919 (2013).
66. Lee, J. J., Jacobsen, E. A., McGarry, M. P., Schleimer, R. P. & Lee, N. A. Eosinophils in health and disease: the LIAR hypothesis. *Clin. Exp. Allergy J. Br. Soc. Allergy Clin. Immunol.* **40,** 563–575 (2010).
67. Jung, Y. & Rothenberg, M. E. Roles and Regulation of Gastrointestinal Eosinophils in Immunity and Disease. *J. Immunol. Baltim. Md 1950* **193,** 999–1005 (2014).
68. Cheng, E., Souza, R. F. & Spechler, S. J. Tissue remodeling in eosinophilic esophagitis. *Am. J. Physiol. Gastrointest. Liver Physiol.* **303,** G1175-1187 (2012).
69. Rosenberg, H. F. & Druey, K. M. Eosinophils, galectins, and a reason to breathe. *Proc. Natl. Acad. Sci.* **113,** 9139–9141 (2016).
70. Lee, J. J. & Rosenberg, H. F. *Eosinophils in Health and Disease*. (Elsevier, 2012).
71. Chu, D. K. *et al.* Indigenous enteric eosinophils control DCs to initiate a primary Th2 immune response in vivo. *J. Exp. Med.* **211,** 1657–1672 (2014).

72. Carlens, J. *et al.* Common -Chain-Dependent Signals Confer Selective Survival of Eosinophils in the Murine Small Intestine. *J. Immunol.* **183,** 5600–5607 (2009).
73. Mowat, A. M. & Bain, C. C. News & Highlights. *Mucosal Immunol.* **3,** 420–421 (2010).
74. Misharin, A. V., Morales-Nebreda, L., Mutlu, G. M., Budinger, G. R. S. & Perlman, H. Flow Cytometric Analysis of Macrophages and Dendritic Cell Subsets in the Mouse Lung. *Am. J. Respir. Cell Mol. Biol.* **49,** 503–510 (2013).
75. Griseri, T. *et al.* Granulocyte Macrophage Colony-Stimulating Factor-Activated Eosinophils Promote Interleukin-23 Driven Chronic Colitis. *Immunity* **43,** 187–199 (2015).
76. Melo, R. C. N., Spencer, L. A., Dvorak, A. M. & Weller, P. F. Mechanisms of eosinophil secretion: large vesiculotubular carriers mediate transport and release of granule-derived cytokines and other proteins. *J. Leukoc. Biol.* **83,** 229–236 (2008).
77. Melo, R. C. N. & Weller, P. F. Piecemeal degranulation in human eosinophils: a distinct secretion mechanism underlying inflammatory responses. *Histol. Histopathol.* **25,** 1341–1354 (2010).
78. Wan, H.-C., Melo, R. C. N., Jin, Z., Dvorak, A. M. & Weller, P. F. Roles and origins of leukocyte lipid bodies: proteomic and ultrastructural studies. *FASEB J. Off. Publ. Fed. Am. Soc. Exp. Biol.* **21,** 167–178 (2007).
79. Weller, P. F., Bozza, P. T., Yu, W. & Dvorak, A. M. Cytoplasmic lipid bodies in eosinophils: Central roles in eicosanoid generation. *Allergol. Int.* **46,** 141–153 (1997).
80. Spencer, L. A. *et al.* Cytokine receptor-mediated trafficking of preformed IL-4 in eosinophils identifies an innate immune mechanism of cytokine secretion. *Proc. Natl. Acad. Sci.* **103,** 3333–3338 (2006).
81. Scepek, S., Moqbel, R. & Lindau, M. Compound exocytosis and cumulative degranulation by eosinophils and their role in parasite killing. *Parasitol. Today* **10,** 276–278 (1994).
82. Hafez, I., Stolpe, A. & Lindau, M. Compound Exocytosis and Cumulative Fusion in Eosinophils. *J. Biol. Chem.* **278,** 44921–44928 (2003).
83. Salcedo, R. *et al.* Eotaxin (CCL11) induces in vivo angiogenic responses by human CCR3+ endothelial cells. *J. Immunol. Baltim. Md 1950* **166,** 7571–7578 (2001).
84. Ahrens, R. *et al.* Intestinal Macrophage/Epithelial Cell-Derived CCL11/Eotaxin-1 Mediates Eosinophil Recruitment and Function in Pediatric Ulcerative Colitis. *J. Immunol. Baltim. Md 1950* **181,** 7390–7399 (2008).
85. Gounni, A. S. *et al.* IL-9-mediated induction of eotaxin1/CCL11 in human airway smooth muscle cells. *J. Immunol. Baltim. Md 1950* **173,** 2771–2779 (2004).
86. Takatsu, K. & Nakajima, H. IL-5 and eosinophilia. *Curr. Opin. Immunol.* **20,** 288–294 (2008).
87. Greenfeder, S., Umland, S. P., Cuss, F. M., Chapman, R. W. & Egan, R. W. Th2 cytokines and asthma — The role of interleukin-5 in allergic eosinophilic disease. *Respir. Res.* **2,** 71–79 (2001).

88. Bouffi, C. *et al.* IL-33 markedly activates murine eosinophils by an NFκB-dependent mechanism differentially dependent upon an IL-4-driven autoinflammatory loop. *J. Immunol. Baltim. Md 1950* **191,** (2013).
89. Pope, S. M. *et al.* IL-13 induces eosinophil recruitment into the lung by an IL-5– and eotaxin-dependent mechanism. *J. Allergy Clin. Immunol.* **108,** 594–601 (2001).
90. Bagnasco, D., Ferrando, M., Varricchi, G., Passalacqua, G. & Canonica, G. W. A Critical Evaluation of Anti-IL-13 and Anti-IL-4 Strategies in Severe Asthma. *Int. Arch. Allergy Immunol.* **170,** 122–131 (2016).
91. Schneider, C. *et al.* A Metabolite-Triggered Tuft Cell-ILC2 Circuit Drives Small Intestinal Remodeling. *Cell* (2018). doi:10.1016/j.cell.2018.05.014
92. Nussbaum, J. C. *et al.* Type 2 innate lymphoid cells control eosinophil homeostasis. *Nature* **502,** 245–248 (2013).
93. Neill, D. R. *et al.* Nuocytes represent a new innate effector leukocyte that mediates type-2 immunity. *Nature* **464,** 1367–1370 (2010).
94. Mao, H. *et al.* Mechanisms of Siglec-F-Induced Eosinophil Apoptosis: A Role for Caspases but Not for SHP-1, Src Kinases, NADPH Oxidase or Reactive Oxygen. *PLOS ONE* **8,** e68143 (2013).
95. Zhang, M. *et al.* Defining the in vivo function of Siglec-F, a CD33-related Siglec expressed on mouse eosinophils. *Blood* **109,** 4280–4287 (2007).
96. Zimmermann, N. *et al.* Siglec-F antibody administration to mice selectively reduces blood and tissue eosinophils. *Allergy* **63,** 1–1163 (2008).
97. Garcia, N. V. *et al.* SIRPα/CD172a Regulates Eosinophil Homeostasis. *J. Immunol.* **187,** 2268–2277 (2011).
98. Muñoz, N. M. *et al.* Eosinophil VLA-4 binding to fibronectin augments bronchial narrowing through 5-lipoxygenase activation. *Am. J. Physiol.* **270,** L587-594 (1996).
99. Anwar, A. R., Walsh, G. M., Cromwell, O., Kay, A. B. & Wardlaw, A. J. Adhesion to fibronectin primes eosinophils via alpha 4 beta 1 (VLA-4). *Immunology* **82,** 222–228 (1994).
100. Dubucquoi, S. *et al.* Interleukin 5 synthesis by eosinophils: association with granules and immunoglobulin-dependent secretion. *J. Exp. Med.* **179,** 703–708 (1994).
101. Muraki, M., Gleich, G. J. & Kita, H. Antigen-specific IgG and IgA, but not IgE, activate the effector functions of eosinophils in the presence of antigen. *Int. Arch. Allergy Immunol.* **154,** 119–127 (2011).
102. Willebrand, R. & Voehringer, D. IL-33-Induced Cytokine Secretion and Survival of Mouse Eosinophils Is Promoted by Autocrine GM-CSF. *PLOS ONE* **11,** e0163751 (2016).
103. Cayrol, C. & Girard, J.-P. IL-33: an alarmin cytokine with crucial roles in innate immunity, inflammation and allergy. *Curr. Opin. Immunol.* **31,** 31–37 (2014).
104. Johnston, L. K. & Bryce, P. J. Understanding Interleukin 33 and Its Roles in Eosinophil Development. *Front. Med.* **4,** (2017).

105. Cherry, W. B., Yoon, J., Bartemes, K. R., Iijima, K. & Kita, H. A NOVEL IL-1 FAMILY CYTOKINE, IL-33, POTENTLY ACTIVATES HUMAN EOSINOPHILS. *J. Allergy Clin. Immunol.* **121,** 1484 (2008).
106. Stolarski, B., Kurowska-Stolarska, M., Kewin, P., Xu, D. & Liew, F. Y. IL-33 exacerbates eosinophil-mediated airway inflammation. *J. Immunol. Baltim. Md 1950* **185,** 3472–3480 (2010).
107. Schmitz, J. *et al.* IL-33, an Interleukin-1-like Cytokine that Signals via the IL-1 Receptor-Related Protein ST2 and Induces T Helper Type 2-Associated Cytokines. *Immunity* **23,** 479–490 (2005).
108. Rankin, A. L. *et al.* IL-33 Induces IL-13–Dependent Cutaneous Fibrosis. *J. Immunol.* **184,** 1526–1535 (2010).
109. Wen, T., Besse, J. A., Mingler, M. K., Fulkerson, P. C. & Rothenberg, M. E. Eosinophil adoptive transfer system to directly evaluate pulmonary eosinophil trafficking in vivo. *Proc. Natl. Acad. Sci. U. S. A.* **110,** 6067–6072 (2013).
110. Liew, F. Y., Girard, J.-P. & Turnquist, H. R. Interleukin-33 in health and disease. *Nat. Rev. Immunol.* **16,** 676–689 (2016).
111. Hodzic, Z., Schill, E. M., Bolock, A. M. & Good, M. IL-33 and the intestine: The good, the bad, and the inflammatory. *Cytokine* **100,** 1–10 (2017).
112. Pastorelli, L., De Salvo, C., Vecchi, M. & Pizarro, T. T. The Role of IL-33 in Gut Mucosal Inflammation. *Mediators Inflamm.* **2013,** (2013).
113. Wu, D. *et al.* Eosinophils Sustain Adipose Alternatively Activated Macrophages Associated with Glucose Homeostasis. *Science* **332,** 243–247 (2011).
114. Kurokawa, M. *et al.* Expression and effects of IL-33 and ST2 in allergic bronchial asthma: IL-33 induces eotaxin production in lung fibroblasts. *Int. Arch. Allergy Immunol.* **155 Suppl 1,** 12–20 (2011).
115. Masterson, J. C. *et al.* Eosinophils and IL-33 perpetuate chronic inflammation and fibrosis in a pediatric population with stricturing Crohn's ileitis. *Inflamm. Bowel Dis.* **21,** 2429–2440 (2015).
116. Salimi, M. *et al.* A role for IL-25 and IL-33–driven type-2 innate lymphoid cells in atopic dermatitis. *J. Exp. Med.* **210,** 2939–2950 (2013).
117. Fort, M. M. *et al.* IL-25 Induces IL-4, IL-5, and IL-13 and Th2-Associated Pathologies In Vivo. *Immunity* **15,** 985–995 (2001).
118. Tang, W. *et al.* IL-25 and IL-25 receptor expression on eosinophils from subjects with allergic asthma. *Int. Arch. Allergy Immunol.* **163,** 5–10 (2014).
119. Behm, C. A. & Ovington, K. S. The Role of Eosinophils in Parasitic Helminth Infections: Insights from Genetically Modified Mice. *Parasitol. Today* **16,** 202–209 (2000).
120. Klion, A. D. & Nutman, T. B. The role of eosinophils in host defense against helminth parasites. *J. Allergy Clin. Immunol.* **113,** 30–37 (2004).
121. Buys, J., Wever, R., van Stigt, R. & Ruitenberg, E. J. The killing of newborn larvae of Trichinella spiralis by eosinophil peroxidase in vitro. *Eur. J. Immunol.* **11,** 843–845 (1981).

122. Capron, M., Torpier, G. & Capron, A. In vitro killing of S. mansoni schistosomula by eosinophils from infected rats: role of cytophilic antibodies. *J. Immunol. Baltim. Md 1950* **123,** 2220–2230 (1979).
123. Butterworth, A. E. *et al.* Eosinophils as mediators of antibody-dependent damage to schistosomula. *Nature* **256,** 727–729 (1975).
124. Lee, J. J. *et al.* Human versus mouse eosinophils: 'that which we call an eosinophil, by any other name would stain as red'. *J. Allergy Clin. Immunol.* **130,** 572–584 (2012).
125. Fabre, V. *et al.* Eosinophil deficiency compromises parasite survival in chronic nematode infection. *J. Immunol. Baltim. Md 1950* **182,** 1577–1583 (2009).
126. Huang, L. *et al.* Eosinophils and IL-4 Support Nematode Growth Coincident with an Innate Response to Tissue Injury. *PLOS Pathog.* **11,** e1005347 (2015).
127. Jacobsen, E. A., Ochkur, S. I., Lee, N. A. & Lee, J. J. Eosinophils and asthma. *Curr. Allergy Asthma Rep.* **7,** 18–26 (2007).
128. Fehrenbach, H., Wagner, C. & Wegmann, M. Airway remodeling in asthma: what really matters. *Cell Tissue Res.* **367,** 551–569 (2017).
129. O'Byrne, P. M., Inman, M. D. & Parameswaran, K. The trials and tribulations of IL-5, eosinophils, and allergic asthma. *J. Allergy Clin. Immunol.* **108,** 503–508 (2001).
130. Humbles, A. A. *et al.* A Critical Role for Eosinophils in Allergic Airways Remodeling. *Science* **305,** 1776–1779 (2004).
131. Jacobsen, E. A., Lee, N. A. & Lee, J. J. Re-defining the Unique Roles for Eosinophils in Allergic Respiratory Inflammation. *Clin. Exp. Allergy J. Br. Soc. Allergy Clin. Immunol.* **44,** 1119–1136 (2014).
132. Rieder, F. & Fiocchi, C. Intestinal fibrosis in inflammatory bowel disease — Current knowledge and future perspectives. *J. Crohns Colitis* **2,** 279–290 (2008).
133. Shimshoni, E., Yablecovitch, D., Baram, L., Dotan, I. & Sagi, I. ECM remodelling in IBD: innocent bystander or partner in crime? The emerging role of extracellular molecular events in sustaining intestinal inflammation. *Gut* **64,** 367–372 (2015).
134. Al-Haddad, S. & Riddell, R. H. The role of eosinophils in inflammatory bowel disease. *Gut* **54,** 1674–1675 (2005).
135. Levy, A. M. *et al.* Increased Eosinophil Granule Proteins in Gut Lavage Fluid From Patients With Inflammatory Bowel Disease. *Mayo Clin. Proc.* **72,** 117–123 (1997).
136. Lampinen, M. *et al.* Eosinophil granulocytes are activated during the remission phase of ulcerative colitis. *Gut* **54,** 1714–1720 (2005).
137. Masterson, J. C. *et al.* Eosinophil-mediated signalling attenuates inflammatory responses in experimental colitis. *Gut* gutjnl-2014-306998 (2014). doi:10.1136/gutjnl-2014-306998
138. Sicherer, S. H. & Sampson, H. A. Food allergy. *J. Allergy Clin. Immunol.* **125,** S116–S125 (2010).
139. Galli, S. J. & Tsai, M. IgE and mast cells in allergic disease. *Nat. Med.* **18,** 693–704 (2012).

140. Kelly, K. J. *et al.* Eosinophilic esophagitis attributed to gastroesophageal reflux: improvement with an amino acid-based formula. *Gastroenterology* **109,** 1503–1512 (1995).
141. Clayton, F. *et al.* Eosinophilic esophagitis in adults is associated with IgG4 and not mediated by IgE. *Gastroenterology* **147,** 602–609 (2014).
142. Kamdar, T. A., Ditto, A. M. & Bryce, P. J. Skin prick testing does not reflect the presence of IgE against food allergens in adult eosinophilic esophagitis patients: a case study. *Clin. Mol. Allergy* **8,** 16 (2010).
143. Nhu, Q. M. & Aceves, S. S. Tissue Remodeling in Chronic Eosinophilic Esophageal Inflammation: Parallels in Asthma and Therapeutic Perspectives. *Front. Med.* **4,** (2017).
144. Renz, H. Neurotrophins in bronchial asthma. *Respir. Res.* **2,** 265 (2001).
145. Rochman, M. *et al.* Neurotrophic tyrosine kinase receptor 1 is a direct transcriptional and epigenetic target of IL-13 involved in allergic inflammation. *Mucosal Immunol.* **8,** 785–798 (2015).
146. Reichman, H., Karo-Atar, D. & Munitz, A. Emerging Roles for Eosinophils in the Tumor Microenvironment. *Trends Cancer* **2,** 664–675 (2016).
147. von Wasielewski, R. *et al.* Tissue eosinophilia correlates strongly with poor prognosis in nodular sclerosing Hodgkin's disease, allowing for known prognostic factors. *Blood* **95,** 1207–1213 (2000).
148. Pretlow, T. P. *et al.* Eosinophil infiltration of human colonic carcinomas as a prognostic indicator. *Cancer Res.* **43,** 2997–3000 (1983).
149. Goldsmith, M. M., Belchis, D. A., Cresson, D. H., Merritt, W. D. & Askin, F. B. The importance of the eosinophil in head and neck cancer. *Otolaryngol.--Head Neck Surg. Off. J. Am. Acad. Otolaryngol.-Head Neck Surg.* **106,** 27–33 (1992).
150. Lotfi, R., Lee, J. J. & Lotze, M. T. Eosinophilic Granulocytes and Damage-associated Molecular Pattern Molecules (DAMPs): Role in the Inflammatory Response Within Tumors. *J. Immunother.* **30,** 16 (2007).
151. Nissim Ben Efraim, A. H., Eliashar, R. & Levi-Schaffer, F. Hypoxia modulates human eosinophil function. *Clin. Mol. Allergy CMA* **8,** 10 (2010).
152. Legrand, F. *et al.* Human Eosinophils Exert TNF-α and Granzyme A-Mediated Tumoricidal Activity toward Colon Carcinoma Cells. *J. Immunol.* **185,** 7443–7451 (2010).
153. Carretero, R. *et al.* Eosinophils orchestrate cancer rejection by normalizing tumor vessels and enhancing infiltration of CD8(+) T cells. *Nat. Immunol.* **16,** 609–617 (2015).
154. Turner, J.-E. *et al.* IL-9–mediated survival of type 2 innate lymphoid cells promotes damage control in helminth-induced lung inflammation. *J. Exp. Med.* **210,** 2951–2965 (2013).
155. Todd, R. *et al.* The eosinophil as a cellular source of transforming growth factor alpha in healing cutaneous wounds. *Am. J. Pathol.* **138,** 1307–1313 (1991).
156. Gouon-Evans, V., Lin, E. Y. & Pollard, J. W. Requirement of macrophages and eosinophils and their cytokines/chemokines for mammary gland development. *Breast Cancer Res. BCR* **4,** 155–164 (2002).

157. Tchernitchin, A. N. & Galand, P. Oestrogen levels in the blood, not in the uterus, determine uterine eosinophilia and oedema. *J. Endocrinol.* **99,** 123–130 (1983).
158. Perez, M. C., Furth, E. E., Matzumura, P. D. & Lyttle, C. R. Role of eosinophils in uterine responses to estrogen. *Biol. Reprod.* **54,** 249–254 (1996).
159. Miguel, R. D. V. *et al.* IL-4–secreting eosinophils promote endometrial stromal cell proliferation and prevent Chlamydia-induced upper genital tract damage. *Proc. Natl. Acad. Sci.* **114,** E6892–E6901 (2017).
160. Molofsky, A. B. *et al.* Innate lymphoid type 2 cells sustain visceral adipose tissue eosinophils and alternatively activated macrophages. *J. Exp. Med.* **210,** 535–549 (2013).
161. Sugawara, R. *et al.* Small intestinal eosinophils regulate Th17 cells by producing IL-1 receptor antagonist. *J. Exp. Med.* **213,** 555–567 (2016).
162. Jung, Y. *et al.* IL-1β in eosinophil-mediated small intestinal homeostasis and IgA production. *Mucosal Immunol.* **8,** 930–942 (2015).
163. Chu, V. T. *et al.* Eosinophils Promote Generation and Maintenance of Immunoglobulin-A-Expressing Plasma Cells and Contribute to Gut Immune Homeostasis. *Immunity* **40,** 582–593 (2014).
164. Yu, C. *et al.* Targeted Deletion of a High-Affinity GATA-binding Site in the GATA-1 Promoter Leads to Selective Loss of the Eosinophil Lineage In Vivo. *J. Exp. Med.* **195,** 1387–1395 (2002).
165. Chu, D. K. *et al.* Indigenous enteric eosinophils control DCs to initiate a primary Th2 immune response in vivo. *J. Exp. Med.* **211,** 1657–1672 (2014).
166. Xenakis, J. J. *et al.* Resident intestinal eosinophils constitutively express antigen presentation markers and include two phenotypically distinct subsets of eosinophils. *Immunology* **154,** 298–308
167. Mishra, A., Hogan, S. P., Lee, J. J., Foster, P. S. & Rothenberg, M. E. Fundamental signals that regulate eosinophil homing to the gastrointestinal tract. (1999). doi:10.1172/JCI6560
168. Ueki, S. *et al.* Retinoic acids up-regulate functional eosinophil-driving receptor CCR3. *Allergy* **68,** 953–956 (2013).
169. Turfkruyer, M. *et al.* Oral tolerance is inefficient in neonatal mice due to a physiological vitamin A deficiency. *Mucosal Immunol.* **9,** 479–491 (2016).
170. Yang, Y., Loy, J., Ryseck, R.-P., Carrasco, D. & Bravo, R. Antigen-Induced Eosinophilic Lung Inflammation Develops in Mice Deficient in Chemokine Eotaxin. *Blood* **92,** 3912–3923 (1998).
171. Walton, K. D. *et al.* Villification in the mouse: Bmp signals control intestinal villus patterning. *Development* **143,** 427–436 (2016).
172. Melo, R. C. N. & Weller, P. F. Piecemeal degranulation in human eosinophils: a distinct secretion mechanism underlying inflammatory responses. *Histol. Histopathol.* **25,** 1341–1354 (2010).

173. Dvorak, A. M., Monahan, R. A., Osage, J. E. & Dickersin, G. R. Crohn's disease: Transmission electron microscopic studies: II. Immunologic inflammatory response. Alterations of mast cells, basophils, eosinophils, and the microvasculature. *Hum. Pathol.* **11,** 606–619 (1980).
174. Saffari, H. *et al.* Electron microscopy elucidates eosinophil degranulation patterns in patients with eosinophilic esophagitis. *J. Allergy Clin. Immunol.* **133,** 1728-1734.e1 (2014).
175. Melo, R. C. N., Perez, S. A. C., Spencer, L. A., Dvorak, A. M. & Weller, P. F. Intragranular Vesiculotubular Compartments are Involved in Piecemeal Degranulation by Activated Human Eosinophils. *Traffic Cph. Den.* **6,** 866–879 (2005).
176. Nagase, H. *et al.* Expression and function of Toll-like receptors in eosinophils: activation by Toll-like receptor 7 ligand. *J. Immunol. Baltim. Md 1950* **171,** 3977–3982 (2003).
177. Turner, J. R. Intestinal mucosal barrier function in health and disease. *Nat. Rev. Immunol.* **9,** 799–809 (2009).
178. Olivares-Villagómez, D. & Kaer, L. V. Intestinal Intraepithelial Lymphocytes: Sentinels of the Mucosal Barrier. *Trends Immunol.* **39,** 264–275 (2018).
179. Powell, D. W., Adegboyega, P. A., Di Mari, J. F. & Mifflin, R. C. Epithelial Cells and Their Neighbors I. Role of intestinal myofibroblasts in development, repair, and cancer. *Am. J. Physiol.-Gastrointest. Liver Physiol.* **289,** G2–G7 (2005).
180. Meran, L., Baulies, A. & Li, V. S. W. Intestinal Stem Cell Niche: The Extracellular Matrix and Cellular Components. *Stem Cells International* (2017). doi:10.1155/2017/7970385
181. Delgado, M. E., Grabinger, T. & Brunner, T. Cell death at the intestinal epithelial front line. *FEBS J.* **283,** 2701–2719 (2016).
182. Nakata, K. *et al.* Commensal microbiota-induced microRNA modulates intestinal epithelial permeability through the small GTPase ARF4. *J. Biol. Chem.* **292,** 15426–15433 (2017).
183. Groschwitz, K. R. *et al.* Mast cells regulate homeostatic intestinal epithelial migration and barrier function by a chymase/Mcpt4-dependent mechanism. *Proc. Natl. Acad. Sci.* **106,** 22381–22386 (2009).
184. Knight, P. A. *et al.* Aberrant Mucosal Mast Cell Protease Expression in the Enteric Epithelium of Nematode-Infected Mice Lacking the Integrin αvβ6, a Transforming Growth Factor-β1 Activator. *Am. J. Pathol.* **171,** 1237–1248 (2007).
185. Gommerman, J. L., Rojas, O. L. & Fritz, J. H. Re-thinking the functions of IgA+ plasma cells. *Gut Microbes* **5,** 652–662 (2014).
186. Vermeer, P. D. *et al.* MMP9 modulates tight junction integrity and cell viability in human airway epithelia. *Am. J. Physiol. Lung Cell. Mol. Physiol.* **296,** L751-762 (2009).
187. Vandenbroucke, R. E. *et al.* Matrix metalloproteinase 13 modulates intestinal epithelial barrier integrity in inflammatory diseases by activating TNF. *EMBO Mol. Med.* **5,** 932–948 (2013).

188. Pawlak, M., Lefebvre, P. & Staels, B. Molecular mechanism of PPARα action and its impact on lipid metabolism, inflammation and fibrosis in non-alcoholic fatty liver disease. *J. Hepatol.* **62,** 720–733 (2015).
189. Bünger, M. *et al.* Genome-wide analysis of PPARα activation in murine small intestine. *Physiol. Genomics* **30,** 192–204 (2007).
190. Manoharan, I. *et al.* Homeostatic PPARα Signaling Limits Inflammatory Responses to Commensal Microbiota in the Intestine. *J. Immunol.* **196,** 4739–4749 (2016).
191. Hu, Y. *et al.* Pathogenic role of diabetes-induced PPAR-α down-regulation in microvascular dysfunction. *Proc. Natl. Acad. Sci. U. S. A.* **110,** 15401–15406 (2013).
192. Feltenmark, S. *et al.* Eoxins are proinflammatory arachidonic acid metabolites produced via the 15-lipoxygenase-1 pathway in human eosinophils and mast cells. *Proc. Natl. Acad. Sci.* **105,** 680–685 (2008).
193. Henderson, W. R., Harley, J. B. & Fauci, A. S. Arachidonic acid metabolism in normal and hypereosinophilic syndrome human eosinophils: generation of leukotrienes B4, C4, D4 and 15-lipoxygenase products. *Immunology* **51,** 679–686 (1984).
194. Ivanov, I. I. *et al.* Induction of intestinal Th17 cells by segmented filamentous bacteria. *Cell* **139,** 485–498 (2009).
195. Atarashi, K. *et al.* Th17 Cell Induction by Adhesion of Microbes to Intestinal Epithelial Cells. *Cell* **163,** 367–380 (2015).
196. Detoraki, A. *et al.* Angiogenesis and lymphangiogenesis in bronchial asthma. *Allergy* **65,** 946–958
197. Puxeddu, I. *et al.* Human peripheral blood eosinophils induce angiogenesis. *Int. J. Biochem. Cell Biol.* **37,** 628–636 (2005).
198. Puxeddu, I. *et al.* The role of eosinophil major basic protein in angiogenesis. *Allergy* **64,** 368–374 (2009).
199. Stzepourginski, I., Eberl, G. & Peduto, L. An optimized protocol for isolating lymphoid stromal cells from the intestinal lamina propria. *J. Immunol. Methods* **421,** 14–19 (2015).
200. Pantoja-Feliciano, I. G. *et al.* Biphasic assembly of the murine intestinal microbiota during early development. *ISME J.* **7,** 1112–1115 (2013).
201. Sommer, F. & Bäckhed, F. The gut microbiota--masters of host development and physiology. *Nat. Rev. Microbiol.* **11,** 227–238 (2013).
202. Smith, K., McCoy, K. D. & Macpherson, A. J. Use of axenic animals in studying the adaptation of mammals to their commensal intestinal microbiota. *Semin. Immunol.* **19,** 59–69 (2007).
203. Bristow, J., Carey, W., Egging, D. & Schalkwijk, J. Tenascin-X, collagen, elastin, and the Ehlers-Danlos syndrome. *Am. J. Med. Genet. C Semin. Med. Genet.* **139C,** 24–30 (2005).

204. Huijing, P. A. *et al.* Muscle characteristics and altered myofascial force transmission in tenascin-X-deficient mice, a mouse model of Ehlers-Danlos syndrome. *J. Appl. Physiol.* **109,** 986–995 (2010).
205. Elefteriou, F., Exposito, J. Y., Garrone, R. & Lethias, C. Binding of tenascin-X to decorin. *FEBS Lett.* **495,** 44–47 (2001).
206. Mao, J. R. *et al.* Tenascin-X deficiency mimics Ehlers-Danlos syndrome in mice through alteration of collagen deposition. *Nat. Genet.* **30,** 421–425 (2002).
207. Desai, J. *et al.* Nell1-deficient mice have reduced expression of extracellular matrix proteins causing cranial and vertebral defects. *Hum. Mol. Genet.* **15,** 1329–1341 (2006).
208. Cowan, C. M. *et al.* Synergistic Effects of Nell-1 and BMP-2 on the Osteogenic Differentiation of Myoblasts. *J. Bone Miner. Res.* **22,** 918–930 (2007).
209. Feitosa, N. M. *et al.* Hemicentin 2 and Fibulin 1 are required for epidermal-dermal junction formation and fin mesenchymal cell migration during zebrafish development. *Dev. Biol.* **369,** 235–248 (2012).
210. Dong, C. *et al.* Hemicentin Assembly in the Extracellular Matrix Is Mediated by Distinct Structural Modules. *J. Biol. Chem.* **281,** 23606–23610 (2006).
211. Gorres, K. L. & Raines, R. T. Prolyl 4-hydroxylase. *Crit. Rev. Biochem. Mol. Biol.* **45,** 106–124 (2010).
212. Trackman, P. C. Diverse Biological Functions of Extracellular Collagen Processing Enzymes. *J. Cell. Biochem.* **96,** 927–937 (2005).
213. Barnes, J. M., Przybyla, L. & Weaver, V. M. Tissue mechanics regulate brain development, homeostasis and disease. *J. Cell Sci.* **130,** 71–82 (2017).
214. Ferrer-Ferrer, M. & Dityatev, A. Shaping Synapses by the Neural Extracellular Matrix. *Front. Neuroanat.* **12,** (2018).
215. Melchior-Becker, A. *et al.* Deficiency of Biglycan Causes Cardiac Fibroblasts to Differentiate into a Myofibroblast Phenotype. *J. Biol. Chem.* **286,** 17365–17375 (2011).
216. Alfano, M. *et al.* The interplay of extracellular matrix and microbiome in urothelial bladder cancer. *Nat. Rev. Urol.* **13,** 77–90 (2016).
217. Slack, E. *et al.* Innate and Adaptive Immunity Cooperate Flexibly to Maintain Host-Microbiota Mutualism. *Science* **325,** 617–620 (2009).
218. Medzhitov, R. *et al.* MyD88 Is an Adaptor Protein in the hToll/IL-1 Receptor Family Signaling Pathways. *Mol. Cell* **2,** 253–258 (1998).
219. Cayrol, C. & Girard, J.-P. Interleukin-33 (IL-33): A nuclear cytokine from the IL-1 family. *Immunol. Rev.* **281,** 154–168 (2018).
220. Garlanda, C., Dinarello, C. A. & Mantovani, A. The Interleukin-1 Family: Back to the Future. *Immunity* **39,** 1003–1018 (2013).
221. Kakkar, R., Hei, H., Dobner, S. & Lee, R. T. Interleukin 33 as a Mechanically Responsive Cytokine Secreted by Living Cells. *J. Biol. Chem.* **287,** 6941–6948 (2012).

222. He, Z., Chen, L., Furtado, G. & Lira, S. IL-33 regulates gene expression in intestinal epithelial cells independently of its nuclear localization. *bioRxiv* 291039 (2018). doi:10.1101/291039
223. Hashimoto, H. & Kusakabe, M. Three-dimensional Distribution of Extracellular Matrix in the Mouse Small Intestinal Villi. Laminin and Tenascin. *Connect. Tissue Res.* **36,** 63–71 (1997).
224. Lee, L., Hashimoto, H. & Kusakabe, M. A note on the preparation of whole mount samples suitable for observation with the confocal laser scanning microscope. *Acta Histochem.* **99,** 101–109 (1997).
225. Veeraveedu, P. T. *et al.* Ablation of IL-33 gene exacerbate myocardial remodeling in mice with heart failure induced by mechanical stress. *Biochem. Pharmacol.* **138,** 73–80 (2017).
226. Calvén, J. *et al.* Rhinoviral stimuli, epithelial factors and ATP signalling contribute to bronchial smooth muscle production of IL-33. *J. Transl. Med.* **13,** (2015).
227. Kouzaki, H., Iijima, K., Kobayashi, T., O'Grady, S. M. & Kita, H. The danger signal, extracellular ATP, is a sensor for an airborne allergen and triggers IL-33 release and innate Th2-type responses. *J. Immunol. Baltim. Md 1950* **186,** 4375–4387 (2011).
228. Kusu, T. *et al.* Ecto-Nucleoside Triphosphate Diphosphohydrolase 7 Controls Th17 Cell Responses through Regulation of Luminal ATP in the Small Intestine. *J. Immunol.* **190,** 774–783 (2013).
229. Perruzza, L. *et al.* T Follicular Helper Cells Promote a Beneficial Gut Ecosystem for Host Metabolic Homeostasis by Sensing Microbiota-Derived Extracellular ATP. *Cell Rep.* **18,** 2566–2575 (2017).
230. Theofilopoulos, A. N., Baccala, R., Beutler, B. & Kono, D. H. TYPE I INTERFERONS (α/β) IN IMMUNITY AND AUTOIMMUNITY. *Annu. Rev. Immunol.* **23,** 307–335 (2005).
231. Pott, J. *et al.* IFN-λ determines the intestinal epithelial antiviral host defense. *Proc. Natl. Acad. Sci.* **108,** 7944–7949 (2011).
232. McFarlane, A. J. *et al.* Enteric helminth-induced type I interferon signaling protects against pulmonary virus infection through interaction with the microbiota. *J. Allergy Clin. Immunol.* **140,** 1068-1078.e6 (2017).
233. Gregorio, J. *et al.* Plasmacytoid dendritic cells sense skin injury and promote wound healing through type I interferons. *J. Exp. Med.* **207,** 2921–2930 (2010).
234. Banchereau, J. & Pascual, V. Type I Interferon in Systemic Lupus Erythematosus and Other Autoimmune Diseases. *Immunity* **25,** 383–392 (2006).
235. Brkic, Z. *et al.* The interferon type I signature is present in systemic sclerosis before overt fibrosis and might contribute to its pathogenesis through high BAFF gene expression and high collagen synthesis. *Ann. Rheum. Dis.* annrheumdis-2015-207392 (2015). doi:10.1136/annrheumdis-2015-207392
236. Luckhardt, T. R. & Thannickal, V. J. Systemic Sclerosis-Associated Fibrosis: An Accelerated Aging Phenotype? *Curr. Opin. Rheumatol.* **27,** 571–576 (2015).
237. Rodier, F. & Campisi, J. Four faces of cellular senescence. *J. Cell Biol.* **192,** 547–556 (2011).

238. Schafer, M. J. *et al.* Cellular senescence mediates fibrotic pulmonary disease. *Nat. Commun.* **8,** (2017).

239. Yu, Q. *et al.* DNA-Damage-Induced Type I Interferon Promotes Senescence and Inhibits Stem Cell Function. *Cell Rep.* **11,** 785–797 (2015).

240. Coppé, J.-P., Desprez, P.-Y., Krtolica, A. & Campisi, J. The Senescence-Associated Secretory Phenotype: The Dark Side of Tumor Suppression. *Annu. Rev. Pathol.* **5,** 99–118 (2010).

241. Jun, J.-I. & Lau, L. F. Cellular senescence controls fibrosis in wound healing. *Aging* **2,** 627–631 (2010).

242. Xiao, C., Stahel, P., Carreiro, A. L., Buhman, K. K. & Lewis, G. F. Recent Advances in Triacylglycerol Mobilization by the Gut. *Trends Endocrinol. Metab.* **29,** 151–163 (2018).

243. Iqbal, J. & Hussain, M. M. Intestinal lipid absorption. *Am. J. Physiol. - Endocrinol. Metab.* **296,** E1183–E1194 (2009).

244. Johnson, A. M. F. *et al.* High Fat Diet Causes Depletion of Intestinal Eosinophils Associated with Intestinal Permeability. *PLOS ONE* **10,** e0122195 (2015).

245. Pauly, J. E. *et al.* Meal timing dominates the lighting regimen as a synchronizer of the eosinophil rhythm in mice. *Cells Tissues Organs* **93,** 60–68 (1975).

246. Zhao, J. *et al.* F-box protein FBXL19–mediated ubiquitination and degradation of the receptor for IL-33 limits pulmonary inflammation. *Nat. Immunol.* **13,** 651–658 (2012).

247. Zhao, J. *et al.* Focal Adhesion Kinase–Mediated Activation of Glycogen Synthase Kinase 3β Regulates IL-33 Receptor Internalization and IL-33 Signaling. *J. Immunol.* **194,** 795–802 (2015).

248. Guerre-Millo, M. *et al.* PPAR-α–Null Mice Are Protected From High-Fat Diet–Induced Insulin Resistance. *Diabetes* **50,** 2809–2814 (2001).

249. Stienstra, R., Duval, C., Müller, M. & Kersten, S. PPARs, Obesity, and Inflammation. *PPAR Res.* **2007,** (2007).

250. Florey, H. Observations on the contractility of lacteals. *J. Physiol.* **62,** 267–272 (1927).

251. Michaudel, C. *et al.* Ozone exposure induces respiratory barrier biphasic injury and inflammation controlled by IL-33. *J. Allergy Clin. Immunol.* (2018). doi:10.1016/j.jaci.2017.11.044

252. Cohen, E. S. *et al.* Oxidation of the alarmin IL-33 regulates ST2-dependent inflammation. *Nat. Commun.* **6,** 8327 (2015).

253. Gomes, I. *et al.* Eosinophil-fibroblast interactions induce fibroblast IL-6 secretion and extracellular matrix gene expression: Implications in fibrogenesis. *J. Allergy Clin. Immunol.* **116,** 796–804 (2005).

254. Hopkins, A. M. *et al.* Organized migration of epithelial cells requires control of adhesion and protrusion through Rho kinase effectors. *Am. J. Physiol.-Gastrointest. Liver Physiol.* **292,** G806–G817 (2007).

255. Vllasaliu, D., Falcone, F. H., Stolnik, S. & Garnett, M. Basement membrane influences intestinal epithelial cell growth and presents a barrier to the movement of macromolecules. *Exp. Cell Res.* **323,** 218–231 (2014).
256. Burgess, J. K., Mauad, T., Tjin, G., Karlsson, J. C. & Westergren-Thorsson, G. The extracellular matrix – the under-recognized element in lung disease? *J. Pathol.* **240,** 397–409 (2016).
257. Lu, P., Takai, K., Weaver, V. M. & Werb, Z. Extracellular Matrix Degradation and Remodeling in Development and Disease. *Cold Spring Harb. Perspect. Biol.* **3,** (2011).
258. Watson, W. H., Ritzenthaler, J. D. & Roman, J. Lung extracellular matrix and redox regulation. *Redox Biol.* **8,** 305–315 (2016).

ACKNOWLEDGEMENTS

There are no words enough to describe my gratitude to all the people that made this journey possible. I owe a great debt to so many who have given me support, shown me kindness and gifted me perseverance over these 3 years. I will never forget these acts, no matter how small – and I can only hope to do them justice, in whatever direction life may take me. The memories I shared with all of you is something I will treasure for years to come, and has become an integral component of my personal growth.

To Nicola, thank you so much for placing so much faith in me these past few years – and for giving me the opportunity to conduct my thesis in your lab. I learnt so much during my time here, and this was only possible with all the support and encouragement you have given me. Your kindness, light-hearted attitude and humanity are a rarity in this world - I dedicate this work to you.

I would also like to thank Prof. Oricchio, Prof. Oxenius Prof. Velin and Prof. De Palma for agreeing to participate in my PhD defense committee.

I would like to thank my collaborators, particularly to Jeremiah – who has taught me so much during the early stages of my PhD, and has immensely broadened my understanding of the intestine. His initial observation of the Δdbl.GATA1 mice has laid the early foundations for the work presented in this thesis, and we are grateful to all the contributions he has made to make this possible.

To members of UPHARRIS - Luc, Bea, Alexis, Tiffany, Mati, Lalit, Manu and Audrey – thank you for your friendship and for making me feel at home over these years. I will always cherish the memories I have shared with all of you. Also, would like to thank our secretary Dagmara for taking care of me and the mini-UPHARRIS 'satellite lab' these past few months.

I would like to give a special thanks to the Melbourne crew – Mati and Tiffany for the exceptional support (both emotional and intellectual) you have given me. I can truly say – that without you two, this thesis really would not have been possible. I wish you the very best in the years ahead, and hope that the world shows you the same kindness that you have shown me. I owe you both a great moral debt.

To my Charlie's Angels crew: Maria, Simone, Selene and Radek – this thesis would also not have been possible without you all. We have all grown so much together, and I'm so proud of all that you have accomplished. Thank you very much for your friendship – and hope that I can do it justice in the years to come.

I would also like to express my gratitude to so many people at SV - particularly to the Blokesch lab, Ablasser lab and Oricchio lab – it is really true that it takes a village to raise a child! Thank you for the generosity and support you have provided me through the course of my studies.

To my non-SV friends and my past roommates - Beba, Cat, Damaris, Nate - thank you for keeping me sane. Although I really love the intestine, it is important to step back from time to time and come out of the cave once in a while – thank you for your friendship and for reminding me to broaden my perspective from time to time.

Lastly, to my love James – thank you for holding me together in difficult times, for being my voice of reason and maintaining my optimism these past few years. After four-long years, I can finally say that I am coming home to you. I look forward to all the adventures we will experience in these years to come.

Kathleen Kris Sanchez Shah

Date/Place of Birth: December 24, 1990 – San Juan, Philippines
Nationality: Canadian
Professional address (current): Laboratory of Intestinal Immunology, EPFL-SV-GHI-UPHARRIS, Station 19, CH-1015 Lausanne
Current position: PhD candidate (3rd year)
Email address: Kathleen.shah@epfl.ch

EDUCATION

Doctor of Philosophy (PhD) Molecular Life Sciences **(2015-current)**
Ecole Polytechnique Federale Lausanne (EPFL), Lausanne Switzerland
Supervisor: Prof. Nicola L. Harris
Thesis title: *An exploratory study on the functional significance of eosinophil residency in the small intestine under homeostatic conditions*
Relevant keywords: Small intestinal eosinophils, structural cells, whole-mount imaging, confocal microscopy, nutrient absorption, villous architecture, flowcytometry, microbiota, metabolic analysis, intestinal physiology/function, circadian rhythm

Master of Science (MSc) Microbiology and Immunology (**2013-2015)**
McGill University, Montreal Canada
Supervisor: Prof. Irah L. King
Thesis title: *A role for microbiota in the homeostatic regulation of type II immunity*
Relevant keywords: Th2/type II immunity, allergy, microbiota, t-follicular helper cells, intestinal eosinophils, flowcytometry, microbiota, immunoblotting

Bachelor of Science (Bsc) Honors spec. In Cell and Developmental Biology (**2008-2012)**
University of Western Ontario, London ON Canada

OTHER RESEARCH/WORK EXPERIENCE

Volunteer, Allergy Clinic
Montreal Children's hospital **(2014)**
Supervisor: Dr. Moshe Ben-Shoshan
Relevant keywords: post-admission clinical surveys, follow-up calls, patients, anaphylaxis, food labeling, montreal pediatric hospitals

Research assistant **(2012-2013)**
Institut de researches cliniques de Montreal (IRCM)
Supervisor: Prof. Marie Trudel
Relevant keywords: Polycystic kidney disease, molecular biology techniques, mouse colony management

POSTER PRESENTATIONS (recent)

"Resident intestinal eosinophils maintain small intestinal structure and function", SSAI meeting 2017 - St. Gallen CH
Bernier-Latmani J.*, **Shah K.***, Davanture S., Petrova T., Harris NL (*equal contribution)

"A role for eosinophils in the regulation of small intestinal structure and function", LIMNA meeting 2017 - Lausanne CH
Shah K.*, Bernier-Latmani J.*, Bouchery T., Moyat M., Petrova T., Harris NL (*equal contribution)

HONORS & AWARDS

Poster award, SSAI meeting (2017)
MIMM FC Harrison fellowship Award for returning students (2014)
MIMM Great Travel Award (2014)
MIMM Graduate Excellence Fellowship (2013)
Dean's list (2011-2012)
Western Scholarship of Distinction (2008)

PUBLICATIONS

T. Bouchery[1*], B. Volpe[1], **K. Shah[1]**, K. Filbey[2], L. Lebon[1], G. LeGros[2], N. Harris[1]. The study of host immune responses elicited by the model murine hookworms, *Nippostronglyus brasiliensis and Heligmosomoides polygyrus. Current Protocols in Mouse Biology* (accepted), (2017)

Vânia Cardoso[1*], Julie Chesné[1*], Hélder Ribeiro[1], Tânia Carvalho[1], Bethania García-Cassani[1], Tiffany Bouchery[2], **Kathleen Shah[2]**, Nuno Barbosa-Morais[1], Nicola Harris[2] and Henrique Veiga-Fernandes[1,3]. Neuronal regulation of type 2 innate lymphoid cells via neuromedin U.
Nature (in press), (2017)

TEACHING

Immunology (Bio-479) **(Sept-Dec, 2017)**
Teaching Assistant

Cellular and Molecular Biology (Bio-205) **(Sept-Dec, 2017)**
Teaching Assistant

Integrated Laboratory in Life Sciences I (Bio-203) **(Jan-May, 2017)**
Teaching Assistant